Development of a General Design Method for Intensifying Distillation and Multiple Reactions

by

James Chin

A Dissertation submitted to the Graduate Faculty in Engineering
in partial fulfillment of the requirements for the degree of
Doctor of Philosophy, The City University of New York

2007

UMI Number: 3288946

Copyright 2007 by
Chin, James

All rights reserved.

UMI Microform 3288946
Copyright 2008 by ProQuest Information and Learning Company.
All rights reserved. This microform edition is protected against
unauthorized copying under Title 17, United States Code.

ProQuest Information and Learning Company
300 North Zeeb Road
P.O. Box 1346
Ann Arbor, MI 48106-1346

© 2007

JAMES CHIN

All Rights Reserved

This manuscript has been read and accepted for the
Graduate Faculty in Engineering in satisfaction of the
dissertation requirement for the degree of Doctor of Philosophy.

Professor Jae W. Lee

Date — Chair of Examining Committee

Professor Mumtaz Kassir

Date — Executive Officer

Professor Jae W. Lee (mentor)

Professor Alexander Couzis

Professor Irven Rinard

Professor David Rumschitzki

Supervisory Committee

THE CITY UNIVERSITY OF NEW YORK

Abstract

Development of a General Design Method for Intensifying Distillation and Multiple Reactions

by

James Chin

Advisor: Professor Jae W. Lee

By using phase and reaction equilibrium information, this thesis derives feasibility criteria for non-extractive and extractive reactive distillation systems. This thesis presents a quick method for estimating column composition profiles for reactive and extractive cascades in a double-feed column without stage calculations. This column profile estimation is based on the feasibility and pinch point analyses. From the pinch point analysis, manifolds of possible composition profiles are generated. This thesis then addresses a general feasibility evaluation method for quaternary reactive distillation based on the feasibility study of isomolar reactions. Critical composition regions (CCRs) are defined as the areas where thermodynamic constraints force extractive composition profiles to travel in infeasible directions. Then, material balance is imposed to determine whether extractive composition profiles can reach desired product compositions.

This thesis also presents a new feasibility evaluation procedure for reactive mixtures where simple homogeneous reactive batch columns cannot produce pure

products and presents three alternatives: a batch reactive rectifier with a decanter, a homogenous batch reactive extractive distillation (BRED) column, or an entrainer that introduces an unstable node heteroazeotrope. Finally, this thesis addresses a new method for estimating the liquid still composition trajectory of batch reactive distillation systems based on material balance and reaction equilibrium data. For a given feed to product flow ratio with constant feed charge and product compositions, the still pot composition trajectory is mathematically confined to the intersection between the reaction equilibrium manifolds and a “material balance plane” defined by stoichiometry and material balance. Starting from this estimated still pot trajectory, we can easily evaluate the feasibility of various batch reactive distillation configurations by applying the batch column feasibility criteria.

Acknowledgements

I wish to first give thanks to God for letting me be born and raised in New York City, which (in my admittedly biased opinion) is the greatest city in the world.

Second, I wish to give thanks to my family and friends, most especially my parents, Jim Chin and Margaret Donohue Chin, who have been loving and supportive all the years of my life.

Third, I wish to acknowledge the City College of New York, itself, for the fine undergraduate and graduate education that I have received here.

Fourth, I wish to acknowledge the faculty of the Chemical Engineering Department and the instruction and guidance they have given me over the combined nine years that I have been a student in this Department, both undergraduate and graduate. Included in this is Professor Robert A. Graff, whom I served as an undergraduate research assistant, and especially included in this is my doctoral advisor, Professor Jae Woo Lee, who has been exceedingly patient in my struggles to retain my sanity, focus, and will to finish this thesis work.

Fifth, I wish to acknowledge the members of my doctoral committee: Doctor Jeff Siirola, Professor Jae Woo Lee, Professor David Rumschitzki, Professor Alexander Couzis, and Professor Irven Rinard.

Sixth, I wish to acknowledge the Chemical Engineering Technical Staff, namely, Zhen Rong Xu and Andrew Eng, whose assistance in technical matters I have found to be valuable.

Finally, I wish to acknowledge the students of the undergraduate Chemical Engineering laboratory classes, whom I have had the honor and pleasure of serving as the Teaching Assistant these past six years. It is my hope that they will take safety issues to heart, most memorably to always wear safety goggles in a laboratory while an experiment is in operation.

Table of Contents

List of Tables

List of Figures

Introduction

Reactive distillation is the execution of chemical reaction and vapor-liquid(-liquid) phase separation in a single piece of equipment. Chemical Research & Licensing Company's process for MTBE was the first patented reactive distillation process to become commercially successful[1]. Other commercial examples of reactive distillation include the synthesis of methyl acetate[2], cumene[3], methylal[4], etc.

The application of reactive distillation can simplify many processes, reduce energy use, and, in some cases, avoid the use of harmful extractive agents[5-7]. Reactive distillation can circumvent azeotropes in phase separation behavior. Conventional processes based on single-function equipment can require a lot of steps (and therefore, a lot of separators) to break and/or circumvent non-idealities. The single reactive column in the Eastman methyl acetate process, for example, replaced a possible system of ten unit operations that would have been needed in a conventional process arrangement[8].

The energy savings realized by reactive distillation come from the fact that much of the repeated heating and cooling in a conventional process is avoided. Additionally, each additional piece of equipment in a plant represents an additional source of thermodynamic inefficiency and heat loss. Because energy production is closely tied to a wide range of environmental issues[9], this is indirectly an environmental benefit in and of itself.

Another environmental benefit of reactive distillation is that, in some processes, the use of a separate entrainer can be avoided. Again taking Eastman's methyl acetate system as an example, the use of a separate extractive agent was avoided because acetic acid was able to act as both a reactant and an extractive agent[8].

However, in spite of these potential benefits to both industry and society, general methods for determining the *feasibility of multi-component, multi-reaction systems* have not been developed.

Therefore, the main objective of this work is to develop a design method for intensifying *multiple reactions* in a single unit or in the smallest possible number of units. To achieve this goal, the detailed research problems, past research activities by other groups, and past research by our group will be presented in the following sections.

Literature Survey

The feasibility and design methods for reactive separation systems that have been formulated and considered to date generally fall into one of three categories: geometric methods, simulation methods, and mathematical programming methods.

Geometrically-based graphical methods for determining feasibility, the first category of design methods discussed here, tend to require visual inspection. Since only three-dimensional systems can be directly visualized in a convenient manner, this limits the application of geometric systems to four components unless some scheme to reduce

the number of dimensions of the problem is applied. One approach that preserved the number of dimensions was Lee et al.[10], who considered the case of a single kinetically-controlled reaction taking place inside a single-feed distillation column. The column was divided into the rectifying and stripping sections, and each section was treated as either reactive or non-reactive. The column profile of a reactive section was estimated according to the critical Damköhler number and the profile of the non-reactive section was estimated according to the Rectification Body Method (RBM) proposed by Bausa et al.[11]. Although this method provided a means of deciding how reaction should be distributed within a column, it's use of the RBM, which is linear, is liable to be inadequate for systems that are highly non-linear.

Static analysis, as studied by Serafimov and coworkers, was another method that preserved the number of dimensions of the system[12-20]. Here, the feed composition was fixed and the possible reaction conversions and product compositions were determined using the simplifying assumption that liquid and vapor molar flow rates are much larger than molar reaction rates on any given stage. Because the assumption does not always hold well in most systems, static analysis could only give indications of the maximum possible reaction conversions and the sizes and locations of the reaction zones and could not guarantee feasibility.

Some geometric approaches assumed reaction equilibrium, and thus allowed the system to be visualized in a number of dimensions smaller than the dimensionality of the full composition space. For example, Barbosa and Doherty[21-23] and Espinosa et al.[24,25]

used a set of transformed composition coordinates to refer to points on the reaction equilibrium surface. Perez-Cisneros et al.[26] introduced element balance variables to reduce the dimensionality of a reactive system. In their approach, they dealt with a Gibbs energy minimization problem by treating energy as a function of elements or functional groups (as opposed to being functions of chemical species). This greatly mitigated the visualization problem in cases where the number of such elements or functional groups under consideration is much smaller than the number of chemical species in the system. Finally, Wibowo and Ng[27] proposed a system of geometric modeling using homogenous coordinates and Janecke projections, and thus projected features of a higher-dimensional composition space onto a projected composition space that is much easier to visualize.

The iterative simulation methods are the second category of design methods and they typically iterated on a particular variable (usually the reflux ratio or the extent of reaction) to arrive at their solutions. Barbosa and Doherty[28] derived a set of differential equations to describe the simple distillation of homogenous reacting mixtures for both ideal and non-ideal systems. They then applied these equations to develop a minimum-reflux calculation technique for single-reaction distillation columns (both single- and double-feed) that is analogous to the minimum-reflux calculation techniques of conventional multicomponent distillation[29,30]. Although applicable to non-ideal systems, Buzad and Doherty[31,32] only applied this to kinetically controlled ternary mixtures. Okasinski and Doherty[33] extended this method to multiple components, but were still limited to a single reaction.

For a specified feed, Chadda et al.[34] determined the regions of feasible distillate and bottom product compositions from a combination of simulation techniques and fixed point methods. These regions are bound by the minimum reflux and the minimum number-of-stages limits. Chadda et al.[35] then extended this algorithm to estimate the column profiles for reaction rates in-between those two limits.

Mathematical programming methods are the third category of design techniques that have been applied. Ciric and Gu[36] presented a MINLP model to optimize the feed tray locations, feed rates, and number of trays in a reactive distillation column.

Papalexandri and coworkers[37,38] proposed a method of using conceptual mass and heat transfer modules to model various processes including, but not limited to, traditional unit operations. In this manner, processes can be conceived without having to directly consider the particular unit operations involved, so particular unit operations don't have to be chosen a priori for any given process under consideration. Only information about the streams feeding the process and the desired product streams are necessary. The structure formed by such mass/heat transfer blocks was also optimized by a MINLP approach. However, numerical and combinatorial problems arise which make solving such a system difficult. Finally, Jackson and Grossman[39] presented an algorithm to optimize feed tray locations, number of trays, operating and design parameters, and sizes and locations of reaction zones. The algorithm employed conditional trays that, if in use, may perform either separation alone or both separation and reaction.

In summary, all of the previous work deals with continuous processes and mostly single-reaction systems. In particular, no geometric design methods for batch reactive distillation have been developed. Also, there is no general design method for combining multiple reactions in various structural configurations of reactive distillation columns.

Prior Research Work

In this section, we will discuss previous reactive separation research conducted by our group. The work described here is the basis for the thesis work presented in the following chapters, which derives a general design method for combining multiple reactions in various batch and continuous configurations. We will look at four categories of our previous research work: feasibility of batch systems, feasibility of BRED systems, feasibility of continuous systems, and thermodynamically-based design methods.

Feasibility of Batch Reactive Distillation for Non-Ideal Systems

Design insights for reactive distillation were developed through understanding the time-dependent interaction between reaction and separation[40]. Figures 1 and 2 illustrate two different flow sheets for producing pure products in the decomposition reaction 2I ↔ L+H. From thermodynamic classification[41,42] (also refer to Thesis Appendix), Residue Curve Map (RCM) 320 was chosen for this example. It features one unstable node (UN), two stable nodes (SN), and two saddles. Two binary azeotropes exist in this mixture and are shown in Figure 0-1(a). One is a minimum-boiling saddle azeotrope (AZ) between I and H. The other is a maximum-boiling stable node azeotrope between I and L. The

order of the boiling points is L < I-H AZ < I < L-I AZ < H. Thus, this ternary mixture forms a separation boundary that simple distillation cannot cross.

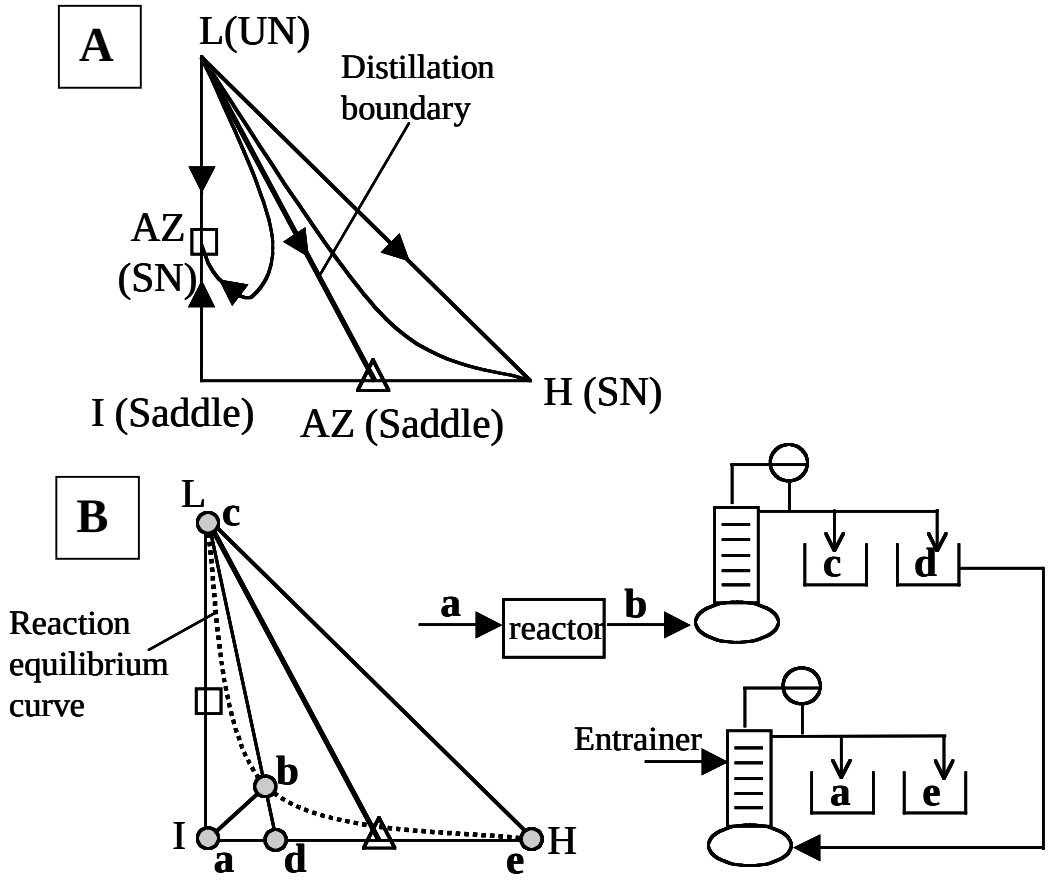

Figure 0-1: Production of pure products L and H with reaction 2I ↔ L+H in a batch system. (a) RCM 320. (b) Conventional flowsheet with one reactor and two columns.

The first process shown in Figure 0-1(b) employs a traditional flowsheeting technique using single-function units. The feed stream (**a**) containing pure reactant I enters a reactor that produces products L and H. Because of the reaction equilibrium limitation, the outlet stream (**b**) of the reactor has unconverted reactant I mixed with these two products. To separate the reactor effluent into pure components, two batch distillation operations are needed. The first rectification produces the lightest product L (**c**) at the top receiver and then recovers the I-H mixture (**d**) that will be separated in the

second rectification. In the second rectification, an extractive agent (entrainer) is provided through a side-feed to break the minimum boiling I-H azeotrope. So, the reactant I (**a**) will be recovered first at the top receiver, then H (**e**), and then the entrainer. Unconverted reactant I (**a**) is then recycled for the next batch. Three single-function operations are required for this production system and an extractive agent is needed to circumvent the separation boundary.

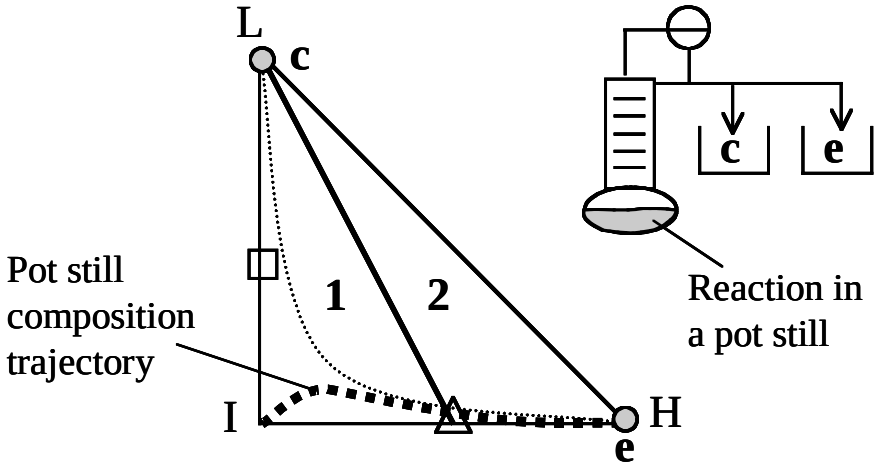

Figure 0-2: Production of pure products L and H with one reactive rectifier (Guo et al., 2003a[39]). There are two different distillation regions, **1** and **2**.

However, only one batch rectification operation is needed to produce pure products if the reaction occurs in the pot still as shown in Figure 0-2. Above the pot still, a large number of non-reactive stages are assumed to be available for the purification of the products. Here, two important considerations should be taken into account: 1) light product L is the most volatile component (or unstable node) in both distillation regions and therefore will be recovered at the top of the rectifier at every instant in time and 2) the forward reaction in the pot still is enhanced by the removal of L and will circumvent the separation boundary to reach the heavy product (H) as time passes. Since the light product (L) is continuously removed at the top, the pot still composition trajectory moves

into the forward reaction zone towards the H-I binary edge. Thus, the forward reaction continues to occur (2I → L+H) and consumes all of the reactant (I). Hence the reactive pot still composition trajectory crosses the separation boundary and reaches the heavy product vertex (H).

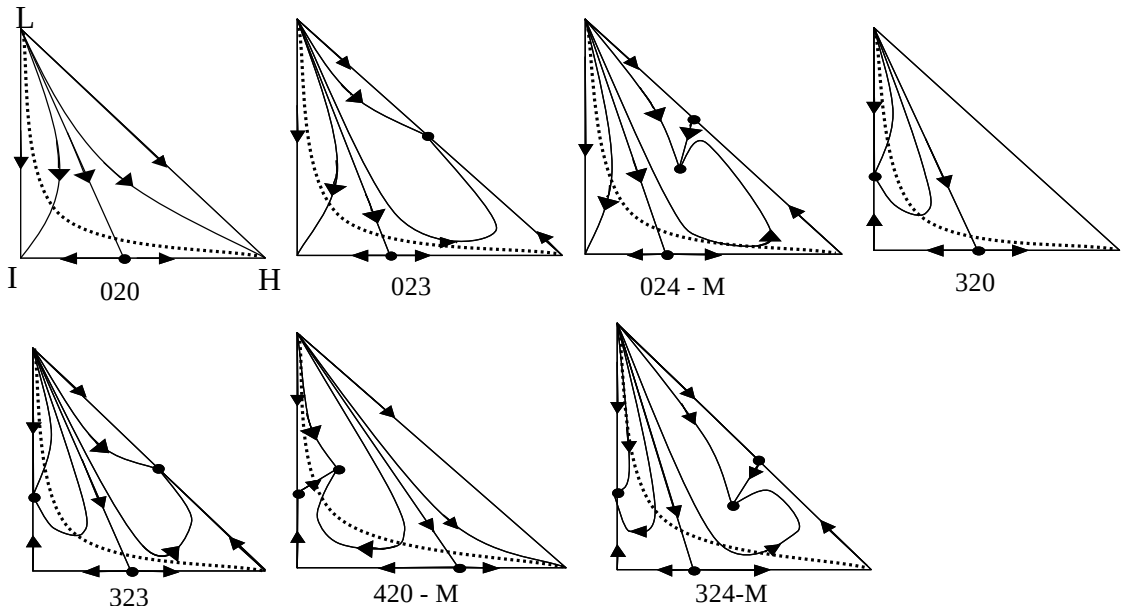

Figure 0-3: RCMs which can lead to the production of pure products in a reactive batch rectifier (Guo et al., 2003a[39])

Here, one generalized design insight for the reactive rectifier has been identified by the examination of Figure 0-2[40]: *if one of the reaction products is an UN (that is, if it is the most volatile) and is reachable from any distillation region*, then *a batch rectifier* with a reactive pot still can produce pure products. The various RCMs shown in Figure 0-3 have different numbers and types of azeotropes but they have one common feature: *each RCM has one UN product (L)*. Since the UN product is continuously removed at the top of the column, the forward reaction occurs. Then, reactant I is completely consumed and heavy product H is produced in the pot still. Any decomposition reaction with

arbitrary stoichiometry, $\alpha I \leftrightarrow \beta L + \gamma H$, can be integrated to produce pure products if L is an UN and is reachable from any distillation region.

A symmetric result holds for systems with a SN product (the least volatile component) that is reachable from any distillation region. In this case, a batch stripper with a reactive overhead drum is used as shown in Figure 0-4(a). With one UN product and one SN product, the middle vessel column in Figure 0-4(b) can be used to produce pure products.

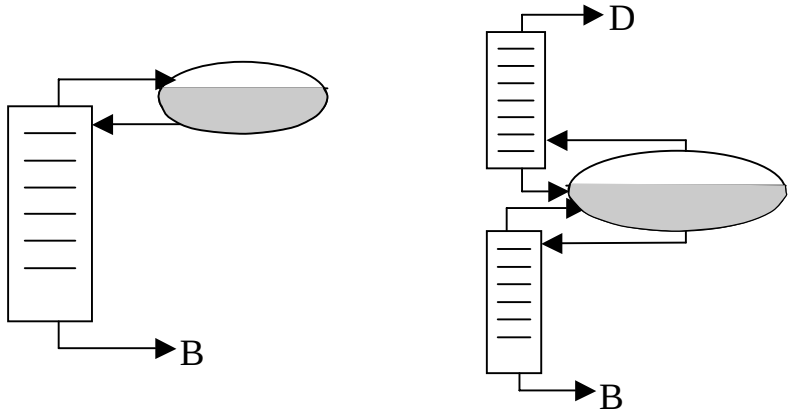

(a) Stripper (b) Middle vessel column

Figure 0-4: Various batch configurations with reactive charge drums (Guo et al. 2003a[29]).

Feasibility of Bath Reactive Extractive Distillation (BRED) for Non-Ideal Systems

Batch rectifiers, strippers, and middle vessel columns as described above can only produce pure products if at least one of the products is a stable or unstable node. However, if both products are saddles, then these configurations will only produce an azeotrope, not pure products. RCM-031 is shown in Figure 0-5(a). There is an unstable node azeotrope in-between the saddle products L and H. It should be noted that if both

products are saddles, then there must be a node azeotrope (stable or unstable) between them. There is also a stable node azeotrope between the reactant, I, and the heavy product, H.

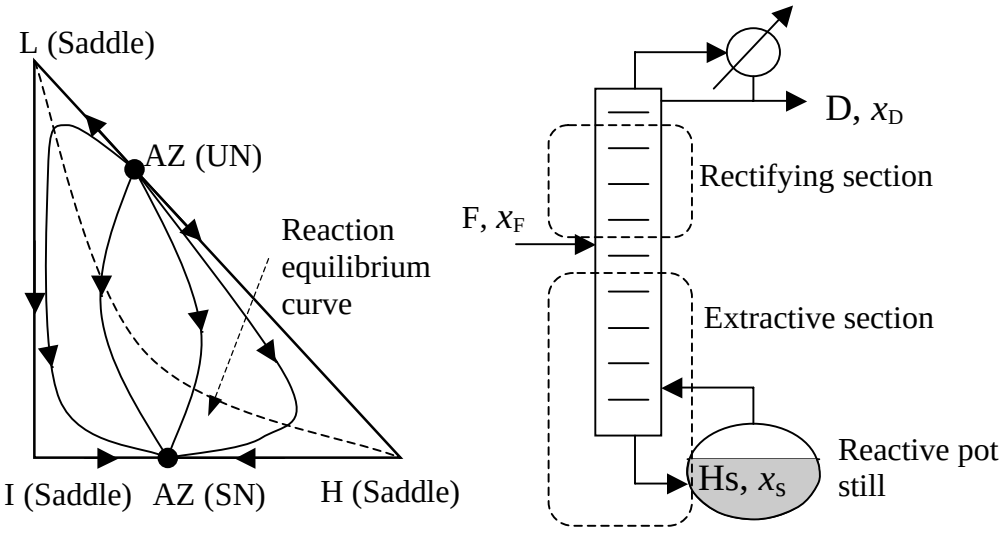

Figure 0-5: (a) Residue Curve Map 031 has an unstable node azeotrope between the two products. Both products are saddles. (b) The structural configuration for a BRED rectifier with a reactive pot still.

If reactant I is charged into the pot still of the batch rectifier shown in Figure 0-2, allowed to react, and distilled, then the L-H azeotrope is formed at the top. As the reaction proceeds, the pot still composition is pushed into the forward reaction zone and additional L and H are produced. Eventually, only H will remain in the pot still for the system shown in Figure 0-5a. It would then be necessary to separate the L-H azeotrope in a separate unit, possibly with the use of an entrainer. Thus, we cannot use the batch rectifier of Figure 0-2 to produce pure products.

If reactant I is charged into the pot still of the batch stripper shown in Figure 0-4a allowed to react, and distilled, then the I-H azeotrope will be formed at the bottom and the pot still composition will be pushed into the reverse reaction zone. Thus, the reverse

reaction will take place and the stable node azeotrope will be produced at the bottom. It would then be necessary to separate the I-H azeotrope in a separate unit. Thus, we cannot use the batch stripper of Figure 0-4a to produce pure products.

If both products are saddles with an UN azeotrope between them, then an extractive agent can be fed into the side of a batch rectifier column. Such batch reactive extractive distillation columns are referred to as BRED columns[43] and their configuration is shown in Figure 0-5b. The extractive agent feed stage divides the BRED column into two sections: the rectifying and extractive sections. Guo and Lee[43] derived balance equations that describe the composition profiles in both sections of the BRED column.

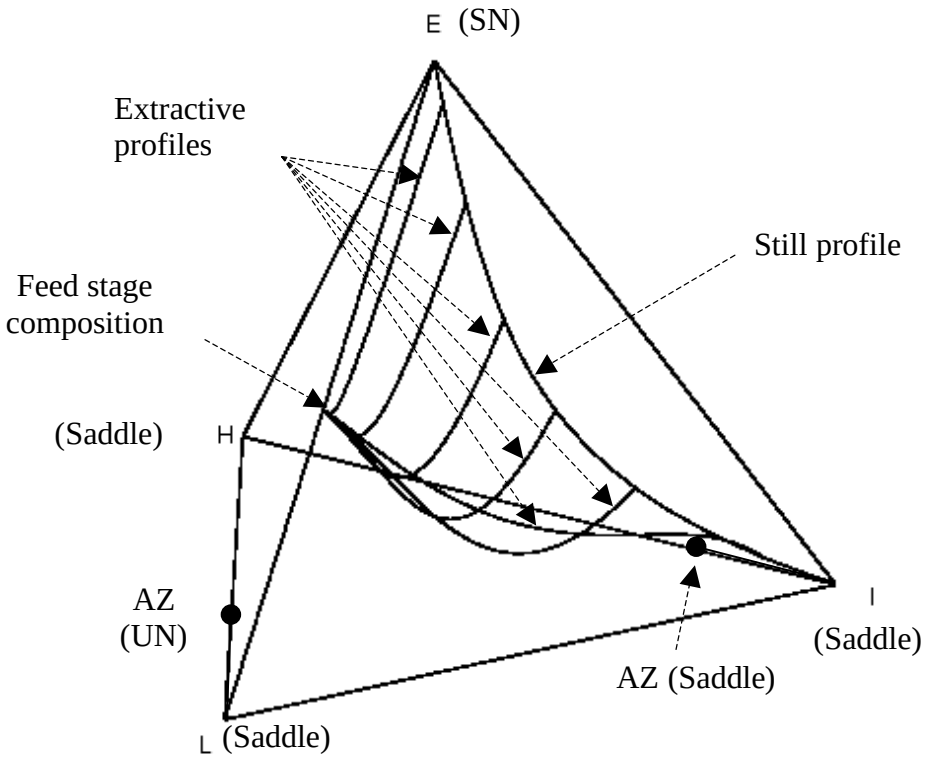

Figure 0-6: The pot still trajectory and the extractive section composition profiles for a BRED rectifier under total reflux (Guo and Lee, 2004[42]).

If an appropriate entrainer, E, is selected such that it is the heaviest component in the system, then its presence changes the dynamic properties of the original ternary system. Specifically, the stable node azeotrope between H and I becomes a saddle in the new quaternary system of Figure 0-6. Because there is only one UN (L-H azeotrope) and one SN (E) in this quaternary system, and all other fixed points are saddles, no distillation boundary exists. It was found from simulations based on the balance equations that, for this quaternary system, the extractive section composition profile would connect any pot still composition to a point on the L-E binary edge of composition space and that the rectifying section composition profile would connect this point to the light product vertex. Thus, light product L will always be produced at the top by the non-reactive rectifying section.

If reactant I is charged to the pot still, allowed to react, and distilled as entrainer E is fed into the column, then L will be removed at the top of the column, pushing the pot still composition into the forward reaction zone. This will cause more I to react to form L and H and more L will be produced at the top of the column. Eventually, as L is removed, I consumed, and E added, only H and E will remain in the pot still and the pot still composition will move towards the entrainer vertex. The extractive section profiles starting from various points on the pot still trajectory are shown in Figure 0-6.

In summary, for the previous two sections, two important strategies were employed for combination of reaction and azeotropic separation in batch systems: 1) the thermodynamic categorizations of feasible combinations of reaction and phase

equilibrium according to the dynamic properties (UN, SN, and saddle) of reactants, products, entrainers, and azeotropes, and 2) the structural variations of equipment to circumvent thermodynamic limitations.

Overview

This thesis consists of five papers, where each paper is a chapter of this thesis. Four of them have been published and the fifth is to be submitted for review soon.

In Chapter 1, "Feasibility of Continuous Reactive Distillation with Azeotropic Mixtures" (Guo, Chin, and Lee 2004), the feasibility criteria for continuous reactive distillation (single-feed) *and* continuous reactive/extractive distillation (double-feed) columns are derived from material balance constraints and phase and reaction equilibrium information.

In Chapter 2, "Rapid Generation of Composition Profiles for Reactive and Extractive Cascades" (Chin and Lee 2005), the critical composition region is defined with the purpose of identifying regions of composition space where phase equilibrium will not allow extractive distillation to produce pure products. The upper and lower bounds of reflux ratios are also defined with the purpose of identifying the minimum entrainer flow needed to perform a non-reactive/extractive distillation. The upper and lower bound calculations are then extended to determine minimum entrainer flow in reactive/extractive distillation. Also, a method is presented for following the trajectory of a pinch point curve under a given entrainer flow.

In Chapter 3, “Generalized Feasibility Evaluation of Equilibrated Quaternary Reactive Distillation Systems” (Chin, Kattukaran, and Lee 2004), the upper and lower bound calculations are extended to cases involving a non-isomolar reaction.

In Chapter 4, “Feasible Products in Complex Batch Reactive Distillation” (Chin, Lee, and Choe 2006), the feasibility criterion of batch reactive rectifiers is modified to exploit any liquid-liquid immiscibility that’s present. Critical composition regions and upper and lower bounds are applied to determine the feasibility of batch reactive/extractive distillation (BRED). Finally, BRED with heterogenous entrainers are considered in exploiting liquid-liquid immiscibilities.

In Chapter 5, “Estimation of Still Trajectory for the Feasibility Evaluation of Batch Reactive Distillation Systems” (Chin and Lee, 2007), the above work is organized into an automated and systematic method for evaluating the feasibility of combining distillation and a single reaction to produce pure products. This feasibility algorithm is then extended to multiple-reaction systems.

The thesis is concluded with “Conclusions and Future Work” wherein we describe possible research avenues that could be explored from the work already presented.

References

1. Smith LA. Catalytic Distillation Process. U.S. Patent 4,307,254: 1981.

2. Agreda VH, Partin LR. Reactive distillation process for the production of methyl acetate. U.S. Patent 4,435,595: 1984.

3. Shoemaker JD, Jones EM. Cumene by Catalytic Distillation. *Hydrocarbon Processing*. 1987;66(6):57-58.

4. Masamoto J, Matsuzaki K. Development of Methylal Synthesis by Reactive Distillation. *J. Chem. Engr. Japan*. 1994;27(1):1-5.

5. Malone MF, Doherty MF. Reactive distillation. *Ind Eng Chem Res*. 2000;39:3953-3957.

6. Taylor R, Krishna R. Modelling reactive distillation. *Chem Eng Sci*. 2000;55:5183-5229.

7. Stankiewicz A, Moulijn JA. Process Intensification. *Ind. Engr. Chem Res.* 2002;41(8):1920-1924.

8. Siirola JJ. An industrial perspective on process synthesis. *AIChE Symp Ser*. 1995;304:222-233.

9. Allen DT, Shonnard D. Green Engineering: Environmentally Conscious Design of Chemical Processes, Prentice Hall PTR, Upper Saddle River, NJ, (2002).

10. Lee JW, Brüggemann S, Marquardt W. Shortcut method for kinetically controlled reactive distillation systems. *AIChE J*. 2003;49:1471-1487.

11. Bausa J, Watzdorf Rv, Marquardt W. Shortcut methods for nonideal multicomponent distillation: 1. Simple columns. *AIChE J*. 1998;44:2181-2198.

12. Giessler S, Danilov RY, Pisarenko YA, Serafimov LA, Hasabe S, Hashimoto I. Feasibility Study of Reactive Distillation Using the Analysis of the Statics. *Ind. Eng. Chem. Res.* 1998;37:4375-4382.

13. Giessler S, Danilov RY, Pisarenko YA, Serafimov LA, Hasabe S, Hashimoto I. "Feasible Separation Modes for Various Reactive Distillation Systems", *Ind. Eng. Chem. Res* 1999;38:4060

14. Giessler S, Danilov RY, Pisarenko YA, Serafimov LA, Hasabe S, Hashimoto I. "Systematic Structure Generation for Reactive Distillation Processes", *Comp. Chem. Engr.* 2001;25:49.

15. Balashov MI, Serafimov LA. Analysis of statics of continuous combined reaction-fractionation process. *Theor. Found. Chem. Engr*. 1980;14:495-500.

16. Balashov MI, Patlasov VP, Serafimov LA. Rules of Primary Reaction Zone Spread in Continuous Combined Reaction-Fractionation Processes, *Theor. Found. Chem. Engr.* 1981;15:406-413

17. Patlasov VP, Balashov MI, Serafimov LA. Computer Analysis of the Statics of Continuous Integrated Reaction-Rectification Processes. *Theor. Found. Chem. Technol.* 1980;14(1):67-72

18. Pisarenko YA, Balashov MI. Statics of Reaction Systems with Selective Exchange. *Teor. Osn. Khim. Teknol.* 1986;20:539.

19. Pisarenko YA, Serafimov LA. Assessing Influence of Selective Transfer on Chemical Conversion in Open Systems. *Theor. Found. Chem. Engr.* 1992;26:611.

20. Pisarenko YA, Danilov RY, Serafimov LA. Infinite-Efficiency Operating Conditions in Analysis of the Statics of Reactive Rectification. *Theor. Found. Chem. Engr.* 1995;29:556.

21. Barbosa D, Doherty MF. Theory of phase diagrams and azeotropic conditions for two-phase reactive system. *Proc. R. Soc. London* 1987;A413:443-458.

22. Barbosa D, Doherty MF. A new set of composition variables for the representation of reactive phase diagram. *Proc. R. Soc. London* 1987;A413:459-464.

23. Barbosa D, Doherty MF. The Influence of Equilibrium Chemical Reactions on Vapor-Liquid Phase Diagrams, *Chem. Engr. Sci.*, 1988;43:529-540.

24. Espinosa J, Aguirre P, Perez G. Product Composition Regions of Single-Feed Reactive Distillation Columns: Mixtures Containing Inerts. *Ind. Eng. Chem. Res.* 1995;34:853.

25. Espinosa J, Aguirre P, Perez G. Some Aspects in the Design of Multicomponent Reactive Distillation Columns Including Nonreactive Species. *Chem. Eng. Sci.* 1996;50:469.

26. Pérez-Cisneros ES, Gani R, Michelsen ML. Reactive separation systems. Part I: Computation of physical and chemical equilibrium. *Chem Eng. Sci.* 1997;52:527-543.

27. Wibowo C, Ng KM. Visualization of High-Dimensional Systems via Geometric Modeling with Homogenous Coordinates. *Ind. Eng. Chem. Res.* 2002;41:2213.

28. Barbosa D, Doherty MF. The Simple Distillation of Homogenous Reactive Mixtures. *Chem. Engr. Sci.*, 1988;43:541.

29. Barbosa D, Doherty MF. Design and Minimum-Reflux Calculations for Single-Feed Multicomponent Reactive Distillation Columns. *Chem. Engr. Sci.*, 1988;43:1523.

30. Barbosa D, Doherty MF. Design and Minimum-Reflux Calculations for Double-Feed Multicomponent Reactive Distillation Columns. *Chem. Engr. Sci.*, 1988;43:2377.

31. Buzad G, Doherty MF. Design of three-component kinetically controlled reactive distillation columns using fixed-point methods. *Chem. Eng. Sci.* 1994;49:1947-1963.

32. Buzad G, Doherty MF. New Tools for the Design of Kinetically Controlled Reactive Distillation Columns for Ternary Mixtures. *Comp. Chem. Engr.* 1995;19:395.

33. Okasinski MJ, Doherty MF. Design Method for Kinetically Controlled, Staged Reactive Distillation Columns. *Ind. Eng. Che. Res.* 1998;37:2821.

34. Chadda N, Malone MF, Doherty MF. Feasible products for kinetically controlled reactive distillation of ternary mixtures. *AIChE J.* 2000;46:923-936.

35. Chadda N, Malone MF, Doherty MF. Effect of Chemical Kinetics on Feasible Splits for Reactive Distillation. *AIChE Journal*. 2001;47:590

36. Ciric AR, Gu D. Synthesis of nonequilibrium reactive distillation processes by MINLP optimization. *AIChE J.* 1994;40:1479-1487.

37. Papalexandri KP, Pistikopoulos EN. Generalized modular representation framework for process synthesis. *AIChE J.* 1996;42:1010-1032.

38. Ismail SR, Papalexandri KP, Pistikopoulos EN. Synthesis of Reactive and Combined Reactor/Separation Systems Utilizing a Mass/Heat Transfer Exchange Module. *Chem. Engr. Sci.* 1999;54:2721.

39. Jackson JR, Grossmann IE. A disjunctive programming approach for the optimal design of reactive distillation columns. *Comp. Chem. Eng.* 2001;25:1661-1673.

40. Guo Z, Ghufran M, Lee JW. Feasible products in batch reactive distillation. *AIChE J.*, 2003;49:3161-3172.

41. Matsuyama H, Nishimura H. Topological and thermodynamic classification of ternary vapor-liquid equilibria. *J Chem Engr Japan*. 1977;10(3):181-187.

42. Doherty MF, Caldarola GA. Design and synthesis of homogeneous azeotropic distillations. 3. The sequencing of columns for azeotropic and extractive distillations. *Ind. Eng. Chem. Fundam.* 1985;24:474-485.

43. Guo Z, Lee JW. Feasible products in batch reactive extractive distillation. *AIChE J*. 2004;50:1484-1492.

44. Chin J, Lee JW. Estimation of Still Trajectory for the Feasibility Evaluation of Batch Reactive Distillation Systems, to be submitted to *AIChE J*. (2007).

Chapter 1: Feasibility of Continuous Reactive Distillation with Azeotropic Mixtures

Reproduced with permission from Ind. Eng. Chem. Res. 2004;43:3758-3769. Copyright 2004 American Chemical Society.

Abstract

By using phase and reaction equilibrium information, the feasibility criteria for single-feed and double-feed reactive distillation systems are derived: When the products are a stable node and an unstable node and a part of the reaction equilibrium curve lies in the same distillation region as the products, both reactive rectifying and reactive stripping sections can feasibly produce pure products in a single-feed column. If one of the products is a saddle and no azeotrope exists between the products, a single-feed column is still feasible, but only with large reaction equilibrium constants. If a saddle product forms a minimum-boiling azeotrope with another product, an entrainer is needed to break this azeotrope in a double-feed column. If both reaction products are saddles, the same double-feed column configuration with an entrainer can produce pure products.

Introduction

Reactive distillation, which combines reaction and separation in a synergistic way, has many advantages over sequential processes. The main advantages of reactive distillation include reduced initial investment and operating costs, higher reaction conversions and selectivities, and reduced heat utilities for condensers and reboilers, among others. Such economic benefits have attracted much interest in the study of

reactive distillation.[1-7] Some useful methods have been developed to determine design feasibilities and parameters such as the minimum reflux ratio, the total number of trays, and the distribution of reaction zones inside a reactive distillation column.[8-14]

In our previous papers,[15,16] we developed several feasibility criteria for batch reactive distillation and batch reactive-extractive distillation (BRED) processes involving multicomponent reacting mixtures. We also demonstrated that, if the reaction products are unstable nodes (UNs) and/or stable nodes (SNs) that can be reached by simple distillation, then a batch reactive distillation column (a rectifier, or a stripper, or a middle vessel) can be used to produce pure products. If all of the reaction products are saddles and one of the binary azeotropes between a desired product and one of the other components is a UN, then a reactive rectifier with a side-feed entrainer (BRED) can produce pure products. For a detailed discussion, see refs 15 and 16.

For *continuous* reactive or reactive-extractive distillation, no geometric feasibility method has been available to identify the possibility of producing pure products according to the position of the reaction equilibrium manifolds and the dynamic properties of the azeotropic mixtures. Thus, a primary goal of this paper is to develop design insights for evaluating the feasibility of continuous reactive distillation using the simple information of reaction and phase equilibrium.

To this end, we apply the graphical methods of binary or ideal ternary reacting mixtures[12,17,18] to azeotropic reacting mixtures. We perform stage calculations to confirm

the geometric feasibility criteria developed for continuous single-feed and double-feed reactive distillation columns.

Ternary Reacting Mixtures in a Single-Feed Reactive Distillation Column

Throughout the single feed column section, the isomolar decomposition reaction (2I ⇔ L + H) is assumed to take place in the liquid phase. Here, I is the intermediate-boiling reactant, and L and H are the light- and heavy-boiling products, respectively. The graphical method of tray-by-tray calculations under reaction equilibrium was proposed for ideal ternary mixtures.[12] A main idea of this method is that the liquid- and vapor-stage compositions are confined to reaction equilibrium curves and their equilibrated vapor curves. Stepping up or stepping down the reactive stages is performed in terms of reactive cascade difference points.[12,19] The assumptions for this method are a constant molar overflow for the overall column, vapor-liquid equilibrium on each stage, negligible vapor and liquid holdups on each stage, a negligible heat of reaction, a saturated liquid feed, and reaction equilibrium.

Material Balance

Material balances are taken around two envelopes in Figure 1-1. For the rectifying reactive section, we obtain equations (1) to (3)[12]:

$$V_{F,s} = L_n + D - \nu_T \xi_n \tag{1}$$

$$V_{Fs} y_{Fs} = L_n x_n + D\delta^r_{R,n} \tag{2}$$

$$\delta^r_{R,n} = \frac{Dx_D + 2\xi_n (c_R - c_P)}{D} \tag{3}$$

For the stripping reactive section, we obtain equations (4) to (6):

$$L_{Fs} = V_m + B - \nu_T \xi_m \tag{4}$$

$$V_m y_m = L_{Fs} x_{Fs} - B\delta^s_{R,m} \tag{5}$$

$$\delta^s_{R,m} = \frac{Bx_B + 2\xi_m (c_R - c_P)}{B} \tag{6}$$

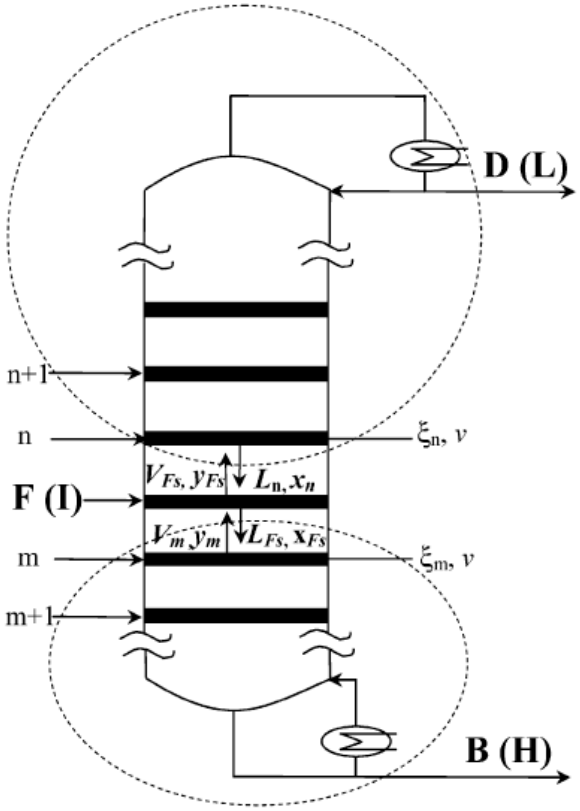

Figure 1-1 A Schematic Diagram of a Single Feed Reactive Distillation Column

Here, ν_T is the sum of the stoichiometric coefficients. Because ν_T is zero for the isomolar decomposition reaction (2I ⇔ L + H), the normalized reactant and product stoichiometric coefficient vectors[20] c_R (=[0, 1, 0]) and c_P (=[1/2, 0, 1/2]) represent reactant I and equimolar products of L and H, respectively. ξ_n, and ξ_m are the accumulated sums of reaction molar turnovers from the top to stage *n* and from the bottom to stage *m*,

respectively. $\delta^{r}_{R,n}$ and $\delta^{s}_{R,m}$ are the reactive cascade difference points[12,19] for the rectifying section and the stripping section, respectively.

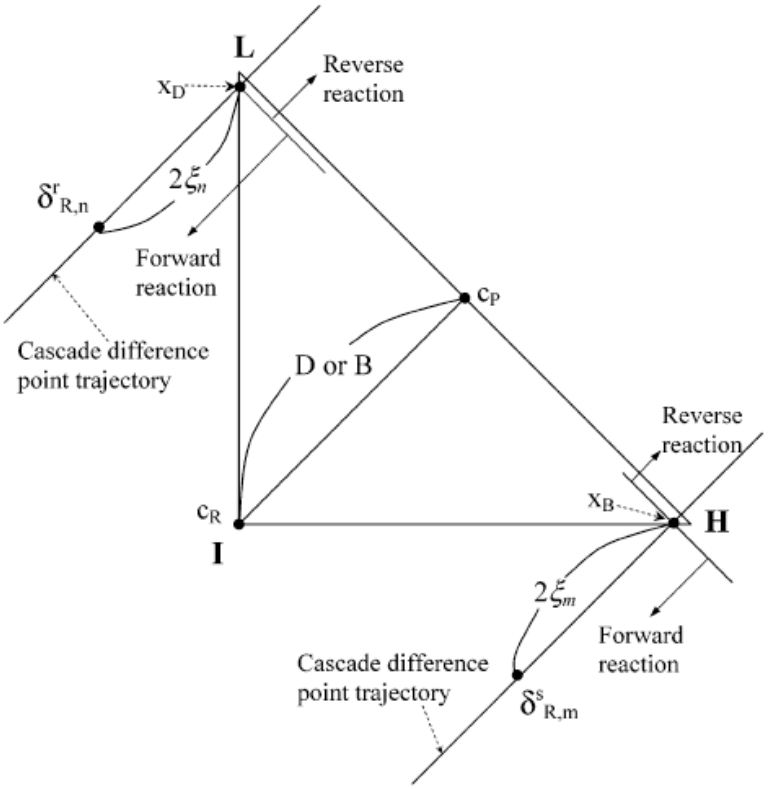

Figure 1-2 The Relative Amounts between Product Flow Rates and Reaction Extents for Graphical Design Method

In Figure 1-2, the trajectories of these two difference points ($\delta^{r}_{R,n}$ and $\delta^{s}_{R,m}$), which start from the top and bottom product compositions, are parallel to the vector (c_R - c_P). The length of the stoichiometric line represents the relative magnitude of the top or bottom product molar flow rate (D or B, respectively). The length of the line connecting the top product composition (x_D) or the bottom product composition (x_B) to the reactive cascade difference point ($\delta^{r}_{R,n}$ or $\delta^{s}_{R,m}$) represents the relative amount of $2\xi_n$ or $2\xi_m$. Detailed explanations and applications of this tray-by-tray calculation method can be found in reference 12.

Feasibility of Reacting Mixtures with Distillation Boundary

In a previous paper,[15] we showed that batch reactive distillation can be used to circumvent minimum- and/or maximum boiling azeotropes and distillation boundaries. Thus batch processes can produce pure products from azeotropic reacting mixtures when the desired product is an unstable node (UN) or a stable node (SN) in spite of distillation boundaries. Here, we evaluate the applications of continuous columns for the similar azeotropic systems to determine the feasible configurations and develop the feasibility criteria.

Example 1: RCM-320

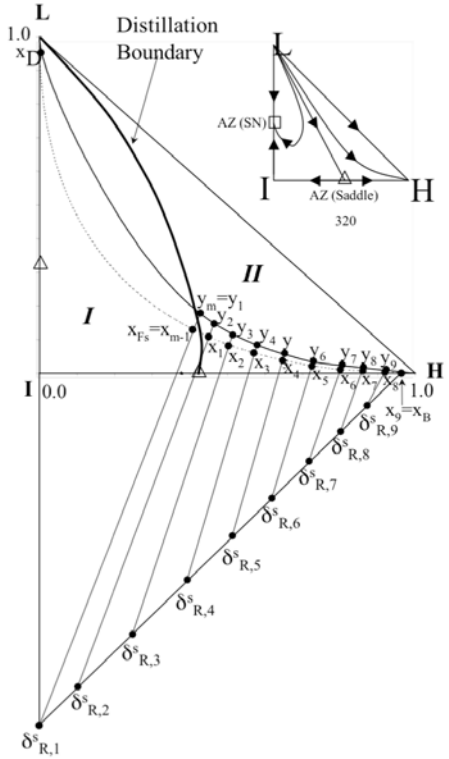

Figure 1-3 Feasible Geometry Tray-by-Tray Calculations with Stripping Section Reaction (Keq=0.25) for Azeotropic System RCM-320. Dotted curve denotes the liquid reaction equilibrium and the solid curve represents the equilibrated vapor compositions.

The first example is the ternary reacting system ($2I \Leftrightarrow L + H$), which has two azeotropes: one is a maximum-boiler (stable node, SN) between *L* and *I* while the other azeotrope is a minimum-boiler (saddle) between *H* and *I*. Its residue curve map (RCM) is called RCM-320[21,22] and is shown in Figure 1-3. The residue curve map is divided into two distillation regions, ***I*** and ***II***, by a distillation boundary. The dotted curve is the reaction equilibrium curve and all possible liquid compositions at reactive stages lie on this curve. The solid curve is the vapor curve in phase equilibrium with the reaction equilibrium curve and denotes all possible vapor compositions at reactive stages.

We can always produce light product *L* at the top of the column from any distillation region, as *L* is the lowest boiler (UN) in the RCM. However, to produce the pure heavy product (*H*) at the bottom, the reactive operating line should cross the distillation boundary separating distillation regions ***I*** and ***II***. We arbitrary select a feed-stage liquid composition (x_{Fs}) in distillation region ***I*** such that the vapor composition (y_m) in equation (5) should be in distillation region ***II***. According to equation (5), the liquid composition of the reactive feed stage (x_{Fs}) should lie in the middle of the line that connects the reactive cascade difference point ($\delta^s_{R,m} = \delta^s_{R,1}$) with the vapor composition at one stage below the feed stage ($y_m = y_1$).

Here, the distance from y_1 to x_{Fs} denotes the bottom molar flow rate (*B*) and the distance from x_{Fs} to $\delta^s_{R,1}$ represents the vapor molar flow rate (V_m) in the stripping section. Thus, the reboil ratio (V_m/B) can be determined by the ratio $|x_{Fs} - \delta^s_{R,1}| / |y_1 - x_{Fs}|$. Because

the liquid composition at the feed stage is fixed, the reboil ratio simultaneously determines the positions of the vapor composition on the vapor equilibrium curve and the reactive cascade difference point. From the phase equilibrium relationship $y_k = Kx_k$, the liquid composition (x_k) can be calculated. In this way, the vapor composition and the reactive cascade difference point on the next stage can be obtained simultaneously. The tray-by-tray calculations (stepping down from the feed stage to the bottom of the column) continue until a liquid composition on some stage coincides with or passes the desired bottom product composition (x_B).

The liquid composition of the feed stage x_{Fs} is fixed as [0.1302, 0.4612, 0.4086], which is in distillation region ***I***. The composition is expressed as [light (L), intermediate (I), heavy (H)], and this order remains the same throughout this paper. The vapor composition ($y_m = y_1$) of one stage below the feed stage is [0.1859, 0.3911, 0.4230] and lies in distillation region ***II***. Thus, the distillation boundary can be circumvented by reaction. The reactive cascade difference point trajectory is known and the two points are fixed. Then, $\delta^s_{R,m}$ and the reboil ratio (V_m/B) can be determined (for this specific system, RCM-320, the reboil ratio V_m/B is 22). From the phase equilibrium relationship, the liquid composition x_1 can be calculated and the composition is [0.1140, 0.4472, 0.4388]. Using x_1 and the fixed reboil ratio, the vapor composition (y_2) and the reactive cascade difference point ($\delta^s_{R,2}$) on the next stage below can be obtained simultaneously. The value of y_2 equals [0.1530, 0.3793, 0.4677]. In this way, we continue to carry out the tray-by-tray calculations as shown in Figure 1-3. To reach the required bottom product

purity, the total number of trays in the reactive stripping section should be 9 in this example.

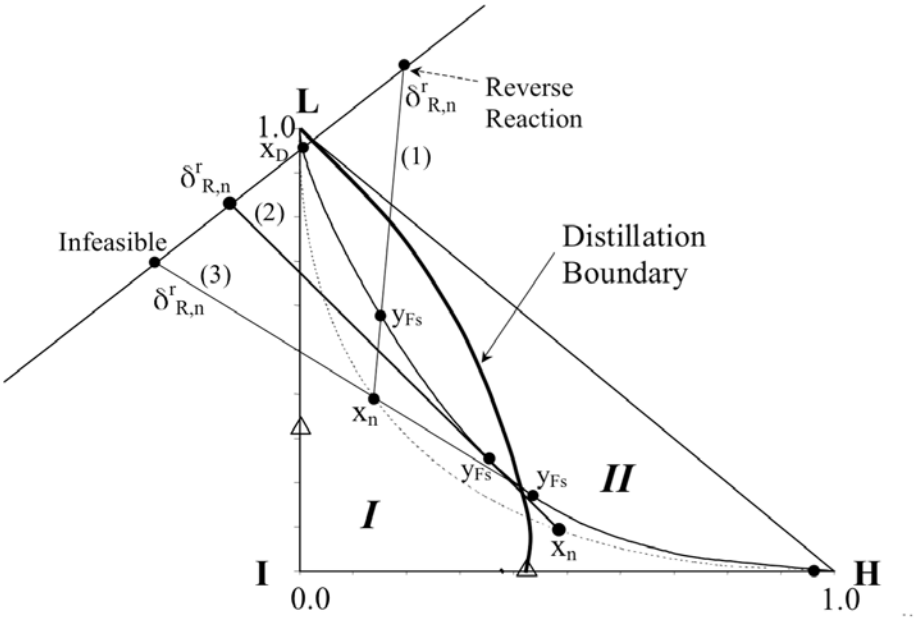

Figure 1-4 An Infeasible Schematic of RCM-320 with Rectifying Section Reaction (Keq=0.25). Dotted curve denotes the liquid reaction equilibrium and the solid curve represents the equilibrated vapor compositions.

What will happen if the reaction zone is put in the rectifying section? From the material balance equations, (1) through (3), the vapor composition of feed stage y_{Fs} should lie between the line connecting the liquid composition x_n and the reactive cascade difference point $\delta^r_{R,n}$. We arbitrarily select the liquid composition x_n and the feed-stage vapor composition y_{Fs} and connect them with line (1) shown in Figure 1-4. The reverse reaction will be dominant in this process[12]. If the forward reaction is dominant, then in most cases x_n lies on the middle of the connection y_{Fs} and $\delta^r_{R,n}$ as with line (2) in Figure 1-4. Then it violates the material balance in equation (2) and leads to an infeasible configuration.

However, if a reactive operating line satisfies the material balance constraint (that is, if y_{Fs} lies between $\delta_{R,n}^{r}$ and x_n) as shown by line (3) of Figure 1-4, then it can feasibly circumvent the distillation boundary. In this case, we can use reaction to force the vapor composition of the feed stage (y_{Fs}) and the liquid composition on next stage above (x_n) to be located in distillation region ***II***. Using the phase equilibrium relationship, we can calculate y_n, the vapor composition on the same stage with x_n. Here, y_n is also in distillation region ***II*** (see Figure 1-4). Thus pure light and heavy products (L and H) are simultaneously produced at the top and bottom of the column since they are a UN and an SN in distillation region ***II*** and can be reached by simple distillation. Here, it needs to be pointed out that, in distillation region ***II***, the heavy product fraction on stage n (y_n) is larger than that on the feed stage (y_{Fs}). Thus we cannot put more reactive stages in the rectifying section like we have done in the stripping section of Figure 1-3 because the composition profile would approach heavy product H while going up the column. Therefore, a large amount of catalyst should be used on the feed stage to get the required reaction conversion, but few reactive stages are needed. In terms of quick feasibility evaluations using phase and reaction equilibrium data, it is observed that either the rectifying or the stripping reaction zone can produce node products in RCM-320. Detailed comparison (catalyst load, heat duty, and tray size and numbers) between these two reaction zones can be carried out with detailed kinetics, but that is beyond the scope of this paper.

Example 2: RCM 410

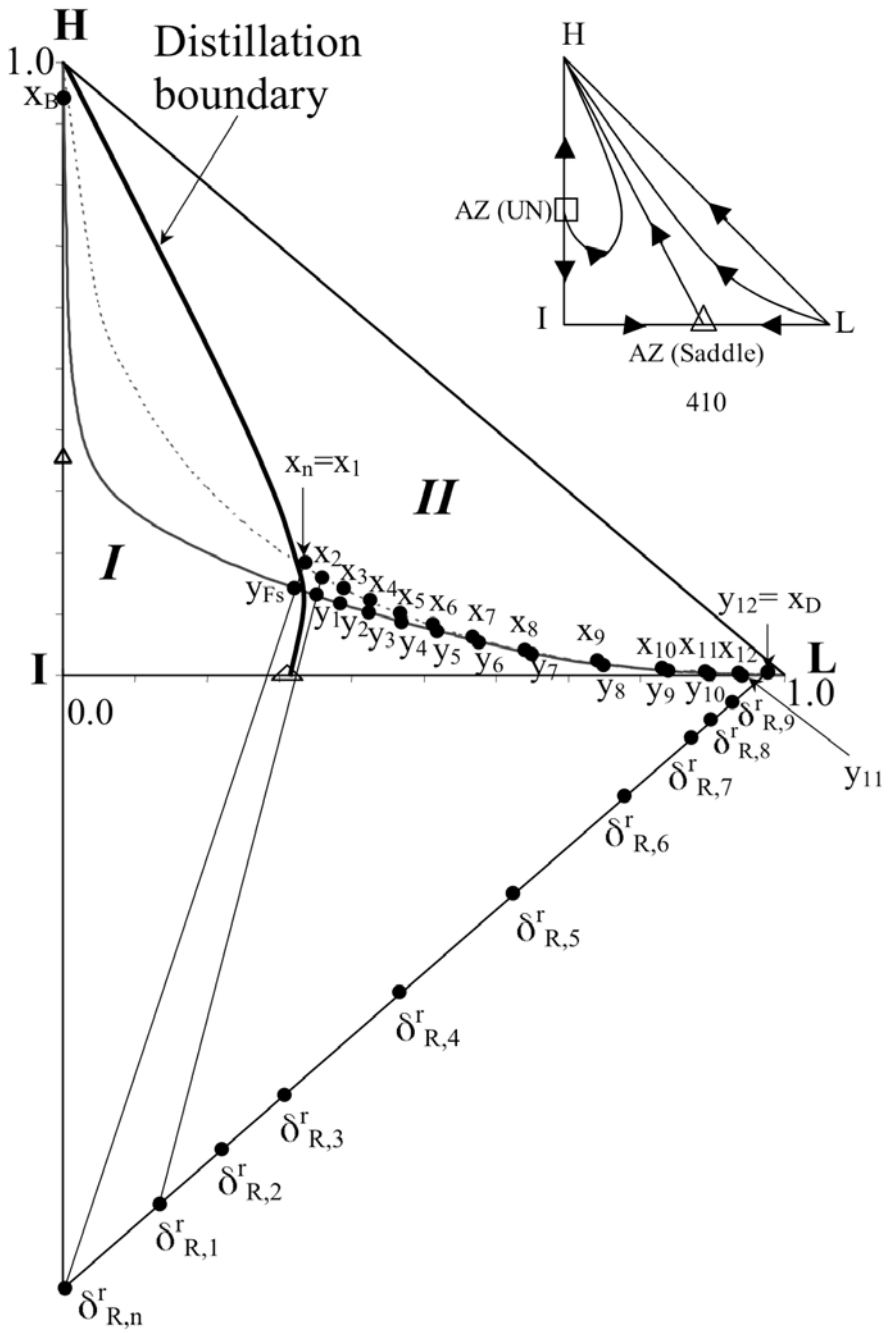

Figure 1-5 Feasible Geometry Tray-by-Tray Calculations with Rectifying Section Reaction (Keq=0.25) for Azeotropic System RCM-410. Dotted curve denotes the liquid reaction equilibrium and the solid curve represents the equilibrated vapor compositions. Note that the vertices are not in the conventional orientation.

The second example RCM-410[21,22] has two binary azeotropes: the maximum-boiler between L and I is a saddle and the minimum-boiler between H and I is an UN. The RCM is divided into two distillation regions, ***I*** and ***II***, by a distillation boundary (see Figure 1-5). The reactive operating line should cross from distillation region ***I*** to ***II*** to produce light product L because the heaviest product (H, SN) is always produced at the bottom of the column. In contrast to Figure 1-3, the vapor curve is located between the reaction equilibrium curve and reactive cascade difference point trajectory in Figure 1-5. Thus, to circumvent the distillation boundary and have only the forward reaction, we put the reaction in the rectifying section.

The tray-by-tray calculations follow the same procedure as in the first example: if we arbitrarily select the feed stage vapor composition (y_{Fs}) in distillation region ***I***, the correlated liquid composition (x_n) in equation (2) should be in distillation region ***II*** to circumvent the distillation boundary. According to equation (2), the reactive feed-stage vapor composition (y_{Fs}) should lie on the line connecting the reactive cascade difference point ($\delta^r_{R,n}$) and the liquid composition (x_n). The reflux ratio (L_n/D) can be determined by the ratio of the length of y_{Fs}—$\delta^r_{R,n}$ to the length of y_{Fs}—x_n. Here, the lengths of y_{Fs}—$\delta^r_{R,n}$ and y_{Fs}—x_n represent the liquid molar flow rate (L_n) in rectifying section and the distillate molar flow rate (D), respectively. Because the vapor composition at the feed stage is fixed, the reflux ratio simultaneously determines the liquid composition (x_n) and the reactive cascade difference point ($\delta^r_{R,n}$) one stage above the feed stage. The vapor composition (y_n) at stage n can be calculated from the phase equilibrium relationship.

Thus the tray-by-tray calculations will proceed in this way until a vapor composition on a certain stage coincides with or passes the desired distillate product composition (x_D).

For the system RCM-410, we arbitrarily place the vapor composition of the reactive feed stage in distillation region ***I*** (y_{Fs}= [0.3238, 0.5019, 0.1743]). To circumvent the existing distillation boundary by reaction, the correlated liquid composition (x_n = [0.3373, 0.4701, 0.1926]) must lie in distillation region ***II***. The reflux ratio (L_n/D) is 30 for this case. The tray-by-tray calculation can be done by using the fixed reflux ratio and y_{Fs}. The graphical result for RCM-410 is shown in Figure 1-5. It indicates that one can produce pure products when the reaction zone is placed in the rectifying section and the total number of trays in this section is 12.

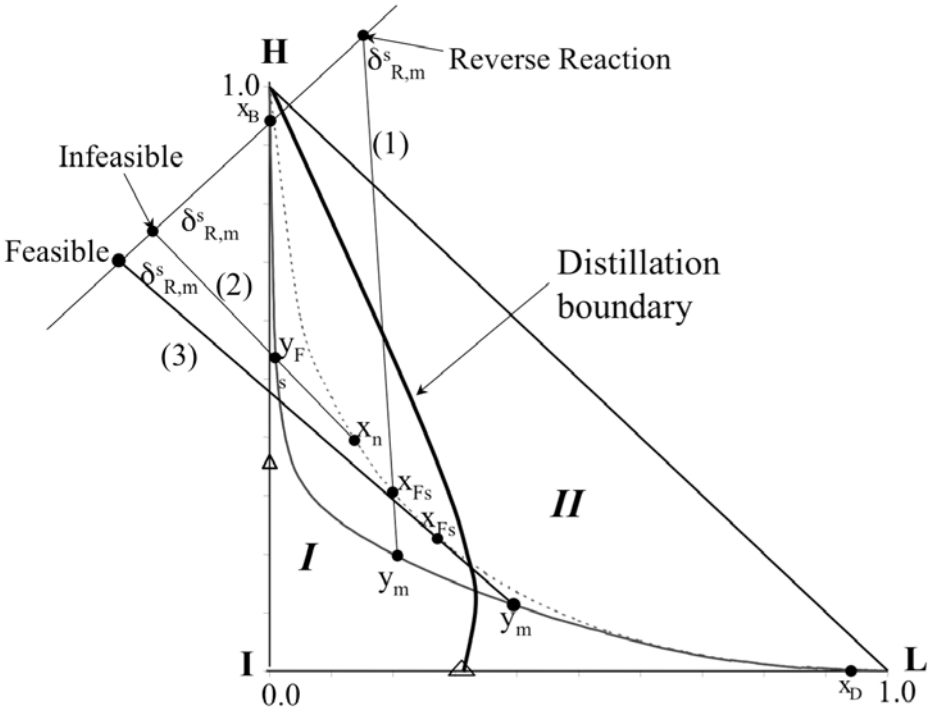

Figure 1-6 An Infeasible Schematic of RCM-410 with Stripping Section Reaction (Keq=0.25). Dotted curve denotes the liquid reaction equilibrium and the solid curve represents the equilibrated vapor compositions. Note that the vertices are not in the conventional orientation.

If reaction is put in the stripping section for RCM-410, then behavior similar to that in Figure 1-4 is observed. The reverse reaction dominantly occurs, as shown in reactive operating line (1) of Figure 1-6. In most cases, operating lines like line (2) of Figure 1-6 would violate material balance equation (5). There is also a feasible reactive operating line where both the liquid composition at the feed stage and the vapor composition at one stage below the feed stage lie in distillation region ***II*** (see line (3) in Figure 1-6). Here, "feasible" means that pure H and L can be simultaneously produced as H and L are an SN and a UN, respectively, in distillation region ***II***. However, for this case, light component (L) becomes richer when more reactive stages are used in the stripping section (compare x_{Fs} with x_1 in distillation region ***II*** of Figure 1-6). This means that few reactive stages can be put in the stripping section. To reach the total conversion requirement, we have to use lots of catalyst on the feed stage. Thus for system RCM-410, either a reactive rectifying section or a reactive stripping section can be used to produce node products.

These two examples show us that, if the reaction products are an SN and a UN in the same distillation region, then either a stripping reaction zone or a rectifying reaction zone can be employed to circumvent distillation limitations and produce pure products in a single-feed column. Real examples are the decomposition of *tert*-butyl alcohol to water and isobutene (TBA $\Leftrightarrow$ W + IBUT)[23] and the decomposition of ethanol to diethyl ether and water (2EtOH $\Leftrightarrow$ DEE +W).[24] The RCMs of these systems are characterized as RCM-020 (see Figure 1-8). The two products are a UN and an SN, which can be directly produced by a single-feed column according to this feasibility criterion.

Now, is this feasibility criterion still valid when any of the products are saddles? To answer this question, several azeotropic systems with saddle products are investigated next for the possibility of producing pure products in a single-feed column.

Example 3: RCM-430

This example, RCM-430, has two maximum binary azeotropes: one is a saddle formed between *L* and *I* while the other is a stable node between *H* and *I*. In Figure 1-7, the reaction equilibrium curve (*Keq* = 0.25) lies between the equilibrated vapor curve and the cascade difference point. According to the material balance, one can easily perform the tray-by-tray calculations for a reactive stripping section following the same procedure as used in example 1. The feed stage liquid composition (x_{Fs}) is [0.099, 0.431, 0.470] and the reboil ratio (V_m/B) is 18. Then, the correlated vapor composition (y_1) on the next stage below is determined as [0.145, 0.378, 0.477]. The liquid composition on the same stage is calculated from the phase equilibrium relationship (x_1= [0.104, 0.436, 0.460]). In the same way, the vapor composition (y_2) and liquid composition (x_2) on the next stage below are obtained and they are [0.152, 0.382, 0.466] and [0.109, 0.442, 0.449], respectively. The compositions of y_3 and x_3 are [0.159, 0.387, 0.454] and [0.114, 0.447, 0.439], respectively.

To produce heavy product at the bottom, the liquid molar fraction of heavy component in the stripping section should increase as the calculations step down from the feed stage to the bottom. Now, the tray-by-tray calculation results show that, while stepping down to the bottom of the column, the molar fraction of heavy product

decreases, x_1=**0.460** > x_2=**0.449** > x_3=**0.439**. This indicates that continuous reactive distillation under reaction equilibrium (*Keq* = 0.25) **cannot** produce the pure heavy product (H). If the reaction is placed in the rectifying section, then a feasible operating line exists that connects y_{Fs} and x_n. However, the fraction of H is much higher in x_n than in x_{Fs} as shown in Figure 1-7. Then, while moving up the column, the heavy product becomes enriched because of the maximum boiling azeotrope between I and H.

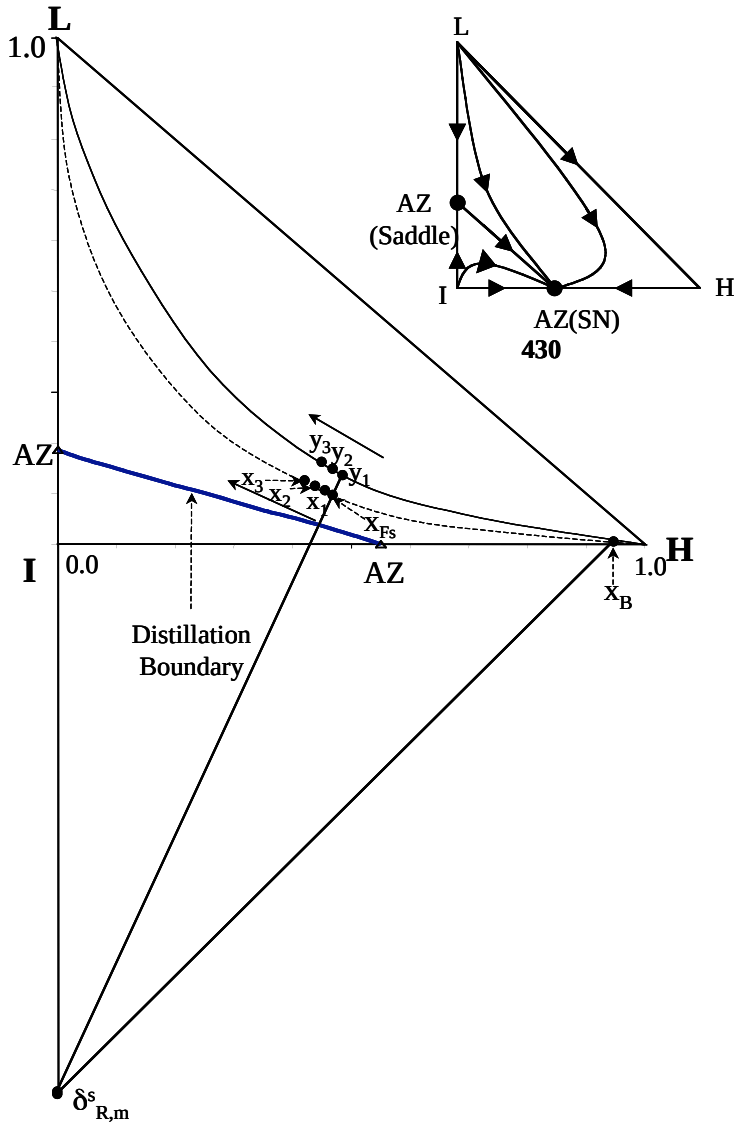

Figure 1-7 An Infeasible Schematic Geometry Tray-by-Tray Calculations with the Reaction (Keq=0.25) for Azeotropic System RCM-430. Dotted curve denotes the liquid reaction equilibrium and the solid curve represents the equilibrated vapor compositions.

Therefore neither a rectifying nor a stripping reaction zone can produce pure products in this example (RCM-430). For examples 1 and 2, all products are nodes and can be reached by simple distillation. Thus, as long as any stage liquid or vapor composition is located in the same distillation region as the top or bottom product composition, a continuous single-feed column is feasible. However, one of the two products in example 3 (heavy product) is a saddle, which means simple distillation cannot lead to desired pure products because the existence of an SN maximum azeotrope. It should be emphasized that examples 1 through 3 are *feasible* in reactive *batch rectifiers and strippers* since these batch configurations only require that one product be a UN or an SN (for detailed discussions, see our previous paper[15]).

RCMs where the two pure products (L and H) can be feasibly produced in a continuous single-feed column are shown in Figure 1-8. Figure 1-9 shows RCMs where a continuous single-feed reactive distillation column cannot lead to the production of the pure products. However, with any of the RCMs in Figures 1-8 and 1-9, the pure products can be produced in reactive batch rectifiers, strippers, and middle-vessel columns.[15] The common characteristics of all feasible RCMs in Figure 1-8 are that all products are UNs and SNs and that the node products share the same distillation region with a part of reaction equilibrium curve. This is exactly the same situation as for a reactive middle-vessel column,[15] which requires that a part of the reaction equilibrium curve should lie in the same distillation region as the products (see RCM-010-S and RCM-310-S in Figure 1-8). Thus, the reaction forces the liquid compositions to be located in the same region and then circumvent distillation boundaries.

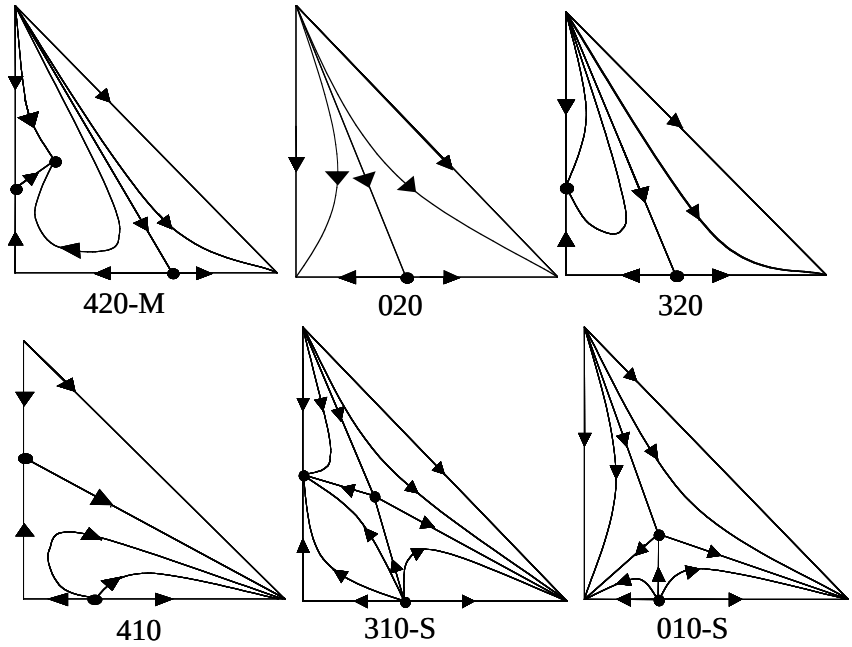

Figure 1-8. Summary of the RCMs for Feasible Single Feed Reactive Distillation Column

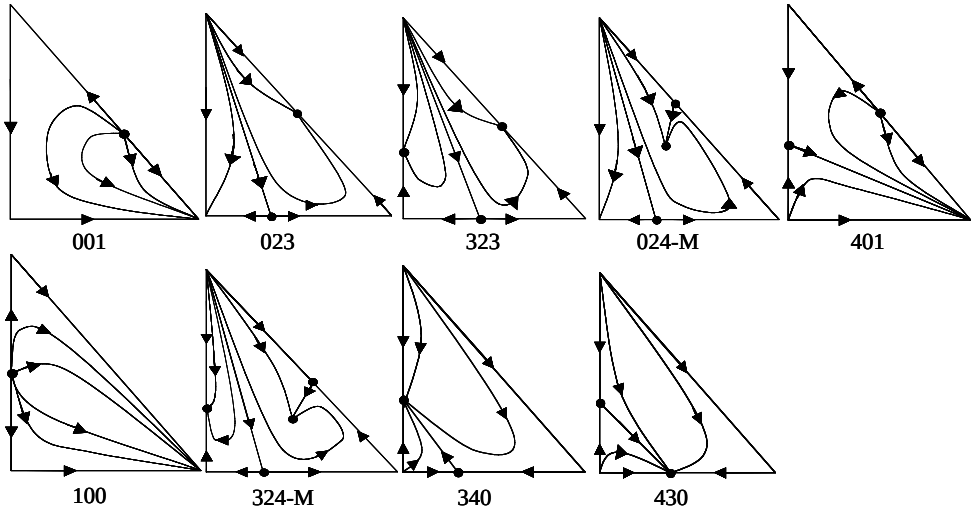

Figure 1-9. Summary of the RCMs for Infeasible Single Feed Reactive Distillation Column.

For the RCMs in Figure 1-9, the common characteristic is that one of products (L or H) is a saddle. These systems cannot feasibly produce pure products with *Keq*=0.25 as already shown in Figure 1-7. *Keq* = 0.25 is relatively small, which means that reaction is not dominant when compared to V/L separation during reactive distillation. In the

following section, we will discuss the feasibility of any system in Figure 1-9 when higher reaction equilibrium constants are used or complex continuous configurations (such as double-feed columns) are employed.

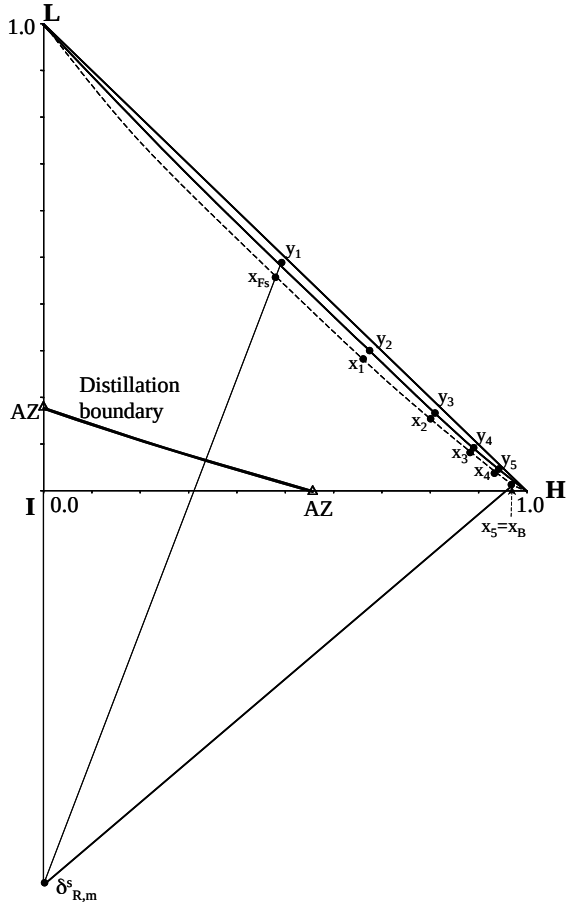

Figure 1-10 A Feasible Schematic Geometry Tray-by-Tray Calculations with the Reaction (Keq=50) for Azeotropic System RCM-430. Dotted curve denotes the liquid reaction equilibrium and the solid curve represents the equilibrated vapor compositions.

It is well known that reaction can circumvent azeotropes during distillation processes[25-27]. Such experiences encourage us to investigate the conditions under which the systems in Figure 1-9 can feasibly circumvent phase equilibrium limitations. Let us again focus on RCM-430 from example 3. Because the azeotrope between H and I is an SN, there is competition between reaction equilibrium and phase equilibrium to reach heavy product H in the stripping reaction zone, as shown in Figure 1-7. The phase

equilibrium effect on reactive distillation is much stronger than the reaction equilibrium effect (*Keq*=0.25). Thus reaction cannot lead to the production of the saddle heavy product. If we assume that we have a different reaction with a higher reaction equilibrium constant (*K*eq = 50) and with the same phase equilibrium and reaction stoichiometry, then the continuous configuration becomes feasible for the production of the products H and L, as shown in Figure 1-10.

Example 4: RCM-001

It is worth noting that large reaction equilibrium constants cannot always lead to feasible production in a single-feed column. If one of the products is a saddle and there is an azeotrope between H and L, then reaction cannot circumvent phase equilibrium limitations even though the reaction equilibrium constant is large. The example of RCM-001, which exhibits this behavior, is studied, and its result is shown in Figure 1-11. The stripping reaction zone can produce the heavy product (H). However, reaction in the stripping section cannot circumvent the UN azeotrope since it is the lowest boiler and is recovered at the top. Thus, we cannot get the desired saddle light product (L) at the top (Figure 1-11a, *Keq*=0.25). Even though reaction is put in the rectifying section, the light product (L) cannot be produced since the vapor composition above the feed stage is not richer in L than the feed stage, as shown in Figure 1-11a. Even when *Keq* is equal to 50, as shown in Figure 1-11b, reaction cannot circumvent the UN azeotrope, and the pure light product cannot be produced. These results show that another method should be proposed to circumvent the azeotrope when reaction has no effect on the elimination of the azeotrope. A possible alternative method is reactive-extractive distillation with an

entrainer to break the azeotrope. This double-feed reactive distillation configuration is investigated in the next section.

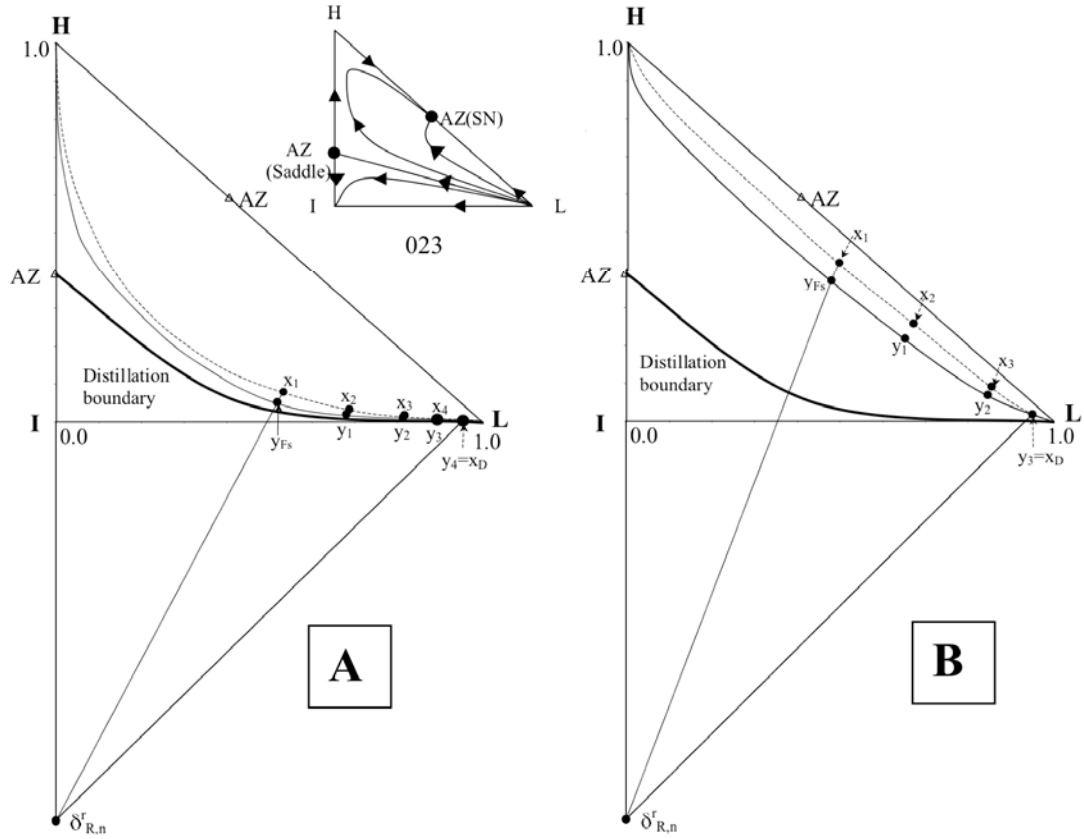

Figure 1-11 Infeasible Schematic Geometry Tray-by-Tray Calculations with the Reaction (a: Keq=0.25 and b: Keq=50) for Azeotropic System RCM-023. Dotted curve denotes the liquid reaction equilibrium and the solid curve represents the equilibrated vapor compositions. Note that the vertices are not in the conventional orientation.

The difference between RCM-430 and RCM-001 is the location of the azeotrope. For RCM-430, the azeotrope is located between product H and reactant I. A large reaction equilibrium constant (*Keq*) can force the reaction equilibrium curve and its equilibrated vapor curve to lie far from the azeotrope. Thus, favorable reaction equilibrium dilutes the effect of the azeotrope, and the heavy product can be reached as shown in Figure 1-10. However, in RCM-001, there is a binary azeotrope between H and L. When a large *Keq* value is used, the two curves get closer to the azeotrope than in

cases with smaller *Keq* values. Thus reaction cannot circumvent the phase equilibrium limitation, and the single-feed column is infeasible (see Figures 1-11a and 1-11b). According to the comparison between RCM-430 and RCM-001, Figure 1-9 is divided into two subgroups: (a) infeasible at small *Keq* but feasible at large *Keq* and (b) infeasible at all values of *Keq*.

Example 5: Effect of different reaction stoichiometries

All systems studied above are reactive distillation systems with the isomolar reaction 2I ⇔ L + H. In this section, a non-isomolar reaction, L + I ⇔ H, is considered to investigate the effect of reaction stoichiometry on feasibility. The reaction difference point, δ_R, of this reaction is [1, 1, -1] for L, I, and H, respectively[5]. Here, the two reactants are light and intermediate boilers, and the product is a heavy boiler. For a single-feed column, the light reactant is provided in excess and the excess light reactant exits at the top of the column while the heavy product (H) is withdrawn from the bottom. Material balance equations[28] for the reactive rectifying section in Figure 1-1 with this non-isomolar reaction are

$$V_{Fs} y_{Fs} = L_n x_n + (D + \xi_n)\delta^r_{R,n} \tag{7}$$

$$\delta^r_{R,n} = \frac{D x_D + \xi_n \delta_R}{D + \xi_n} \tag{8}$$

For the stripping reactive section, we obtain equations (9) and (10):

$$V_m y_m = L_{Fs} x_{Fs} - (B + \xi_m)\delta^s_{R,m} \tag{9}$$

$$\delta^s_{R,m} = \frac{B x_B + \xi_m \delta_R}{B + \xi_m} \tag{10}$$

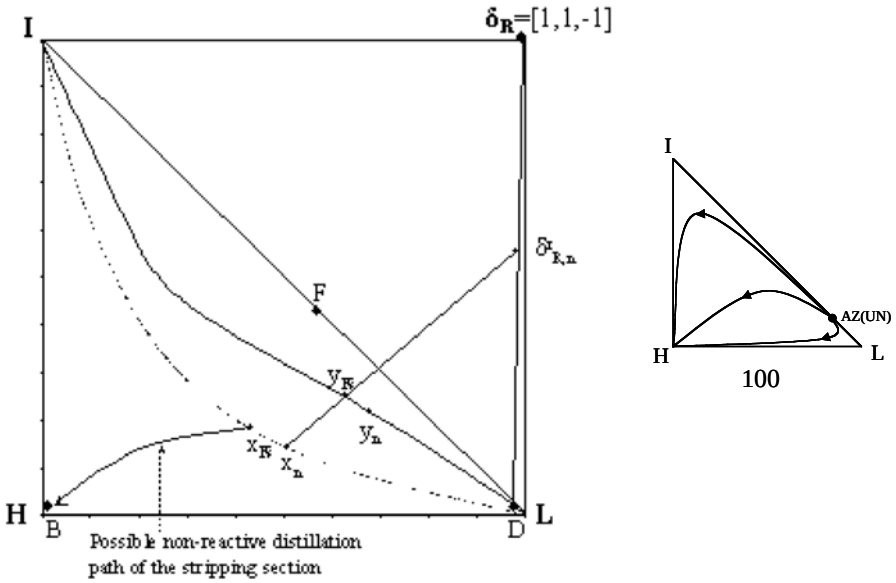

Figure 1-12 Feasible geometry scheme for RCM-100 reactive distillation with the nonisomolar reaction L + I ↔ H for K_{eq} = 5.0. Note that the vertices are not in the conventional orientation.

RCM-100 is first chosen for this example and is shown in Figure 1-12. In the reactive rectifying section, the vapor composition (y_{Fs}) should lie between the liquid composition (x_n) and the cascade difference point ($\delta_{R,n}^{r}$) according to equation (7). The cascade difference point for the rectifying section is a linear combination of the distillate composition (x_D) and the reaction difference point (δ_R). Thus, it lies between the line connecting x_D and δ_R. Figure 1-12 shows that the vapor curve is located between the reaction equilibrium curve and the cascade difference point. Because of their positions in composition space, it was already shown that the stripping reaction zone causes reverse reaction and lower forward reaction conversion to occur[29]. Thus, the reaction is placed in the rectifying section to give positive reaction conversions.

Because the heavy product (H) is the SN in this system (with no distillation boundary) and can always be reached by simple distillation, pure H can be produced at

the bottom as shown in Figure 1-12. If the locations of the cascade difference points and the liquid and vapor compositions fulfill the requirements of material balance equation (7), then a single-feed column with a reactive rectifying section can feasibly produce pure H. The production of MTBE from isobutene and methanol[30] or the production of TAME from methanol and 2-methyl-2-butene[31] is an example of such a system. These mixtures show the phase equilibrium behavior of RCM-120. A single-feed column with a reactive rectifying section can produce the SN heavy products.

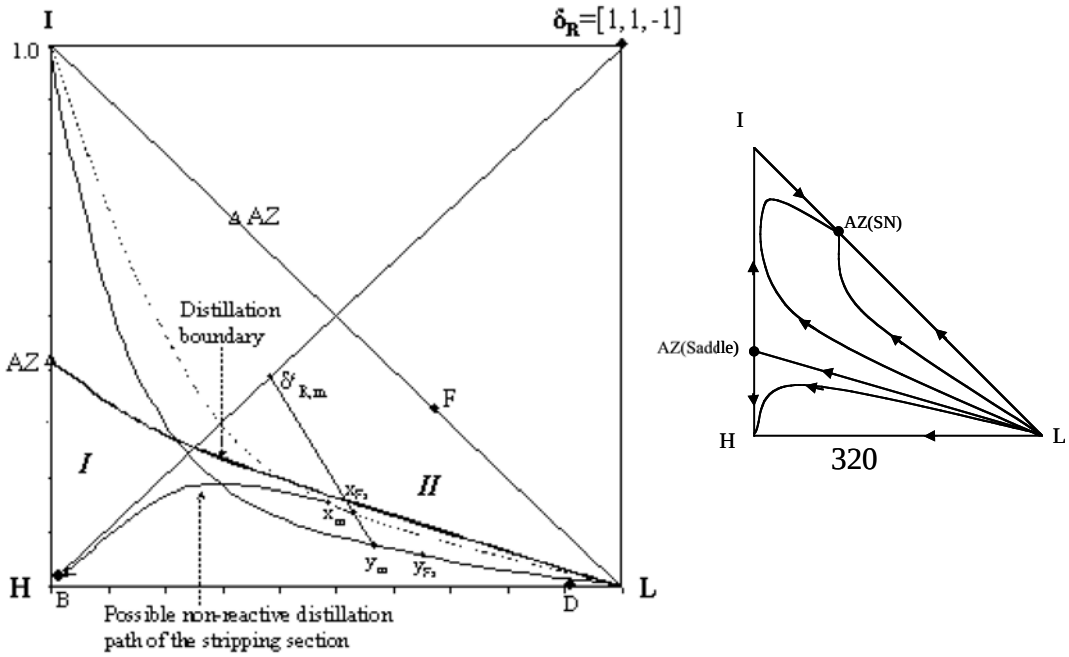

Figure 1-13 Feasible geometry scheme for RCM-320 reactive distillation with the nonisomolar reaction L + I ↔ H for K_{eq} = 5.0. Note that the vertices are not in the conventional orientation.

A complex RCM with a distillation boundary (RCM-320) is also investigated, and the results are shown in Figure 1-13. In distillation region ***I***, the light and heavy product (L and H) are a UN and an SN, respectively, that can be reached by simple distillation. Because the liquid reaction equilibrium curve lies between the vapor curve and the reaction difference point, we place reaction in the stripping section to have a positive reaction conversion according to material balance equation (9). Whenever a part of the

reaction equilibrium curve shares the same distillation region with H, a single-feed column with a stripping reaction zone can produce the heavy product H even though a distillation boundary exists in this system.

In accordance with all of the above examples (examples 1 through 5), we can generate the feasibility criteria for continuous azeotropic reactive distillation in a single feed column. (i) If the products are an SN and a UN, then both rectifying and stripping reaction zones can lead to the production of pure products when a part of the reaction equilibrium curve and the node products share the same distillation region. (ii) If one of the two products is a saddle and there is no azeotrope between the two products, then the single-feed continuous column is still feasible with a sufficiently high value of Keq. (iii) If there is an azeotrope between the two products, then a single-feed column is infeasible. An extractive agent might be needed to break an azeotrope if it is a minimum-boiling UN, as explained in the next section. (iv) For a system with a nonisomolar reaction such as L + I ⇔ H and one SN heavy product, the single feed column is feasible with either a reactive rectifying section or a reactive stripping section as long as the reaction equilibrium curve shares the same distillation region as H.

Ternary Reacting Mixtures with Entrainer in a Double Feed Column

For the ternary reacting mixture (2I ⇔ L + H), if both of the products (L and H) are saddles and the binary azeotrope formed by L and I or L and H is an unstable node, then pure products can be produced by using batch reactive-extractive distillation (BRED)[16]. A side-feed stream of an entrainer is needed to break the azeotrope in such a process. A

continuous process in analogy to BRED is a double-feed *reactive-extractive distillation* column as shown in Figure 1-14.

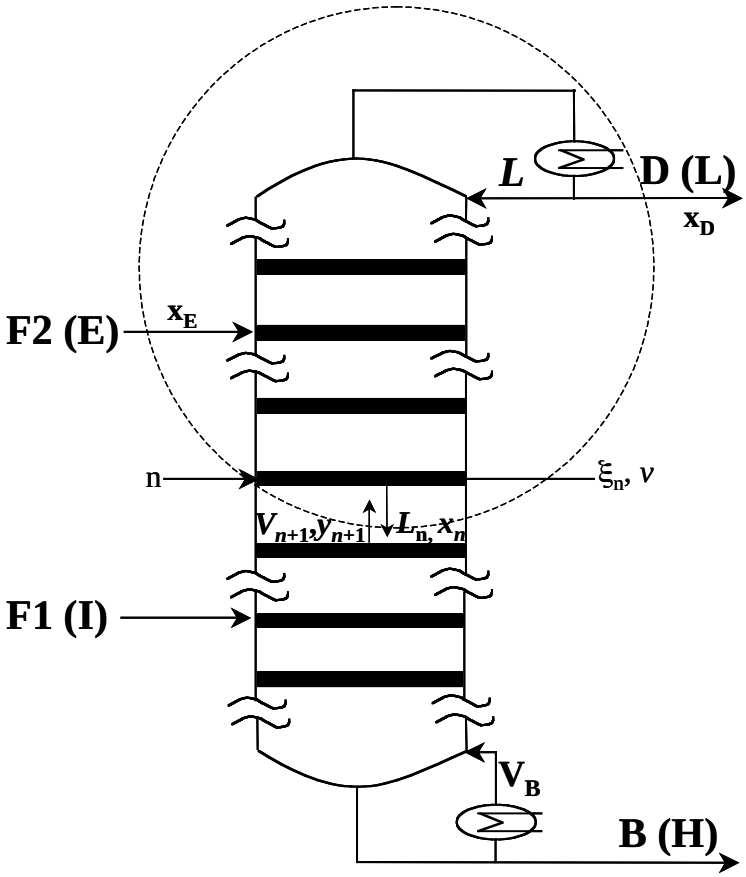

Figure 1-14 A Schematic Diagram of a Double Feed Reactive Extractive Distillation Column.

This column includes a nonreactive rectifying section, a reactive middle section between the two feed streams, and a nonreactive stripping section (or a reactive stripping section if the catalyst is a nonvolatile liquid). Here, the lower and upper feeds are reactant I and entrainer E, respectively, and the selection of entrainer is based on references 32 through 34. Because no azeotrope is formed between any reacting component (L, I, or H) and E, a double feed column can produce pure products if and only if L and E are dominant in the liquid and vapor compositions at the upper feed stage. Through the nonreactive rectifying section, light product L can be enriched at the top of the column.

Heavy product H and reactant I in the column are extracted by the entrainer. Reactant I will be consumed by reaction, and heavy product H will be recovered at the bottom. Here, the feasibility study of double-feed reactive distillation columns focuses on systems whose saddle products form a minimum-boiling azeotrope, as shown in Figure 1-9b.

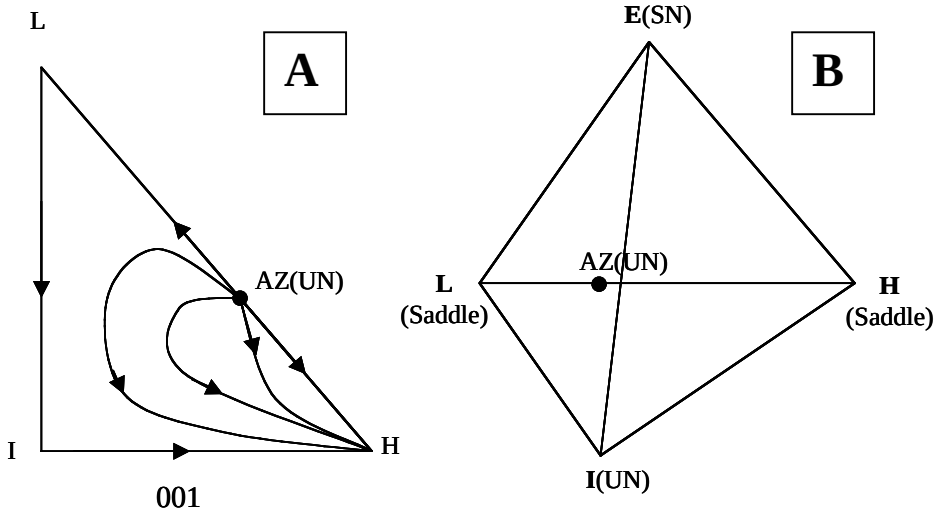

Figure 1-15 (a) Residue Curve Map of Ternary Reacting Mixture RCM-001;
(b) Tetrahedral Composition Space of the Reacting Mixture with Entrainer.

Example 6: RCM-001

The system studied here is a quaternary reactive-extractive distillation system with ternary reaction 2I ⇔ L + H (see RCM-001 in Figure 1-15a). There is one minimum binary azeotrope, a UN, between products L (saddle) and H (SN). Once the entrainer (E) is introduced into this ternary mixture, the stable node H becomes a saddle in the quaternary system because the entrainer E is the heaviest boiler in the whole system, as shown in Figure 1-15b. Other singular points (I, L, and L-H minimum azeotrope) retain the same dynamic properties after introducing the entrainer E. No distillation boundary exists in this quaternary system as there is only one UN (L-H azeotrope) and one SN (E) and all other fixed points are saddles.

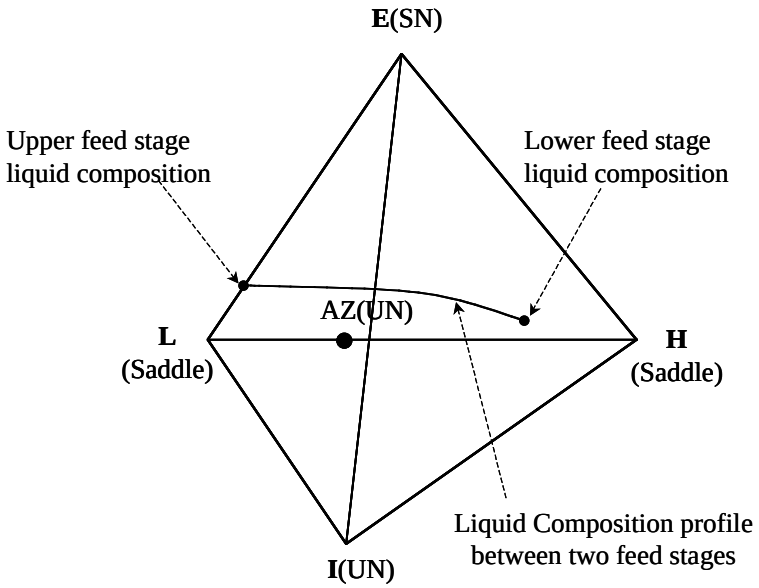

Figure 1-16 Profile Map of RCM-001 with Entrainer in the Continuous Reactive Extractive Distillation System.

For example 6, the reflux ratio (*L/D*) is fixed as 15 and *E/D* ratio as 3.0. The starting liquid composition (x_n in Figure 1-16) is [0.250, 0.400, 0.250, 0.100] for L, I, H, and E, respectively. The composition profile obtained by tray-by-tray calculations for this system is shown in Figure 1-16. The liquid composition profile moves from the starting point and eventually reaches the binary edge of E and L, where the ending point at the binary edge is the upper feed-stage liquid composition (see Figure 1-16). Reaching this binary edge indicates that the intermediate reactant is completely consumed by the reaction and that the lowest-boiling azeotrope (between L and H) has been broken by the entrainer. Thus, the pure light product can be recovered at the top by nonreactive rectification. Also, the heavy product is extracted by the entrainer and can be recovered at the bottom.

Figure 1-11 already showed that a single-feed reactive distillation column could not produce pure products with RCM-001 where one product is a saddle. However, this

system can feasibly produce those products in a double-feed distillation column with an entrainer as shown in Figure 1-16. In the next two examples we will discuss the feasibility of the reacting mixture when both products are saddles.

Example 7: RCM-031

The system under consideration here is a ternary reacting mixture with reaction 2I ⇔ L + H and RCM-031 (see Figure 1-17a). There are two azeotropes, one UN and one SN, in this ternary mixture. In the presence of the entrainer, the SN azeotrope becomes a saddle in the quaternary system as shown in Figure 1-17b. All other fixed points (I, L, H, and the L-H minimum azeotrope) retain the same dynamic properties after introducing the entrainer, E. No distillation boundary exists in this quaternary system as there are only one UN (azeotrope between L and H) and one SN (E). All other fixed points are saddles.

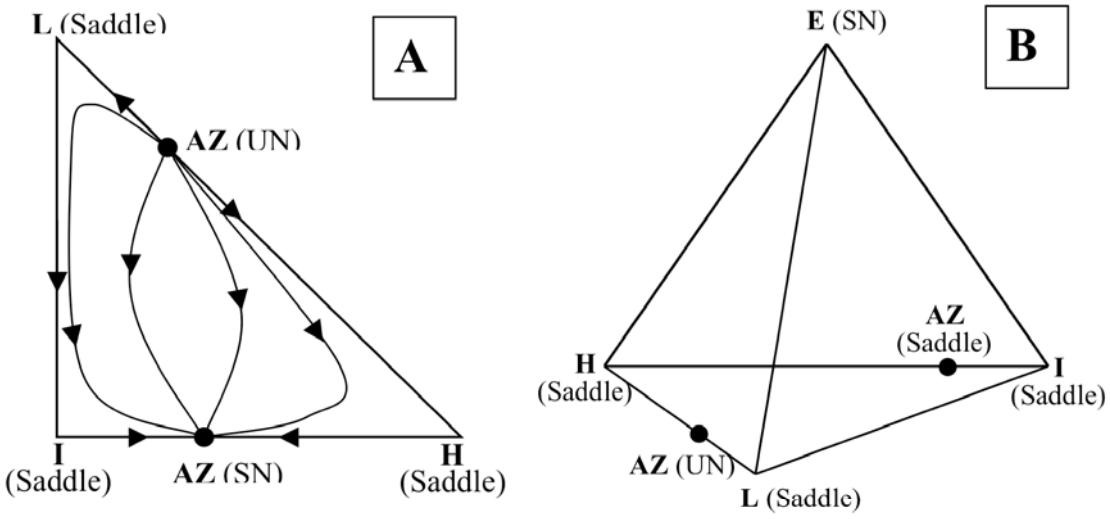

Figure 1-17 (a) Residue Curve Map of Ternary Reacting Mixture RCM-031;
(b) Tetrahedral Composition Space of the Reacting Mixture with Entrainer

For the example 7, the selected *L/D* ratio is 12, the *E/D* ratio is 2.5, and the starting composition is [0.225, 0.450, 0.225, 0.100]. The simulation results for this system are shown in Figure 1-18. The liquid composition profile, which is obtained by tray-by-tray calculations, moves from the starting point (near the lower feed stage liquid composition) and eventually reaches the binary edge of E and L. Thus, the pure light product (L) can be purified from the binary mixture of E and L at the top, and the heavy product can be recovered at the bottom with the entrainer. The result shown in Figure 1-18 demonstrate that the quaternary reacting mixture that was feasible in batch reactive-extractive distillation[16] is also feasible in a *continuous reactive* double-feed distillation column.

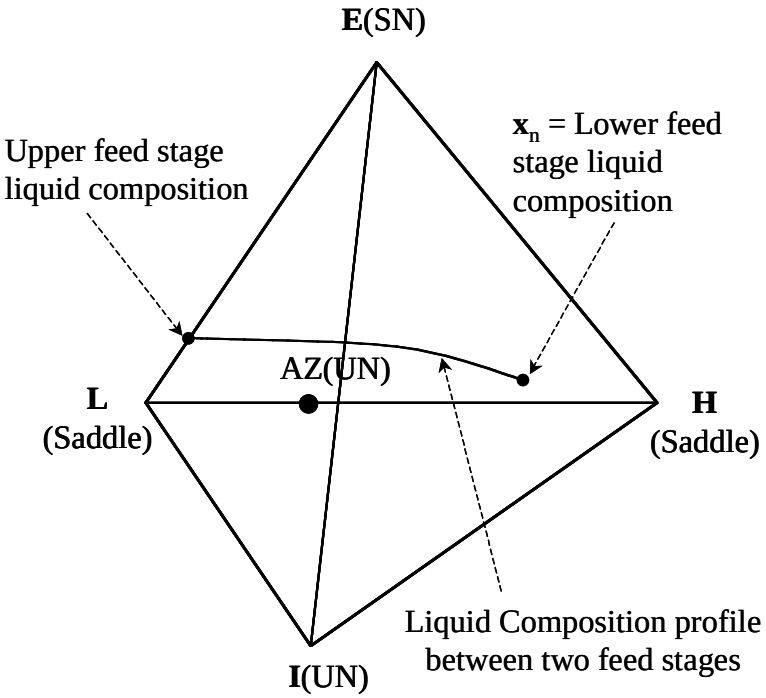

Figure 1-18 Profile Map of RCM-031 with Entrainer in the Continuous Reactive Extractive Distillation System.

Examples 6 and 7 studied above are relatively simple since no distillation boundary exists. In the next example, RCM-441-M, which has one distillation boundary with all saddle products, is considered for a feasibility study in a double-feed column.

Example 8: RCM-441-M

RCM-441-M has one ternary maximum-boiling azeotrope and three binary azeotropes. The binary azeotrope between products L and H is a minimum-boiling UN, and the other two azeotropes, H—I and L—I, are both maximum-boiling saddles. The ternary maximum-boiling azeotrope formed between L, H, and I, is an SN (Figure 1-19a). After the introduction of entrainer E (the heaviest boiler in the whole system), the SN ternary azeotrope in the ternary system becomes a saddle in the quaternary system. Other singular points retain the same dynamic properties. There are two UN's, one SN, and five saddles in this quaternary system. With these singular points, the connections of saddle—saddle and saddle—node form distillation boundaries[35]. Thus, a distillation boundary surface exists in this system as shown in Figure 1-19b. Because of this distillation boundary surface, two distillation regions (***I*** and ***II***) exist.

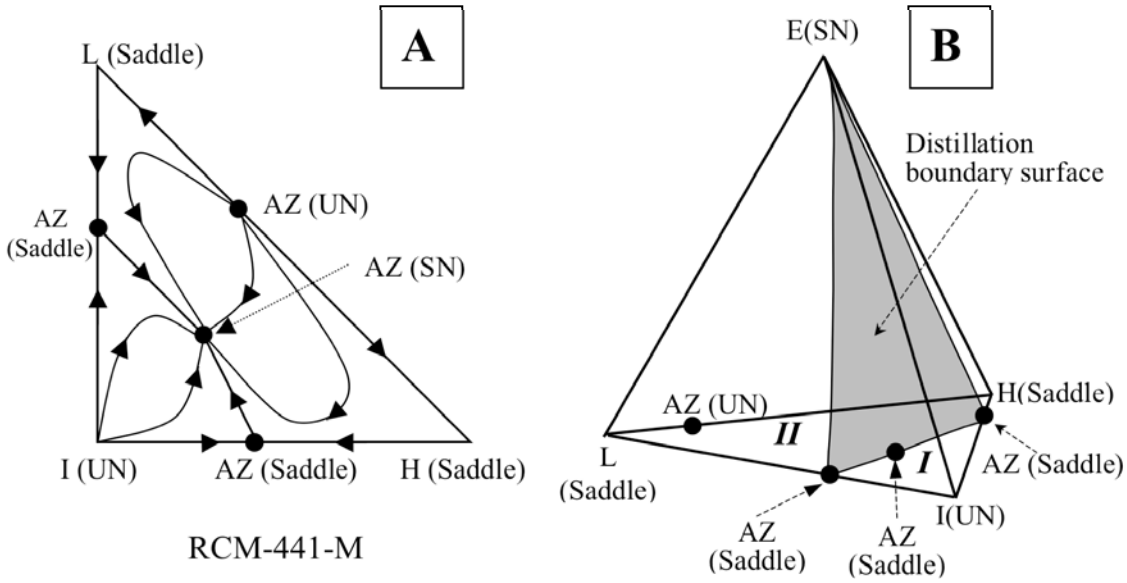

Figure 1-19 (a) Residue Curve Map of Ternary Reacting Mixture RCM-441-M;
(b) Tetrahedral Composition Space of the Reacting Mixture with Entrainer.

For the calculations of example 8, the selected ratios of *L/D* and *E/D* are 15 and 2.0, respectively. To investigate the effect of the distillation boundary surface on the continuous reactive-extractive distillation, the selected starting composition [0.152, 0.646, 0.152, 0.050] for L, I, H, and E, respectively, lies in distillation region ***I***. The result of tray-by-tray calculations for this system is shown in Figure 1-20. It can be easily seen that reaction and extractive distillation force the liquid composition profile to cross the distillation boundary surface. After crossing the surface, the liquid composition profile moves from distillation region ***I*** (starting point) to region ***II*** and eventually reaches the binary edge of E and L. Here, the ending point at the E—L binary edge is the liquid composition on the upper feed stage.

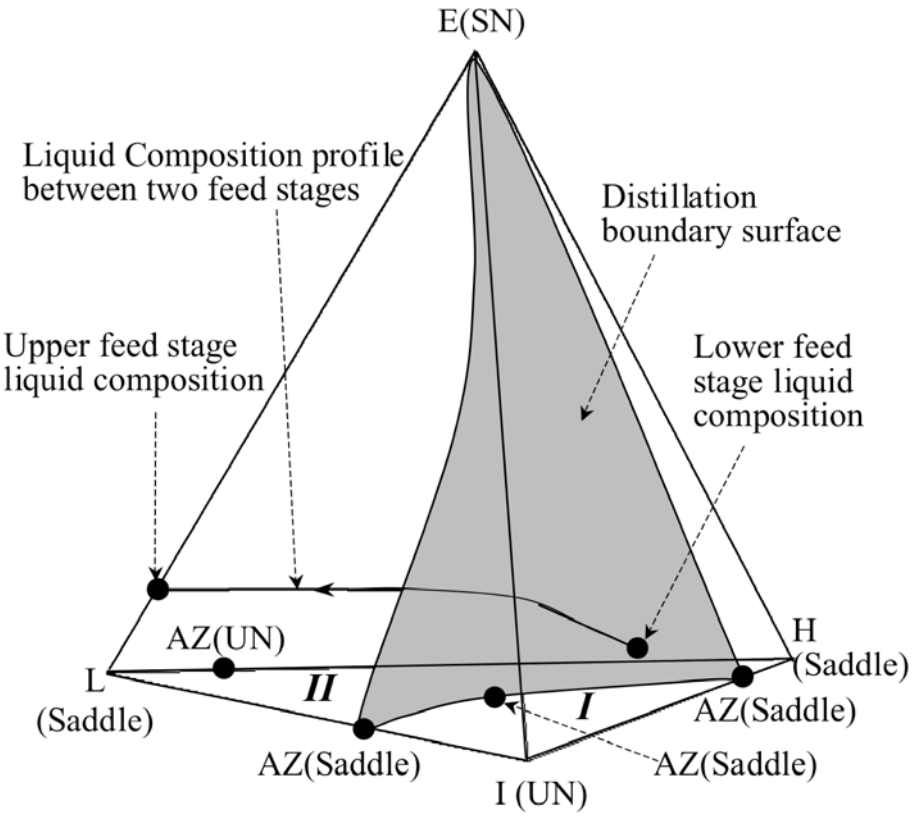

Figure 1-20 Profile Map of RCM-441-M with Entrainer in the Continuous Reactive Extractive Distillation System.

Reaching this binary edge indicates that the pure light product can be recovered at the top of the distillation column, and thus, such a configuration is feasible. Here, the lowest-boiling azeotrope (between L and H) has to be broken by the entrainer feed. In industrial applications, respective reactive distillation and extractive distillation are effective methods for circumventing azeotropes. However, it is necessary to combine these two methods together to avoid all azeotropes in systems with highly non-ideal phase equilibrium, as shown in examples 6 through 8 when any one single method cannot be used to produce the desired products.

In summary, for reacting mixtures that have a saddle product forming a minimum-boiling azeotrope with another product, a double-feed reactive distillation column with an appropriate entrainer can circumvent phase equilibrium limitations and produce pure products. A successful industrial application of double-feed reactive distillation is the production of methyl acetate from acetic acid and methanol,[36] where acetic acid works not only as a reactant, but also as an entrainer to break the azeotrope between water and methyl acetate.

Conclusion

The feasibility criteria for single-feed and double-feed reactive distillation systems are derived for azeotropic systems. When the two products are an SN and a UN and a part of the reaction equilibrium curve shares the same distillation region as the node products, then both reactive rectifying and reactive stripping sections can lead to the

production of pure products. When one of the two products is a saddle with no azeotrope between the products, a single-feed column can still be feasible if the value of *K*eq is large. However, if the saddle product forms an azeotrope with another product, then a single-feed configuration is infeasible regardless of the value of *K*eq, and an entrainer is needed to break the azeotrope. If there is only one SN heavy product in a nonisomolar reaction, then a single-feed column with either a reactive rectifying or a reactive stripping section is feasible whenever the reaction equilibrium curve lies in the same distillation region as the heavy product. It has been demonstrated that batch reactive-extractive distillation configurations can be replaced by double-feed continuous reactive-extractive distillation when all of the products are saddles and they form a minimum-boiling azeotrope.

Because these feasibility criteria have been developed according to arbitrary thermodynamic properties of reactants and products, they are easily applicable to any real systems once the relevant physical property data are available. This thermodynamic categorization of arbitrary azeotropic systems with a single reaction will be used for the feasibility studies of multiple reaction systems.

Nomenclature

B = bottom molar flow rate
c_R = normalized reactant stoichiometric coefficient vector
c_P = normalized product stoichiometric coefficient vector
D = distillate molar flow rate
E = upper feed molar flow rate

Keq = reaction equilibrium constant

L_n = liquid flow rate at stage n

V_{n+1} = vapor flow rate at stage $n + 1$

x_B = bottom composition vector

x_D = distillate composition vector

x_E = upper feed composition vector

x_{Fs} = feed liquid composition vector

x_n = liquid composition vector at stage n

y_{Fs}= feed vapor composition vector

y_{n+1} = vapor composition vector at stage $n + 1$

δ_R = reaction difference point

$\delta_{R,n}^{r}$ = reactive cascade difference points for the rectifying section at stage n

$\delta_{R,m}^{s}$ = reactive cascade difference points for the stripping section at stage m

ν = stoichiometric coefficient vector

ν_T = sum of stoichiometric coefficients

ξ_n = accumulated molar reaction extent from the top to stage n

ξ_m = accumulated molar reaction extent from the bottom to stage m

Literature Cited

1. Malone, M. F.; Doherty, M. F. Reactive Distillation. *Ind. Eng. Chem. Res.* **2000;** *39,* 3953.

2. Peng J, Lextrait S, Edgar TF, Eldridge RB. A Comparison of Steady-State Equilibrium and Rate-Based Models for Packed Reactive Distillation Columns. *Ind. Eng. Che. Res*. 2002;41:2735.

3. Al-Arfaj MA, Luyben WL. Design and Control of an Olefin Metathesis Reactive Distillation Column. *Chem. Eng. Sci*. 2002;57:715.

4. Baur R, Taylor R, Krishna R. Dynamic Behaviour of Reactive Distillation Columns Described by a Nonequilibrium Stage Model. *Chem. Eng. Sci.* 2001;56:2085.

5. Hauan S, Westerberg AW, Lien KM. Phenomena based analysis of fixed points in reactive separation systems. *Chem. Eng. Sci.*, 2000;55:1053-1075.

6. Kreul LU, Górak A, Barton PI. Modeling of Homogeneous Reactive Separation Processes in Packed Columns. *Chem. Eng. Sci*. 1999;54:19.

7. Taylor R, Krishna R. Modelling reactive distillation. *Chem Eng Sci*. 2000;55:5183-5229.

8. Okasinski MJ, Doherty MF. Design Method for Kinetically Controlled, Staged Reactive Distillation Columns. *Ind. Eng. Che. Res*. 1998;37:2821.

9. Barbosa D, Doherty MF. Design and Minimum-Reflux Calculations for Single-Feed Multicomponent Reactive Distillation Columns. *Chem. Engr. Sci.*, 1988;43:1523.

10. Lee JW. Feasibility studies on quaternary reactive distillation systems. *Ind Eng Chem Res*. 2002;41:4632-4642.

11. Giessler S, Danilov RY, Pisarenko YA, Serafimov LA, Hasabe S, Hashimoto I. Feasibility Study of Reactive Distillation Using the Analysis of the Statics. *Ind. Eng. Chem. Res.* 1998;37:4375-4382.

12. Lee JW, Westerberg AW. Visualization of Stage Calculations in Ternary Reacting Mixtures. *Comput. Chem. Eng.* 2000;24:639.

13. Ciric AR, Gu D. Synthesis of nonequilibrium reactive distillation processes by MINLP optimization. *AIChE J.* 1994;40:1479-1487.

14. Jackson JR, Grossmann IE. A disjunctive programming approach for the optimal design of reactive distillation columns. *Comp. Chem. Eng.* 2001;25:1661-1673.

15. Guo Z, Ghufran M, Lee JW. Feasible products in batch reactive distillation. *AIChE J.*, 2003;49:3161-3172.

16. Guo Z, Lee JW. Feasible products in batch reactive extractive distillation. *AIChE J*. 2004;50:1484-1492.

17. Lee JW, Hauan S, Lien KM, Westerberg AW. A Graphical Method for Designing Reactive Distillation Columns I: The Ponchon—Savarit Diagram. *Proc. R. Soc. London, Ser. A* 2000;456:1953-1964.

18. Lee JW, Hauan S, Lien KM, Westerberg AW. A Graphical Method for Designing Reactive Distillation Columns II: The McCabe—Thiele Diagram. *Proc. R. Soc. London, Ser. A* 2000;456:1965-1978.

19. Hauan S, Ciric AR, Westerberg AW, Lien KM. Difference points in extractive and reactive cascades. I - Basic properties and analysis. *Chem. Eng. Sci.* 2000;55(16):3145-3159.

20. Lee JW, Hauan S, Lien KM, Westerberg AW. Difference points in extractive and reactive cascades. II - Generating design alternatives by the lever rule for reactive systems. *Chem. Eng. Sci.* 2000;55(16):3161-3174.

21. Matsuyama H, Nishimura H. Topological and thermodynamic classification of ternary vapor-liquid equilibria. *J Chem Engr Japan*. 1977;10(3):181-187.

22. Doherty MF, Caldarola GA. Design and synthesis of homogeneous azeotropic distillations. 3. The sequencing of columns for azeotropic and extractive distillations. *Ind. Eng. Chem. Fundam.* 1985;24:474-485.

23. Velo E, Puigjaner L, Recasens F. Inhibition by product in the liquid-phase hydration of isobutene to tert-butyl alcohol: Kinetics and equilibrium studies. *Ind. Eng. Chem. Res.* 1988;27:2224.

24. Ung S, Doherty MF. Vapor-liquid phase equilibrium in systems with multiple chemical reactions. *Chem. Eng. Sci.* 1995;50:23.

25. Doherty MF, Buzad G. Reactive distillation by design. *Chemical Engineering Research and Design, Transactions of the Institution of Chemical Engineers, Part A.* 1992;70:448.

26. Lee JW, Hauan S, Westerberg AW. Circumventing an azeotrope in reactive distillation. *Ind. Eng. Chem. Res.* 2000;39:1061.

27. Hoffmaster W, Hauan S. Analysis of complex separation schemes in the presence of chemical reactions. *Sep. Sci. Technol.* 2003;38:2763.

28. Lee JW, Hauan S, Westerberg AW. Feasibility of a reactive distillation column with ternary mixtures. *Ind. Eng. Chem. Res.* 2001;40:2714-2728.

29. Lee JW, Westerberg AW. Graphical design applied to MTBE and methyl acetate reactive distillation processes. *AIChE J.*, 2001;47:1333.

30. Nisoli A, Malone MF, Doherty MF. Attainable regions for reaction with separation. *AIChE J.* 1997;43:374.

31. Sundmacher K, Uhde G, Hoffmann U. Multiple reactions in catalytic distillation processes for the production of the fuel oxygenates MTBE and TAME: Analysis by rigorous model and experimental validation. *Chem. Eng. Sci.* 1999;54:2839.

32. Foucher ER, Doherty MF, Malone MF. Automatic Screening of Entrainers for Homogeneous Azeotropic Distillation. *Ind. Eng. Chem. Res.*, 1991;30:760.

33. Wahnschafft OM, Westerberg AW. The product composition regions of azeotropic distillation columns. 2. Separability in two-feed columns and entrainer selection. *Ind. Eng. Chem. Res.* 1993;32:1108-1120.

34. Dyk BV, Nieuwoudt I. Design of Solvents for Extractive Distillation. *Ind. Eng. Chem. Res.*, 2000;39:1423.

35. Rooks RE, Julka V, Doherty MF, Malone MF. Structure of distillation regions for multicomponent azeotropic mixtures. *AIChE J*. 1998;44:1382-1391.

36. Agreda VH, Partin LR, Heise WH. High purity methyl acetate via reactive distillation. *Chem Eng Prog*. 1990;86(2):40-46.

Chapter 2: Rapid Generation of Composition Profiles for Reactive and Extractive Cascades

Reproduced with permission from AIChE J. 2005;51:922-930. Copyright 2005 American Institute of Chemical Engineers.

Abstract

This paper presents a quick method for estimating composition profiles for reactive and extractive cascades in a double-feed column without stage calculations. This profile estimation is based on the feasibility and pinch point analyses. The trajectories of pinch points are determined using material balance equations and phase and reaction equilibrium data. From these pinch point trajectories, the ranges of feasible external reflux ratios and required entrainer flow rates are calculated for a given reaction extent and product purity. Then, for given external reflux ratios, heat balance constraints are imposed to determine the positions of pinch points. Finally, using the internal reflux ratios of these pinch points, manifolds of possible composition profiles are generated. Composition profiles of a reactive/extractive cascade can lie in the section of the reaction equilibrium surface where the internal reflux ratio of a saddle pinch is between the upper and lower bounds of the internal reflux ratio.

Introduction

Extractive distillation has been used for separating azeotropic mixtures or other mixtures with low relative volatilities. It can also be combined with reaction to circumvent azeotropic compositions. A representative example is Eastman's system for producing methyl acetate by reactive distillation[1-2]. In this reactive extractive distillation, one minimum boiling azeotrope between methyl acetate (MA) and methanol (MT) is

broken through the complete consumption of MT in the reaction while the other azeotrope between MA and water (W) is circumvented by extractive distillation with acetic acid (AC).

Extractive distillation columns are feasible if an extractive agent and a desired top product are dominantly present at the extractive (or upper) feed stage. Thus, the composition profile around the extractive feed stage approaches or lies on the binary edge between those two components in composition space[3-6]. This feasibility consideration is also applicable to reactive extractive distillation in a double-feed column[7]. For example, the composition profile of the MA reactive distillation column approaches the binary edge of extractive agent (and reactant) AC and product MA while moving up the column from the lower feed stage to the upper feed stage. If a binary mixture of AC and MA exists at the upper feed stage, then the non-reactive rectifying section above that stage can separate pure MA from the binary mixture since no minimum-boiling azeotrope exists between AC and MA.

Using the above simple feasibility information, this article will address how to determine feasible composition profiles for double-feed distillation columns based on the concept of the upper and lower bounds of the internal reflux ratio[7] and the stability analysis of pinch points[8-10].

This work will review the first key concept of the upper and lower reflux ratios. The upper and lower bounds of the internal reflux ratio are determined from the phase

equilibrium behavior of the system, the feed and product specifications, and an application of material balance constraints. This application of material balance constraints will determine the set of all possible pinch points in the middle section of a double-feed column. An eigenvalue analysis will be used to determine which possible pinch points are stable or unstable nodes and which are saddle points.

Then, for a given external reflux ratio (that is, for a given heat balance), it will be shown that the internal reflux ratio of the saddle pinch point lies between the upper and lower bounds of the internal reflux ratio of every stage in the middle section composition profile. Thus, the manifold of all possible composition profiles for the middle section can be drawn for any desired external reflux ratio by calculating the upper and lower bounds at every point in composition space. Rigorous stage calculations are used to verify this method. Two real systems will be intensively considered in this paper: the non-reactive acetone (AT)─MT─W system and the reactive MA production system.

Upper and Lower Reflux Ratios for a Non-reactive System

As shown in Figure 2-1, a material balance envelope is drawn from the top of the column to an arbitrary stage (n) in the middle section of the column. Here, we consider non-reactive extractive distillation, so ξ_n in Figure 2-1 is equal to zero. Column parameters are specified: namely, the ratio of the extractive feed and the distillate molar flow rates (E/D), the distillate composition ($\boldsymbol{x}_D$), and the extractive feed composition ($\boldsymbol{x}_E$). Then, an arbitrary composition is selected and is assumed to be the liquid-phase composition on the arbitrary stage ($\boldsymbol{x}_n$). It is then of interest to determine whether or not a

column profile passing through this arbitrary composition can reach the binary edge of an extractive agent and a top product.

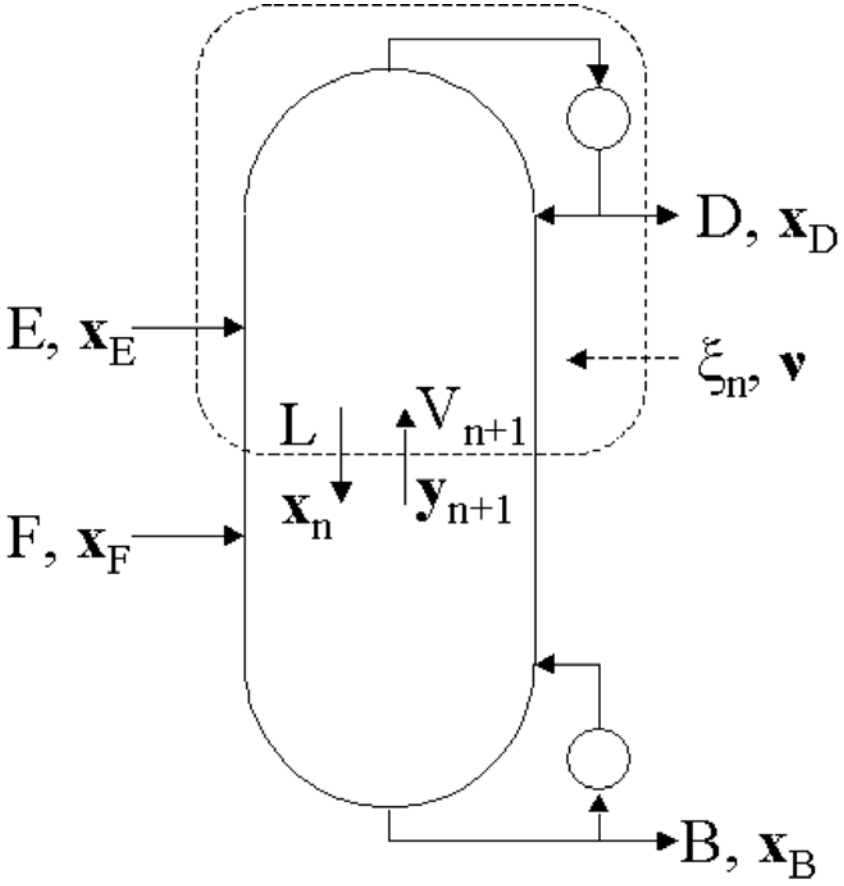

Figure 2-1: Double feed extractive/reactive distillation column.
$\xi_n=0$ for a non-reactive case and $\xi_n\neq0$ for a reactive case.

This determination begins with the assumption that this arbitrary stage is pinched. Therefore, the vapor stream ($\boldsymbol{y}_{n+1}$) entering the material balance envelope is identical to the vapor stream ($\boldsymbol{y}_n$) that is in phase equilibrium with the liquid stream ($\boldsymbol{x}_n$) leaving the material balance envelope. With these liquid and vapor compositions ($\boldsymbol{y}_n$ and $\boldsymbol{x}_n$) and the compositions of the distillate ($\boldsymbol{x}_D$) and the extractive feed ($\boldsymbol{x}_E$), material balance lines are drawn in composition space according to the following material balance equations:

$$L_n x_n + D x_D = V_n y_n + E x_E = (L_n + D)x^* = (V_n + E)x^* \qquad (1)$$

$$L_n x_n + D x_D = (L_n + D)x^* \qquad \frac{L_n}{D} = \frac{\overline{x^* x_D}}{\overline{x^* x_n}} \qquad (2)$$

$$V_n y_n + E x_E = (V_n + E)x^* \qquad \frac{V_n}{E} = \frac{\overline{x^* x_E}}{\overline{x^* y_n}} \qquad (3)$$

where $\boldsymbol{x}^*$ is the point of intersection of the material balance lines, L_n is the liquid molar flow rate leaving stage n, V_n is the vapor molar flow rate leaving stage n, D is the molar flow rate of the distillate, and E is the molar flow rate of the extractive feed. An overbar refers to the length of a line segment connecting two points on a composition diagram. For example, $\overline{x^* x_D}$ indicates the length of the line segment connecting $\boldsymbol{x}^*$ and $\boldsymbol{x}_D$.

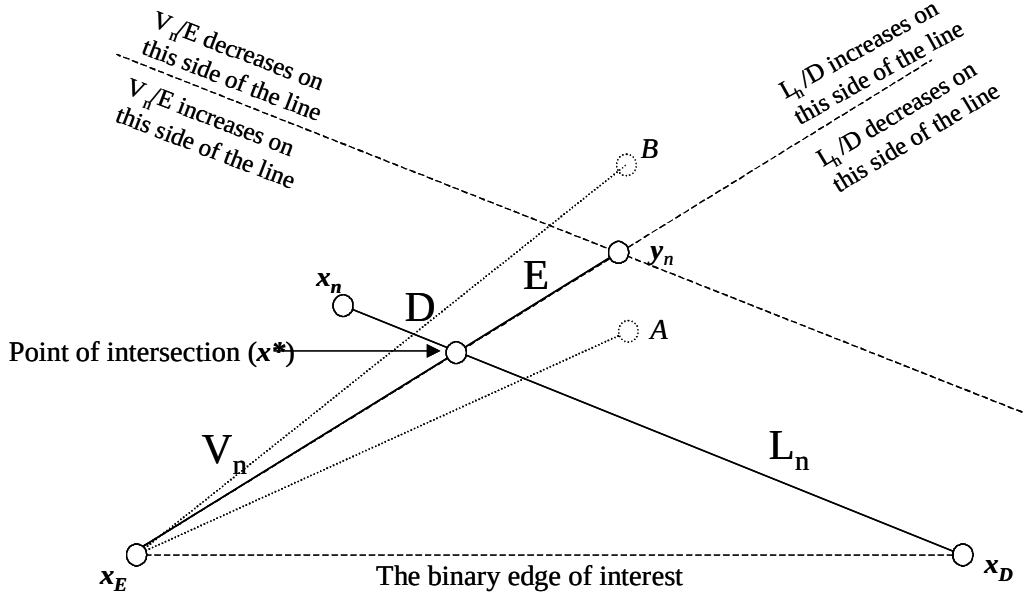

Figure 2-2: Calculation of the upper and lower bounds of the IRR in the acetone-methanol-water system. A and B denote possible $\boldsymbol{y}_{n+1}$.

Through the use of the lever rule shown in equations 2 and 3, the ratios of the lengths of line segments are related to the ratios of flow rates in and out of the material balance envelope, thus providing for two different means of calculating the internal

reflux ratio on this stage. The ratio of the lengths of the line segments labeled L_n and D in Figure 2-2 is taken as the internal reflux ratio because the internal reflux ratio for a particular stage n is defined as L_n/D. The ratio of the lengths of the line segments labeled V_n and E are related to the internal reflux ratio by manipulating the total molar material balance equation in the following manner:

$$L_n + D = V_n + E \tag{4}$$

$$\frac{L_n}{D} + 1 = \frac{V_n}{D} + \frac{E}{D} \tag{5}$$

$$\frac{L_n}{D} = \frac{V_n}{E}\frac{E}{D} + \frac{E}{D} - 1 \tag{6}$$

If the stage under consideration were actually pinched and E is equal to D ($E/D=1$), then the two calculated values of the reflux ratio (L_n/D and V_n/E) would be equal in equation 6. However, since a liquid-phase composition was arbitrarily chosen, the stage is most likely not pinched and the two calculated values for the internal reflux ratio are different. We recall that it is desired to approach a particular boundary of the composition space (the AT-W binary edge in this example) while going up the middle-section between the two feed stages. Therefore the composition of the vapor stream entering the material balance envelope ($\boldsymbol{y}_{n+1}$) must be further away from this binary edge than the composition of the vapor stream leaving stage n ($\boldsymbol{y}_n$). If this is not the case, then the composition profile will head away from the binary edge while moving up to the upper feed stage. Geometrical considerations then dictate that one of the calculated ratios has to be greater than the other calculated ratio in order for a column composition profile

passing through this point ($\boldsymbol{x}_n$) to reach the binary edge. These two calculated ratios are therefore called the upper and lower bounds of the internal reflux ratio.

Again consider Figure 2-2. Suppose that $\boldsymbol{y}_{n+1}$ is closer to the desired edge than $\boldsymbol{y}_n$ (at point *A*); this would represent an infeasible case as the column composition profile would head away from the binary edge while going up the column from stage *n+1* to stage *n*. If the true $\boldsymbol{y}_{n+1}$ were used to redraw the material balance lines, then the true internal reflux ratio would be less than L_n/D and greater than V_n/E. Now suppose that $\boldsymbol{y}_{n+1}$ was further away from the desired edge than $\boldsymbol{y}_n$ (at point *B* in Figure 2-2); this would represent a feasible case as the column composition profile would head towards the binary edge while going up the column from stage *n+1* to stage *n*. In this case, if the true $\boldsymbol{y}_{n+1}$ were used to redraw the material balance lines, then the true internal reflux ratio would be greater than L_n/D and less than V_n/E. Hence, L_n/D is referred to as the lower bound of the internal reflux ratio and V_n/E is used to calculate the upper bound of the internal reflux ratio by the use of equation 6 shown above.

A feasible composition profile can pass through a liquid-phase composition ($\boldsymbol{x}_n$) when the upper reflux ratio is greater than the lower reflux ratio at that $\boldsymbol{x}_n$. Under arbitrary *E/D* ratios, the upper and lower reflux ratios are the right and left sides, respectively, of equation 6. This calculation can be quickly and easily repeated using any phase-equilibrated pair of compositions $\boldsymbol{x}_n$ and $\boldsymbol{y}_n$ in composition space. Thus, it is possible to draw a region in composition space where the upper bound is greater than the

lower bound; this is the region where column composition profiles head towards the binary edge.

Upper and Lower Reflux Ratios for a Reactive System

In the AT-MT-W system, drawing these material balance lines is a simple matter as we only require that the two material balance lines intersect in a two-dimensional (three-component) composition space as shown in Figure 2-2. However, in the reactive MA production system, the points used to draw the liquid, vapor, extractive, and distillate compositions do not lie on the same plane in composition space.

Lee (2002)[7] proposed the following: given a distillate composition and the reaction stoichiometry, a line can be drawn on a composition diagram through the distillate composition and parallel to the reaction stoichiometry vector. This line is called the "cascade difference point trajectory" and combines the distillate and reaction terms of the material balance equations[11-12]. For any given liquid composition ($\boldsymbol{x}_n$) on a hypothetical stage in the reactive section of the column, Lee (2002)[7] shows that there exists a unique point on this trajectory called the "cascade difference point" such that material balance lines can be drawn. Specifically, this is the point where the cascade difference trajectory intersects the plane containing the liquid, vapor, and extractive feed compositions as shown in Figure 2-3. The lever rule is then applied to the segments of the material balance lines to determine the upper and lower bounds of the reflux ratio with the simple modification that the cascade difference point, $\boldsymbol{\delta}_n$, is used in these calculations instead of the distillate composition, $\boldsymbol{x}_D$.

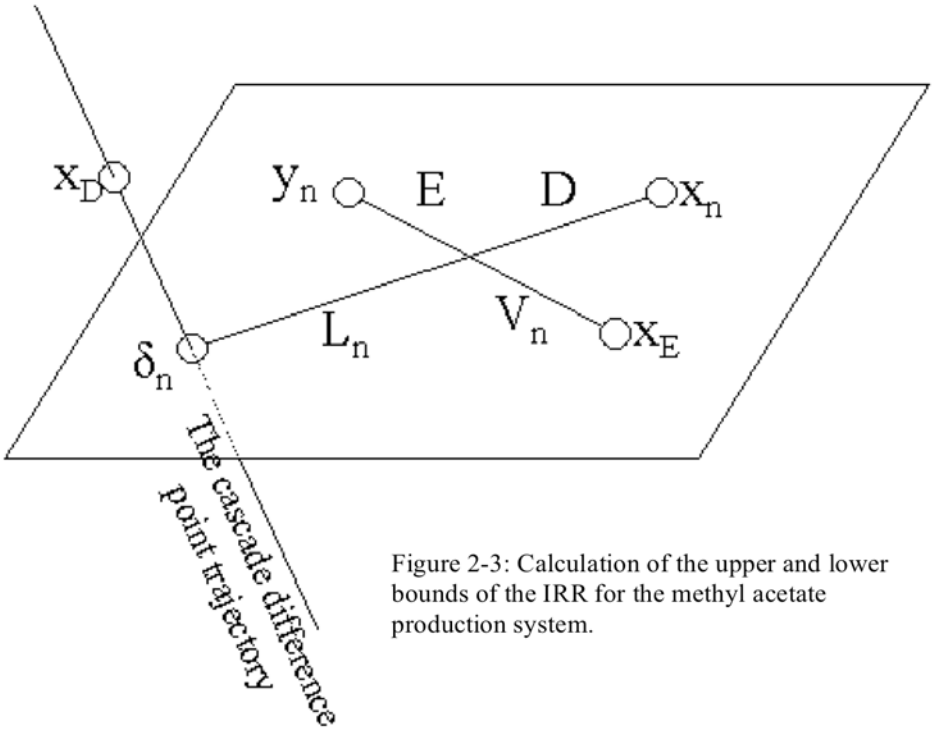

Figure 2-3: Calculation of the upper and lower bounds of the IRR for the methyl acetate production system.

The upper and lower reflux calculations required only phase equilibrium information, material balance constraints, the extractive feed composition, the desired distillate composition, and the ratio of the extractive and distillate flow rates. In the reactive case, reaction stoichiometry and reaction equilibrium information were also used. From these upper bound and lower bound calculations, the region where the upper bound is greater than the lower bound can be drawn. A column profile must travel through this region in order to reach the binary edge of the extractive feed composition and the desired distillate product composition.

Since possible pinch points exist wherever the upper bound equals the lower bound, this region is bound by the pinch point trajectories. If the upper and lower bounds are calculated at points sampled throughout composition space, then this region is easily visible and the boundaries of this region are the pinch point trajectories. In both Figures

2-5 (for the AT-MT-W system, page 67) and 2-6 (for the MA production system, page 68), it can be seen that there are two pinch point trajectories between which the upper bounds are greater than the lower bounds. These figures also show the nature of the pinch points and their internal/external reflux ratios (IRR/r_{ext}), which will be discussed in the following section.

Determination of Pinch Point Trajectories

In the previous section, it was shown how the pinch point trajectories could be located by sampling points in composition space and selecting those points where the upper and lower bounds of the internal reflux ratio are equal. Although effective in quickly determining the approximate locations of pinch trajectories, this method is slightly time-consuming when trying to locate these trajectories with precision. Thus, this section will show the mathematical determination of the pinch point trajectories by using material balance constraints and equilibrium data.

The pinch point trajectories in the AT-MT-W system can be described by the following N_{comp} molar component material balance equations:

$$\frac{V_n}{D} y_{n,i} + \frac{E}{D} x_{E,i} - \frac{L_n}{D} x_{n,i} - x_{D,i} = 0 \quad \text{for i=1..}N_{comp} \quad (7)$$

where $\frac{V_n}{D} = \frac{L_n}{D} + 1 - \frac{E}{D}$, N_{comp} is the number of components, and $y_{n,i}$ is the vapor phase fraction of component i (a function of the liquid phase composition). In the MA system, there is also a reaction term, $\frac{\xi_n}{D}\nu_i$, on the left-hand side of each occurrence of equation

(7) where ξ_n is the molar extent of reaction on all of the trays in the material balance envelope and v_i is the reaction stoichiometry coefficient of component i.

The MA production system also has an additional equation that requires any liquid phase composition to be on the reaction equilibrium surface (because the reaction takes place in the liquid phase):

$$K_{equil} = \frac{x_{n,MA} x_{n,W} \gamma_{n,MA} \gamma_{n,W}}{x_{n,AC} x_{n,MT} \gamma_{n,AC} \gamma_{n,MT}} \qquad (8)$$

where $x_{n,i}$ and $\gamma_{n,i}$ are the mole fraction and activity coefficient, respectively, of component i on arbitrary stage n and K_{equil} is the reaction equilibrium constant, which is a function of temperature (K_{equil} = 0.83983 +782.98/T in Song et al., 1998[13]).

Thus, the AT-MT-W system has seven unknowns ($\frac{L_n}{D}$, $\boldsymbol{x}_A$, $\boldsymbol{x}_{MT}$, $\boldsymbol{x}_W$, $\boldsymbol{y}_A$, $\boldsymbol{y}_{MT}$, $\boldsymbol{y}_W$) and six equations (the three material balance equations and the three phase equilibrium equations). The MA production system has ten unknowns ($\frac{L_n}{D}$, $\frac{\xi_n}{D}$, $\boldsymbol{x}_{AC}$, $\boldsymbol{x}_{MT}$, $\boldsymbol{x}_{MA}$, $\boldsymbol{x}_W$, $\boldsymbol{y}_{AC}$, $\boldsymbol{y}_{MT}$, $\boldsymbol{y}_{MA}$, $\boldsymbol{y}_W$) and nine equations (the four material balance equations, the four phase equilibrium equations, and the reaction equilibrium equation). In either case, the pinch trajectory has one degree of freedom. Because the pinch trajectories are dependent upon phase equilibrium (which can be severely non-linear), the trajectories are double-valued at some values of the internal reflux ratio; they cannot be a priori relied upon to be single-valued anywhere.

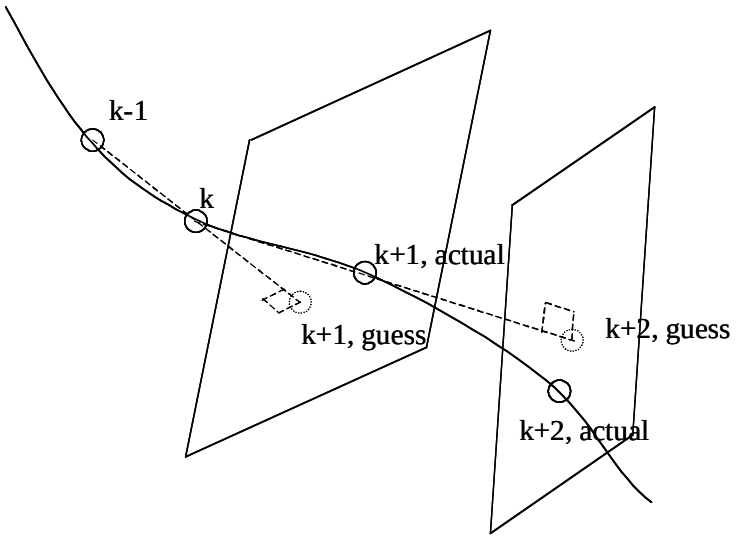

Figure 2-4: Continuation method for the calculation of pinch trajectories.

Seyde and Hlavack (1989)[14] and Seider et al. (1991)[15] described what they refer to as the continuation method for calculating trajectories of functions that are not always single valued with respect to a particular continuation parameter. Knapp and Doherty (1994)[4] performed a bifurcation analysis of such non-linear systems. The continuation method is applied here in the following manner illustrated in Figure 2-4: if the coordinates of two closely-spaced points on that trajectory are known (k-1 and k), then the coordinates of a third point on the pinch trajectory (k+1) can be guessed by drawing a line through the two given points and extending that line some arbitrary distance as shown in Figure 2-4; where the line ends is an initial guess for the next point on the pinch trajectory (k+1).

A linear variation is then drawn through this guessed point and perpendicular to the aforementioned line. (The linear variation is represented as a plane in Figure 2-4, but actually has N_{param}-1 dimensions.) This linear variation is represented by a single

equation and constrains the only degree of freedom held by the pinch trajectory. That equation is

$$0 = \sum_{i=1}^{Nparam} normal_i (x_i - x_{i,guess}) \qquad (9)$$

where N_{param} is the number of continuation method parameters, $normal_i$ is the i-th parameter of the vector pointing from one known point to the other, x_i is the i-th parameter of the coordinates being solved for (the coordinates of the next point on the pinch trajectory), and $x_{i,guess}$ is the i-th parameter of the initial guess for this point. Remember that the parameters are the liquid and vapor mole fractions, the internal reflux ratio, and the extent of reaction (if the system is reactive).

Where the pinch trajectory intersects this linear variation is the solution to both the equation of the linear variation and the equations that describe the pinch trajectory and is taken as a third known point on the trajectory (k+1). Thus, there is an equation for each unknown and the set of algebraic equations can be solved by any numerical method found fit for the task (the Newton-Raphson method, for example). The second and third known points (k and k+1) are then used to find a fourth point (k+2) and repeat the process. Thus, the coordinates of points along the trajectory can be obtained. Because each successive solution is used to calculate the initial guess for the next solution on the trajectory, the method can follow the trajectory regardless of how many twists and turns the trajectory takes as long as the spacing of the two known points being used at each step is sufficiently small (that is, smaller than the radius of curvature of the trajectory at any point on the trajectory).

Once the pinch trajectories are determined by the continuation method, we can also calculate external reflux ratios along the trajectories by applying a heat balance to the envelope shown in Figure 2-1. The heat balance equation is:

$$\frac{V_n}{D}H_n + \frac{E}{D}h_E = \frac{L_n}{D}h_n + h_D - (r_{ext}+1)*(h_D - H_D) \quad (10)$$

where $\frac{V_n}{D} = \frac{L_n}{D} + 1 - \frac{E}{D}$, h_n is the saturated liquid enthalpy of the liquid on the arbitrary stage n, H_n is the saturated vapor enthalpy also on stage n, h_E is the saturated liquid enthalpy of the upper (extractive) feed stream, and h_D and H_D are the saturated liquid and vapor enthalpies, respectively, of the distillate stream. Then, the external reflux ratio associated with a particular pinch point can be calculated for each point on a pinch trajectory by using equation (10) with the internal reflux ratio determined by the continuation method.

In the AT-MT-W system shown in Figure 2-5, one pinch trajectory travels from the MT vertex to the W vertex. Along this trajectory, the internal and external reflux ratios begin at very large values near the MT vertex and decrease until they each go through a minimum at the point where the saddle pinches become stable nodes. They then increase until they reach the point where the pinches become saddles again. The reflux ratios then decrease again until the pinch points become unstable nodes, and then increase to very large values again as they approach the W vertex. The second trajectory starts at the AT-MT azeotrope, travels towards the W-AT binary edge, and then turns towards the AT vertex. Along this trajectory, the internal and external reflux ratios begin

at very high values near the azeotrope, go through minima, and then increase to very large values again as they approach the AT vertex.

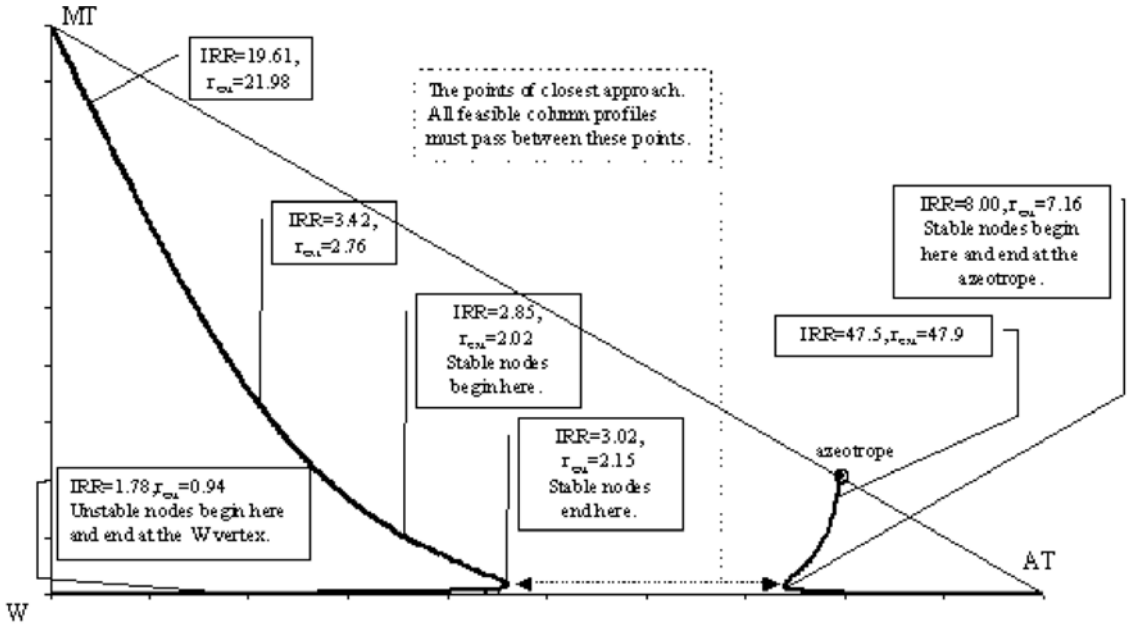

Figure 2-5: Pinch point trajectories for the acetone-methanol-water system. Given conditions[3] are $\boldsymbol{x}_E$=[0.000004 0.000496 0.9995] and $\boldsymbol{x}_D$=[0.995 0.001 0.004] for AT, MT, and W, respectively, E/D=1.0955. All pinch points are saddles unless otherwise marked.

In the MA production system shown in Figure 2-6, one pinch trajectory begins at the W vertex and travels towards the AC vertex. Along this trajectory, the internal and external reflux ratios both start at very high values near the W vertex, go through a minimum, and become very large again as they approach the AC vertex. The other pinch trajectory begins at the MT-MA azeotrope and travels towards the AC-MA binary edge before turning towards the MA vertex. Along this trajectory, the internal and external reflux ratios also begin at very high values, go through minima, and return to very high values again.

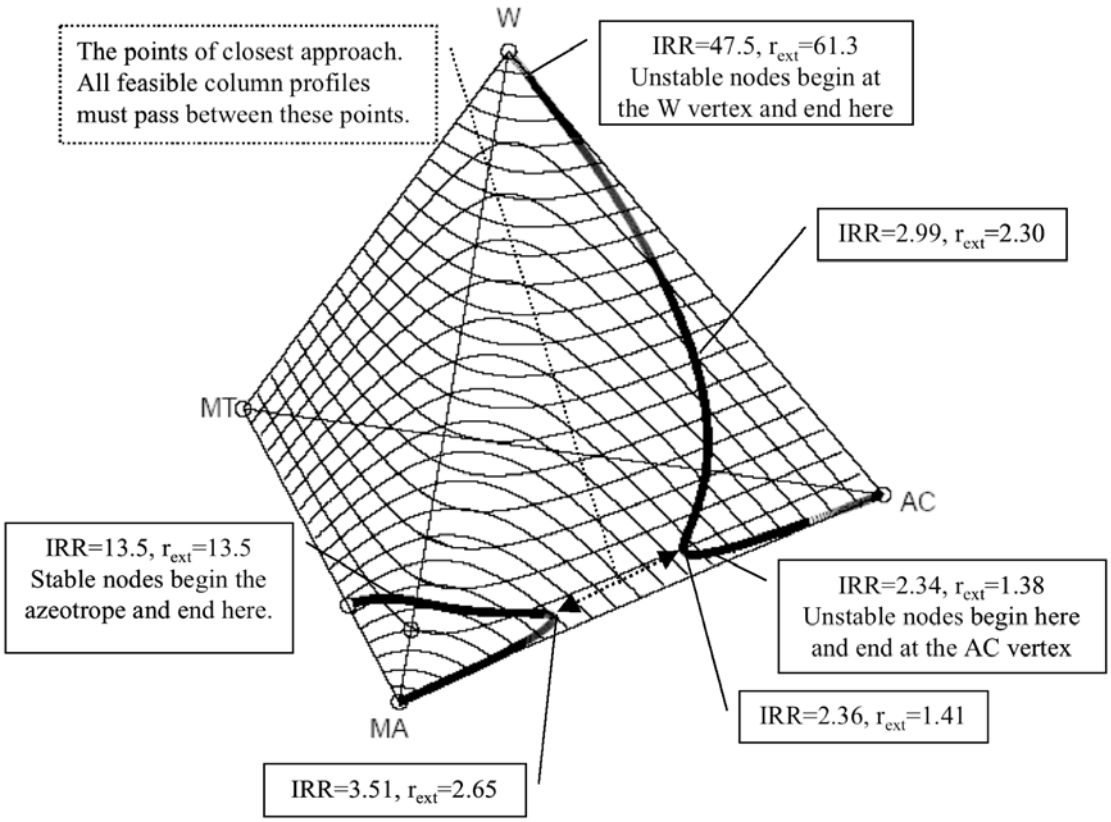

Figure 2-6: Pinch point trajectories for the methyl acetate production system. Given conditions[7] are $\boldsymbol{x}_E$=[1 0 0 0] and $\boldsymbol{x}_D$=[0.001 0.008 0.990 0.001] for AC, MT, MA, and W, respectively, E/D=1. All pinch points are saddles unless otherwise marked. Hereafter, open circles are azeotropes and pure component vertices.

The pinch points of any system affect the behavior of column profiles. Hence, the dynamic properties of pinch points are typically of interest. That is, it is usually desired to know whether a pinch point is a stable node, a saddle, or an unstable node. For a particular pinch point, these properties can be determined by calculating the eigenvalues and eigenvectors of the following matrix[8-10]:

$$\overline{\overline{J}} = \left(\frac{\partial f_i}{\partial x_j} \right) \qquad \text{i, j = 1..Ncomp} \qquad (11)$$

where f_i (for the acetone-methanol-water system using the balance envelope described above) is defined as $x_{n+1,i} = x_{n,i} = f_i(\bar{x}) = \frac{V_{n+1}}{L_n} y_{n+1,i} + \frac{E}{L_n} x_{E,i} - \frac{D}{L_n} x_{D,i}$, that is, the mole

fraction of component i in the liquid phase of stage n+1 (which is the same as on stage n because it is pinched). The MA production system has an additional term, $+\frac{\xi_n}{L}\nu_i$, in the f_i expression.

Julka et al. (1990)[8] also showed that for an N_{comp} component system, there are N_{comp}-1 real, positive eigenvalues. A pinch point is a stable node if all of its eigenvalues are less than unity. A pinch point is an unstable node if all of its eigenvalues are greater than unity. All other pinch points are saddles and they each have at least one eigenvalue greater than unity and at least one eigenvalue less than unity.

Because we hold the extractive and distillate compositions and their molar flow rates constant, the derivative of f_i is merely a constant times the derivative of y_i, which can be calculated for any analytical representation of the phase equilibrium behavior. In the MA production system, the reaction stoichiometry vector is given and the extent of reaction is prescribed by the reaction equilibrium. Thus, we can also use equation (11) for the MA production system to determine eigenvalues and eigenvectors.

Estimation of Operating Parameters and Composition Profiles

General Behavior of Column Profiles

For a given value of the external reflux ratio, it is possible to calculate different middle-section column profiles using various arbitrary starting points throughout composition space as the liquid composition on the tray above the lower feed stage.

These rigorously calculated column profiles are plotted in Figure 2-7 for the AT-MT-W system and Figure 2-8 for the MA production system.

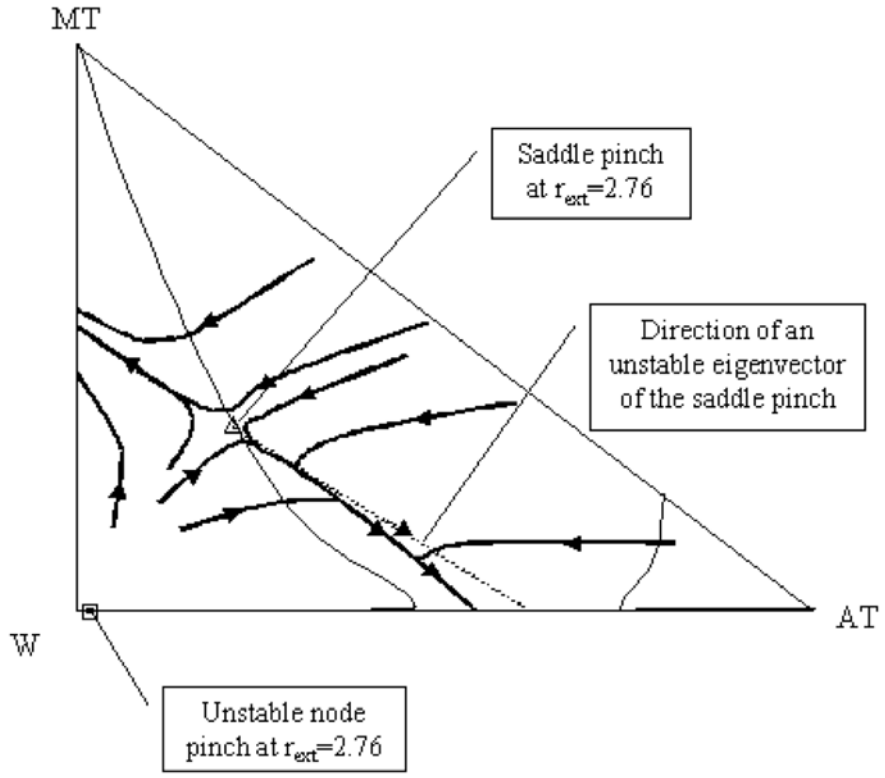

Figure 2-7: Various tray-by-tray calculated profiles in the acetone-methanol-water system at r_{ext}=2.76.

In the AT-MT-W system of Figure 2-7, all of the column profiles that begin sufficiently far away from the feasible section of the AT-W edge approach the saddle pinch point before proceeding to either the AT-W or MT-W edges of composition space. Those that go to the AT-W edge are always drawn to the same point on that edge for a given external reflux ratio. Because any middle-section profile must reach the AT-W binary edge to represent a feasible column profile, it should move through the feasible region where the upper reflux bound is greater than the lower reflux bound and then end at the AT-W binary edge. At r_{ext}=2.76, there are two pinch points present: the saddle

pinch at [0.214 0.324 0.462] and an unstable node at [0.015 0.000 0.985] for AT, MT, and W, respectively. Those profiles that started near the unstable node were first attracted to the saddle before traveling to the AT-W edge.

The tray-by-tray profiles in the MA production system show similar behavior. As shown in Figure 2-8, all of the feasible composition profiles were attracted to the saddle pinch before traveling to the same spot on the AC-MA binary edge. In the MA production system at r_{ext}=2.3, there are again two pinch points present: the saddle pinch at [0.536 0.008 0.109 0.347] and an unstable node at [0.874 0.000 0.122 0.005] for AC, MT, MA, and W respectively.

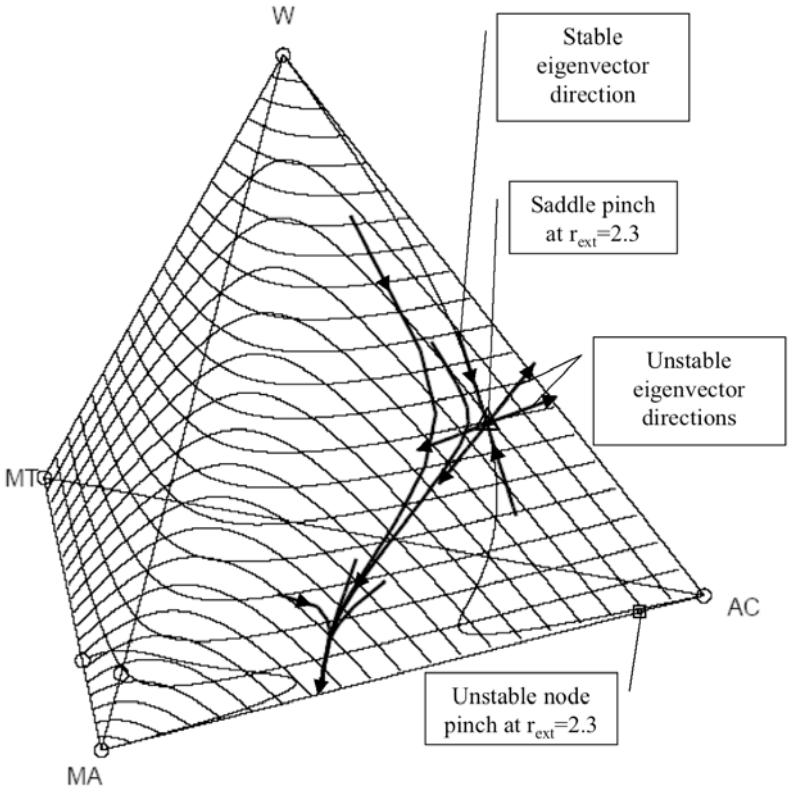

Figure 2-8: Various tray-by-tray calculated profiles in the methyl acetate production system at r_{ext}=2.30.

Brüggemann and Marquardt (2004)[16] discussed a profile estimation based upon the calculation of the eigenvectors of the pinch points of the system and take the direction of the eigenvectors as being the direction of the non-reactive column profiles. Consistent with their estimate, the column profiles in the AT-MT-W system travel away from the saddle pinch along the unstable eigenvector as shown in Figure 2-7. The saddle pinch for the MA production system shown in Figure 2-8 possesses three eigenvectors, one stable and two unstable. The two unstable eigenvectors repel the column profiles away from the saddle pinch and one of them moves towards the feasible destination on the AC-MA binary edge.

The Feasible Range of Column External Reflux Ratios

It has been noted that extractive distillation processes exhibit both a minimum and a maximum feasible external reflux ratio[4-5, 16-17]. As shown in the previous section, the feasible composition profiles always proceed towards, and end in, the region where upper reflux bounds are greater than lower reflux bounds. Thus, for the feasible composition profiles to move towards the AT-W or AC-MA edge, they must pass between the two pinch trajectories as shown in Figures 2-7 and 2-8. In each of the two systems presented in this paper, the two pinch point trajectories have points of closest approach as shown in Figures 2-5 and 2-6, that is, points where they come closest to each other. Therefore, all feasible profiles must pass between these two points of closest approach. Then, by using equation (10) and the internal reflux ratios (L_n's) of these pinch points, the range of external reflux ratios that allows feasible operation is determined as 2.2 to 7.2 for the AT-

MT-W system and as 1.4 to 2.7 for the MA system for the conditions given in Figures 2-5 and 2-6.

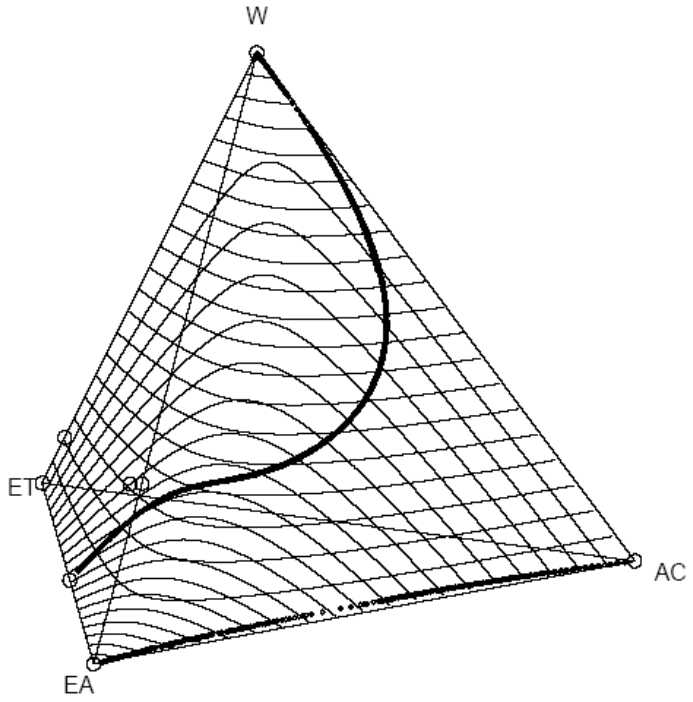

Figure 2-9: Pinch point trajectories for the ethyl acetate production system with E/D=1.

The Effects of Varying E/D

The parameter *E/D* was fixed when calculating the upper and lower bounds of the internal reflux ratio in the previous sections. However, these upper and lower bounds are dependent upon the values of E/D. In some systems, merely combining reaction and separation will not result in the feasible production of pure products from a stoichiometric feed (*E/D*=1). For example, Figure 2-9 shows the pinch point trajectories for the ethyl acetate (EA) production system when *E/D* is equal to 1. There is one trajectory that travels from the W vertex to the ET-EA azeotrope and a second pinch trajectory that travels from the EA vertex to the AC vertex along the EA-AC edge. Between these two pinch trajectories, the lower bound is greater than the upper bound. It

is then clear that pure EA cannot be produced from a stoichiometric feed of ET and AC since the EA-AC binary edge cannot be reached.

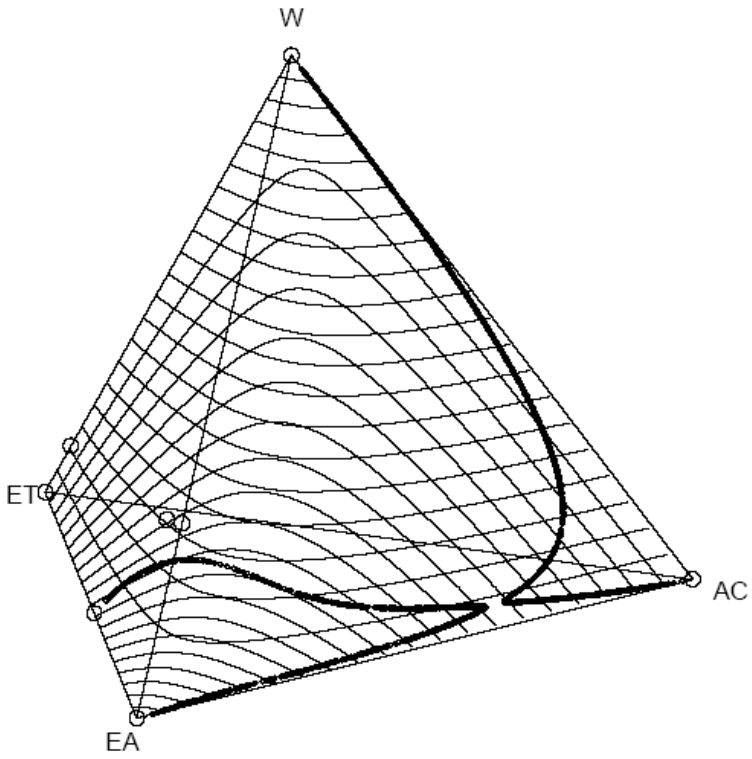

Figure 2-10: Pinch point trajectories for the ethyl acetate production system with E/D=5.

However, if E/D is increased to 5 (that is, a 400% AC excess is introduced to act as entrainer), then the pinch point trajectories in Figure 2-10 result. These trajectories resemble the pinch trajectories shown in Figure 2-6 for the MA production system; between them, the upper bound is greater than the lower bound and it is possible for feasible column profiles to pass between them to reach the AC-EA edge. By generating pinch trajectories with different E/D ratios, we can easily determine the feasible ranges of E/D.

Composition Profile Estimation

The region through which the feasible column profiles travel after turning from the saddle pinch can be determined by first selecting an external reflux ratio and then finding the saddle pinch associated with that external reflux ratio. To determine this region, two conditions will be applied in terms of the concept of the upper and lower reflux ratios and the general behavior of middle section profiles in Figures 2-7 and 2-8:

1) The saddle pinch attracts the feasible composition profiles.
2) The feasible composition profile must move into the region where the upper bounds of the internal reflux are greater than the lower bounds of the internal reflux ratio and must end in the binary edge connecting the desired top product and upper feed vertices.

To satisfy these two conditions, we can draw the region between the two pinch trajectories where the internal reflux ratio of the saddle pinch lies between the upper and lower bounds of the internal reflux ratio as shown in Figures 2-11 and 2-12. Thus, the range of the upper and lower reflux ratios evaluated at this feasible region includes the internal reflux ratio of the saddle pinch.

Figure 2-11 shows a column composition profile for the middle section of the AT-MT-W system. This profile was generated by a rigorous tray-by-tray algorithm for particular values of $\boldsymbol{x}_E$, $\boldsymbol{x}_D$, E/D, and the external reflux ratio. The column profile proceeds from an arbitrarily chosen lower feed stage composition towards a pinch point and then turns to the AT-W binary edge. Notice that while the profile travels from the

saddle pinch to the binary edge, it remains inside the feasible region drawn for this system.

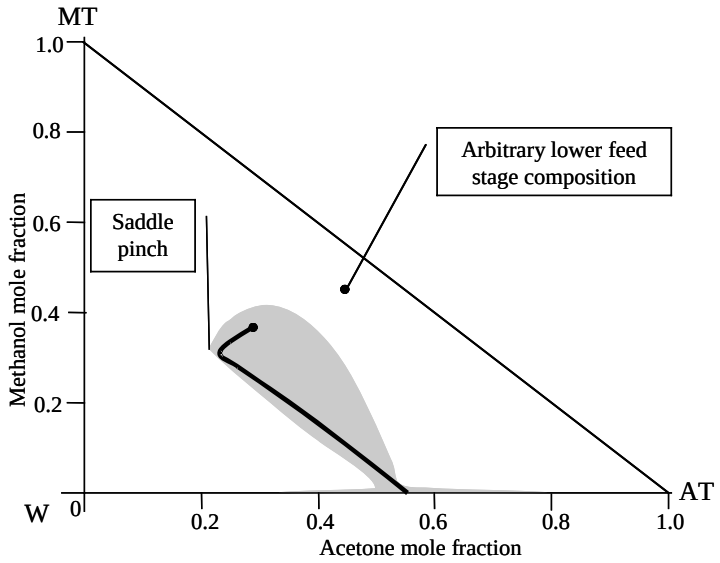

Figure 2-11: Tray-by-tray-calculated column profile and the feasible region. r_{ext}=2.76, IRR of the saddle pinch =3.42, x_D=[0.995 0.001 0.004] x_E=[0.000004 0.000496 0.9995], x_F=[0.5 0.5 0], E/D=1.0955.

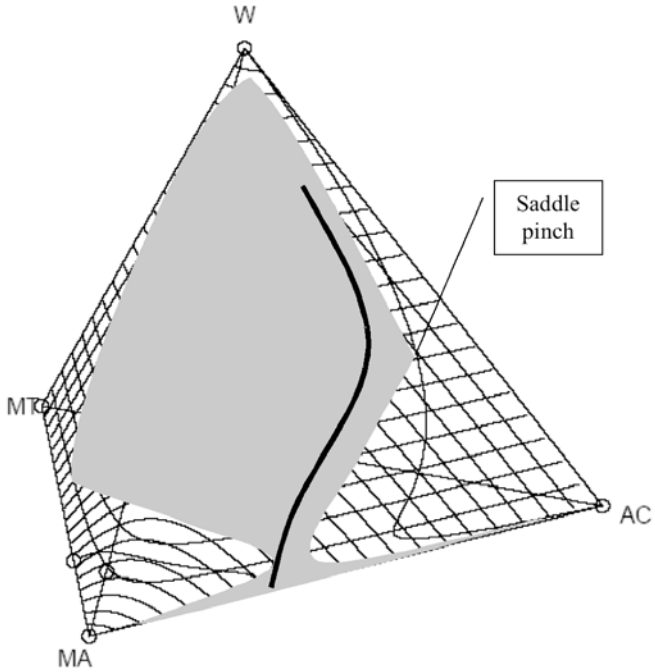

Figure 2-12: Tray-by-tray-calculated column profile and the feasible region. rext=2.30, IRR of the saddle pinch =2.993, xD=[0.001 0.008 0.990 0.001], xE=[1 0 0 0], xF=[0 1 0 0], E/D=1.0.

Figure 2-12 also shows a rigorously calculated composition profile for the middle section of the MA production system. Again, values of $\boldsymbol{x}_E$, $\boldsymbol{x}_D$, E/D, and the external reflux ratio are chosen. This profile also travels from the arbitrarily chosen lower feed stage composition towards the saddle pinch before turning towards the binary edge.

Summary and Conclusions

We have developed a quick and reliable method for estimating reactive composition profiles in a double-feed reactive distillation column. Its implementation procedure is summarized in Figure 2-13. For given entrainer and product compositions, E/D ratio, and phase and reaction equilibrium data, the upper and lower bounds of the internal reflux ratio are calculated throughout composition space. Then, we determine the region where the upper bound is greater than the lower bound. If this region does not extend to the desired binary edge, then a feasible column is not possible for the parameters chosen and a different set of parameters should be selected as shown in Figure 2-13. Then the continuation method is applied to find pinch trajectories and their dynamic properties. The last step is to select an external reflux ratio for the column and determine the saddle pinch associated with that external reflux ratio. Finally, we draw the feasible region of all liquid compositions where the upper and lower bounds of the internal reflux ratio include the internal reflux ratio of the saddle pinch.

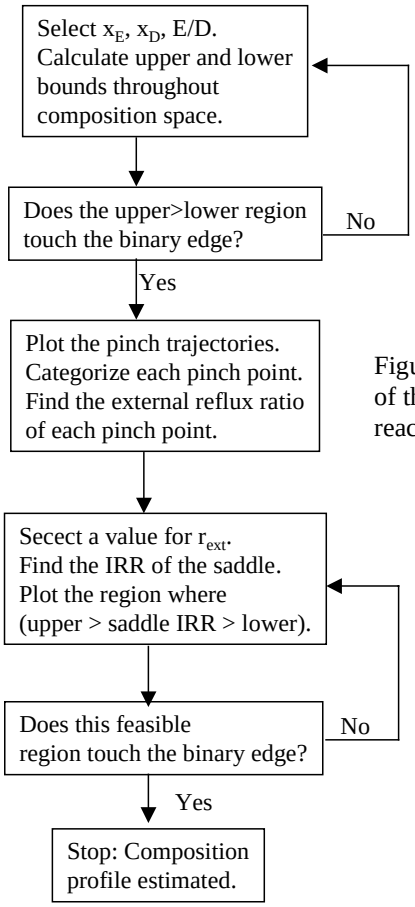

Figure 2-13: A summary flowsheet of the estimation of feasible reactive composition profiles.

In the proposed scheme of estimating possible composition profiles for the middle section of reactive and non-reactive extractive distillation columns, only phase and reaction equilibrium calculations with the pinch point analysis are needed to replace rigorous tray-by-tray calculations. From the pinch analysis, the column feasibility and the feasible range of the operating parameters are determined by using the concept of the upper and lower bounds of the internal reflux ratio.

This method can be used in combination with other shortcut design methods such as the rectification body method[9,16,18-19] to implement the nonlinearity of column profiles and to determine key design parameters. By combining the concept of critical

composition regions[7], it can also be used to screen suitable entrainers for a particular separation before conducting extensive bench scale separation experiments. Adapting this method to estimate profiles for systems with multiple components and reactions will be the subject of future work in this area.

Acknowledgements

The corresponding author is grateful for the support of Professional Staff Congress City University of New York (PSC-CUNY) and American Chemical Society – Petroleum Research Fund (ACS-PRF, G). The authors are also thankful to Prof. Marquardt at RWTH for his permission to use the code of a shortcut algorithm.

Notation

D = molar flow rate of the distillate stream.

E = molar flow rate of the extractive (upper feed) stream.

f_i = mole fraction of chemical component i in the liquid phase of a pinched stage.

h_D = specific enthalpy of the liquid distillate (exiting the total condenser).

H_D = specific enthalpy of the vapor distillate (entering the total condenser).

h_E = specific enthalpy of the extractive (upper feed) stream.

h_n = specific enthalpy of the liquid leaving stage n.

H_n = specific enthalpy of the vapor leaving stage n.

IRR = internal reflux ratio (L_n/D)

$\overline{\overline{J}}$ = jacobian matrix of the derivatives of f_i with respect to x_j.

K_{equil} = reaction equilibrium constant.

L_n = molar flow rate of the liquid leaving stage n.

N_{comp} = number of chemical components.

N_{param} = number of continuation method parameters.

$normal_i$ = i-th parameter in the vector pointing from the first known pinch point to the second known pinch point in the continuation method scheme.

r_{ext} = external reflux ratio (L_0/D)

V_n = molar flow rate of the vapor leaving stage n.

x_i = value of parameter i of the next pinch point determined by the continuation method

$x_{D,i}$ = mole fraction of chemical component i in the distillate.

$x_{E,i}$ = mole fraction of chemical component i in the extractive feed.

$x_{i,guess}$ = value of parameter i in the initial guess for the next pinch point in the continuation method.

$x_{n,i}$ = mole fraction of chemical component i in the liquid leaving stage n.

$y_{n,i}$ = mole fraction of chemical component i in the vapor leaving stage n.

Greek Letters

$\boldsymbol{\delta}_{n,i}$ = mole fraction of component i in the cascade difference point.

$\gamma_{n,i}$ = activity coefficient of component i on stage n.

ν_i = stoichiometric coefficient of component i

ξ_n = cumulative reaction extent from the top of the column to stage n.

Literature Cited

1. Agreda VH, Partin LR. Reactive distillation process for the production of methyl acetate. U.S. Patent 4,435,595: 1984.

2. Agreda VH, Partin LR, Heise WH. High purity methyl acetate via reactive distillation. Chem. Eng. Prog. 1990;86: 40-46.

3. Knapp JP, Doherty MF. Thermal integration of homogeneous azeotropic distillation sequence. AIChE J. 1990;36: 969-984.

4. Knapp JP, Doherty MF. Minimum entrainer flows for extractive distillation: a bifurcation theoretic approach. AIChE J. 1994;40:243-268.

5. Wahnschafft OM, Westerberg AW. The product composition regions of azeotropic distillation columns. 2. Separability in two-feed columns and entrainer selection. Ind. Eng. Chem. Res. 1993;32:1108-1120.

6. Lelkes Z, Lang P, Benadda B, Moszkowicz P. Feasibility of extractive distillation in a batch rectifier. AIChE J. 1998; 44:810-822.

7. Lee JW. Feasibility studies on quaternary reactive distillation systems. Ind. Eng. Chem. Res. 2002;41:4632-4642.

8. Julka V, Doherty MF. Geometric behavior and minimum flows for nonideal multicomponent distillation. Chem. Eng. Sci. 1990;45:1801-1822.

9. Bausa J, Watzdorf Rv, Marquardt W. Shortcut methods for nonideal multicomponent distillation: 1. Simple columns. AIChE J.1998;44:2181-2198.

10. Reder C, Remme U, Bausa J, Marquardt W. Design of reactive distillation processes using a new shortcut method for minimum-reflux calculation. AIChE Annual Meeting, Miami, November (1998).

11. Hauan S, Ciric AR, Lien KM, Westerberg AW. Difference points in extractive and reactive cascades. I – Basic properties and analysis. Chem. Eng. Sci. 2000;55:3145-3159.

12. Lee JW, Hauan S, Westerberg AW. Feasibility of a reactive distillation column with ternary mixtures. Ind. Eng. Chem. Res. 2001;40:2714- 2728.

13. Song W, Venimadhavan G, Manning JM, Malone MF, Doherty MF. Measurement of residue curve maps and heterogeneous kinetics in methyl acetate synthesis. Ind. Eng. Chem. Res.1998;37:1917-1928.

14. Seydel R, Hlavacek V. Role of continuation in engineering analysis. Chem. Eng. Sci. 1987;42:1281-1295.

15. Seider WD, Brengel DD, Widagdo S. Nonlinear analysis in process design. AIChE J. 1991;37;1-38.

16. Brüggemann S, Marquardt W. Shourtcut methods for nonideal multicomponent distillation: 3. Extractive distillation columns. AIChE J. 2004;50;1129-1149.

17. Andersen HW, Laroche L, Morari M. Effect of design on the operation of homogeneous azeotropic distillation. Comp. Chem. Eng. 1995;19:105-122.

18. Watzdorf Rv, Bausa J, Marquardt W. Shortcut method for non-ideal multicomponent distillation: 2. Complex columns. AIChE J. 1999;45:1615-1628.

19. Lee JW, Brüggemann S, Marquardt W. Shortcut method for kinetically controlled reactive distillation systems. AIChE J. 2003;49:1471-1487.

Chapter 3: Generalized Feasibility Evaluation of Equilibrated Quaternary Reactive Distillation Systems

Reproduced with permission from Ind Eng Chem Res. 2004;43:7092-7102. Copyright 2004 American Chemical Society.

Abstract – This article addresses a general feasibility evaluation method for quaternary reactive distillation based on the feasibility study of isomolar reactions[1]. With an arbitrary reaction stoichiometry and feed ratio, the general algorithm can be applied to evaluating the feasibility of a double-feed reactive distillation column. The feasibility evaluation relies on the desired directions of column composition profiles for reaching pure products or achieving complete reaction conversion without performing rigorous stage calculations. Critical composition regions (CCRs) are defined as the areas where thermodynamic constraints force composition profiles to travel in infeasible directions. After identifying the CCRs, material balance is imposed to determine whether composition profiles can move to desired directions in terms of upper and lower bounds of the internal reflux ratio. If the upper and lower bounds permit composition profiles to approach a desired boundary, then a double-feed column can achieve almost 100% reaction conversion and produce pure products.

1. Introduction

Reactive distillation is the combination of reaction and distillation in a single process unit. The combination of these two operations yields synergistic effects between reaction and distillation. The three main effects[2-4] are: (a) a shift in chemical equilibrium resulting from the simultaneous separation and removal of the products, (b) the

circumvention of phase equilibrium limitations such as azeotropes and distillation boundaries, and (c) the utilization of reaction heat for the separation of educts and products. These synergistic effects give reactive distillation the following advantages over traditional two-step processes: (a) lower capital investment, (b) lower energy consumption, and (c) higher product yields. These benefits make reactive distillation an attractive means for improving process efficiency.

However, before the implementation of reactive distillation technology in any new process, or before the re-engineering of an existing process, we should know whether or not the combination of reaction and distillation could achieve a desired reaction conversion and produce pure products. To answer this question, we need to develop a quick and reliable method for determining feasibility. In previous work[1], we proposed a method to determine the feasibility of quaternary *isomolar* reactive distillation systems in a double feed column under a stoichiometric feed ratio. We evaluated the feasibility of the integration of an isomolar reaction with distillation by introducing the concept of critical composition regions and by enforcing material balance constraints on the reactive middle section of a double-feed column.

The purpose of this work is to generalize this feasibility evaluation method for quaternary reaction systems with arbitrary stoichiometries and reactant feed ratios. To do that, a special emphasis is given to quaternary *non-isomolar* reactive distillation systems with *inerts* since the feed ratios for this type of reaction usually deviate from the stoichiometric ratios (meaning that one of the reactants is provided in excess). Thus, the

methyl *tert*-butyl ether (MTBE) production system will be taken as an example to illustrate the generalized feasibility algorithm.

First, the feasible directions of composition profiles will be discussed in terms of reaching complete reaction conversion and obtaining pure products. Then, the concept of critical composition regions will be explained in terms of the feasible directions of composition profiles. Then, a quick and reliable algorithm will be proposed for checking the feasibility of quaternary reactive systems by using the concept of *the upper and lower bounds of the internal reflux ratios*. These upper and lower reflux ratios will be calculated by associating material balance constraints with the geometry of material balance lines in composition space. The *tert*-amyl methyl ether (TAME) production system will be employed to show the applicability of this method using only chemical and phase equilibrium information.

2. Feasible Directions of Composition Vectors in a Double-Feed Reactive Distillation Column

The schematic of a double-feed reactive distillation column is shown in Figure 3-1. This column has non-reactive rectifying and stripping sections with a reactive middle section in-between the two feed streams. The following liquid-phase reaction occurs in the double-feed reactive distillation column.

$$MT + IC4 \leftrightarrow MTBE \qquad (1)$$

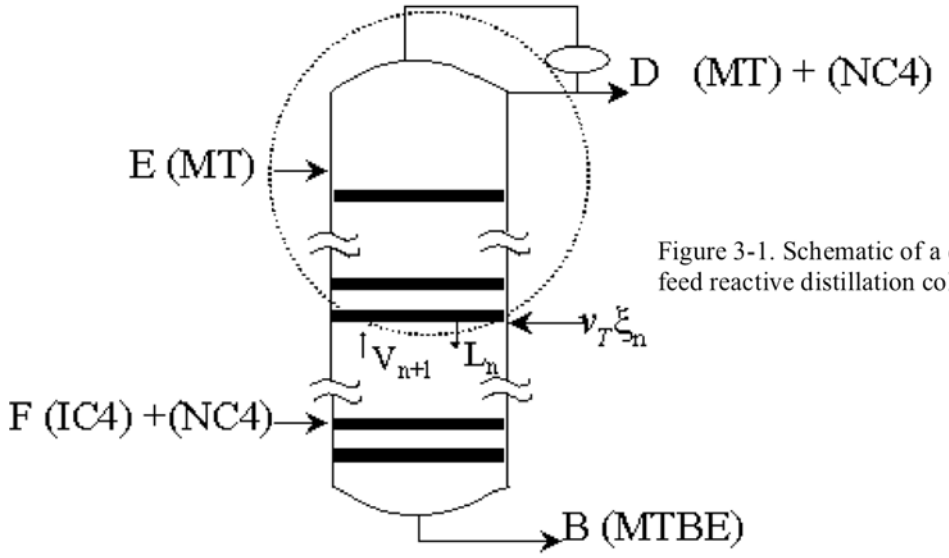

Figure 3-1. Schematic of a double-feed reactive distillation column.

Here MT and IC4, which represent methanol and isobutene respectively, are the two reactants. MTBE (methyl *tert*-butyl ether) is the product and NC4 (n-butene) is an inert component that enters the column with IC4 in the lower feed stream. Here, MT is less volatile than NC4 and IC4. IC4 is the most volatile of the four components. Three binary minimum-boiling azeotropes exist in this system as shown in Figure 3-2: IC4-MT, NC4-MT, and MT-MTBE. The equilibrium data for all systems used in this chapter is collected in the chapter Appendix. The lowest-boiler in the MTBE production system is the IC4-MT azeotrope. MT is supplied in slight excess compared to IC4 in order to achieve higher conversions[5] and, due to its lower volatility, it is fed to the upper feed stage whereas the stream containing IC4 and NC4 is fed to the lower feed stage. Product MTBE is the heaviest component in this system and is recovered at the bottom. Simultaneous reaction and phase equilibria are assumed for the middle reactive section.

A double-feed reactive distillation column can completely convert IC4 *if MT and NC4 are dominantly present at the upper feed stage.* MTBE is the heaviest component

and is not significantly present at the upper feed stage. It is naturally recovered at the bottom. Under this condition, we notice that *the stage composition profiles between the two feed stages must approach the MT-NC4 binary edge* as we follow the composition profiles up through the column. If the binary edge is reached, then this indicates that light reactant IC4 is completely consumed by the reaction. Otherwise unconverted IC4 will appear in the distillate due to the IC4-MT azeotrope (the lowest-boiling composition in the system). Pure product MTBE will always be obtained at the bottom of the column since it is the least volatile component in the system.

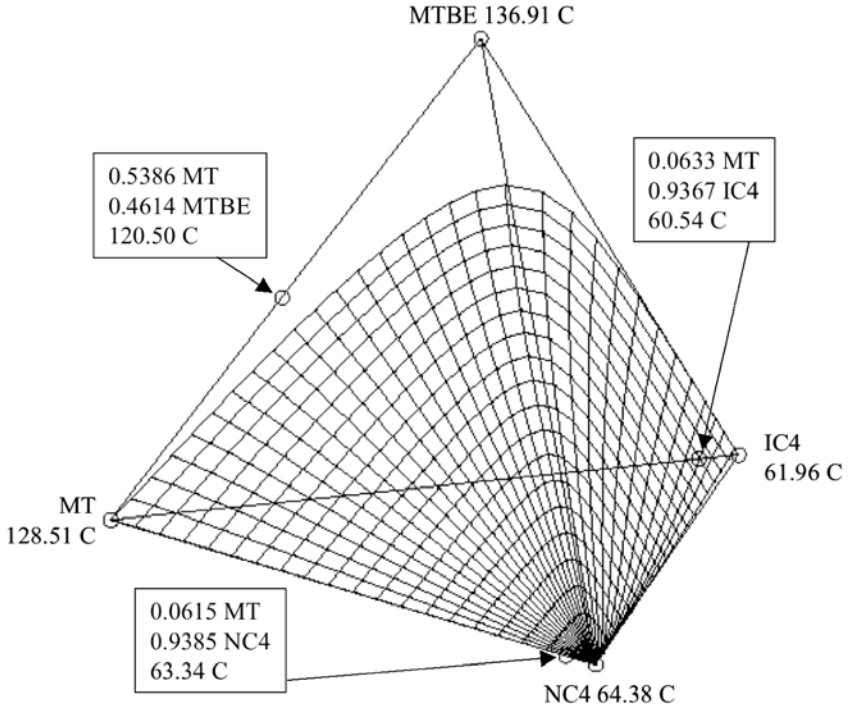

Figure 3-2. Reaction equilibrium surface and azeotropes for the MTBE production system at 8 atm.

One might consider providing excess IC4 to the lower feed stage in an attempt to convert all of the MT in the upper feed stream. However, this can lead to a difficult separation between IC4 and NC4 due to the low relative volatilities[5]. Also, this may not lead to a high reaction conversion of MT since excess IC4 forms the IC4-MT azeotrope

and some of the MT would be recovered at the top without being converted. Therefore, to have higher reaction conversion, excess MT should be used. Then, feasible stage profiles that move up through the middle reactive section will point to the NC4-MT binary edge.

3. Critical Composition Region

In this section, the concept of critical composition regions[1] (CCRs) is revisited. CCRs are quickly determined by using phase and reaction equilibrium data. Because we want the stage column profiles to move in a particular direction (usually towards a particular boundary of composition space), the CCR is defined as the region of liquid phase compositions whose equilibrated vapor compositions lie further away from the desired boundary than the liquid compositions. Those liquid/vapor compositions that are equally far away from the desired boundary are known as critical compositions. How "closer" and "further away" are defined is explained below.

In the MTBE production system, we want all of the IC4 to react before it reaches the upper feed stage. For this reason, the column composition profiles should approach the MT-NC4 binary edge as they approach the upper feed stage. To determine whether or not a vapor composition is closer to that edge than its equilibrated liquid, we calculate and compare the projected compositions. In the MTBE production system, there are two points of projection that we can use: the MT vertex and the NC4 vertex. A projected composition is obtained by drawing a line from the point of projection, through the composition being projected, and extended to the face opposite the point of projection.

This is numerically calculated by taking the original composition, ignoring the component that's acting as the point of projection, and then renormalizing the remaining component fractions so that they add up to one. In other words, dividing each original component fraction by the sum of the non-projecting components. For example, the projected liquid composition (using MT as a point of projection) is calculated as $\tilde{x}_{n,NC4}=x_{n,NC4}/(1-x_{n,MT})$, $\tilde{x}_{n,IC4}=x_{n,IC4}/(1-x_{n,MT})$, and $\tilde{x}_{n,MTBE}=x_{n,MTBE}/(1-x_{n,MT})$. If MT is used as the point of projection, then the closer $\tilde{x}_{n,NC4}$ is to 1, the closer $\boldsymbol{x_n}$ is to the MT-NC4 binary edge. If NC4 is used as the point of projection, then the closer $\tilde{x}_{n,MT}$ is to 1, the closer $\boldsymbol{x_n}$ is to the MT-NC4 binary edge.

To demonstrate the calculations, let us consider the liquid-phase composition, $\boldsymbol{x_n}$ = [0.2, 0.045452, 0.35201, 0.402538] for NC4, IC4, MT and MTBE, respectively. The phase-equilibrated vapor composition is $\boldsymbol{y_n}$ = [0.583449, 0.131292, 0.143469, 0.141791]. To determine if this liquid composition is in the critical composition region, we do two projections. The first is the NC4 projection. To calculate the NC4-projected compositions of the liquid and vapor, we exclude the NC4 fraction and renormalize the other three components. Thus, in the liquid, $\tilde{x}_{n,MT} = x_{n,MT}/(1- x_{n,NC4}) = 0.35201 / (1 – 0.2) = 0.44001$. In the vapor, $\tilde{y}_{n,MT} = y_{n,MT}/(1-y_{n,NC4}) = 0.14347 / (1 – 0.58345) = 0.34442$. This can be done for all three remaining fractions in both phases, so $\tilde{x}_n$ = [0.056815, 0.4400125, 0.5031725] and $\tilde{y}_n$ = [0.31518754, 0.344420384, 0.340392076] for IC4, MT, and MTBE, respectively. For this liquid/vapor composition pair under an

NC4 projection, we find that $\tilde{y}_{n,MT} < \tilde{x}_{n,MT}$, so the vapor is further away from the MT-NC4 binary edge than the liquid as shown in Figure 3-3(a).

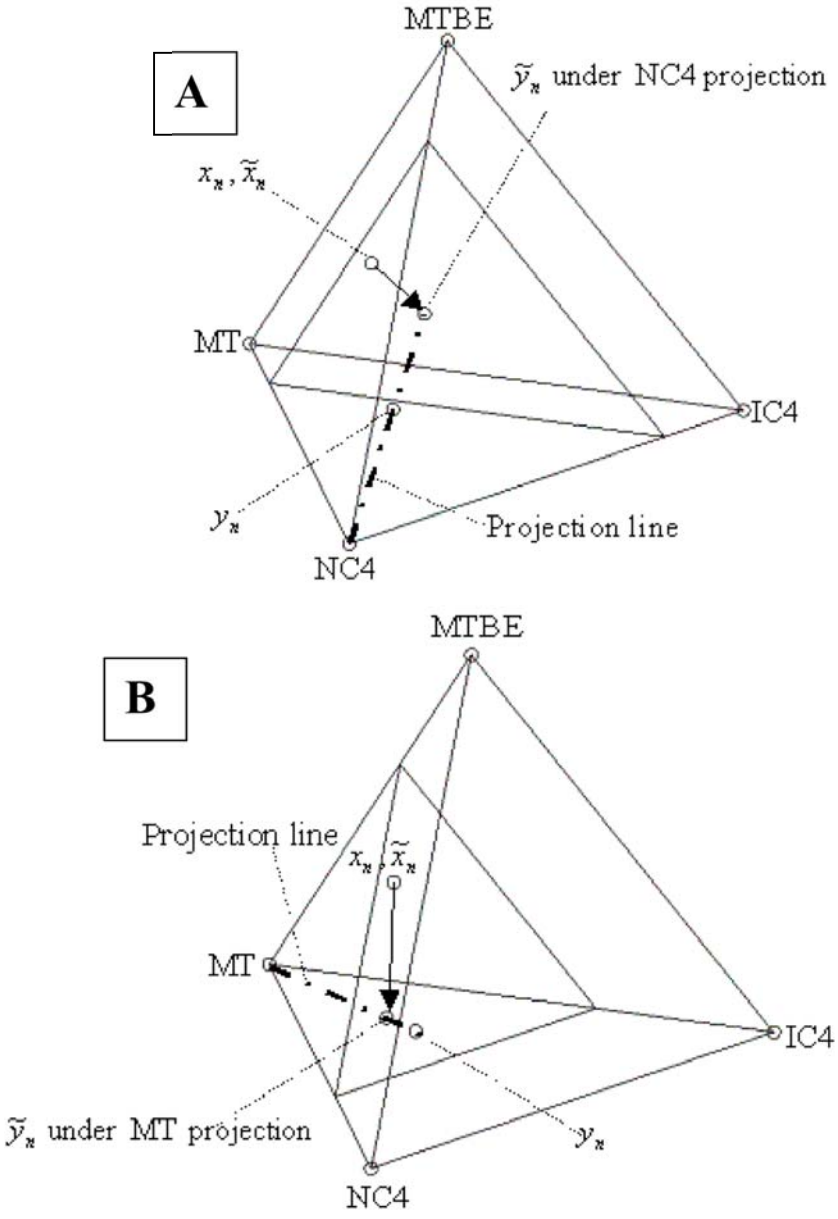

Figure 3-3. Liquid and vapor compositions under two different projections. (a) Infeasible direction under NC4 projection. (b) Feasible direction under MT projection.

However, under the MT projection, we calculate the projected compositions of liquid and vapor as $\tilde{x}_{n,NC4}$ = $x_{n,NC4}/(1-x_{n,MT})$ = 0.2 / (1 – 0.35201) = 0.30865 and $\tilde{y}_{n,NC4}$ = $y_{n,NC4}/(1-y_{n,MT})$ = 0.58345 / (1 – 0.14347) = 0.68118. This can be done for all three non-

projected components in both phases, so $\tilde{x}_n$ = [0.308646738, 0.070143058, 0.621210204] and $\tilde{y}_n$ = [0.681175951, 0.15328324, 0.165540809] for NC4, IC4, and MTBE, respectively. For this liquid/vapor composition pair under a MT projection, we find that $\tilde{y}_{n,NC4} > \tilde{x}_{n,NC4}$, so the vapor is closer to the MT-NC4 binary edge than the liquid as shown in Figure 3-3(b). Even though we cannot approach the NC4-MT binary edge in the NC4 projected space, we can approach that binary edge in the MT projected space. In order to approach this binary edge, the vapor must be closer to the binary edge than the liquid in at least one of the projections. So, the CCR is the set of all points on the reaction equilibrium surface where the projected vapor is further away from the binary edge than the projected liquid in all of the relevant projections (in the MTBE system, there are only two relevant projections: MT and NC4). For the MTBE system, if we do these calculations in both projected spaces for any point on the reaction equilibrium surface, then we notice that the projected vapor is always closer to the binary edge than the projected liquid under a MT projection and, therefore, we can always approach the NC4-MT binary edge. So, no CCR is found for the MTBE system.

Note that there is a significant difference when we compare this with the CCR of the isomolar methyl acetate (MA) production system as shown in Figure 3-4[1]. In the MA production system, a CCR exists in the vicinity of the MA vertex, the MA-MT azeotrope, and part of the MA-AC edge. If the middle reactive section profile enters the CCR, it cannot reach the desired boundary of the MA-AC binary edge as we move up the column. Then, we cannot produce pure MA at the top.

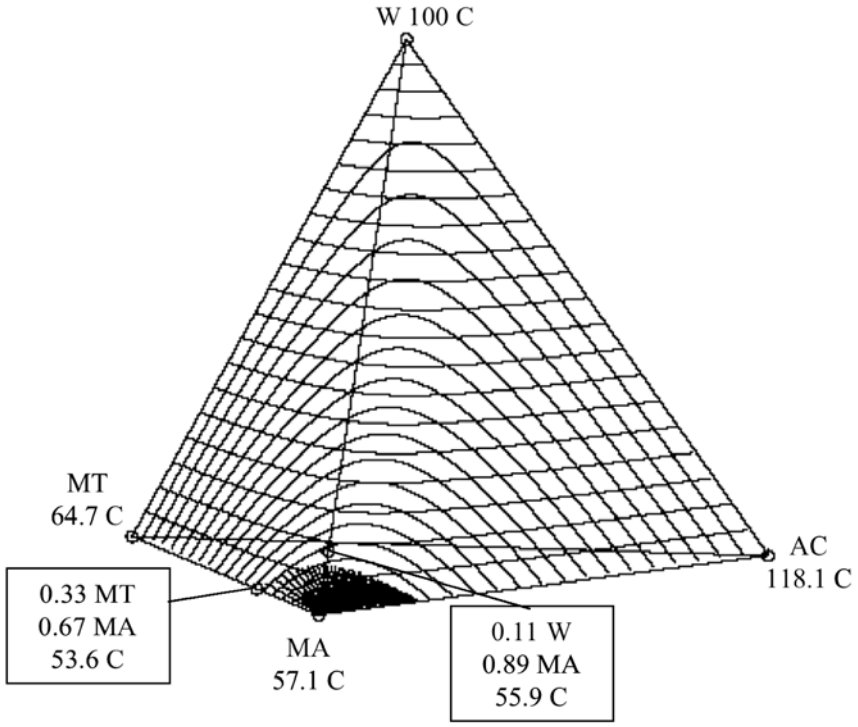

Figure 3-4. Critical composition region (CCR) for the MA production system at 1 atm. Here, the reaction equilibrium surface is for the reaction AC + MT ↔ MA +W.

Here is a summarized procedure for determining CCRs:

Step 1. Using chemical equilibrium data, plot the chemical reaction equilibrium surface in the original composition space as shown in Figure 3-2.

Step 2. For all liquid compositions lying on the chemical reaction equilibrium surface (if the reaction occurs in the liquid phase), calculate their corresponding equilibrated vapor compositions using the phase equilibrium data.

Step 3: Find the set of all liquid compositions on the reaction equilibrium surface where the projected vapor is further away from the desired boundary than the projected liquid (i.e. $\tilde{y}_{n,MT} < \tilde{x}_{n,MT}$ and $\tilde{y}_{n,NC4} < \tilde{x}_{n,NC4}$).

Step 4: Plot all of the liquid compositions found from Step 3 in the original composition space.

4. Material Balance Constraints on Feasibility: Upper and Lower Reflux Ratios

After determining the critical composition region, material balance constraints will be imposed on any equilibrated liquid and vapor compositions ($\boldsymbol{x}_n$ & $\boldsymbol{y}_n$) lying outside the critical composition region. From the material balance constraints of the middle reactive section, we will determine whether any composition profile passing through the chosen liquid or vapor compositions can approach the NC4-MT binary edge. As mentioned in the previous section, this feasibility criterion is based on one important objective: to obtain total conversion of one of the reactants (specifically, IC4). The middle section composition profile should point to the NC4-MT binary edge under a slight excess of MT. Otherwise, unconverted IC4 will appear at the top of the column due to the minimum-boiling IC4-MT azeotrope. The feasibility study can be carried out step-by-step by visualizing the material balance constraints in composition space.

Step 1: Position $\boldsymbol{x}_D$ & $\boldsymbol{x}_E$ in composition space. Here, $\boldsymbol{x}_D$ is the desired distillate composition and lies on the NC4-MT binary edge under an excess MT. $\boldsymbol{x}_E$ is the extractive feed composition. It is pure methanol, so it is located on the MT vertex.

Step 2: Choose an arbitrary position (on the reaction equilibrium surface) for $\boldsymbol{x}_n$ and calculate the corresponding $\boldsymbol{y}_n$. Here $\boldsymbol{x}_n$ is a liquid composition outside the critical

composition region at an arbitrary stage n and $\boldsymbol{y}_n$ is the vapor composition in phase equilibrium with $\boldsymbol{x}_n$.

Step 3: Generate material balance equations that can be used as the basis for drawing material balance lines and representing any quaternary reactive distillation system geometrically.

A total material balance over the envelope shown in Figure 3-1 yields the following equation:

$$V_{n+1} = L_n + D - E - \boldsymbol{\nu}_T \xi_n \qquad (2)$$

where stage numbers are counted from the top.

A component-wise material balance gives

$$V_{n+1}\, \boldsymbol{y}_{n+1} = L_n\, \boldsymbol{x}_n + D\, \boldsymbol{x}_D - E\, \boldsymbol{x}_E - \boldsymbol{\nu}\, \xi_n \qquad (3)$$

Since $\boldsymbol{\nu} = \boldsymbol{\nu}_T \boldsymbol{\delta}_R$, where $\boldsymbol{\delta}_R$ is the reaction difference point[6-8], equation (3) can be rearranged as follows:

$$V_{n+1}\, \boldsymbol{y}_{n+1} = L_n\, \boldsymbol{x}_n + D\, \boldsymbol{x}_D - E\, \boldsymbol{x}_E - \nu_{\boldsymbol{T}}\, \boldsymbol{\delta}_R\, \xi_n \qquad (3)$$

For the *MTBE* production system, $\boldsymbol{\delta}_R$ is given by the coordinates [0, 1, 1, -1] for NC4, IC4, MT, and MTBE, respectively.

Finally equation (4) can be rearranged as follows:

$$V_{n+1}\, \boldsymbol{y}_{n+1} + E\, \boldsymbol{x}_E = L_n\, \boldsymbol{x}_n + (\, D - \nu_{\boldsymbol{T}}\, \xi_n\,)\, \boldsymbol{\delta}_n \qquad (5)$$

$$\rightarrow \boldsymbol{\delta}_n = (\, D\, \boldsymbol{x}_D - \nu_{\boldsymbol{T}}\, \boldsymbol{\delta}_R\, \xi_n\,) \,/\, (\, D - \nu_{\boldsymbol{T}}\, \xi_n\,) \qquad (6)$$

where $\boldsymbol{\delta}_n$ is the cascade difference point [9-11]. This is a geometric and mathematical representation of the combination of the distillate composition and the reaction difference point. It is not a physical quantity and can lie outside the valid composition simplex like

the reaction difference point. However, its location varies according to reaction extents inside the material balance envelope.

For the *MTBE* production system, ν_T = -1–1+1= -1. Hence equations (5) and (6) can be rewritten as follows:

$$V_{n+1}\, \boldsymbol{y}_{n+1} + E\, \boldsymbol{x}_E = L_n\, \boldsymbol{x}_n + (\, D + \xi_n \,)\, \boldsymbol{\delta}_n \qquad (7)$$

$$\rightarrow \boldsymbol{\delta}_n = (\, D\, \boldsymbol{x}_D + \boldsymbol{\delta}_R\, \xi_n \,) / (\, D + \xi_n \,) \qquad (8)$$

Step 4: For given $\boldsymbol{x}_n$ & $\boldsymbol{y}_n$ lying outside the critical composition region, identify important ratios and construct material balance lines in the original composition space (see Figure 3-5) based on the material balance constraints stated in *Step 3*.

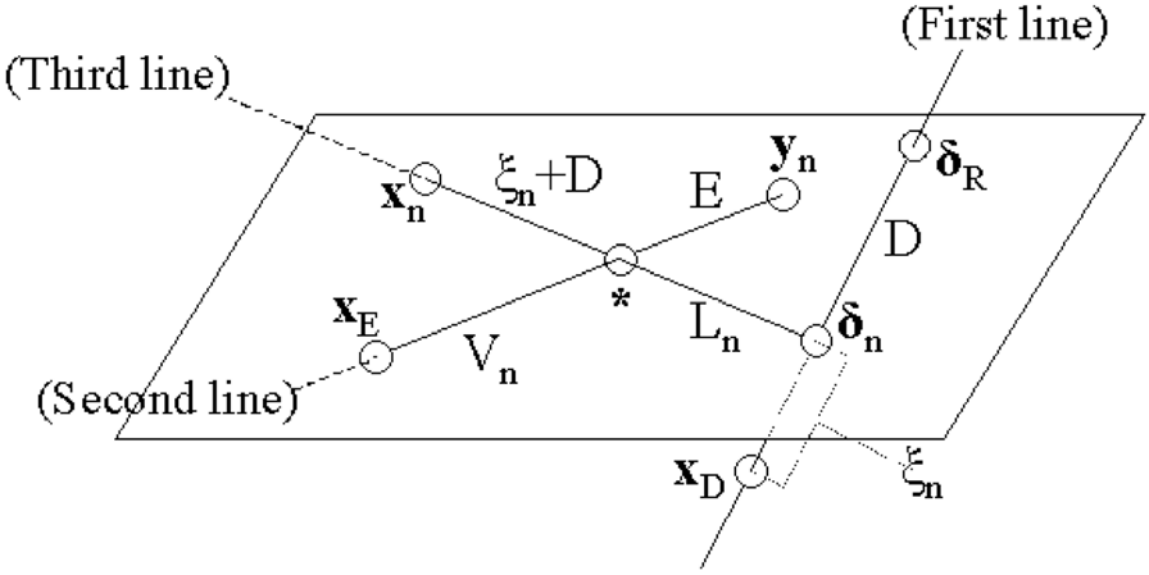

Figure 3-5. Construction of the material balance lines under a pinch assumption.

Assuming pinch conditions, i.e. $\boldsymbol{y}_n = \boldsymbol{y}_{n+1}$, the application of the lever rule on equation (8) tells us that the points $\boldsymbol{\delta}_n$, $\boldsymbol{x}_D$, and $\boldsymbol{\delta}_R$ must lie on a straight line connecting the three points, such that $|\boldsymbol{\delta}_n - \boldsymbol{x}_D| / |\boldsymbol{\delta}_n - \boldsymbol{\delta}_R| = \xi_n / D$. Construct a line passing through the points $\boldsymbol{x}_D$

and $\boldsymbol{\delta}_R$. Let us now draw a second line by connecting $\boldsymbol{x}_E$ and $\boldsymbol{y}_n$. Then, construct a third line passing through $\boldsymbol{x}_n$ such that it intersects the other two lines as shown in Figure 3-5. The intersection between the first and third lines is $\boldsymbol{\delta}_n$. Application of the lever rule in equation (7) tells us that the line connecting the points $\boldsymbol{x}_n$ and $\boldsymbol{\delta}_n$ (the third line) must intersect the line connecting $\boldsymbol{x}_E$ and $\boldsymbol{y}_n = \boldsymbol{y}_{n+1}$ (the second line). Here, we shall refer to this intersection as the combined point. This combined point is denoted by (*) in Figure 3-5.

Two important ratios, $|\boldsymbol{\delta}_n - *|/|* - \boldsymbol{x}_n| = L_n/(\xi_n+D)$ and $|\boldsymbol{x}_E - *|/|* - \boldsymbol{y}_n| = V_n/E$, are derived by constructing the three lines shown in Figure 3-5. The positions of the points (*) and $\boldsymbol{\delta}_n$ are uniquely determined because only one line can be drawn through $\boldsymbol{x}_n$ and the two given lines ($\overline{\boldsymbol{x}_D\ddot{\boldsymbol{a}}_R}$ and $\overline{\boldsymbol{y}_n\boldsymbol{x}_E}$, the first and second lines referred to, respectively). The geometric verification for the uniqueness of the points (*) and $\boldsymbol{\delta}_n$ is given in Appendix 1. For the determined position of $\boldsymbol{\delta}_n$ in Figure 3-5, the ξ_n/D ratio is fixed by equation (7). The $L_n/(\xi_n+D)$ ratio is also fixed for the determined (*) and $\boldsymbol{\delta}_n$ in Figure 3-5. From these two ratios, the internal reflux ratio L_n/D is fixed as a result since $L_n/(\xi_n+D)$ can be rewritten as $(L_n/D)/(\xi_n/D+1)$.

It must be understood that all of the material balance lines and their corresponding ratios were drawn as shown in Figure 3-5 under the assumption of a pinch situation. Thus, except for pinch points, our assumption is not true, so we need to determine where $\boldsymbol{y}_{n+1}$ can possibly lie. To determine this, we should investigate in what direction the composition vectors must move to satisfy the material balance constraints. This

investigation is carried out in the next step. Before doing that let us call the geometrically calculated ratio of $|\boldsymbol{x}_E - *|/|* - \boldsymbol{y}_n| = (V_n/E)_G$. The subscript 'G' denotes that the ratio is geometrically determined for the given $\boldsymbol{x}_n$ & $\boldsymbol{y}_n$.

Step 5: For any $\boldsymbol{x}_n$ & $\boldsymbol{y}_n$ which are not pinched, we manipulate the position of $\boldsymbol{y}_{n+1}$ in the composition space for fixed positions of the points (*) and $\boldsymbol{\delta}_n$ until the material balance constraints are satisfied.

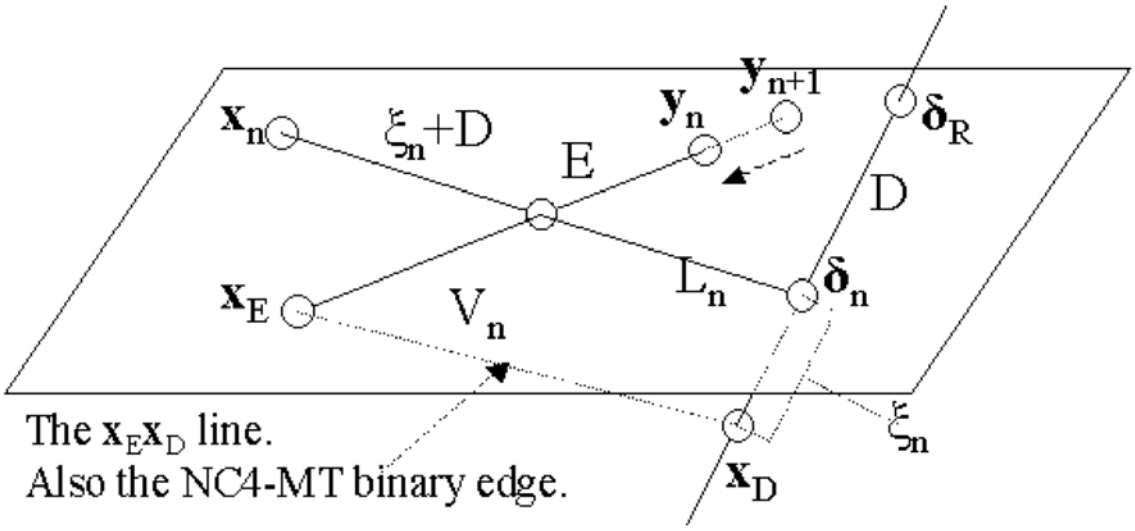

Figure 3-6. Determination of possible $\mathbf{y}_{n+1}$ for non-pinch situations.

Rearranging equation (2), which is the total material balance equation, we get the following relation:

$$V_{n+1}/E = \left[\left(L_n/D\right)\left(D/E\right) + D/E - 1 - \nu_T\left(\xi_n/D\right)D/E\right] \qquad (9)$$

In equation (9) the ratios of L_n/D and ξ_n/D can be easily evaluated from geometry for fixed $\boldsymbol{x}_n$, (*), and $\boldsymbol{\delta}_n$. Moreover if the E/D ratio is known, then we can easily determine the value of the ratio V_{n+1}/E.

If the calculated value of the ratio V_{n+1}/E in equation (9) is less than the geometrically calculated value of the ratio $(V_n/E)_G$, then that implies that the point $\boldsymbol{y}_{n+1}$ lies further away from the MT-NC4 binary edge than $\boldsymbol{y}_n$ as shown in Figure 3-6. Therefore, the vapor composition at stage n is closer to the MT-NC4 binary edge than the vapor composition at stage n+1. This is necessary for the system to be feasible since the composition vectors must move to the MT-NC4 binary edge while going up the column from stage n+1 to stage n. On the other hand, if $V_{n+1}/E > (V_n/E)_G$, then the point $\boldsymbol{y}_{n+1}$ lies closer to the MT-NC4 binary edge than $\boldsymbol{y}_n$. This tells us that the vapor composition in the column at stage n lies farther away from the MT-NC4 binary edge than the vapor composition at stage n+1. So, column profiles would head away from the binary edge while going from stage n+1 to stage n. Therefore, this is an infeasible direction. So, the feasibility criteria can be written mathematically in the form of an inequality as follows:

$$(V_{n+1}/E)\,(\text{Calculated Analytically}) \le (V_n/E)_G\,(\text{Calculated Geometrically}) \qquad (10)$$

Here the equality is conserved for pinch points. Inserting equation (9) into equation (10), equation (10) becomes

$$\lfloor (L_n/D) \le (V_n/E)_G (E/D) - 1 + (E/D) + \nu_T (\xi_n/D) \rfloor \qquad (11)$$

Equation (11) is the generalized feasibility condition applicable to *isomolar* ($\nu_T = 0$) and *non-isomolar* ($\nu_T \neq 0$) reactions for any value of the ratio *E/D*. In equation (11), the L.H.S is called the *lower bound* of the reflux ratio whereas the R.H.S is called the *upper bound* of the reflux ratio. For given $\boldsymbol{x}_n$ and $\boldsymbol{y}_n$, the actual internal reflux ratio will lie between these upper and lower bounds.

For an isomolar reaction with a stoichiometric feed ratio (E/D = 1), we can obtain the condition of $L_n/D \leq (V_n/E)_G$ from equation (11) as already used for the feasibility condition of isomolar reaction systems[1]. For the non-isomolar *MTBE* production system (ν_T = -1), equation (11) can be rewritten as follows:

$$\left[(L_n / D) \leq (V_n / E)_G (E / D) - 1 + (E / D) - (\xi_n / D)\right] \qquad (12)$$

Equation (12) is the feasibility condition for the *MTBE* production system and other ether production systems.

A similar exercise can be carried out for a different situation where the points $\boldsymbol{y}_n$, (*), and $\boldsymbol{\delta}_n$ are fixed. In this case, we should manipulate the position of $\boldsymbol{x}_{n-1}$ until the material balance is satisfied. Equation (11) can also be derived for this case and the detailed derivation is given in Appendix 2.

Special case for no intersection in step 5:

One remarkable feature of the MTBE system is that there is a region of points next to the NC4-MT binary edge where the material balance lines do not intersect under a pinch assumption. In this case, we have a situation like the one shown in Figure 3-7. Here, we can extend the $\overline{\boldsymbol{x}_E \boldsymbol{y}_n}$ line segment to find the combined point, *, on the $\overline{\boldsymbol{x}_n \boldsymbol{\delta}_n}$ line segment and calculate the lower bound. However, since the combined point does not lie on the line segment $\overline{\boldsymbol{x}_E \boldsymbol{y}_n}$, we cannot calculate the upper bound. We can, however, determine feasibility by noting that $\mathbf{y}_{n+1}$ must lie at a position such that $\overline{\boldsymbol{x}_E \boldsymbol{y}_{n+1}}$ *does*

intersect $\overline{x_n \delta_n}$ to satisfy the material balance. When that observation is made, it then becomes clear that $\mathbf{y}_{n+1}$ must lie further away from the binary edge than $\boldsymbol{y}_n$. Therefore, column profiles passing through positions of $\boldsymbol{x}_n$ where this is the case can always approach the binary edge regardless of what the lower bound is. So, in cases where we have this kind of a failure-to-intersect, we treat the upper bound as infinite. All points near the NC4-MT binary edge exhibit this behavior.

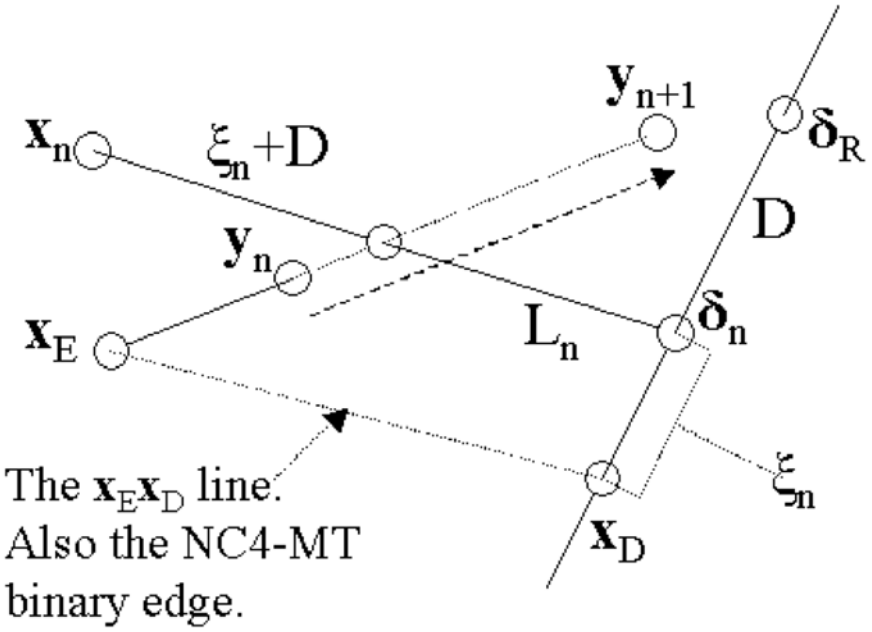

Figure 3-7. Determination of $\mathbf{y}_{n+1}$ when the material balance lines do not intersect under a pinch assumption.

It should be noted that there are additional variations on situations where the material balance lines do not intersect under a pinch assumption (not all of them feasible cases like the case above), and these are treated in detail in Appendix 3.

Step 6: Find the upper and lower bounds of the reflux ratios using equation (12) with an equilibrium pair ($\boldsymbol{x}_n$ and $\boldsymbol{y}_n$) at a characteristic point next to the MT-NC4 edge. The shaded region in Figure 3-8 is the region on the reaction equilibrium surface where the

upper bounds are greater than the lower bounds. Next, check for the existence of a continuous set of points whose reflux ratio ranges overlap the upper bound/ lower bound reflux range at the selected characteristic point. For a composition profile to move to the MT-NC4 binary edge from any given point in the shaded region, the internal reflux ratio range evaluated at that point should overlap the reflux ratio range at the characteristic point[1]. If there exists a continuous region of points that have upper/lower bounds overlapping the upper/lower bound range at the characteristic point near the MT-NC4 binary edge, then the MTBE production system is feasible to consume IC4 completely. At all candidates of characteristic points near the MT-NC4 binary edge, the upper and lower bounds of reflux ratios are almost infinite and zero, respectively, as shown in Figure 3-7 (and Figure 3-15 in Appendix 3). This reflux ratio range can include any reflux ratio range found in the feasible shaded region in Figure 3-8 so that, from any point within that shaded region, composition profiles can move towards the MT-NC4 binary edge. Thus, we can conclude that the MTBE production system can feasibly achieve a complete conversion of IC4 under excess MT.

In order to confirm our conclusion about the MTBE production system, we have simulated this system using rigorous tray-by-tray calculations employing a material and energy balance and specified external reflux ratios. Several middle-section reactive profiles with arbitrary starting points were generated at each of three different external reflux ratios (2.0, 5.0, and 7.0). The simulated profiles for an external reflux ratio of 2.0 are shown as thick curves in Figure 3-8. The liquid and vapor compositions on each stage of each middle section profile were taken and feasibility calculations were

performed on them in order to determine the corresponding upper and lower bounds of the reflux ratios. These upper and lower bounds were then compared with the actual internal reflux ratios calculated from the rigorous simulation results. The rigorously calculated reflux ratios always remained between the upper and lower bounds of the internal reflux ratios. Figure 3-9 shows the actual reflux ratio and the upper and lower bounds for the longest profile shown in Figure 3-8. The upper bound increases to infinity and the lower bound decreases to zero as the profile approaches the binary edge. Thus, the range between the upper and lower reflux ratios at the upper feed stage overlaps with other reflux ratio ranges at the lower stages.

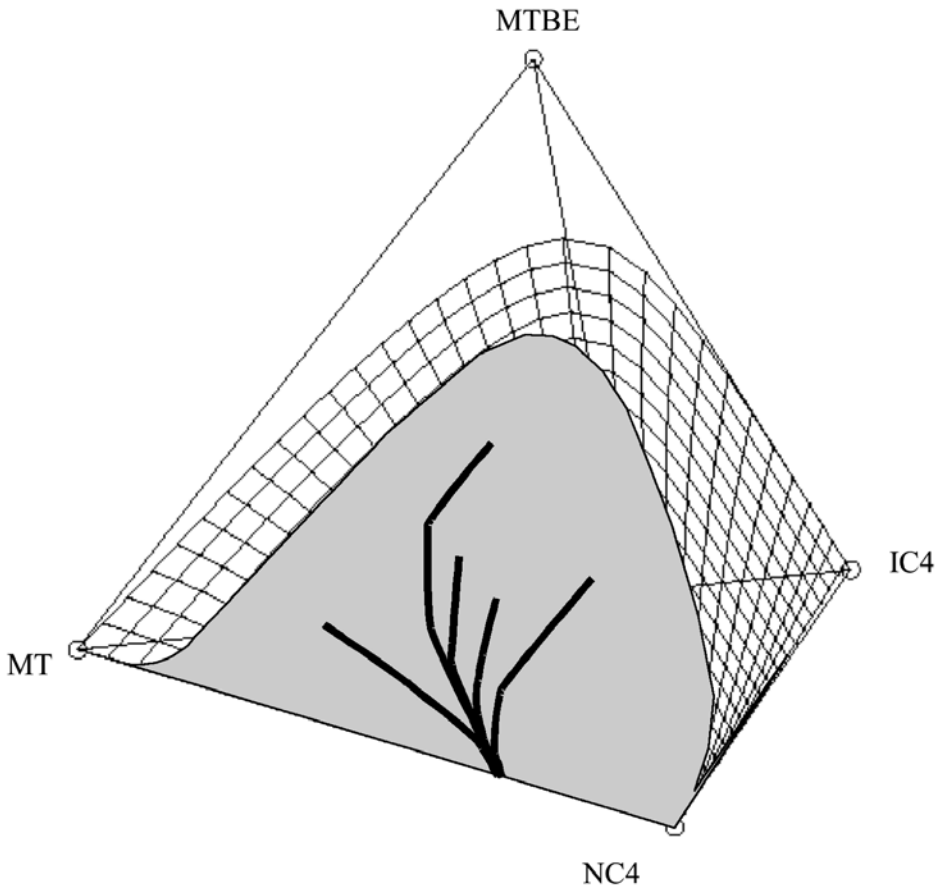

Figure 3-8. Shaded region where the upper bounds are greater than the lower bounds for the MTBE production system. Several rigorously calculated composition profiles are shown.

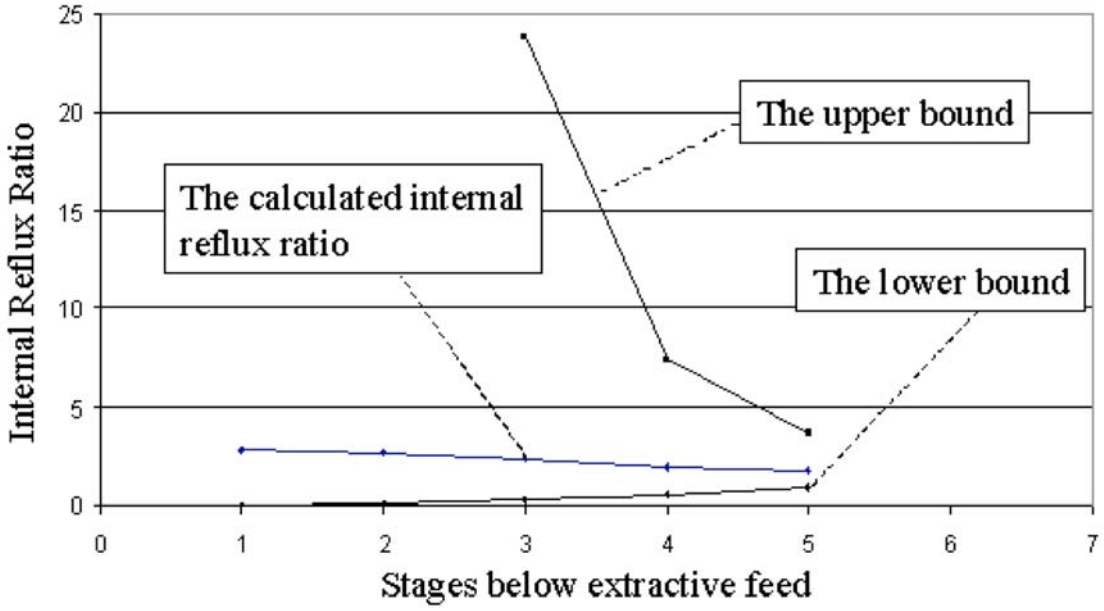

Figure 3-9. Actual internal reflux ratios with upper and lower bounds for one of the composition profiles shown in Figure 3-8.

Feasible column composition profiles must travel through the region where the upper bounds are greater than the lower bounds in order to approach the binary edge. This region is bounded by points where the upper bounds are equal to the lower bounds. Since the upper bounds are equal to the lower bounds only at pinch points, this region is therefore bounded by the pinch point trajectory. This region is also bound by the MT-NC4 binary edge and provides a clear path for feasible column composition profiles to approach the MT-NC4 binary edge.

5. Generalization of Feasibility Evaluation Algorithm

A general procedure for evaluating the feasibility of quaternary double-feed reactive distillation systems is summarized based on the two previous sections as shown in Figure 3-10.

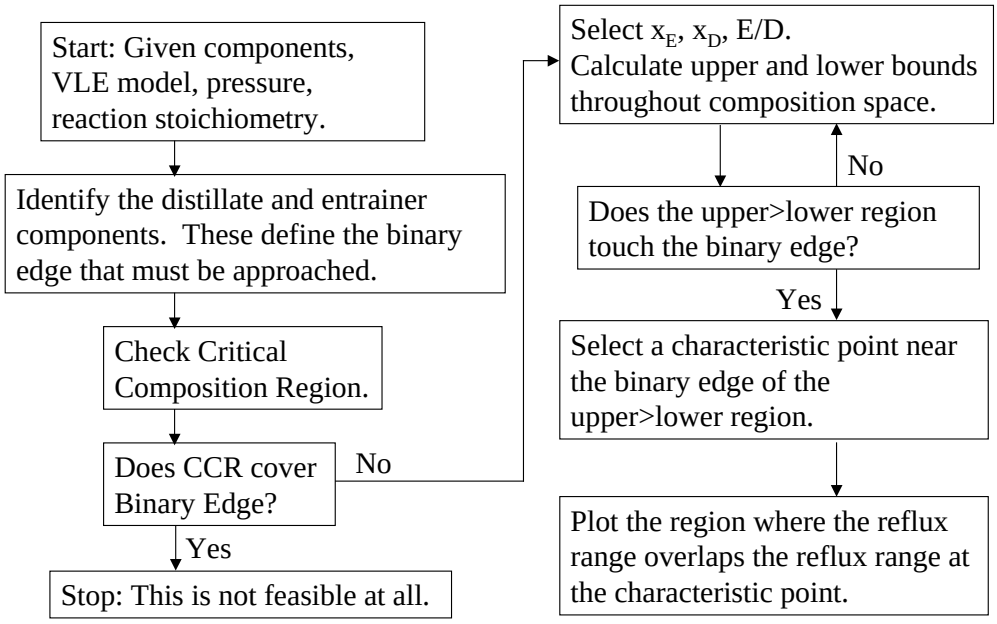

Figure 3-10. Summary flowsheet for determining the feasibility of quaternary double-feed reactive distillation.

First, it will be determined in what direction column composition profiles should travel to reach desired products and/or to achieve complete reaction conversion. For example, in the non-reactive extractive distillation, this means that composition profiles should move to the binary edge connecting a heavy extractive agent and a desired light product[12-14]. In the same sense, to produce pure product MA in the distillate and to achieve nearly complete reaction conversion in the MA reactive distillation system, the upper feed stage composition must lie on the AC-MA binary edge[1]. For MTBE production, the composition at the upper feed stage should be on the NC4-MT binary

edge because it is desired to completely convert IC4. Here, MTBE is the least volatile component and thus can be always recovered with high purity at the bottom.

Once the desired direction is identified, critical composition regions can be determined from phase and reaction equilibrium data. In the MA production system, any given liquid composition on the reaction equilibrium manifold is included in the critical composition region if $\tilde{y}_{AC} < \tilde{x}_{AC}$ under a MA projection and $\tilde{y}_{MA} < \tilde{x}_{MA}$ under an AC projection. Similarly, for the MTBE production system, a liquid composition on the reaction equilibrium manifold is included if $\tilde{y}_{MT} < \tilde{x}_{MT}$ under a NC4 projection and $\tilde{y}_{NC4} < \tilde{x}_{NC4}$ under a MT projection.

After determining the critical composition region, the upper and lower bounds of the internal reflux ratios (r_{nU} & r_{nL}) are calculated by choosing a characteristic point preferably near the desired destination of the middle section composition profiles (e.g.: near the NC4-MT edge for the MTBE case and near the MA-AC edge for the MA case). Once a characteristic point is selected, a continuous set of liquid compositions is plotted where the ranges of $r_{nU} \sim r_{nL}$ overlaps the range evaluated at the characteristic point. If this continuous region exists, then composition profiles can approach the desired binary edge and a column can feasibly produce pure products with a high reaction conversion.

6. Application of the Feasibility Algorithm to *Tert*-Amyl Methyl Ether (TAME) Reactive Distillation System

The following reaction describes the production of TAME.

$$MT + 2MB2 \leftrightarrow TAME \qquad (13)$$

Here MT, 2MB2, and TAME represent methanol, 2-methyl-2-butene, and *tert*-amyl methyl ether respectively. 3-methyl-1-butene (3MB1) is an inert impurity that enters with 2MB2. Here, MT is less volatile than 2MB2 and MT is supplied in slight excess compared to 2MB2 in order to achieve higher conversions. MT enters the upper feed stage whereas the stream containing 2MB2 and 3MB1 is fed to the lower feed stage. The product TAME is the least volatile component and is recovered at the bottom.

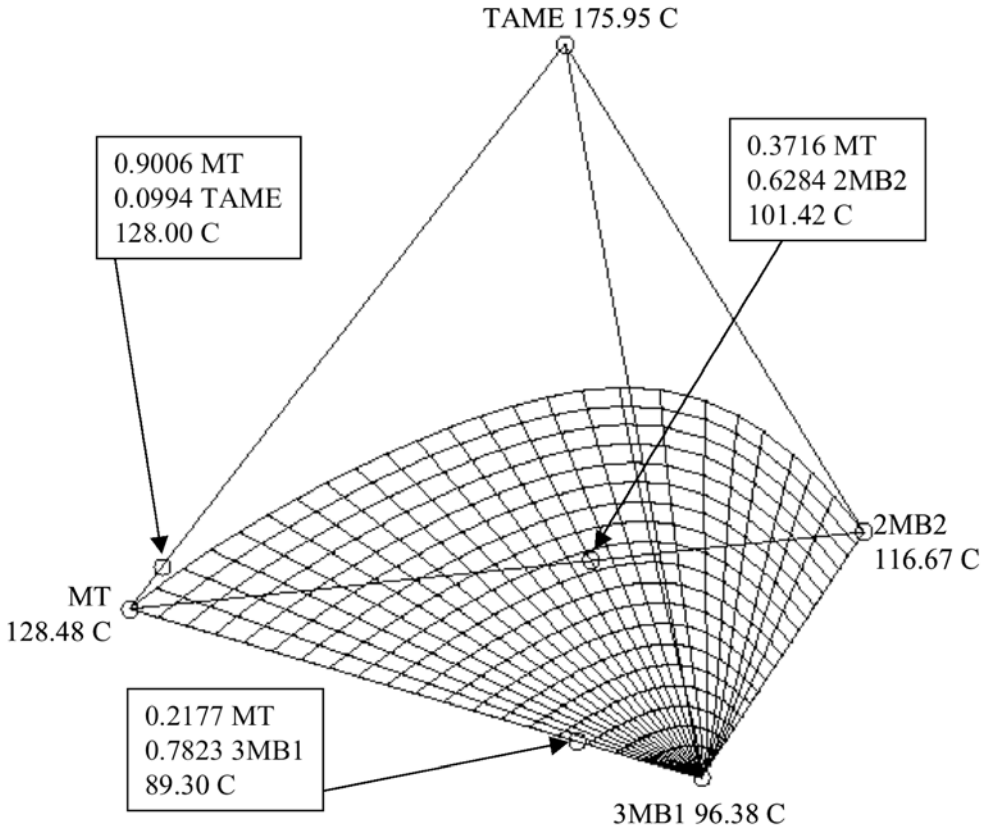

Figure 3-11. Reaction equilibrium surface and azeotropes for the TAME production system at 8 atm.

There are three minimum boiling binary azeotropes in this reaction mixture, as shown in Figure 3-11: MT-2MB2, MT-3MB1, and MT-TAME. In the TAME production system, a double-feed reactive distillation column can achieve a complete conversion of 2MB2 under an excess of MT if MT and 3MB1 are dominantly present at the upper feed stage. In other words, we want the composition profiles to approach the MT-3MB1 binary edge as we move up the column. Approaching this binary edge indicates that reactant 2MB2 is completely consumed by the reaction ensuring almost 100% conversion and that the heaviest component, TAME, is completely recovered at the bottom.

The critical composition region for the TAME production system is determined by enforcing the conditions $\tilde{y}_{MT} < \tilde{x}_{MT}$ under a 3MB1 projection and $\tilde{y}_{3MB1} < \tilde{x}_{3MB1}$ under a MT projection. No points on the reaction equilibrium surface meet the second condition for the TAME system, so no CCR exists for this system.

The upper and lower bounds are calculated in the same manner as for the MTBE system. For given extractive feed and distillate compositions, the material balance lines are drawn and the upper and lower bounds are calculated on the reaction equilibrium surface. Figure 3-12 shows the region where the upper bounds are greater than the lower bounds. This region is bounded by the MT-3MB1 binary edge, the 3MB1-2MB2 binary edge, and the pinch point trajectory. It includes most of the reaction equilibrium surface. The upper and lower bounds in the TAME production system show the same behavior near the MT-3MB1 binary edge as the upper and lower bounds in the MTBE system. Namely, that as column composition profiles approach that binary edge, the upper bounds

increase until the material balance lines fail to intersect under a pinch assumption. The lines fail to intersect in such a way that the upper bounds must again be taken as infinite. Thus, for a characteristic point near the binary edge, all points in the feasible region have an upper/lower bound range that overlaps the range at the characteristic point. So, it is possible to have nearly complete conversion of 2MB2 and to produce pure TAME at the bottom.

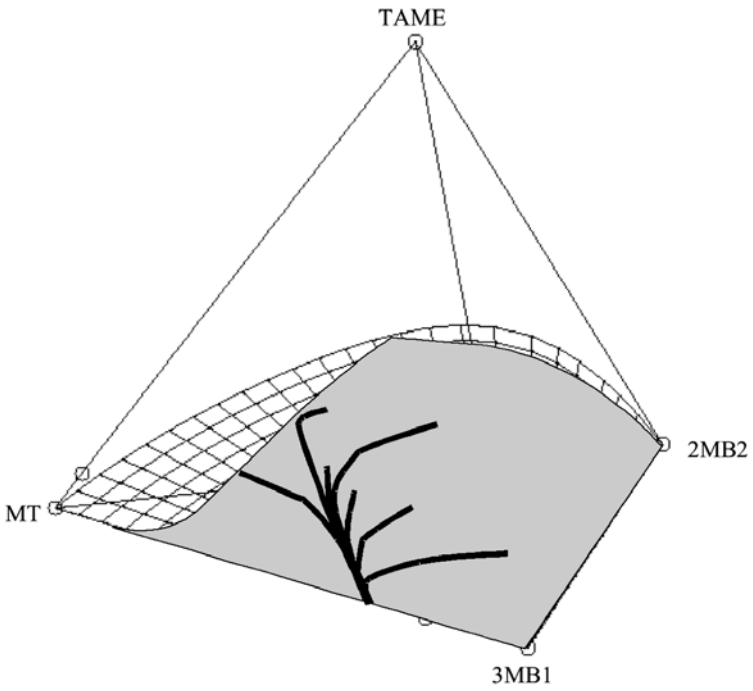

Figure 3-12. Shaded region where the upper bounds are greater than the lower bounds for the TAME production system. Several rigorously calculated composition profiles are shown.

Conclusion

A quick and reliable method has been developed for determining the feasibility of non-isomolar reactive distillation systems. The critical composition region (CCR) shows where the combination of reaction and distillation is thermodynamically infeasible. This CCR is determined by calculating the projected compositions of phase-equilibrated

liquid-vapor composition pairs; If the projected liquid is closer to the desired boundary of composition space than the projected vapor in all of the relevant projections, then that liquid composition is in the critical composition region. The upper and lower bounds of reflux ratios show where the combination of reaction and distillation is feasible for given upper feed stream and distillate stream compositions and a given entrainer/distillate flow ratio. If there exists an extended region of points in composition space where the upper bounds are greater than the lower bounds at each point *and* the upper/lower bound range at each point overlaps the upper/lower bound range near the binary edge, then feasible column composition profiles may approach the desired boundary of composition space. This will ensure nearly 100% reaction conversion and the production of pure products.

Acknowledgement

J.W.L. is grateful for the partial support of the Professional Staff Congress City University of New York (PSC-CUNY) and the donors of the Petroleum Research Fund, administered by the American Chemical Society. J.W.L. is also thankful to Prof. Marquardt at RWTH (Aachen, Germany) for his permission to use the DREIECK visualization code.

Nomenclature

D = molar flow rate of the distillate stream

E = molar flow rate of the entrainer

L_n = molar flow rate of the liquid stream leaving stage n

r_{nL} = lower bound of the internal reflux ratio at stage n

r_{nU} = upper bound of the internal reflux ratio at stage n

V_n = molar flow rate of the vapor stream leaving stage n

$(V_n/E)_G$ = ratio geometrically determined in Figure 3-5

$\mathbf{x}_D$ = molar composition of the distillate stream

$\mathbf{x}_E$ = molar composition of the entrainer feed

$\mathbf{x}_n$ = molar composition of the liquid on an arbitrary stage n.

$\tilde{x}_n$ = molar projected-composition of the liquid on stage n.

$x_{n,i}$ = mole fraction of component i in the liquid on stage n

$\tilde{x}_{n,i}$ = fraction of component i in the projected liquid composition

$\mathbf{y}_n$ = molar composition of the vapor on stage n. $\mathbf{y}_n$ is always in phase equilibrium with $\mathbf{x}_n$

$\tilde{y}_n$ = molar projected-composition of the vapor on stage n.

$y_{n,i}$ = mole fraction of component i in the vapor on stage n

$\tilde{y}_{n,i}$ = mole fraction of component i in the projected vapor composition

Greek Letters

$\boldsymbol{\delta}_n$ = cascade difference point defined in equation (6)

$\boldsymbol{\delta}_R$ = reaction difference point, defined as $\boldsymbol{\nu}/\nu_T$

ξ_n = accumulated reaction turnover from the top to stage n

$\boldsymbol{\nu}$ = stoichiometric vector for the reaction being conducted

ν_i = stoichiometric coefficient of component i

ν_T = sum of the stoichiometric coefficients

Abbreviations

2MB2 = 2-methyl-2-butene

3MB1 = 3-methyl-1-butene

AC = acetic acid

IC4 = isobutene

MA = methyl acetate

MT = methanol

MTBE = methyl *tert*-butyl ether

NC4 = n-butene

TAME = *tert*-amyl methyl ether

W= water

Appendix 3-1: Reaction and phase equilibrium data

The Wilson equation is used for the calculations of the liquid activity coefficients and also estimated by Aspen Plus. The Wilson parameters are estimated as $\Lambda_{ij} = \exp(a_{ij} + b_{ij}/T)$, where $\Lambda_{ii} = 1$. Antoine equation is $\ln(P^{sat}) = A + B/[C+T]$ where pressure is in Pa and temperature is in Kelvin.

Table 3-1. Wilson Binary Parameters for the MTBE System

Component i	Component j	a_{ij}	a_{ji}	b_{ij}	b_{ji}
NC4	IC4	0.0	0.0	59.00019320	-72.18223610
NC4	MT	0.0	0.0	-339.2808290	-791.1722050
NC4	MTBE	0.0	0.0	94.13483790	-192.3888110
IC4	MT	-0.8412	0.8412	-56.7519	-1219.9069
IC4	MTBE	0.0	0.0	-342.5077	208.5720
MT	MTBE	1.0725	-1.0725	-752.2975	223.7027

Table 3-2. Antoine Equation Coefficients for the MTBE System

Component	A	B	C
NC4	21.2936	-2531.47	-8.256
IC4	20.64556	-2125.74886	33.160
MT	23.49989	-3643.31362	-33.434
MTBE	20.71616	-2571.58460	-48.406

Table 3-3. Wilson Binary Parameters for the TAME System

Component i	Component j	a_{ij}	a_{ji}	b_{ij}	b_{ji}
3MB1	2MB2	0.0	0.0	-59.03506880	45.56520210
3MB1	MT	0.0	0.0	-433.6785880	-729.4326730
3MB1	TAME	0.0	0.0	79.59217960	-167.9853990
2MB2	MT	-0.9555	0.9555	-247.6993	-1036.0654
2MB2	TAME	0.0	0.0	67.9151	-127.456
MT	TAME	0.0	0.0	-278.9775	-298.7962

Table 3-4. Antoine Equation Coefficients for the TAME System.

Component	A	B	C
3MB1	20.6065	-2331.488	-36.503
2MB2	20.9339	-2588.859	-36.55
MT	23.4927	-3638.2606	-33.65
TAME	62.342	-5911.70	0.0*

* For TAME, the extended Antoine equation ($A+B/(T+C) +D +E\ln(T) + F10^{G}T^{H}$) is used with D=0.0, E = -5.8464, F = 1.6141, G= -17, and H=6.

The temperature-dependent reaction equilibrium constants for the MTBE and TAME are used from the literature[15-16]. The equilibrium data for the MA acetate production system were obtained from Song et al. (1998)[17].

Appendix 3-2: Uniqueness for the Line Intersecting Two Lines in a Skew Position

The geometric verification for the uniqueness of the combined point (*) and δ_n makes the assertion that for two given lines that are skew to one another and a given point that is not on either line, there is at most one line that passes through the given point and both given lines. This geometric proof is carried out using the following principles: that two non-parallel planes in a 3-space must intersect at a straight line and that a plane can be defined by a line and a point not on that line. Given the above, we can easily construct a plane in composition space as shown in Figure 3-13. On the basis of the above definition

let us draw a plane (P1), which includes $\boldsymbol{x}_n$ and the line connecting the points $\boldsymbol{y}_n$ and $\boldsymbol{x}_E$ (L1). Let us draw another plane (P2) containing $\boldsymbol{x}_n$ and the difference point trajectory (L2). The line $\overline{x_n x^* \delta_n}$ (L3) must intersect the $\overline{y_n x_E}$ line, so L3 must lie on plane P1. Similarly, the line L3 must intersect the cascade difference point trajectory, so L3 must lie on plane P2. It can be clearly seen as shown in Figure 3-13 that, because L3 must lie on both planes P1 and P2, L3 must be the intersection of those two planes. The two planes intersect at a unique line, therefore L3 is unique. L3 intersects L1 and L2 at the combined point (*) and the cascade difference point $\boldsymbol{\delta}_n$, respectively, and hence these two points are uniquely determined.

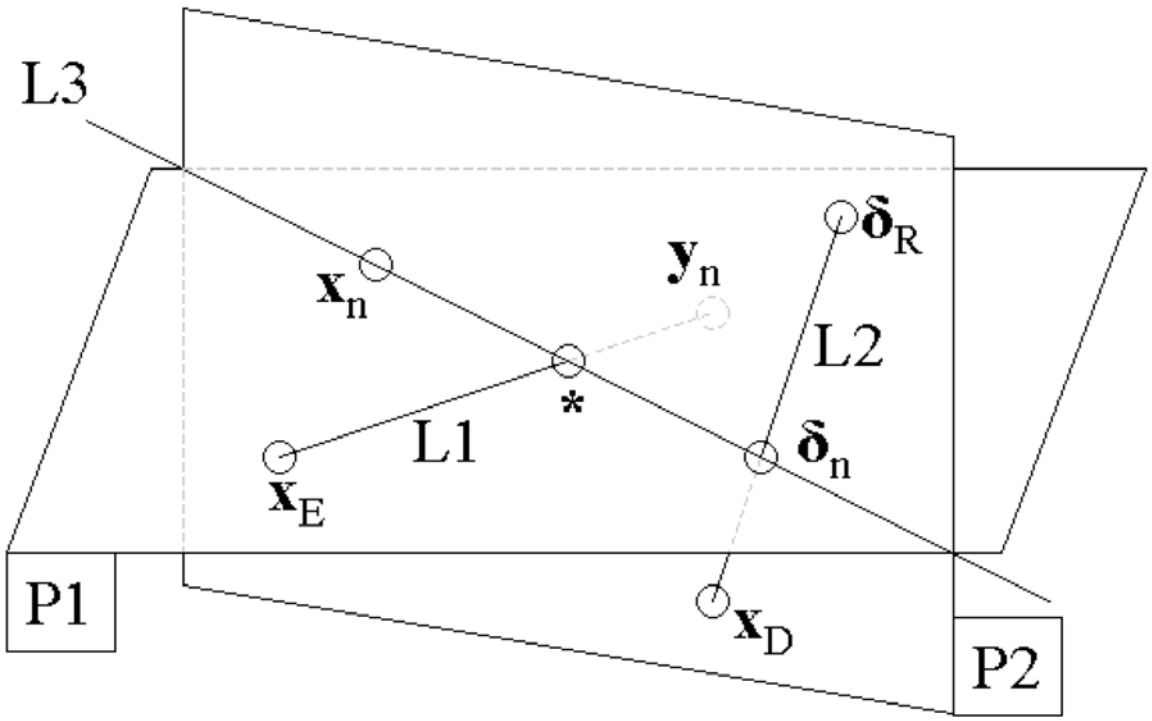

Figure 3-13. Uniqueness for the line intersecting two lines in a skew position for non-isomolar reaction.

Thus we have shown geometrically, the uniqueness for line L3 intersecting the two lines L1&L2, which are skew to each other in the original composition space.

Appendix 3-3: Derivation of Equation (11) for fixed y_n, (*), and δ_n

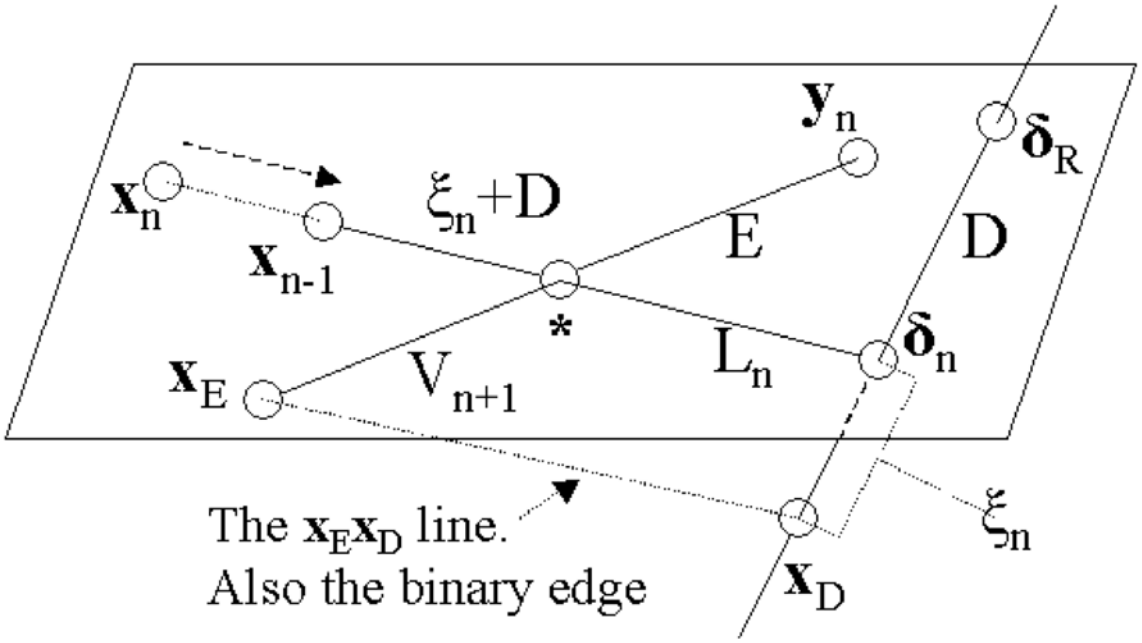

Figure 3-14. Determination of possible $\mathbf{x}_{n-1}$ for non-pinch situations.

Let us now consider the case where the points $\boldsymbol{y}_n$, (*), and $\boldsymbol{\delta}_n$ are fixed in the original composition space. Once these points are fixed, the ratio of $L_n/(\xi_n+D)$ is fixed and can be easily calculated from geometry, thus the ratios ξ_n/D & L_n/D are also fixed. Then, the ratio L_{n-1}/D can be calculated from the following material balance equation:

$$L_{n-1} = V_n + E - D + v_T\xi_n \tag{14}$$

Dividing equation (14) throughout by $(D+\xi_n)$ gives the following equation:

$$L_{n-1} / (D + \xi_n) = (V_n/E)_G [(E / D) / (1 + \xi_n / D)] + (E / D) / (1 + \xi_n / D)$$
$$- 1 / (1 + \xi_n / D) + v_T [(\xi_n / D) / (1 + \xi_n / D)] \tag{15}$$

In equation (15) the ratios of $(V_n/E)_G$ and ξ_n/D can be easily evaluated from geometry. Moreover if the E/D ratio is known, we can easily determine the ratio, $L_{n-1}/(\xi_n+D)$.

If the analytically calculated value of the ratio $L_{n-1}/(D+\xi_n)$ is less than the geometrically calculated value of the ratio $L_n/(D+\xi_n)$, then it implies that the point $\boldsymbol{x}_{n-1}$ lies further away from the MT-NC4 binary edge than the point $\boldsymbol{x}_n$. This implies that the liquid composition at stage n is closer to the MT-NC4 binary edge than the liquid composition at stage n-1, from which we can conclude that the system is not feasible.

On the other hand, if $L_{n-1}/(D+\xi_n) > L_n/(D+\xi_n)$, then it implies that the point $\boldsymbol{x}_{n-1}$ lies closer to the MT-NC4 binary edge than the point $\boldsymbol{x}_n$ as shown in Figure 3-14. This tells us that the liquid composition in the column at stage n lies farther away from the MT-NC4 binary edge than the liquid composition at stage n-1 and hence proving that this is a feasible condition.

Therefore the feasibility criteria can be written mathematically in the form of an inequality as follows:

$\left(L_{n-1}/(D+\xi_n)\right)$ (Calculated analytically) $\geq \left(L_n/(D+\xi_n)\right)$(Calculated geometrically) (16)

Substituting equation (14) into equation (16), we get the following equation:

$$(V_n/E)_G\,[\,(E/D)/(1+\xi_n/D)\,] + (E/D)/(1+\xi_n/D) - 1/(1+\xi_n/D) + v_T\,[(\xi_n/D)/(1+\xi_n/D)\,] \geq L_n/(D+\xi_n) \quad (17)$$

The above equation can be rearranged to

$$L_n/D \leq (V_n/E)_G\,(E/D) - 1 + (E/D) + v_T\,(\xi_n/D) \quad (18)$$

Equation (18) is exactly identical to equation (11). The L.H.S of equation (18) is called the *lower bound* of the reflux ratio and the R.H.S is called the *upper bound* of the reflux

ratio. One should note that these lower and upper reflux ratios are identical at a pinch point.

Appendix 3-4: Cases where the material balance lines do not intersect

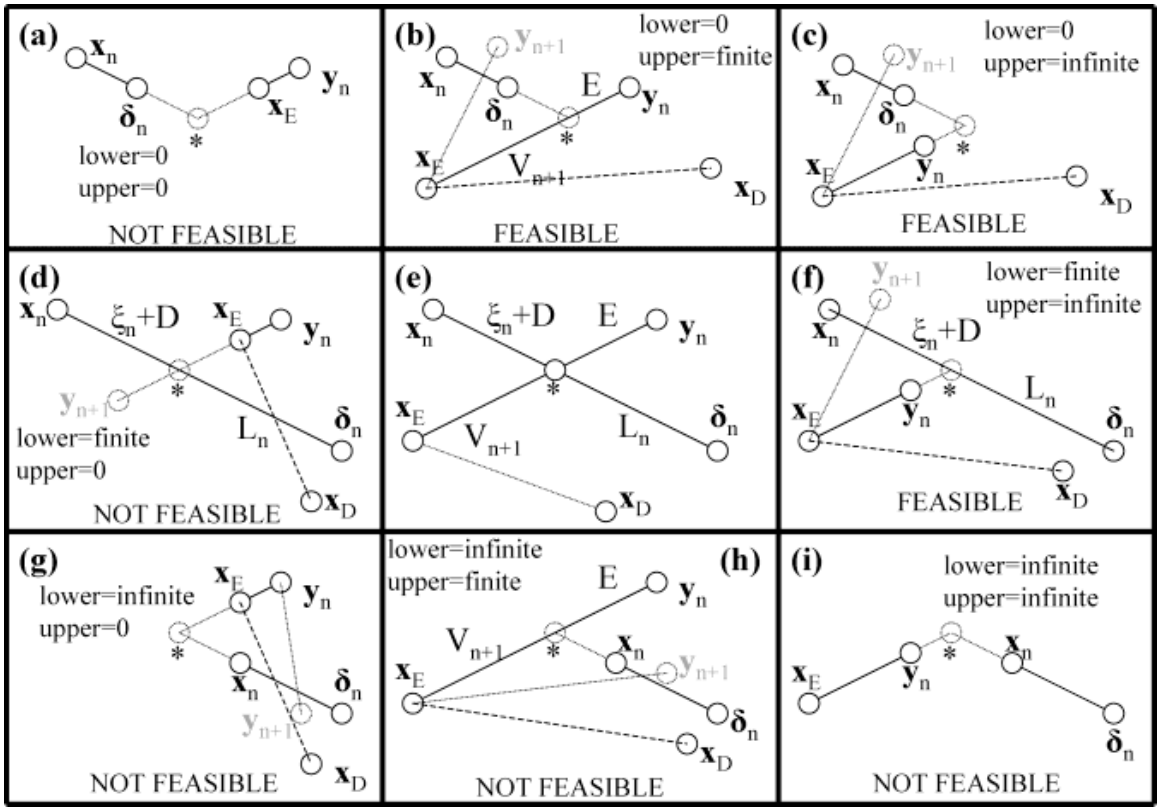

Figure 3-15. All types of intersection of material balance lines for given phase equilibrium points.

To calculate the upper and lower bounds, we make a pinch assumption (specifically, that $\mathbf{y}_n = \mathbf{y}_{n+1}$), draw the material balance lines, find the combined point, *, and calculate the ratios from the lengths of the line segments. However, phase equilibrium behavior can result in cases where these material balance lines don't intersect. In these cases, we remember that $\boldsymbol{\delta}_n$ is chosen such that it lies on the same plane as $\mathbf{x}_n$, $\mathbf{y}_n$, and $\mathbf{x}_E$ and that any lines drawn using these four points must also lie on the same plane. Thus, we can always extend $\overline{\mathbf{x}_n\boldsymbol{\delta}_n}$ and $\overline{y_n x_E}$ such that they do intersect.

There are then three sets of cases to consider for extending $\overline{\mathbf{x}_n\boldsymbol{\delta}_n}$ as shown:

1) The combined point, *, does not lie in-between $\mathbf{x}_n$ and $\boldsymbol{\delta}_n$, but rather has moved out of that segment past $\boldsymbol{\delta}_n$. In these cases, L_n has been reduced to zero and the lower bound becomes zero. This is shown in the top row of Figure 3-15, cases (a), (b), and (c).

2) The combined point, *, lies in-between $\mathbf{x}_n$ and $\boldsymbol{\delta}_n$, so we can calculate the lower bound normally. This is shown in the middle row of Figure 3-15, cases (d), (e), and (f).

3) The combined point, *, does not lie in-between $\mathbf{x}_n$ and $\boldsymbol{\delta}_n$, but rather has moved out of that segment past $\mathbf{x}_n$. In these cases, ξ_n+D has been reduced to zero and the lower bound becomes infinite. This is shown in the bottom row of Figure 3-15, cases (g), (h), and (i).

There are similarly three sets of cases to consider for $\overline{\boldsymbol{y}_n\boldsymbol{x}_E}$:

1) The combined point, *, does not lie in-between $\mathbf{y}_n$ and x_E, but rather has moved out of that segment past $\mathbf{x}_E$. In these cases, V_n has been reduced to zero and the upper bound becomes zero. This is shown in the left column of Figure 3-15, cases (a), (d), and (g).

2) The combined point, *, lies in-between $\mathbf{y}_n$ and $\mathbf{x}_E$, so we can calculate the upper bound normally. This is shown in the left column of Figure 3-15, cases (b), (e), and (h).

3) The combined point, *, does not lie in-between $\mathbf{y}_n$ and $\mathbf{x}_E$, but rather has moved out of that segment past y_n. In these cases, E has been reduced to zero and the upper bound becomes infinite. This is shown in the left column of Figure 3-15, cases (c), (f), and (i).

The above two trends are independent of one another and form a matrix of nine cases, as shown in Figure 3-15. Case (e) represents the typical case where the material balance lines do intersect under a pinch assumption as shown in Figure 3-5. There are eight types

of abnormal cases where there is no intersection between the material balance lines and an intersection must be obtained by extending one (or both) of the material balance lines.

Cases (b), (c), and (f) of Figure 3-15 are the three abnormal cases that are considered feasible. In these cases, the lower bound is either zero or finite and the upper bound is either finite or infinite. Here, we can compare the upper and lower bounds and we can see that the upper bounds are greater than the lower bounds.

Cases (d), (g), and (h) of Figure 3-15 are the three abnormal cases that are considered infeasible. In three of these cases, the lower bound is either finite or infinite and the upper bound is zero or finite. Here, we can compare the upper and lower bounds and we can see that the lower bounds are greater than the upper bounds.

In the last two abnormal cases, both the upper and lower bounds are zero in case (a) and both the upper and lower bounds are infinite in case (i). Here, we cannot make any sensible comparisons between the upper and lower bounds and we can say nothing about the feasibility. However, when drawing the region where upper bounds are greater than the lower bounds, we have treated these cases as being infeasible.

Literature cited

1. Lee JW. Feasibility studies on quaternary reactive distillation systems. *Ind Eng Chem Res*. 2002;41:4632-4642.

2. Doherty MF, Buzad G. Reactive Distillation by Design. *Trans. Inst. Chem. Eng.* 1992;70:448.

3. Taylor R, Krishna R. Modelling reactive distillation. *Chem Eng Sci.* 2000;55:5183-5229.

4. Malone MF, Doherty MF. Reactive distillation. *Ind Eng Chem Res*. 2000;39:3953-3957.

5. Degarmo JL, Parulekar VN, Pinjala V. Consider Reactive Distillation. *Chem. Eng. Prog.* 1992;88(3):43.

6. Hauan, S.; Omtveit, T.; Lien, K.M. Analysis of Reactive Separation Systems. paper 5f, AIChE Annual Meeting 1996, Chicago, Nov., 1996.

7. Hauan S, Westerberg AW, Lien KM. Phenomena based analysis of fixed points in reactive separation systems. *Chem. Eng. Sci.*, 2000;55:1053-1075.

8. Stichlmair, J. G.; Fair, J. R. *Distillation: Principle and Practice*; Wiley-VCH: New York, 1998.

9. Hauan S, Ciric AR, Westerberg AW, Lien KM. Difference points in extractive and reactive cascades. I - Basic properties and analysis. *Chem. Eng. Sci.* 2000;55(16):3145-3159.

10. Lee JW, Hauan S, Lien KM, Westerberg AW. Difference points in extractive and reactive cascades. II - Generating design alternatives by the lever rule for reactive systems. *Chem. Eng. Sci.* 2000;55(16):3161-3174.

11. Lee JW, Hauan S, Westerberg AW. Feasibility of a reactive distillation column with ternary mixtures. *Ind. Eng. Chem. Res.* 2001;40:2714-2728.

12. Knapp JP, Doherty MF. Minimum entrainer flows for extractive distillation: a bifurcation theoretic approach. *AIChE J*. 1994;40:243-268.

13. Lelkes Z, Lang P, Benadda B, Moszlowicz P. Feasibility of extractive distillation in a batch rectifier. *AIChE J.* 1998;44:810-822.

14. Westerberg AW, Wahnschafft OM. Synthesis of Distillation-Based Separation Systems. *Adv. Chem. Eng.* 1996;23:63.

15. Venimadhavan G, Buzad G, Doherty MF. Effects of Kinetics on Residue Curve Maps for Reactive Distillation. *AIChE J.* 1994;39:169.

16. Rihko LK, Krause AO. Kinetics of Heterogeneously Catalyzed *tert*-Amyl Methyl Ether Reactions in the Liquid Phase. *Ind. Eng. Chem. Res.* 1995;34:1172.

17. Song W, Venimadhavan G, Manning JM, Malone MF, Doherty MF. Measurement of residue curve maps and heterogeneous kinetics in methyl acetate synthesis. *Ind. Eng. Chem. Res.* 1998;37:1917-1928.

Chapter 4: Feasible Products in Complex Batch Reactive Distillation

Reproduced with permission from AIChE Journal. 2006;52:1790). Copyright 2006 American Institute of Chemical Engineers.

Abstract - This paper presents a new feasibility evaluation procedure for reactive mixtures where simple homogeneous reactive batch columns cannot produce pure products. Such columns are not feasible for producing pure products if no node products exist that are reachable by residue curves from the reaction equilibrium manifold. We present three alternatives here. If an unstable node heterogenous azeotrope decants to an almost-pure product *and* that azeotrope is always reachable from the reaction equilibrium manifold, then a batch reactive rectifier can produce pure products with a decanter. If a homogenous entrainer allows extractive section profiles to connect the reaction equilibrium manifold to an entrainer-product binary edge, then a homogenous batch reactive extractive distillation (BRED) column can produce pure product. If these criteria are not met, then an entrainer that induces an unstable node heterogenous azeotrope between itself and one of the products should be used in a rectifier, a middle-vessel column, or a BRED column.

Introduction

Reactive distillation has become an attractive process technology in recent years because of the potential reductions in capital costs, operating costs, and environmental impacts. In particular, reactive distillation can be used to conduct processes that would be prohibitively complicated and unwieldy if handled in a conventional process consisting solely of many single-operation units. This is because of two thermodynamic

advantages in carrying out reaction and separation simultaneously rather than sequentially[1-2]: 1) Phase separation can overcome reaction equilibrium limitations and 2) chemical reaction can circumvent phase equilibrium limitations such as azeotropes and distillation boundaries. The Eastman Chemical process for producing methyl acetate is a prime example of the benefits of reactive distillation[3-5]. However, it is not a widely applied technology primarily because most of the commercial reactive distillation processes in use today were developed in a trial-and-error manner with little understanding of how reaction and separation phenomena interact when performed in the same piece of equipment.

Batch production systems are commonly used in the small-scale production of pharmaceuticals, fine chemicals, and specialty chemicals. Batch distillation systems have the advantages of low capital costs, considerable flexibility, the ability to separate multiple components from a single column, being easy to handle, being easy to perform quality control checks on, and usually being able to accept a wide range of feed compositions.

Various studies have been conducted regarding the operating policies and parameters for batch distillation systems[6-8] and batch extractive distillation systems[9-14]. There have been many feasibility studies on non-reactive batch distillation that use residue curve maps (RCMs) to determine feasible product cuts[10,13,15-18]. There have also been studies into the operating policies[19-20], simulation[21], and reaction selectivities[22] of batch reactive distillation systems.

However, little attention has been paid to the feasibility study of reactive batch distillation. As a result of this, it has rarely been understood under what conditions simultaneous reaction and V-L separation can lead to the production of pure products. Before performing numerous experiments and simulations, we want to answer this feasibility question by using the relatively simple information of equilibrium data. In our previous work[23], we determined the following thermodynamic feasibility criteria for simple batch reactive distillation with reactions of the form aK+bI↔ cL+dH or bI ↔ cL +dH:

1. With an unstable node (UN) product that is reachable from the entire reaction equilibrium curve by simple distillation, a batch rectifier with a reactive pot can produce pure products regardless of the number of azeotropes or their dynamic properties. A symmetric result is obtained in a batch stripper with a stable node (SN).
2. If the products are an UN and a SN and share the same distillation region as a part of the reaction equilibrium curve, then pure products can be produced in a batch reactive middle-vessel column (MVC).

Even though the above feasibility criteria apply to a wide range of azeotropic mixtures, there are many phase equilibrium systems that do not meet the criteria listed above for simple batch reactive columns (rectifier, stripper, MVC) that is shown in Figure 4-1. If there is no node product that is always reachable from the reaction equilibrium curve, then pure products cannot be produced in rectifiers, strippers, or MVC columns. This can happen under any one of the following circumstances: 1) if both products are nodes of the same type (both unstable or both stable), 2) if one of the products is a saddle and a

distillation boundary separates the products, and 3) if both products are saddles with or without bounded distillation regions.

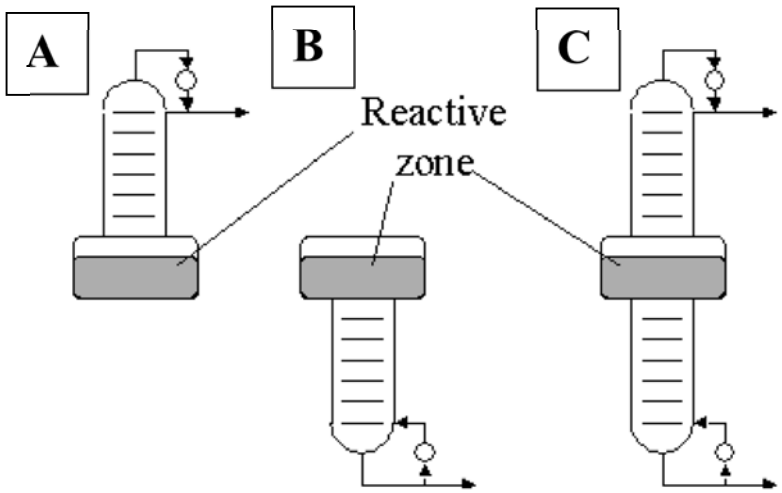

Figure 4-1: Simple batch column structures. (a) Rectifier (b) Stripper (c) MVC

In this work, we will first introduce phase equilibrium systems where pure products cannot be produced in the simple batch reactive columns and will show why these columns do not work. To explore the possibility of producing pure products in these systems, we will introduce three alternatives: reactive rectifier with a decanter, homogeneous BRED column, and heterogeneous BRED column (i.e. BRED with a decanter). For the two types of BRED, we will introduce the new concept of *projected* upper and lower bounds of reflux ratios with the thermodynamically infeasible region (critical composition region (CCR)[24-25]). We will propose new feasibility criteria by using internal heterogeneity and by using external homogeneous and heterogeneous agents. Some actual reactive systems will be used to highlight our new feasibility studies.

Homogeneous Reactive Rectifiers, Strippers, and Middle-Vessel Columns

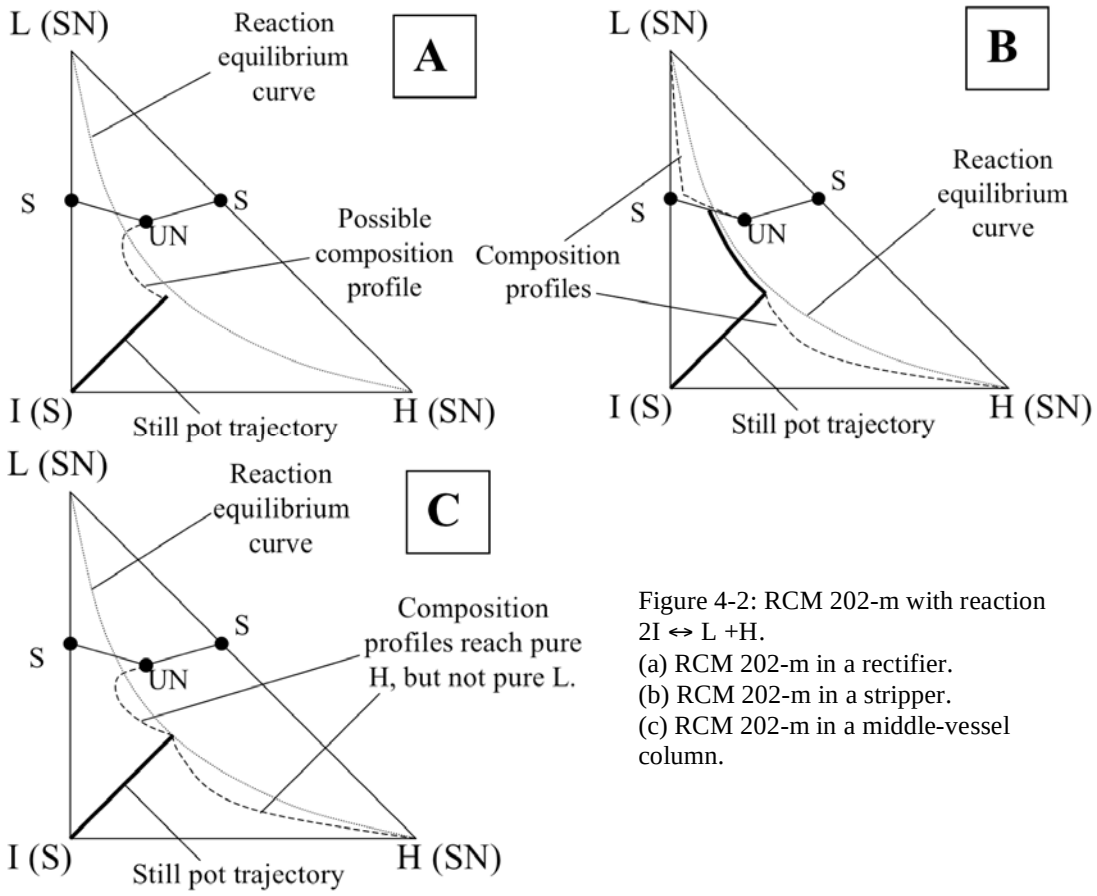

Figure 4-2: RCM 202-m with reaction $2I \leftrightarrow L + H$.
(a) RCM 202-m in a rectifier.
(b) RCM 202-m in a stripper.
(c) RCM 202-m in a middle-vessel column.

In this section, we will examine cases where reactive systems do not meet the feasibility criteria of reactive rectifiers, strippers, or MVCs. A 202-m system (according to Matsuyama and Nishimura's classification[26]) is shown in Figure 4-2. Suppose a reaction of the form $bI \leftrightarrow cL + dH$ where product L forms two minimum boiling saddle (S) azeotropes with product H and reactant I, and there is an unstable node (UN) ternary azeotrope. Products H and L are stable nodes (SNs) that are separated by a distillation boundary. This system is not feasible in a batch reactive rectifier because none of the reaction products are UNs as shown in Figure 4-2a. It is not feasible in a batch reactive stripper because, while the products are both stable nodes, the distillation boundary cuts

across the reaction equilibrium curve (regardless of the value of the reaction equilibrium constant). Thus, pure product would be produced at the bottom only until the still pot composition crossed the distillation boundary; thereafter, a different bottoms composition would be obtained (Figure 4-2b). Batch reactive middle vessel columns cannot produce pure products as the products are separated by a distillation boundary and column profiles can't lead to both product vertices from a still pot composition (Figure 4-2c).

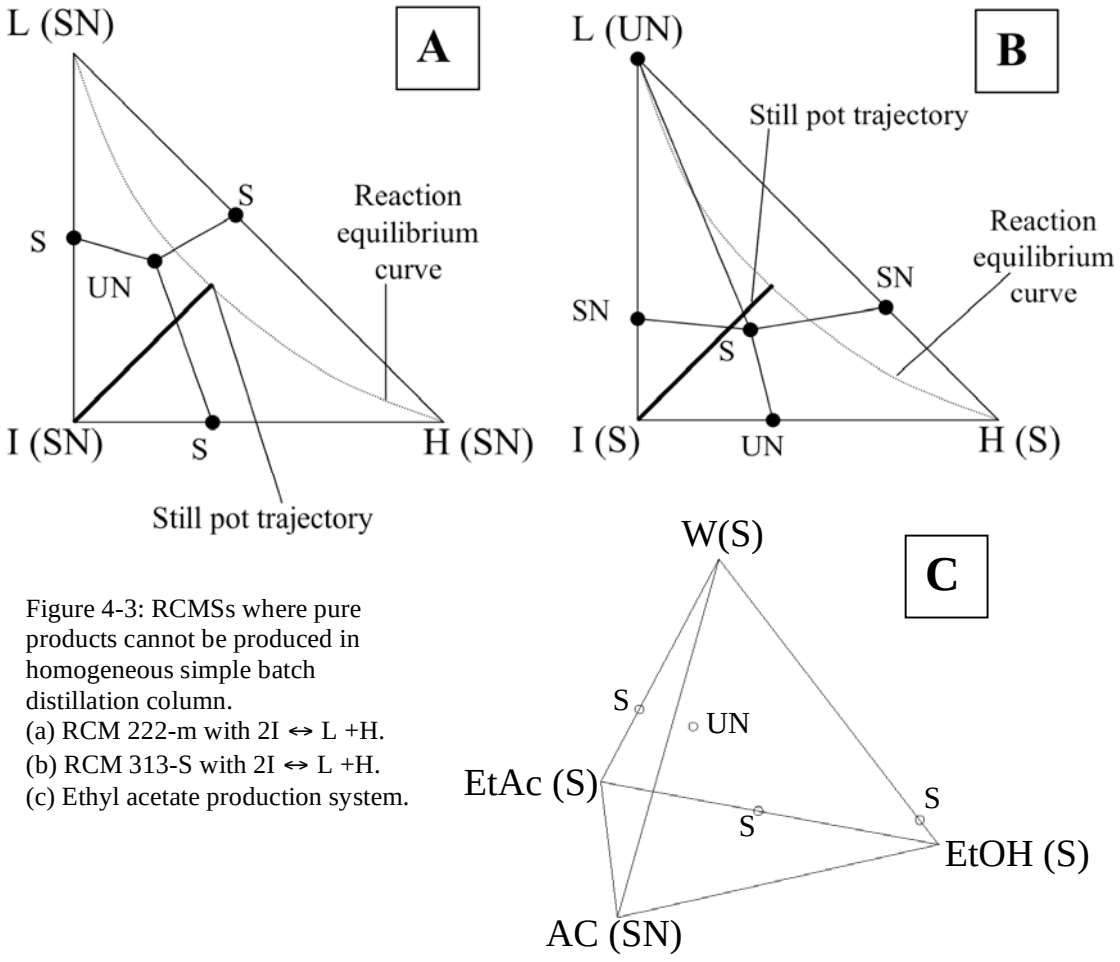

Figure 4-3: RCMSs where pure products cannot be produced in homogeneous simple batch distillation column.
(a) RCM 222-m with 2I ↔ L +H.
(b) RCM 313-S with 2I ↔ L +H.
(c) Ethyl acetate production system.

A 222-m system is shown in Figure 4-3a. Here, the node products are separated by a distillation boundary. This system is not feasible in a batch reactive rectifier because none of the reaction products are UNs. It's not feasible in a batch reactive stripper because the distillation boundary cuts across the reaction equilibrium curve, so pure

product H would only be produced until the still pot composition crossed the distillation boundary. It's not feasible in a batch reactive MVC because the products are separated by a distillation boundary and column profiles can't lead to both product vertices from one still pot composition.

A 313-S system is shown in Figure 4-3b. Again suppose a reaction of the form bI ↔ cL + dH where products L and H are a UN and an S that are separated by a distillation boundary. This system is not feasible in a batch reactive rectifier because a distillation boundary cuts across the reaction equilibrium curve. It's not feasible in a batch reactive stripper because none of the reaction products are SNs. The system is not feasible in a batch reactive MVC because product H is a saddle.

The ethyl acetate production system is shown in Figure 4-3c where both of the products are saddles with three binary azeotropes and one ternary azeotrope. The reaction is acetic acid (AC) + ethanol (ETOH) ↔ ethyl acetate (EtAc) + water (W). The only UN is the ethanol-ethyl acetate-water ternary azeotrope and the only stable node is pure acetic acid. This system is not feasible in a batch reactive rectifier, stripper, or middle vessel column because both of the reaction products (EtAc and W) are saddles.

In all four examples, the thermodynamic feasibility criteria are not met in the simple batch reactive columns in Figure 4-1. To investigate the possibility of producing pure products with these phase equilibrium systems, we propose in the next section a

general feasibility evaluation algorithm where different column structures or inert entrainers should be introduced.

Feasibility Evaluation Algorithm

For a single-reaction system, Figure 4-4 summarizes which of the column structures considered can be used to produce pure products. The overall algorithm is as follows:

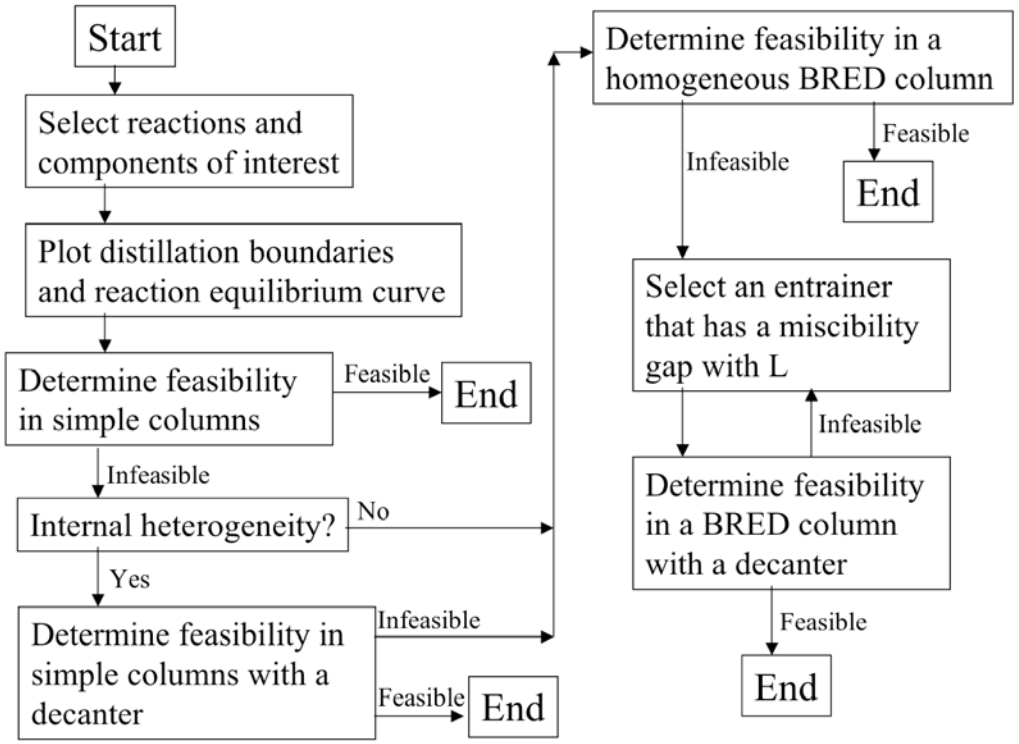

Figure 4-4: Feasibility evaluation algorithm for complex batch reactive distillation.

Step #1: Determine if the pure products can be feasibly produced in any of the simple columns (batch rectifier, stripper, or MVC) without decanter. If reaction equilibrium allows node products to be connected to the still pot composition by residue curves or distillation curves, then the rectifier/stripper/MVC can feasibly produce pure products. If feasible, then no further steps in this algorithm need be performed.

Step #2: If the system does not meet the criteria of Step #1, then determine if pure products can be produced with the addition of a decanter. If the system is not feasible in any of the simple columns due to saddle products or distillation boundaries, then check to see if any heterogeneous azeotrope exists in the mixture. If one does exist, then it may be possible to use a batch reactive rectifier *with a decanter* to isolate the heterogenous azeotrope and then separate the azeotrope into two liquid phases containing at least one pure product (or an almost-pure product that can be put through a final purification step in a downstream process). This azeotrope should be an unstable node that is reachable from the reaction equilibrium curve.

Step #3: If the system does not meet the criteria of Steps #1 or #2, then determine if it is feasible in a BRED system with a homogenous entrainer. Here, we should determine the critical composition region (CCR) and upper and lower bounds of reflux ratios as will be described in the Section of Homogenous Batch Reactive Extractive Distillation. In short, if the CCR blocks the path of the column profiles or pot trajectories, then the system is thermodynamically infeasible in a homogeneous BRED system under that entrainer. If the CCR does not cover the desired binary edge of light product and heavy entrainer, then perform the upper and lower bound calculations to find feasible ratios of entrainer flow to distillate flow. The column composition profiles and the still pot trajectory must always be in the region where the upper/lower bounds allow the column profiles to isolate a pure product.

Step #4: If the system does not meet the criteria of Steps #1, #2, or #3, then determine if it is feasible in the presence of an external entrainer that forms a liquid-liquid split with one of the existing components. If the system is not feasible under any homogenous entrainer, then see if it is feasible under a heterogeneous entrainer (specifically, an entrainer that shares a heterogeneous unstable node azeotrope with one of the products). Then see if a batch reactive rectifier or a BRED column or an MVC can isolate the heterogeneous azeotrope. If so, then a decanter can separate the azeotrope into pure products (or into almost-pure products that can be put through a final purification step in a downstream process).

Reactive Rectifier with a Decanter for 222-m system

Diisopropyl ether (DIPE) is produced by the dehydration of isopropyl alcohol (IPOH). The equilibrium-governed reaction is 2IPOH ↔ DIPE + W. The phase equilibrium behavior is that of a 222-m system with a liquid-liquid split between DIPE and water (W) as shown in Figure 4-5 (using NRTL binary parameters in Aspen Plus[27]: VLE-LIT for IPOH-DIPE & IPOH-W and LLE-ASPEN for DIPE-W). Thus, pure DIPE and W cannot be produced in the homogeneous simple batch columns as already shown in Figure 4-3a. However, if we take advantage of the large miscibility gap, we can produce almost pure DIPE and water using a rectifier with a decanter as suggested in Step 2 of the Feasibility Evaluation Algorithm. The azeotropes are marked with their boiling point temperatures and dynamic properties and they are connected by distillation boundaries. The reaction equilibrium curve is drawn as a dashed curve going from the water vertex to the DIPE vertex by using information from Aspen Plus (ln(Keq) = -

3.00561 + 1464/T +61892.8/T^2, as fitted by Mathematica[28]). The solid curve going from the IPOH vertex, to the reaction equilibrium curve, and then to the DIPE vertex is a rigorously simulated still pot trajectory with coupled heat and material balances. Constant reflux policy is adopted with a reflux ratio of 10. Since no reaction occurs on the trays and fast reaction is assumed to take place in the still pot, pseudo-steady state is assumed for these trays[19]. The detailed simulation model is given in the Appendix.

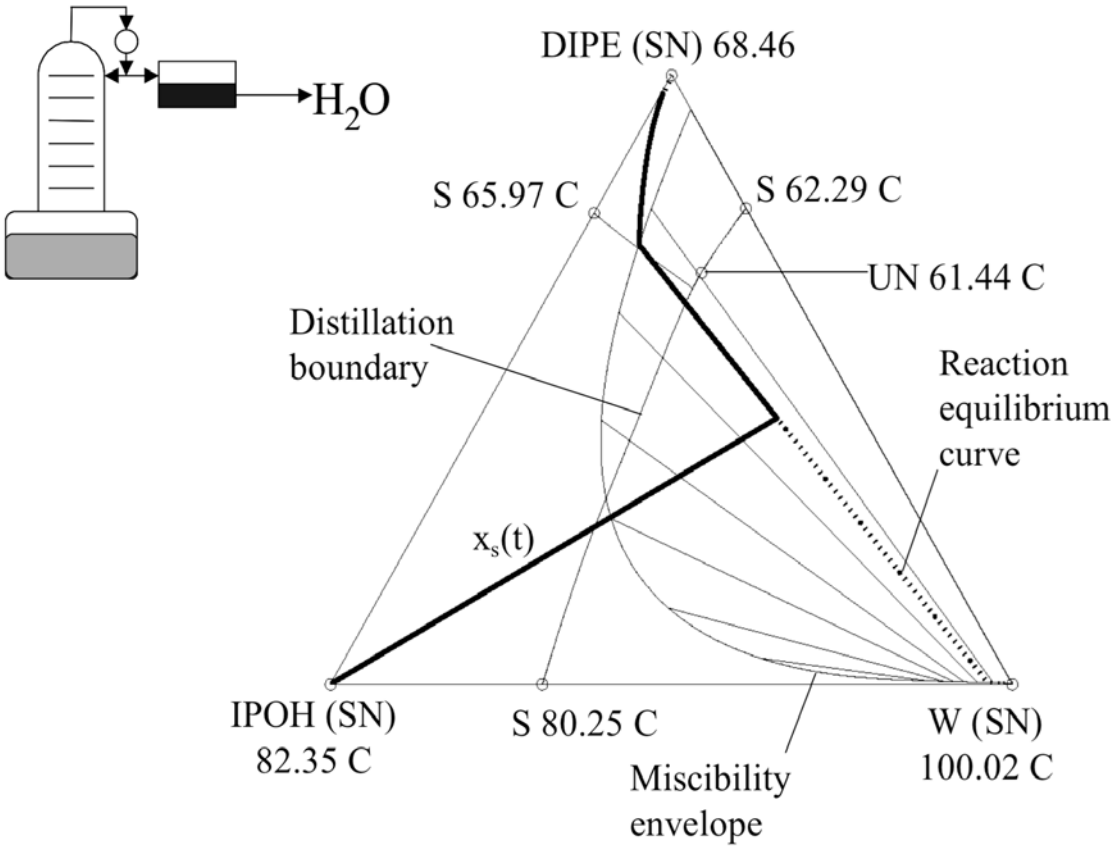

Figure 4-5. Simulation result of one of 222-m systems: 2IPOH ↔ DIPE+W (10 rectifying stages and 97.4% conversion of IPOH).

The features of interest to us in the DIPE system are that the unstable node ternary azeotrope is inside the miscibility gap *and* that one end of the liquid-liquid tie line going through this azeotrope falls near the water vertex. So, when the azeotropic composition is condensed, it splits into two liquid phases: an aqueous phase of relatively pure water

(97.27 mol%), and an organic phase that is 78.69 mol% DIPE, 13.37 mol% IPOH, and 7.93 mol% water. *The ternary azeotrope is the only unstable node in the system, so it is always possible to use a rectifier to produce this azeotrope and then use a decanter to remove a portion of the aqueous phase; the organic phase is completely refluxed.* Thus, we have the same overall effect as a batch reactive rectifier in a feasible homogeneous system: the reaction is driven forward by the continuous removal of one product (water) while the other pure product (DIPE) remains in the pot.

Generalization of Feasibility Criteria in Reactive Rectifier or MVC with a Decanter

Listed in Figures 4-6 and 4-7 are the ternary RCMs (as classified in the literature[26]) where the simple homogeneous batch distillation columns shown in Figure 4-1 cannot lead to the production of pure products with reactions of the form $bI \leftrightarrow cL + dH$ or $aL + bI \leftrightarrow cH$ because distillation boundaries or both saddle products prevent simple distillation from reaching pure product vertices. However, with a decanter in a batch reactive rectifier, we can produce pure products *if the unstable node azeotrope is heterogeneous, reachable from any point in a reaction equilibrium manifold by simple distillation, and the liquid-liquid split from the azeotrope can lead to a pure product vertex.*

The RCMs in Figures 4-6 (a through c) can have these important features. For example, let's take RCM-021. Reactant I converts to products L and H ($bI \leftrightarrow cL + dH$) in the reactive still of the rectifier and simple distillation in the column section can lead to an UN heterogeneous azeotrope at the top. This azeotrope is split into the pure L and the

L-H mixture in the top decanter. The L is withdrawn as a top product and the L-H mixture is recycled to the column. The continuous removal of product L forces the reactive still composition trajectory to lie within the forward reaction region. Then, reactant I will be consumed and finally heavy product H will be left in the still pot. Even though all of the other RCMs in Figure 4-6a have different numbers and types (UN, SN, or S) of azeotropes, the UN azeotrope is reachable from any distillation region or reaction equilibrium curve. Thus, we can isolate pure product L at the top decanter from that azeotrope.

Several systems in Figure 4-6b have two heterogeneous azeotropes (UNs). These RCMs can also lead to the production of pure product L at the top decanter if the L-H UN azeotrope shares the same distillation region with the reaction equilibrium curve and is reachable from the reaction equilibrium curve by simple distillation. If UN heterogeneous azeotropes exist only on the I-H edges as shown in Figure 4-6c, then pure product H can be withdrawn at the top decanter.

With a reactive rectifier-decanter, most of the RCMs in Figure 4-6 can also lead to the production of pure product H with the reaction of $aL + bI \leftrightarrow cH$. However, the H product cannot be isolated at the top decanter when the UN heterogeneous azeotrope exists only between L and I as shown in Figure 4-7a. In this case, a single product H cannot be produced as a pure form in a reactive rectifier-decanter. In contrast, Figure 4-7b shows the RCMs where reaction $bI \leftrightarrow cL + dH$ cannot lead to production of pure L and H in a reactive rectifier-decanter. This is because the only UN azeotrope between I

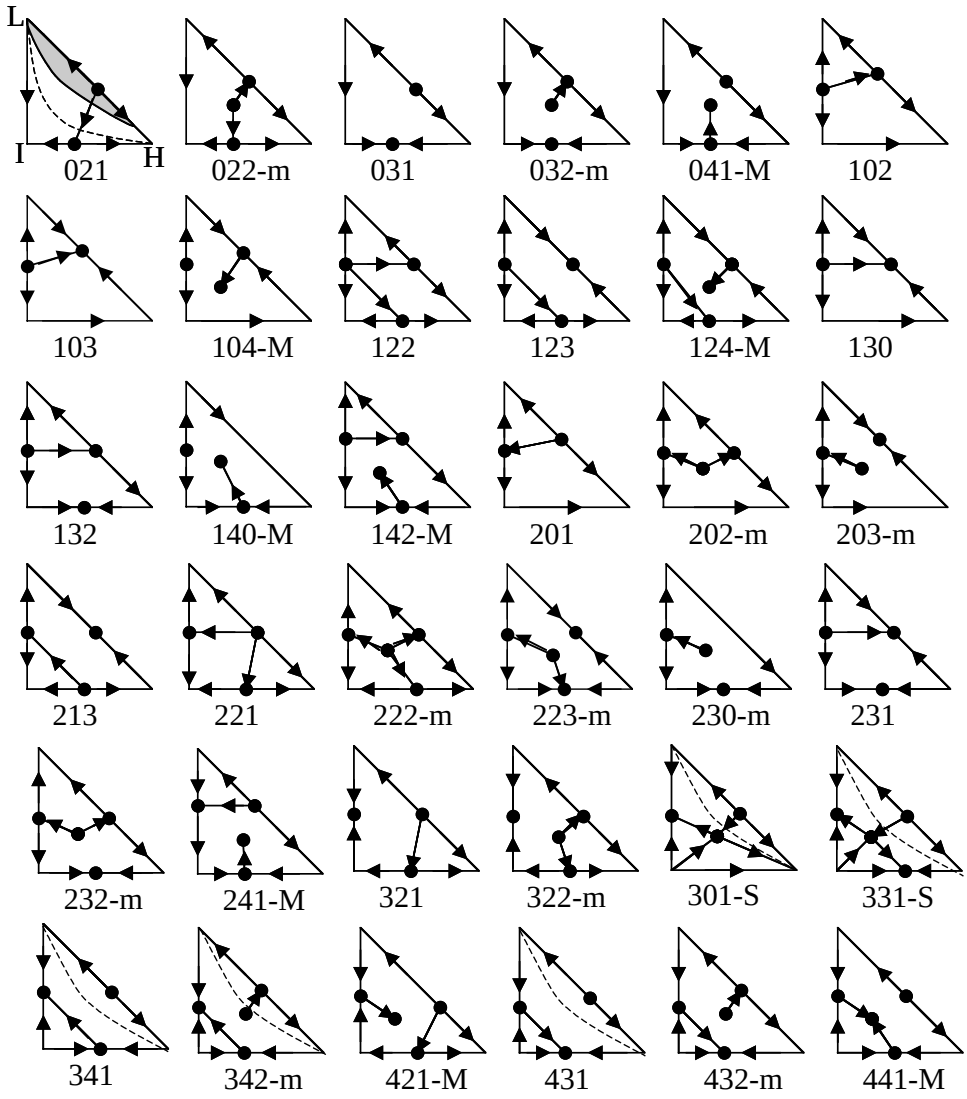

(a) RCMs for possible production of product L at the top decanter.

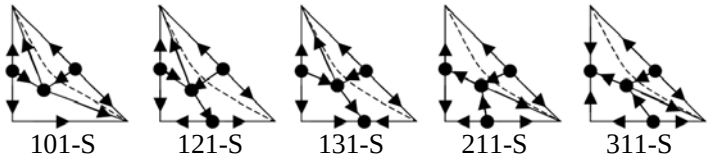

(b) RCMs for possible two UNs of heterogeneous azeotropes.

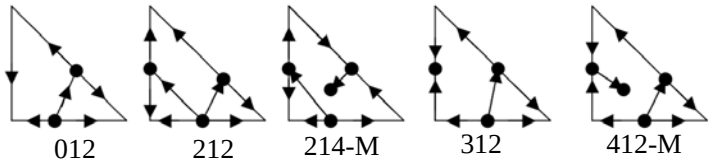

(c) RCMs for possible production of product H at the top decanter.

Figure 4-6. Feasible RCMs producing pure products with bI ↔ cL+dH in a reactive rectifier – decanter. Dotted lines are reaction equilibrium curves and a hatched region is a possible L-L split.

and H is not accessible from the reaction equilibrium curve due to distillation boundaries. However, with the composition reaction of aL + bI ↔ cH, pure product H can be isolated at the top decanter as long as the reaction causes the still composition to move to any distillation region where the UN heterogeneous I-H azeotrope is accessible.

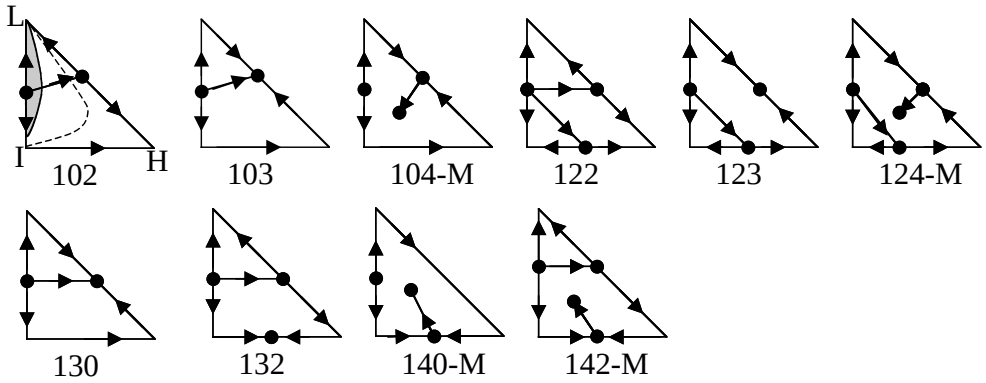

(a) Infeasible RCMs for production of product H at the top decanter with aL+ bI ↔ cH.

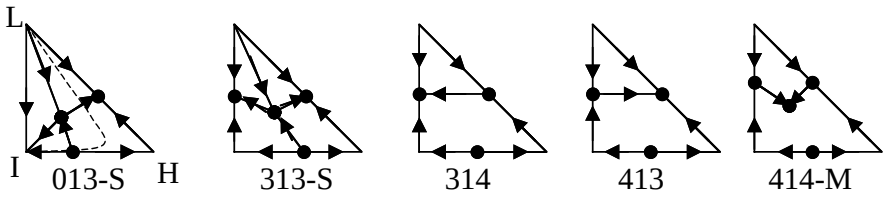

(b)Feasible RCMs with aL+ bI ↔ cH but infeasible RCMs with bI ↔ cL+ dH.

Figure 4-7. Infeasible and feasible RCMs for producing pure product H with aL+ bI ↔ cH in a reactive rectifier – decanter. Dotted lines are reaction equilibrium curves and a hatched region is a possible L-L split.

In the same sense, a quaternary system with an internal heterogeneity (aK+bI ↔ cL+dH) will be feasible if a miscibility gap exists between a product and any other component, if that gap has an unstable node heterogenous azeotrope in it, if that azeotrope has a sharp split with that product, and if that azeotrope is always reachable from the reaction equilibrium surface by simple distillation like the butyl acetate production system[19].

Homogenous Batch Reactive Extractive Distillation

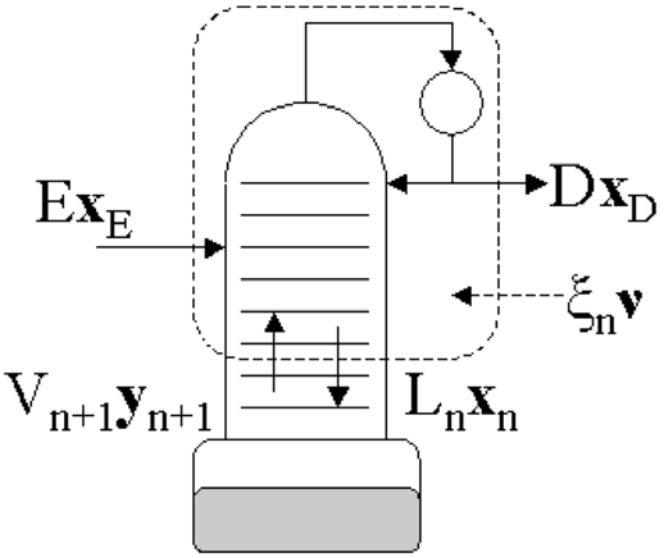

Figure 4-8. Schematic of a batch reactive extractive distillation column (BRED).

We now consider homogeneous batch reactive extractive distillation (BRED) systems that do not split two liquid phases as shown in Step 3 of the Feasibility Evaluation Algorithm. A BRED column is similar in construction to a batch reactive rectifier, with the exception that an extractive agent is fed into the column on one of the trays above the still pot as shown in Figure 4-8. We have developed design techniques for extractive sections in double-feed continuous columns[24-25,29]. These techniques are concerned with a column profile approaching the extractive feed stage from below, so a balance envelope is drawn around the column from the condenser down to an arbitrary tray in the extractive section. As such an envelope can be drawn in both batch and continuous cases, the techniques apply identically to the extractive section of a BRED column. Different from this previous work[24-25,29], we need to define the projected upper and lower bounds of reflux ratios since we will analyze non-reactive trays with four

components in Figure 4-8. First, we revisit projected compositions and the critical composition region and then derive the projected upper and lower bounds of reflux ratios.

Projected Compositions

To obtain a projected composition, one of the pure components of the system is excluded from the composition vector and the remaining components are renormalized to a sum of 1. Geometrically, this means that in composition space, a line is drawn from the point-of-projection (POP), through the composition to be projected, to the boundary of composition space opposite the POP. The POP is the pure component vertex of the component being excluded from the composition vector. A projected fraction (for either the liquid or the vapor) is defined as

$$\tilde{x}_{i,POP} = \frac{x_i}{(1 - x_{POP})} = \frac{x_i}{\sum_{j=1(\neq POP)}^{N} x_j} \quad (1) \qquad \tilde{y}_{i,POP} = \frac{y_i}{(1 - y_{POP})} = \frac{y_i}{\sum_{j=1(\neq POP)}^{N} y_j} \quad (2)$$

where i is any component *not* being used as the POP, $\tilde{x}_{i,POP}$ is the projected mole fraction of component i under a projection by the POP component, x_i is the actual mole fraction of component i, and x_{POP} is the actual mole fraction of the excluded component (that is, the component used as the POP). $\boldsymbol{x}$ refers to liquid mole fractions and $\boldsymbol{y}$ refers to vapor mole fractions. Both projected liquids and projected vapors will be used to determine critical composition regions[24-25] and new projected lower and upper bounds of reflux ratios in the next sections.

Figure 4-9 shows two different projections of the same composition, which is a mixture of four components that we shall call L, I, H, and E. The two L and E projections will be used in the next subsection since these projections clearly tell us whether possible composition profiles can reach the L-E binary edge as we go up to the feed stage[25].

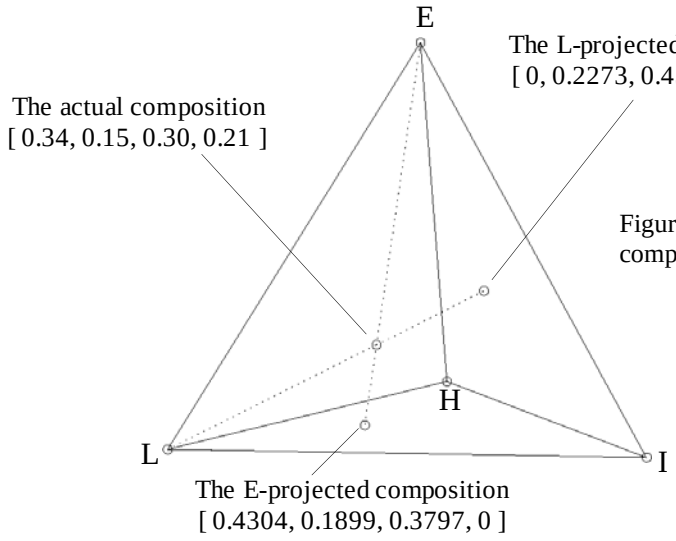

Figure 4-9. Projection of a quaternary composition to two ternary triangles.

Feasible Directions for Composition Profiles - Critical Composition Region

We now employ the concept of feasible directions for composition profiles, as determined by the critical composition region[24-25]. Consider the reaction $2I \leftrightarrow L + H$ in the presence of inert entrainer E where L, I, and H are the light-, intermediate-, and heavy-boiling components. Pure product L is a saddle in both the L-I-H and the L-I-H-E systems and simple batch reactive columns (rectifier, stripper, and MVC) cannot be used to produce pure products. In a homogenous BRED system, an entrainer is chosen such that L and E do not form a binary minimum boiling azeotrope. Then, a rectifying section can separate the mixture and isolate L in the distillate once the extractive composition profile approaches the L-E edge in the feed stage. For a BRED column to be feasible in a

given reaction/phase equilibrium system, the extractive column profiles must be able to reach the L-E edge of composition space from any possible still pot composition. However, there is a region in composition space where phase equilibrium does not allow composition profiles to approach the L-E edge. This region is called the critical composition region (CCR)[24-25] and is defined as the region in composition space where, for a given liquid/vapor pair in phase equilibrium, the projected fraction of L in the liquid is greater than the projected fraction of L in the vapor (under an E projection) **and** the projected fraction of E in the liquid is greater than the projected fraction of E in the vapor (under an L projection). That is, the CCR is the set of compositions where the inequalities $\tilde{x}_{L,E} > \tilde{y}_{L,E}$ and $\tilde{x}_{E,L} > \tilde{y}_{E,L}$ are both true[25]. Any composition profile entering the CCR cannot reach the L-E edge while moving up the column[24-25].

The CCR must also not cover the H-E edge of composition space because, towards the end of the reactive distillation, H and E will accumulate in the still pot to the exclusion of L (which is being distilled out) and I (which is being consumed by reaction). Column composition profiles start from the time-dependent still pot composition. Consequently, a column composition profile must be able to go from compositions near the H-E edge (where the final still pot compositions are) to the L-E edge (where the extractive section profiles join with the rectifying section profiles). *So, for a system to be feasible, the CCR must not cover either the L-E edge or the H-E edge nor block all paths between the two.* The CCR is based only on equilibrium information, process structure, and the choice of desired compositions (we want to isolate an L-E mixture). This

criterion does not employ process operation conditions. It constitutes a necessary, but not sufficient, condition for feasible BRED systems.

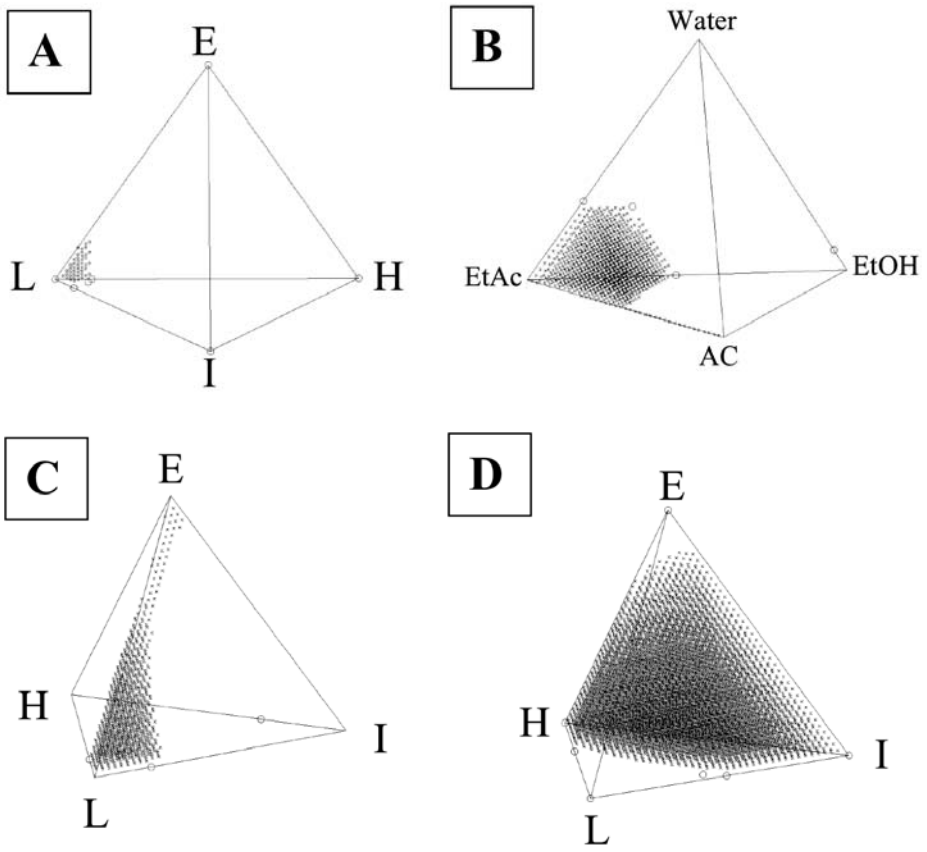

Figure 4-10. All shaded regions are critical composition regions (CCRs).
(a) 202-m. (b) Ethyl acetate production system. (c) 222-m. (d) 313-S.

We take a 202-m system and assume the use of a homogeneous entrainer. The CCR for this region is plotted in Figure 4-10a. Note that neither the L-E nor H-E edges are completely covered by the CCR. The CCR for the EtAC production system is shown in Figure 4-10b. In this system, still pot compositions will move towards the W vertex (or the W-AC binary edge, if an excess of AC is used). The CCR allows composition profiles to approach the EtAC-AC binary edge from the W-AC binary edge. Thus, for both of these systems, we can move to the next step (described in the next section), which is applying the upper/lower bound calculation method. However, in the 222-m and 313-S

systems, the CCR covers the L-E and H-E edges (as shown in Figures 4-10c and 4-10d), so when still pot trajectories enter the CCR, column profiles are unable to approach the L-E edge.

The CCR was only drawn on the reaction equilibrium surface in previous work[24-25]. This is because our consideration was limited to the reactive trays of a continuous distillation column. The calculation of the CCR does not require this limitation and, in BRED systems, the trays above the reactive pot are assumed to be non-reactive. Thus, for columns with non-reactive trays as in Figure 4-8, it is necessary to perform the CCR calculations everywhere in composition space using only phase equilibrium data.

Feasible Directions for Composition Profiles - Projected Upper and Lower Bounds of the Internal Reflux Ratio

The CCR in the previous sub-section is the thermodynamically infeasible region of a BRED column. Now, in this section, material balance constraints will be imposed for given liquid and vapor compositions to see whether BRED column profiles can reach a desired binary edge between the light product and heavy entrainer vertices.

In previous work[24-25,29], the feasible regions for column composition profiles were calculated for the non-reactive acetone-methanol-water system and several esterification and etherification systems. This was done by drawing a material balance envelope around the top of the column down to some arbitrary stage in the extractive section as shown in Figure 4-8. The material balance equations are

$$E + V_{n+1} = L_n + D - \nu_T \xi \quad (3)$$

$$E\boldsymbol{x}_E + V_{n+1}\boldsymbol{y}_{n+1} = L_n\boldsymbol{x}_n + D\boldsymbol{x}_D - \boldsymbol{\nu}\xi \quad (4)$$

where E and $\boldsymbol{x}_E$ are the molar flow rate and molar composition of the entrainer feed stream, V_{n+1} and $\boldsymbol{y}_{n+1}$ are the molar flow rate and molar composition of the vapor stream leaving stage $n+1$ and entering the balance envelope, L_n and $\boldsymbol{x}_n$ are the molar flow rate and molar composition of the liquid stream leaving stage n and leaving the balance envelope, and D and $\boldsymbol{x}_D$ are the molar flow rate and molar composition of the distillate stream. ν_T is the total sum of the stoichiometric coefficients and $\boldsymbol{\nu}$ is the stoichiometric coefficient vector.

By assuming that this arbitrary stage n was pinched ($\boldsymbol{y}_n = \boldsymbol{y}_{n+1}$ or $\boldsymbol{x}_n = \boldsymbol{x}_{n-1}$), the material balance lines described in equations (3) and (4) become pseudo-balance lines instead. For given phase equilibrium data, the following feasibility condition to approach the L-E edge was derived[25]

$$\frac{L_n}{D} \le \left(\frac{V_n}{E}\frac{E}{D} + \frac{E}{D} + \nu_T \frac{\xi_n}{D} - 1 \right) \quad (5)$$

where the left and right sides are the lower and upper bounds of the internal reflux ratios for arbitrary equilibrated compositions of $\boldsymbol{x}_n$ and $\boldsymbol{y}_n$ at arbitrary stage n. If the upper bound is greater than the lower bound at these arbitrary equilibrated compositions, then the composition profiles passing those compositions can move to the desired binary edge between the light product and the entrainer while going up the column.

With a 3-component system such as the methanol-acetone-water extractive distillation, the arbitrary pseudo-balance lines intersect in a 2-dimensional composition

space[29]. The same is true of reactive 4-component systems since the liquid compositions of reactive trays are constrained to the reaction equilibrium manifolds[24-25]. However, if the number of components exceeds the number of equilibrium-governed reactions by more than 3 (for example, a 4-component system with no reaction), then the pseudo-balance lines will not intersect. Thus, the pseudo-balance lines generally do not intersect in multicomponent systems. However, the determination of the upper and lower bounds requires having a point-of-intersection. A point-of-intersection can be obtained if the pseudo-balance lines are projected from the full composition space onto 3-component (2-dimensional) subspaces; the projected pseudo-balance lines are then forced to intersect.

The *projected* pseudo-balance equations without reaction are derived from equation (4)

$$\tilde{E}_{POP}\tilde{\boldsymbol{x}}_{E,POP} + \tilde{V}_{n,POP}\tilde{\boldsymbol{y}}_{n,POP} = \tilde{L}_{n,POP}\tilde{\boldsymbol{x}}_{n,POP} + \tilde{D}_{POP}\tilde{\boldsymbol{x}}_{D,POP}$$

$$= (\tilde{E}_{POP} + \tilde{V}_{n,POP})\tilde{\boldsymbol{x}}^{*}_{POP} = (\tilde{L}_{n,POP} + \tilde{D}_{POP})\tilde{\boldsymbol{x}}^{*}_{POP} \qquad (6)$$

For the geometrical considerations used in the upper/lower bound approach to make sense, we cannot use a vertex as a POP if that vertex is part of the boundary that we want composition profiles to approach. For example, if one wishes to reach the L-E edge in the extractive section, then any projected subspace to be analyzed must include the L-E edge. Therefore, neither L nor E may be used as a POP to calculate upper and lower bounds. This contrasts with the CCR calculations, where *only* L and E could be used as POPs.

$\tilde{\boldsymbol{x}}^{*}_{POP}$, the point-of-intersection between the projected pseudo-balance lines, can be determined. From this, the ratios $\tilde{V}_{n,POP}/\tilde{E}_{POP}$ and $\tilde{L}_{n,POP}/\tilde{D}_{POP}$ can be calculated; they are the ratios of the lengths of the segments of the projected pseudo-balance lines. Because we want a feasible projected $\tilde{\boldsymbol{y}}_{n+1}$ to lie further away from the binary edge than $\tilde{\boldsymbol{y}}_{n}$, we require the projected upper bound (the right hand side of equation (7)) to be greater than the projected lower bound (the left hand side of equation (7)). That is,

$$\frac{\tilde{L}_{n,POP}}{\tilde{D}_{POP}} \le \left(\frac{\tilde{V}_{n,POP}}{\tilde{E}_{POP}} \frac{\tilde{E}_{POP}}{\tilde{D}_{POP}} + \frac{\tilde{E}_{POP}}{\tilde{D}_{POP}} - 1 \right) \tag{7}$$

Equality is conserved for pinch points as mathematically proved in the Appendix. Applying the definitions $\tilde{E}_{POP} = E\left(1 - x_{E,POP}\right)$ and $\tilde{D}_{POP} = D\left(1 - x_{D,POP}\right)$ to calculate the upper and lower bounds with a given value of *E/D*, this becomes

$$\frac{\tilde{L}_{n,POP}}{\tilde{D}_{POP}} \le \left(\frac{\tilde{V}_{n,POP}}{\tilde{E}_{POP}} \frac{E}{D} \frac{\left[1 - x_{E,POP}\right]}{\left[1 - x_{D,POP}\right]} + \frac{E}{D} \frac{\left[1 - x_{E,POP}\right]}{\left[1 - x_{D,POP}\right]} - 1 \right) \tag{8}$$

Figures 4-11 and 4-12 show a pair of pseudo-balance lines for a 4-component system, L, I, H, and E. In both figures, the same liquid and vapor compositions are used, pure E is the entrainer composition, and pure L is the assumed distillate composition. The pseudo-balance lines, themselves, do not intersect, but when projected onto either the L-I-E or the L-H-E faces, the projected pseudo-balance lines do intersect. Figure 4-11 shows the projection onto L-I-E (H is the POP) and Figure 4-12 shows the projection onto L-H-E (I is the POP). Then, the lengths of the line segments on both projected

pseudo-balance lines can be calculated and, from that, the projected upper and lower bounds can be calculated.

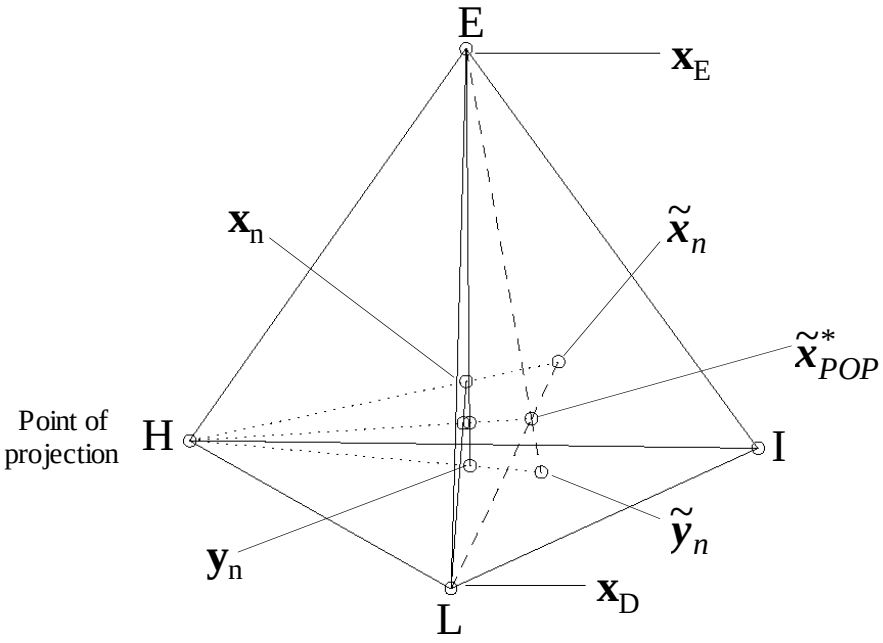

Figure 4-11. H projection in a quaternary mixture.

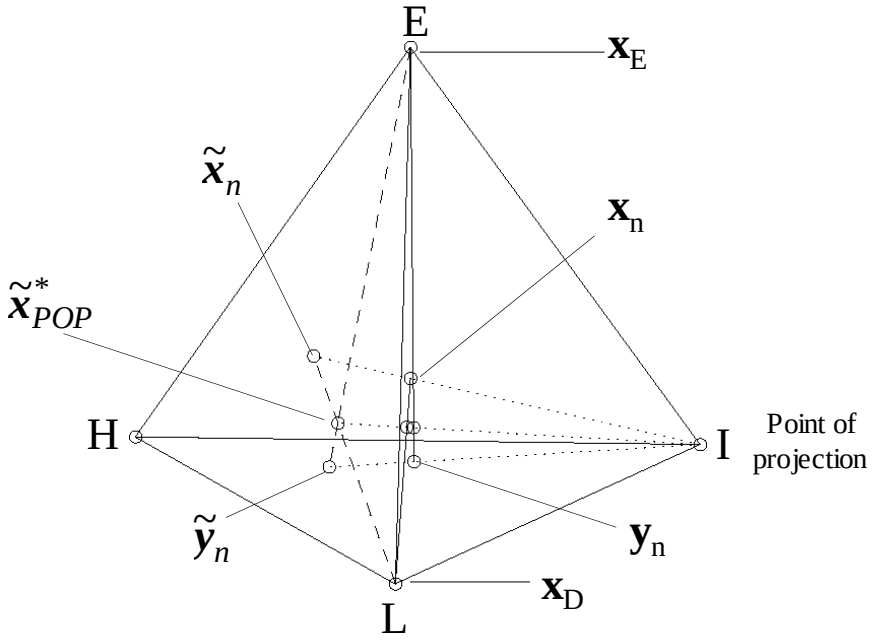

Figure 4-12. I projection in a quaternary mixture.

Because it is possible to project the pseudo-balance lines in two different ways, the projected upper and lower bounds are different under the two projections. A column composition profile passing through that liquid composition is feasible if both projected upper bounds are greater than their respective projected lower bounds. As all of the projected upper and lower bounds are functions of the E/D molar flow ratio, the size and shape of the feasibility region will also be a function of the E/D ratio. *For a given E/D ratio, the still pot trajectory and possible column composition profiles should remain inside the feasibility region.*

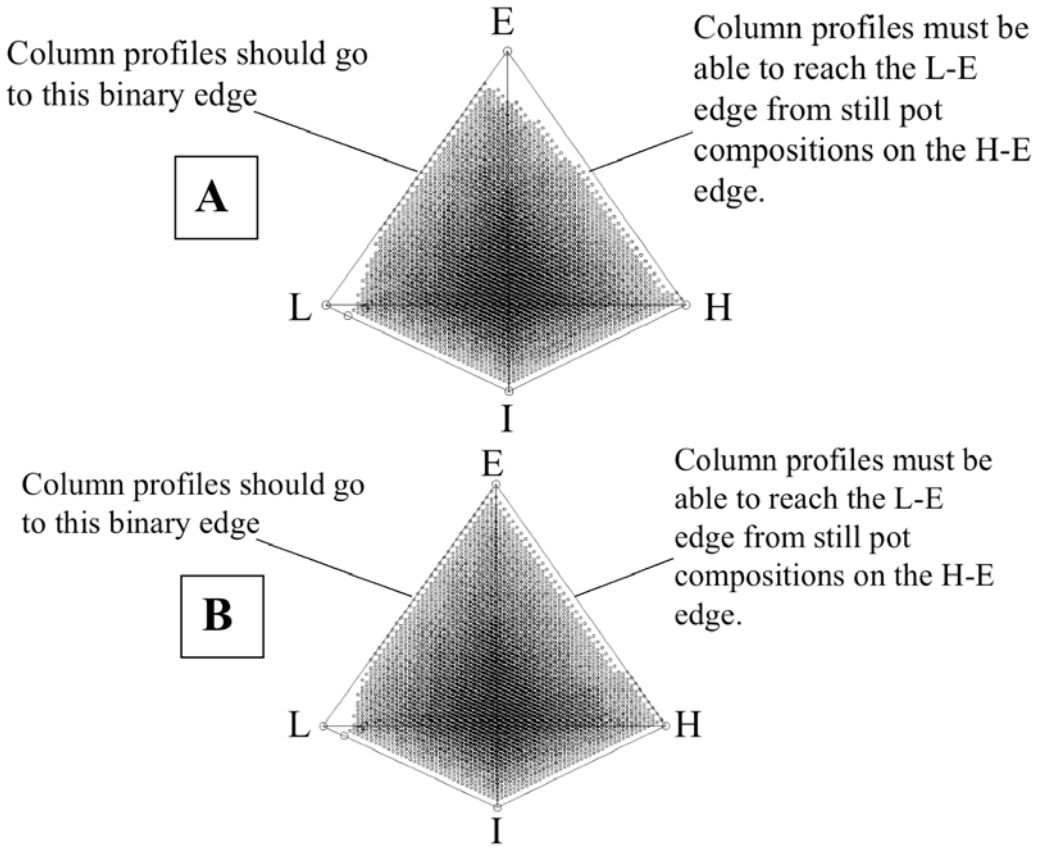

Figure 4-13. Feasible regions (shaded regions) where upper reflux ratios are greater than lower ratio in RCM 202-m under a homogeneous entrainer. (a) E/D = 5.0 (b) E/D = 23.0

The feasibility region must cover some part of the L-E edge so that the column profiles may approach it. Since column profiles start at the still pot trajectories and the

still pot trajectories will move towards the H-E edge with time, the feasibility region must also cover some part of the H-E edge. *Thus, the feasibility region must cover parts of both the L-E and H-E edges for the column to be feasible at a given E/D ratio.*

Figures 4-13a and b show the feasibility region for the 202-m system (the same system as shown in Figure 4-10a under E/D ratios of 5.0 and 23.0, respectively). As the E/D ratio increases, the size of the feasibility region also increases, thus making it easier for the extractive section of the column to isolate an L-E mixture at the entrainer feed stage of the column. A comparison of Figure 4-10a with Figures 4-13a and b shows that the feasibility region does not intersect the CCR.

Figure 4-14a shows a rigorously simulated still pot trajectory and column profiles for the 202-m system ($2I \leftrightarrow L+H$, $Keq=K_xK_\gamma=3.0$) under a homogenous entrainer. The detailed dynamic model is available in the appendix. The grid of small dots marks the region where the projected upper bounds are greater than the projected lower bounds (E/D=23.0, the same as in Figure 4-13b). The still pot composition starts as pure I. It is then allowed to react under total reflux without entrainer to generate L and H in the still pot. Then, we switch to finite reflux and introduce entrainer to the system. Because of the high E/D ratio used, the still pot trajectory quickly travels towards the E vertex of composition space. Although increasing the E/D ratio increases the size of the feasibility region, it does not extend all of the way to the boundary of composition space near the E vertex. So, flooding the column with entrainer causes the still pot composition to leave the feasibility region quickly. Our simulated column was only able to convert 76.1 % of

the reactant (I) initially charged to the still pot. However, while the still pot composition is in the feasibility region, the extractive profile can reach the L-E edge as shown in Figure 4-14a and from this we can produce pure product L using a rectifying section.

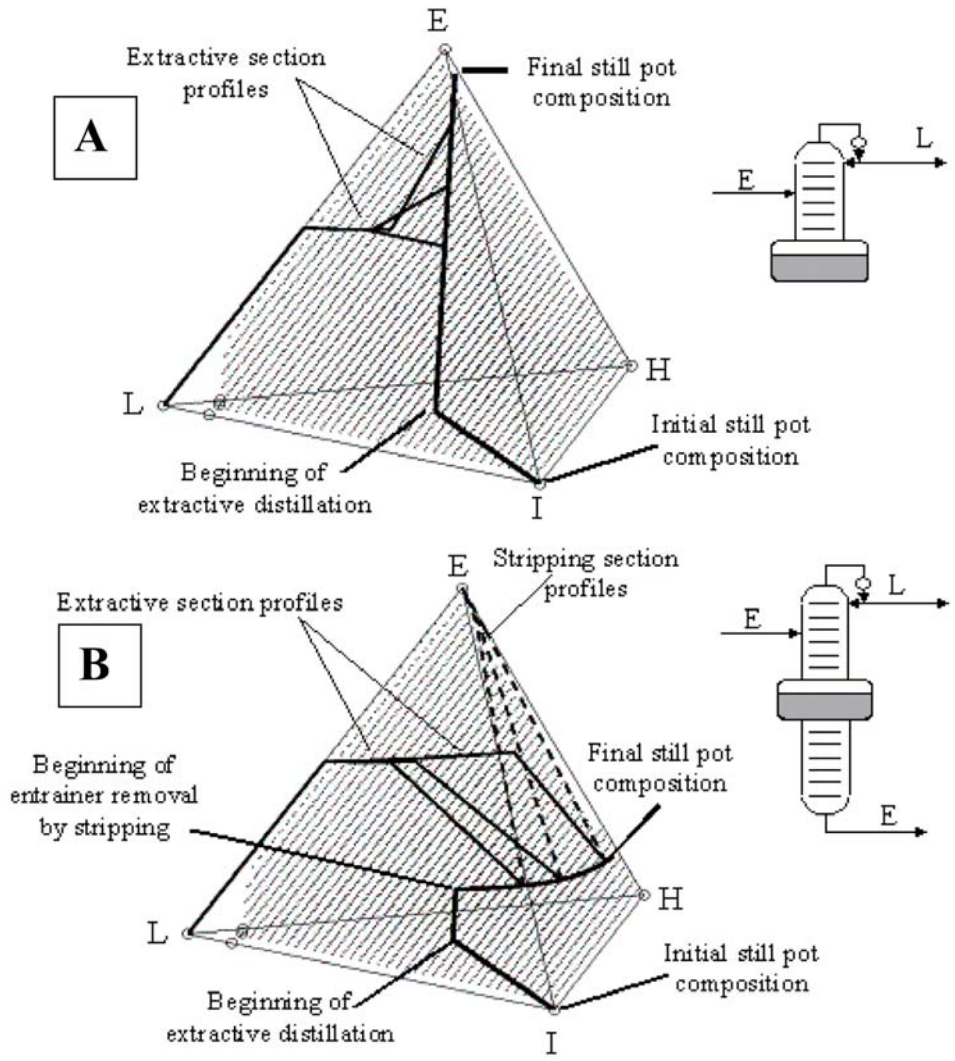

Figure 4-14. Dynamic simulation results in RCM 202-m with reaction 2I ↔L+H and non-reactive entrainer E. (a) BRED column (15 rectifying stages and 50 extractive stages). (b) MVC with a side-fed entrainer (15 rectifying stages, 50 extractive stages, and 9 stripping stages).

To prevent the still pot from being flooded by entrainer, we added a stripping column below the still pot to isolate E and remove it from the reaction mixture as shown in Figure 4-14b; E is the only stable node in this system, so a stripping column can

remove E from the system without removing other components. This makes the column a middle-vessel column with a side-fed entrainer. The simulation result for this column is shown in Figure 4-14b. Here, the still pot composition travels towards the middle of the H-E edge of composition space. This simulated column was able to convert 97.4% of the I charged to the still pot. The slop cut from this batch reactive distillation can be rectified in a non-reactive rectifier to recover small quantities of L-I-H and I-H azeotrope for recycling to the next reactive distillation batch. An additional advantage of using a stripping section is that the E recovered in the bottoms can be recycled immediately back to the entrainer feed stream during the batch reactive distillation; this avoids accumulating a large quantity of E in the still pot and reduces the total amount of E that needs to be present in the system at any given time.

202-m is feasible in a BRED or a MVC BRED column because the CCR and projected upper/lower bounds allow the extractive section composition profile to approach the L-E binary edge. However, in the 222-m and 313-S systems, the CCR prevents column profiles from approaching the L-E edge as shown Figure 4-10. The CCR is determined only from thermodynamic information, the column structure, and the choice of top product and entrainer. The upper and lower bound calculations require this same information and the choice of E/D ratio, which is the only process operating variable used in this calculation. Note that the choice of entrainer is important, here. Different entrainers will yield different shapes for the CCR and the feasibility regions. For the 313-S and 222-m systems, we should either exploit an internal heterogeneity like

the DIPE system in Figure 4-5 or create L-L splits by introducing an external heterogeneous entrainer as described in the next section.

Heterogeneous Batch Reactive Distillation with an External Entrainer

If the components of interest do not show a miscibility gap and the CCR and upper/lower bound reflux ratios tell us that there is no feasible homogenous entrainer that will make a BRED system feasible, then we should consider the possibility of using a heterogenous entrainer as suggested in Step 4 of the Feasibility Evaluation Algorithm in Figure 4-4. The main idea is to introduce an external entrainer that shares an unstable node heterogenous azeotrope with one of the reaction products. If internal heterogeneity does not provide a sharp L-L split, an external heterogenous entrainer that causes sharper L-L splits can be used to obtain purer products.

RCM 313-S system with two external entrainers

From Figures 4-6 and 4-7, the RCM 313-S system cannot lead to the production of pure products with decomposition reaction (bI↔cL+dH) even if there is an internal heterogeneity. If we further assume that there is no such internal heterogeneity, we still may not produce pure products in a homogeneous entrainer in the BRED column since the CCR in the RCM 313-S system covers the E-H edge as shown in Figure 4-10d.

If an entrainer E can be introduced such that E and L share a heterogenous split by forming a UN azeotrope, then, depending upon the size of the miscibility gap, either there is no need to distill L from E or such a distillation would be relatively easy. The

rectifying section can isolate the L-E mixture and a decanter can separate the mixture. Here, two external entrainers are used for producing pure products with $2I \leftrightarrow L + H$ ($Keq= K_xK_\gamma=20$).

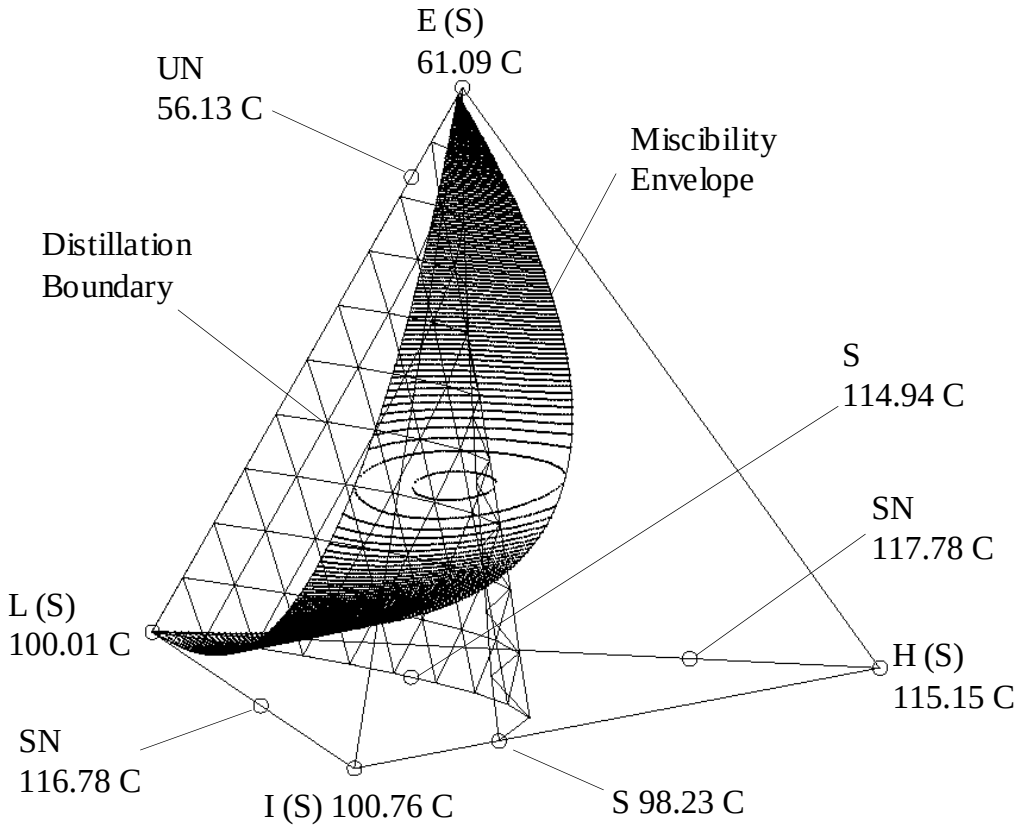

Figure 4-15. VLLE behavior of 313-S with a light heterogeneous entrainer.

The system shown in Figure 4-15 is a 313-S system under a light heterogeneous entrainer (E). A sharp miscibility gap exists between L and E and one distillation boundary is present. A reactive rectifier with a decanter can still be used for producing pure products since the UN azeotrope between L and E is shared by both distillation regions and is reachable by simple distillation. Figure 4-16 shows the dynamic simulation result. The still trajectory starts with reactant I and entrainer E and it ends on the E-H edge. From the still trajectory, all column profiles reach the UN heterogeneous azeotrope at the top stage that is split to light product (L) and L-E mixture. As product L is

continuously removed at the top decanter, the reaction equilibrium shifts to the forward reaction and reactant I is completely consumed as the still trajectory approaches the H-E edge.

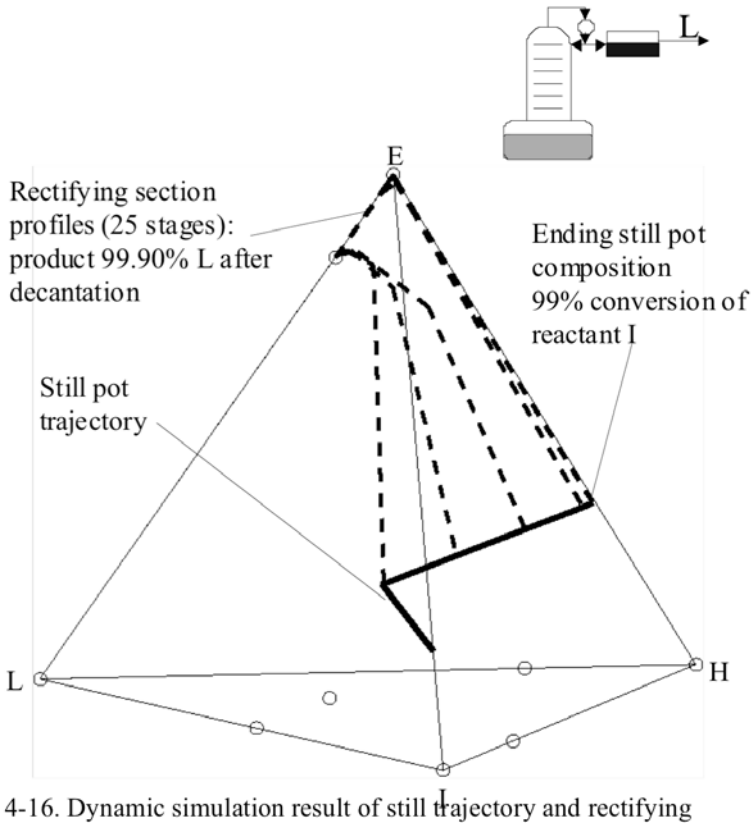

Figure 4-16. Dynamic simulation result of still trajectory and rectifying section profiles of 313-S with a light heterogeneous entrainer.

If a heavy entrainer is introduced to a 313-S system, then two distillation regions are also formed by a distillation boundary as shown in Figure 4-17. The quaternary mixture has two UNs: the heterogeneous L-E azeotrope and the homogeneous I-H azeotrope. Pure E is the only stable node in this system. A batch reactive rectifier (that uses an I-E mixture as the initial still charge) will produce the I-H azeotrope instead of the L-E azeotrope if the still pot composition is in the wrong distillation region. Thus, there must be enough entrainer present to keep the still pot composition out of the distillation region containing the I-H azeotrope. In addition, notice that the distillation

boundary includes the H-E binary edge. Although the distillation boundary closely follows the E-I-H ternary face at high E fractions, it is possible that a batch reactive rectifier would stop producing the L-E azeotrope as the still pot composition approaches the distillation boundary.

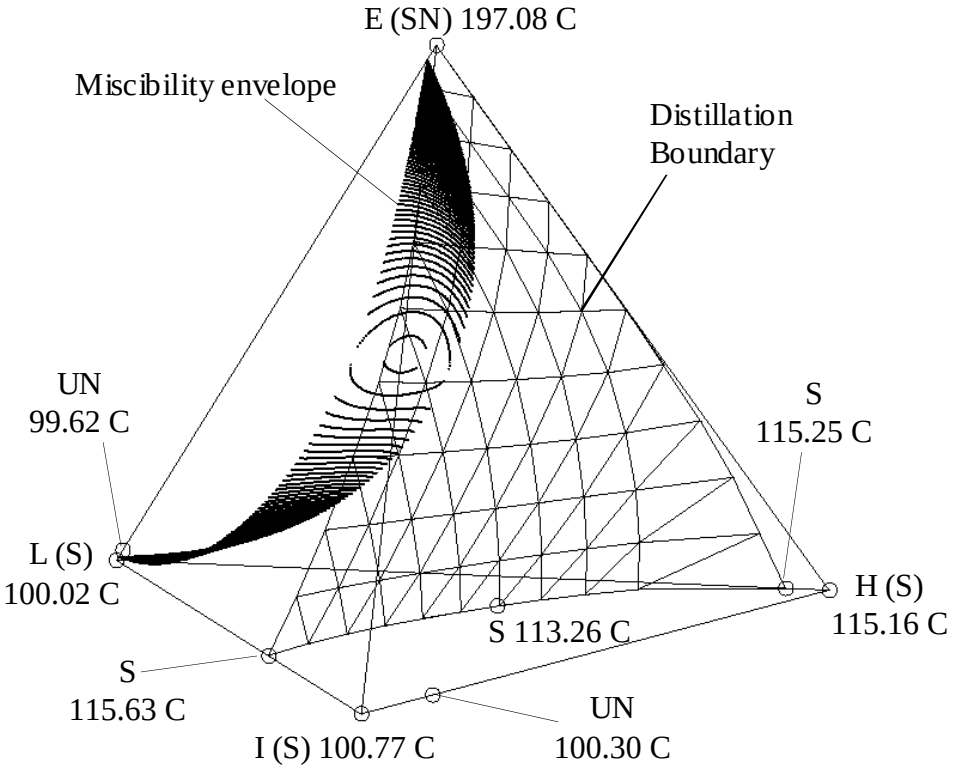

Figure 4-17. VLLE behavior of 313-S with a heavy heterogeneous entrainer.

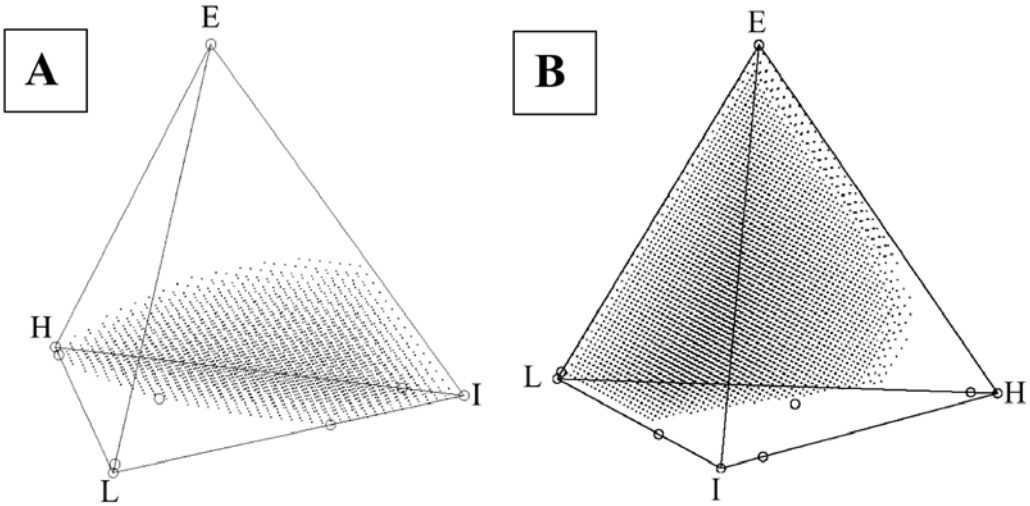

Figure 4-18. CCR and feasible region in the 313-S system with a heavy entrainer.
(a) CCR (shaded region). (b) Feasible shaded region with E/D=20.0.

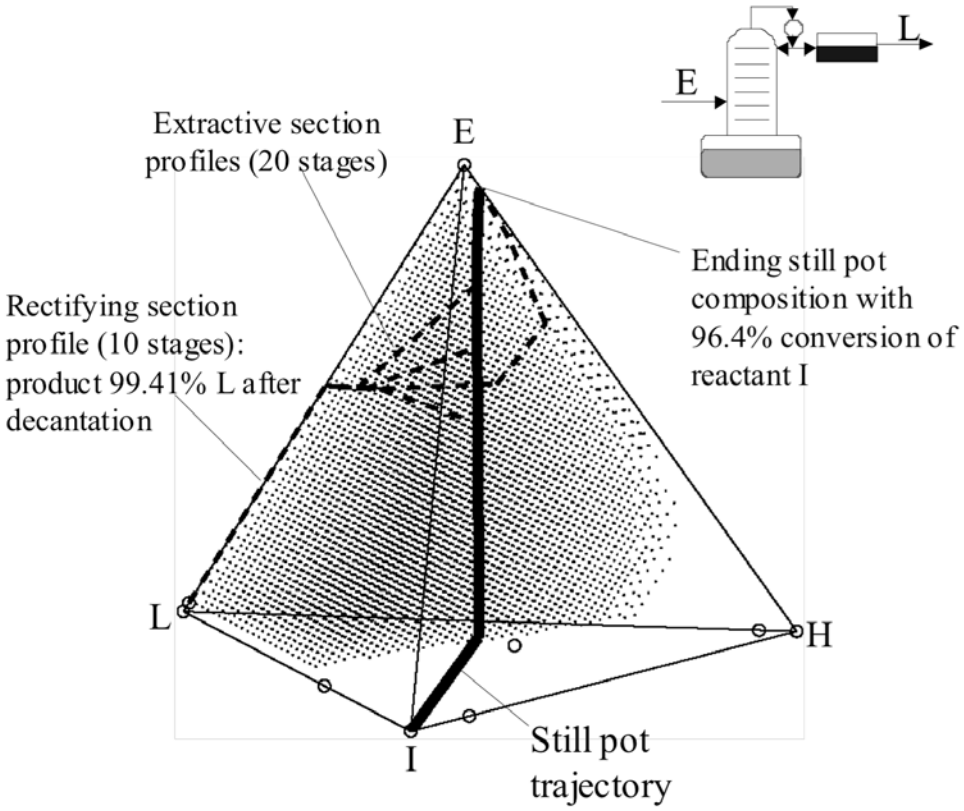

Figure 4-19. Dynamic simulation result of 313-S in a BRED column-decanter with a heavy heterogeneous entrainer (E/D=20).

We perform the CCR calculations for this VLLE system to determine if side-feeding this entrainer can circumvent the distillation boundary. In Figure 4-18a, we see that the CCR does not cover the L-E or H-E edges. We then perform the upper/lower bound calculations to determine the feasible region in Figure 4-18b. The feasible region includes the L-E and H-E edges. It allows an extractive section profile to cross the distillation boundary and the rectifying section profile can proceed to the L-E unstable node azeotrope from there. So, a BRED column with side-fed E is used to cross the distillation boundary as shown in Figure 4-19 and the rectifying section isolates the L-E azeotrope. This azeotrope is then decanted to recover pure L.

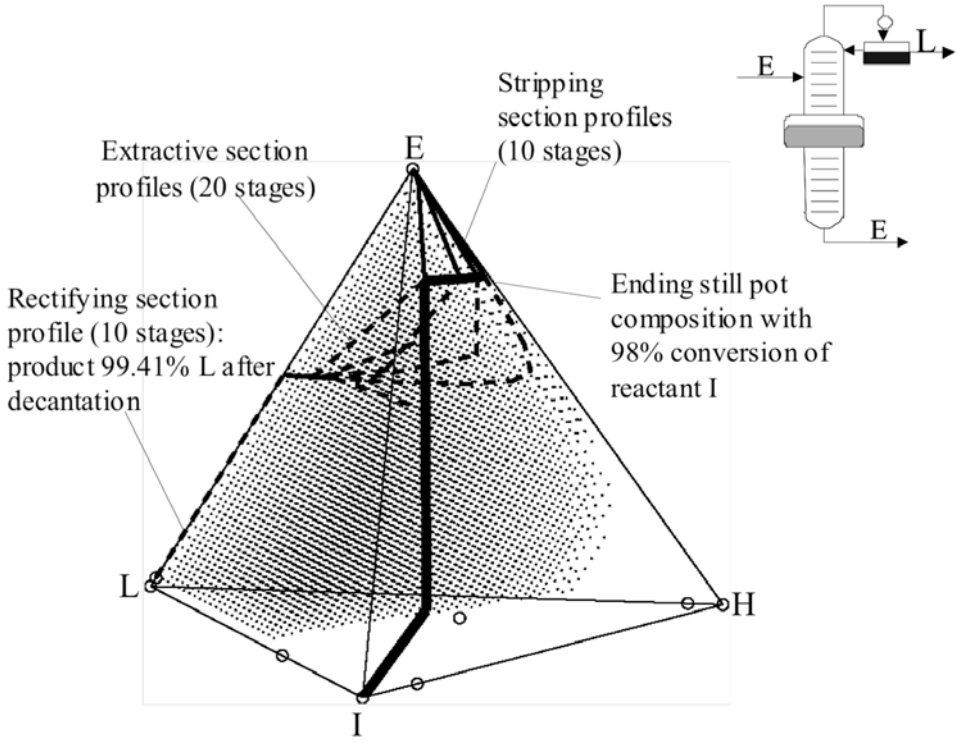

Figure 4-20. Dynamic simulation result of 313-S in a BRED MVC -decanter with a heavy heterogeneous entrainer (E/D=20).

The reaction conversion of reactant I is 96.4% in a BRED column-decanter due to the dilution effect of entrainer (E) as seen in Figure 4-14a. To prevent the flooding of the side-fed entrainer, a middle-vessel column is used to recover the entrainer at the bottom as shown in Figure 4-20 and it achieves 98% conversion of reactant I. The middle vessel is first charged with an I-E mixture because the feasibility region does not extend to low E fractions. The mixture is allowed to react towards equilibrium without distillation or entrainer. The mixture is then simultaneously distilled under the side-fed entrainer, stripped of entrainer from the still pot, and reacted. The still pot trajectory stays within the feasible region as shown in Figure 4-20, so column profiles are always able to go to the L-E azeotrope. It is not strictly necessary to use a stripping section to remove pure E from the still pot because the feasible region in Figure 4-18b includes the E vertex.

However, we do not consider it desirable to have E accumulated in the still pot since it is increasingly difficult to distill other components from a reaction mass that is being increasingly diluted by entrainer.

Isopropyl Acetate Production System

Isopropyl acetate (IPAc) is produced by the esterification of acetic acid (AC) with isopropyl alcohol (IPOH). Water (W) is a byproduct. AC shares no azeotropes with any of the other three components and is the only stable node in the four-component system. IPOH, IPAc, and W have 3 minimum binary azeotropes and a minimum heterogeneous ternary azeotrope between them that is the only unstable node in the system. Although there are no distillation boundaries, neither the stable node (AC) nor the unstable node (IPOH-IPAc-W azeotrope) is a pure product, so the simple columns will not suffice to produce pure IPAc.

We note that the minimum ternary azeotrope is heterogenous and splits to an organic phase (27.44% IPOH, 45.60% IPAc, 26.96% W) and an aqueous phase (3.21% IPOH, 0.04% IPAc, and 96.75% W). A batch reactive rectifier with a decanter can be used to remove W from the reaction mixture and drive the reaction forward. However, because of the significant presence of IPOH in the aqueous phase, further purification is necessary to recover the reactant IPOH by using an additional non-reactive distillation column[30]. Even if a BRED column is used with a side-feed of AC as an entrainer like the methyl acetate production system, pure IPAc cannot be produced since the CCR covers the whole AC-IPAC binary edge as shown in Figure 4-21a. Here, if we introduce an

external heterogeneous entrainer to a reactive rectifier-decanter such that a sharp split with water is provided, then almost pure water is obtained at the top. The reaction equilibrium constant is 8.7[31] based on the activities of the components in the still pot.

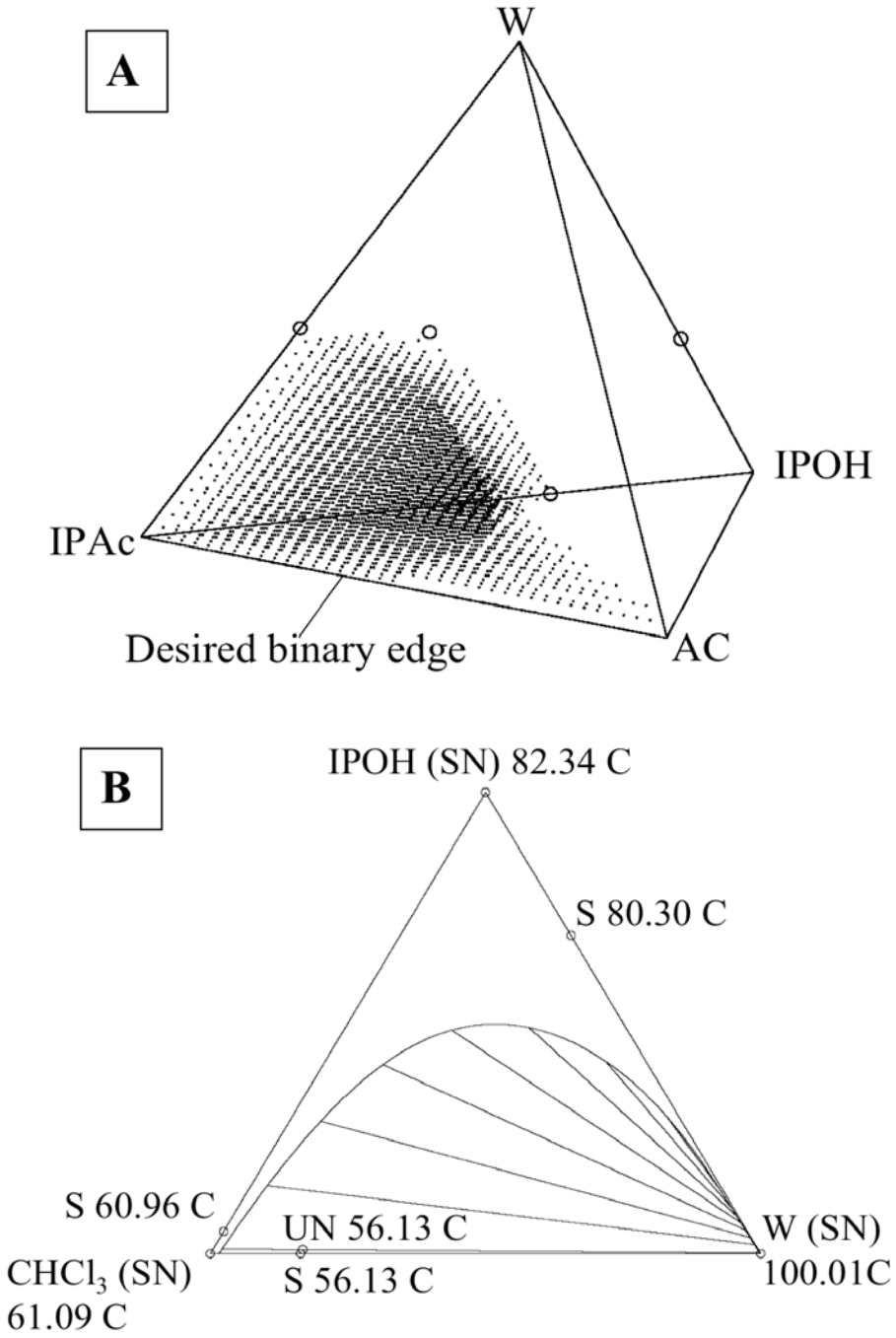

Figure 4-21. VLLE behavior of the isopropyl acetate production system. (a) CCR (shaded region). (b) L-L splits between CHCl3 and W.

We simulate the case where chloroform ($CHCl_3$) is used as an inert heterogeneous entrainer. The NRTL parameters in Aspen Plus[27] was used for phase equilibrium calculations. Pure AC is the only stable node in the five-component system, but there are two unstable nodes: the IPOH-IPAc-W and the IPOH-W-$CHCl_3$ ternary azeotropes. So, there are two distillation regions according to the algorithm of Rook et al.[32]. One region contains IPOH, IPAC, W, and AC with the azeotropes of IPOH-IPAc-W, IPAc-W, IPOH-W, and IPOH-IPAC. The other distillation region includes all five pure components with the azeotropes of IPOH-W-$CHCl_3$, W-$CHCl_3$, IPOH-CHCl3, IPAC-W, and IPOH-W. The IPOH-W-$CHCl_3$ azeotrope is heterogenous and the aqueous phase is 0.17% IPOH, 99.73% W, and 0.11% $CHCl_3$ as shown in Figure 4-21b.

Note that the IPOH-IPAc-W azeotrope lies within the reverse reaction region and the IPOH-W-$CHCl_3$ azeotrope sits on the reaction equilibrium manifold and is reachable from any point in the forward reaction region by distillation in the column section. Since the initial feed charge containing AC and IPOH with an entrainer ($CHCl_3$) lies within the forward reaction zone, the column section in a rectifier allows its composition profiles to reach the IPOH-W-$CHCl_3$ azeotrope. Once this azeotrope is split to pure water in a decanter and is removed at the top, it will push the reactive still trajectory into the forward reaction zone. Then, reactants IPOH and AC are totally consumed and only IPAc with the entrainer will be left in the still.

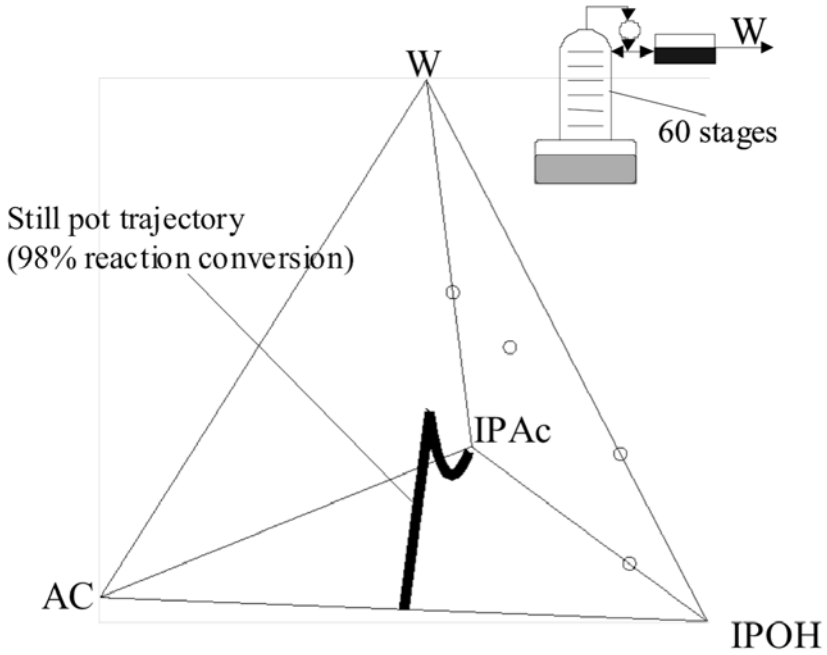

Figure 4-22. Dynamic simulation result of iso-propyl acetate production in a reactive rectifier –decanter. Shown is the projected composition space by excluding an entrainer.

The simulation run begins with 42 mol% each of AC and IPOH and 16 mol% $CHCl_3$. The entrainer-projected still pot trajectory is shown in Figure 4-22. We begin with reaction in the still pot and the column operating at total reflux (so no product is collected) and wait for IPAc and W to accumulate in the still pot. We then switch to finite reflux and begin simultaneous reaction and distillation. The column composition profiles connect the still pot composition to the IPOH-W-$CHCl_3$ azeotrope at all times, so the aqueous phase can be decanted from the condensed azeotrope and water removed at the top. Again, the removal of water from the reaction mixture drives the reaction forward, consuming AC and IPOH and producing more IPAc and W. Eventually, only IPAc and $CHCl_3$ remain in the still pot at the end of the batch reactive distillation. In the same way, we can apply an external heterogeneous entrainer for producing pure ethyl acetate (EtAc) in the esterification of acetic acid (AC) with ethyl alcohol (EtOH) in a

reactive rectifier-decanter. Adding an external entrainer will also be very helpful for producing pure EtAC since the UN heterogeneous EtOH-EtAc-W azeotrope is *barely* within the L-L miscibility gap.

Conclusions

We have derived feasibility criteria for complex batch reactive distillation including rectifier-decanter and homogeneous and heterogeneous BRED columns (or middle vessel BRED columns). If none of the products are nodes in RCMs with reaction bI ↔ cL +dH or aL+bI↔ cH or aK+bI↔ cL+dH, then homogeneous simple rectifiers, strippers, and MVCs cannot produce pure products. Even with a node product being present, these homogeneous batch columns cannot produce pure products if distillation boundaries block column profiles from reaching them. For these cases, we have introduced three alternative ways to produce pure products by using internal or external heterogeneity and by providing a homogeneous entrainer. If an unstable node heterogenous azeotrope exists between a product and another component (or external entrainer) and it is reachable from the reaction equilibrium manifold using simple or extractive distillation, then a rectifier or a BRED with a decanter can be used to separate a pure product. With no heterogeneity, we can introduce a homogeneous entrainer to a BRED (or middle vessel BRED) column. New projected upper and lower bounds of internal reflux ratios are introduced to analyze non-reactive sections of quaternary distillation in a BRED (or middle vessel BRED) column. This can be extended to multi-component and multi-reaction cases to check feasible directions of composition vectors.

Acknowledgements

We are grateful for the support of American Chemical Society – Petroleum Research Fund (ACS-PRF). We also wish to thank Prof. Wolfgang Marquardt at RWTH Aachen for the continued use of his phase equilibrium calculation code, material properties calculation code, and quaternary system visualization program code.

Notation

a, b, c, d Stoichiometric coefficients in ternary and quaternary reactions

D Molar flow rate of the distillate stream

$\tilde{D}_i$ Molar flow rate of the distillate stream under an i projection

E Molar flow rate of side-feed entrainer stream

$\tilde{E}_i$ Molar flow rate of side-feed entrainer stream under an i projection

H, L, K, I Products and reactants in ternary and quaternary reactions

H_S Molar holdup in the still

L_n Molar flow rate of the liquid stream leaving stage n

$\tilde{L}_{n,i}$ Molar flow rate of the liquid stream leaving stage n under an i projection

K_{eq} Reaction equilibrium constant

k_f Forward reaction rate constant (1/time)

V_n Molar flow rate of the vapor stream leaving stage n

$\tilde{V}_{n,i}$ Molar flow rate of the vapor stream leaving stage n under an i projection

V_{n+1} Molar flow rate of the vapor stream leaving stage n+1

x_i^* Mole fraction of component i at intersection point of the pseudo-balance lines

$\mathbf{x}_D$ Molar composition of the distillate stream

$\tilde{\boldsymbol{x}}_{D,POP}$ Composition of the distillate stream under a POP projection

$x_{D,i}$ Mole fraction of component i in the distillate

$\mathbf{x}_E$ Molar composition of the entrainer stream

$x_{E,i}$ Mole fraction of component i in the entrainer feed stream

$\tilde{\boldsymbol{x}}_{E,POP}$ Composition of the entrainer stream under a POP projection

x_i Mole fraction of component i in an unspecified liquid

$\tilde{x}_{i,j}$ Projected liquid mole fraction of component i under a j projection

$\mathbf{x}_n$ Molar composition of the liquid on stage n

$x_{n,i}$ Mole fraction of component i in the liquid leaving stage n

$\tilde{\boldsymbol{x}}_{n,POP}$ Composition of the stage n liquid under a POP projection

$\tilde{\boldsymbol{x}}_{POP}^*$ Composition of the pseudo-balance intersection under a POP projection

x_{POP} Liquid mole fraction of the projecting component. That is x_i where i = POP

$x_{S,i}$ Mole fraction of component i in the still pot

y_i Mole fraction of component i in an unspecified vapor

$\tilde{y}_{i,j}$ Projected vapor mole fraction of component i under a j projection

$y_{n,i}$ Mole fraction of component i in the vapor leaving stage n

y_{POP} Vapor mole fraction of the projecting component. That is y_i where i = POP

$\mathbf{y}_n$ Molar composition of the vapor on stage n

$\tilde{\boldsymbol{y}}_{n,POP}$ Composition of the stage n vapor under a POP projection

Greeks

$\gamma_{S,i}$ Activity coefficient of component i in the still pot

$\boldsymbol{\delta}_n$ Composition of the cascade different point on stage n

$\delta_{n,i}$ Mole fraction of component i in the cascade different point on stage n

$\boldsymbol{\upsilon}$ Reaction stoichiometry vector

υ_i Stoichiometric coefficient of component i

υ_T Sum of the stoichiometric coefficients

ξ_n Total rate-of-reaction within the material balance envelope of Figure 4-8

Appendix 4-1: Dynamic Simulation Model

The simulations presented in this paper are based on material balance equations derived from references 19, 23, and 33. Their derivation is reproduced here with only minor modifications. We consider a batch column that consists of, at most, a rectifying section, an extractive section, and a stripping section. Pseudo-steady state is adopted for non-reactive column sections since no reaction occurs in the column section and fast reaction assumes to take place in the still pot. We adopt a relatively simple operating policy as shown in Table 4-1 for each case.

Table 4-1. Dynamic simulation conditions

Operating policy	Constant Reflux Ratio	Product withdrawal rate
Figure 4-5 (DIPE)	10	Proportional to the reactive holdup in the reactive still pot.
Figure 4-14 (202-m)	23	
Figure 4-16 (313-S with a light entrainer)	20	
Figure 4-19 (313-S with a heavy entrainer)	20	
Figure 4-20 (313-S with a heavy entrainer in BRED MVC)	20	
Figure 4-22 (IPA system)	Increasing 80.0, 120.0, and 200.0*.	

* The aqueous reflux ratio increases over time to compensate for decreasing amounts of water in the still pot as distillation proceeds.

The time-dependent material balance equations around such a column are

$$\frac{dH_S}{dt} = -D - B + E + \nu_T H_S r \tag{A-1}$$

$$\frac{d\left(H_S x_{S,i}\right)}{dt} = -Dx_{D,i} - Bx_{B,i} + Ex_{E,i} + \nu_i H_s r \tag{A-2}$$

A standard middle-vessel column may be considered by setting E=0. A batch reactive stripper may be considered by setting D=0 and E=0. A BRED column may be considered by setting B=0. A batch reactive rectifier may be considered by setting B=0 and E=0. Stage heat balance is coupled with material balance using a special procedure called “mexprops” in the matlab[34]. For any test run, please contact the corresponding author.

We assume a reaction rate of the following form

$$r = k_f \left(\prod_i^{react} \left(x_{S,i} \gamma_{S,i} \right)^{|\nu_i|} - \prod_i^{prod} \left(x_{S,i} \gamma_{S,i} \right)^{\nu_i} \Big/ K_{eq} \right) \tag{A-3}$$

Here, we use a constant reaction rate constant (k_f=*50*) for all dynamic simulations (assume fast reaction). K_{eq} is given as

$$K_{eq} = \prod_i^{all} \left(x_{S,i} \gamma_{S,i} \right)^{\nu_i} = \frac{\prod_i^{prod} \left(x_{S,i} \gamma_{S,i} \right)^{\nu_i}}{\prod_i^{react} \left(x_{S,i} \gamma_{S,i} \right)^{|\nu_i|}} \tag{A-4}$$

We can rewrite equation (A-3) in terms of the following Damköhler number

$$Da = \frac{H_S k_f}{D + B} \tag{A-5}$$

Substituting (A-4) and (A-5) into (A-3) gives

$$r = \frac{(D + B) Da}{H_S} \left(\prod_i^{react} x_{S,i} \gamma_{S,i} - \prod_i^{prod} x_{S,i} \gamma_{S,i} \Big/ K_{eq} \right) \tag{A-6}$$

and the time-dependent material balance equations become

$$\frac{dH_S}{dt} = -D - B + E + \nu_T (D + B) Da \left(\prod_i^{react} x_{S,i} \gamma_{S,i} - \prod_i^{prod} x_{S,i} \gamma_{S,i} \Big/ K_{eq} \right) \tag{A-7}$$

$$H_S \frac{dx_{S,i}}{dt} = D(x_{S,i} - x_{D,i}) + B(x_{S,i} - x_{B,i}) - E(x_{S,i} - x_{E,i})$$

$$+ (\nu_i - \nu_T x_{S,i})(D + B) Da \left(\prod_i^{react} x_{S,i} \gamma_{S,i} - \prod_i^{prod} x_{S,i} \gamma_{S,i} \Big/ K_{eq} \right) \tag{A-8}$$

Finally, it should be noted that if a decanter is used at the top of the column, then x_D in these equations represents only the composition of the phase being removed as product.

Appendix 4-2: Equality of projected upper and lower bounds at a pinch point

We are interested in looking at the projected upper and lower bounds because they tell us if column profiles can travel in feasible directions. The calculations are based on a pinch assumption which generally isn't true; the projected upper bound is different from the projected lower bound as a result. It is of interest to confirm that the projected upper bound is equal to the projected lower bound at a true pinch point. That is, we wish to confirm that the following equation from equation (7) is true at a pinch point

$$\left(\frac{\tilde{V}_{n,POP}}{\tilde{E}_{POP}}\frac{\tilde{E}_{POP}}{\tilde{D}_{POP}}+\frac{\tilde{E}_{POP}}{\tilde{D}_{POP}}-1\right)=\frac{\tilde{L}_{n,POP}}{\tilde{D}_{POP}} \tag{A-9}$$

This will be proven by working backwards from this equation to known statements.

Inserting $\tilde{D}_{POP}=D\left[1-x_{D,POP}\right]$, $\tilde{E}_{POP}=E\left[1-x_{E,POP}\right]$, $\tilde{L}_{n,POP}=L_n\left[1-x_{n,POP}\right]$,

and $\tilde{V}_{n,POP}=V_n\left[1-y_{n,POP}\right]$ to (A-9) gives

$$\frac{V_n}{E}\frac{E}{D}\frac{\left[1-y_{n,POP}\right]}{\left[1-x_{D,POP}\right]}+\frac{E}{D}\frac{\left[1-x_{E,POP}\right]}{\left[1-x_{D,POP}\right]}-1=\frac{L_n}{D}\frac{\left[1-x_{n,POP}\right]}{\left[1-x_{D,POP}\right]} \tag{A-10}$$

Multiply all terms by $[1-x_{D,POP}]$ and rearranging this equation gives

$$\frac{V_n}{E}\frac{E}{D}+\frac{E}{D}-1-\frac{L_n}{D}=\frac{V_n}{E}\frac{E}{D}y_{n,POP}+\frac{E}{D}x_{E,POP}-x_{D,POP}-\frac{L_n}{D}x_{n,POP} \tag{A-11}$$

Multiplying all terms by D, we get

$$V_n+E-D-L_n=V_n y_{n,POP}+Ex_{E,POP}-Dx_{D,POP}-L_n x_{n,POP} \tag{A-12}$$

The expression on the left is the overall material balance and is zero at a pinch point. The expression on the right is a component-wise material balance and is also zero at a pinch point. Thus, both sides of the equation are zero, they are equal, and the starting equation is true.

References

1. Taylor R, Krishna R. Modelling reactive distillation. *Chem. Eng. Sci.* 2000;55:5183-5229.
2. Malone MF, Doherty MF. Reactive distillation. *Ind. Eng. Chem. Res.* 2000;39:3953-3957.
3. Agreda VH, Partin LR. Reactive distillation process for the production of methyl acetate". U.S. Patent 4,435,595: 1984.
4. Agreda VH, Partin LR, Heise WH. High purity methyl acetate via reactive distillation. *Chem. Eng. Prog.* 1990;86(2):40-46.
5. Siirola JJ. An industrial perspective on process synthesis. *AIChE Symp. Ser.* 1995;304:222-233.
6. Hasebe S, Noda M, Hashimoto I. Optimal operation policy for multi-effect batch distillation system. *Comp. Chem. Eng.* 1997;21:S1221-S1226.
7. Bonny L. Multicomponent batch distillation: study of operating parameters. *Ind. Eng. Chem. Res.* 1999;38:4759-4768.
8. Kim K, Diwekar UM. Comparing batch column configurations: parametric study involving multiple objectives. *AIChE J.* 2000;46:2475-2488.
9. Lelkes Z, Lang P, Benadda B, Moszlowicz P. Feasibility of extractive distillation in a batch rectifier. *AIChE J.* 1998;44:810-822.
10. Lelkes Z, Lang P, Moszlowicz P, Benadda B, Otterbein M. Batch extractive distillation: the process and the operational policies", *Chem. Eng. Sci.* 1998;53:1331-1348.
11. Phimister JR, Seider WD. Semicontinuous, middle-vessel extractive distillation. *Comp. Chem. Eng.* 2000;24:879-885.
12. Phimister JR, Seider WD. Semicontinuous, middle-vessel distillation of ternary mixtures. *AIChE J.* 2000;46:1508-1520.
13. Safrit BT, Westerberg AW, Diwekar U, Wahnschafft OM. Extending continuous conventional and extractive distillation feasibility insights to batch distillation. *Ind. Eng. Chem. Res.* 1995;34:3257-3264.
14. Safrit BT, Westerberg AW. Improved operation policies for batch extractive distillation columns. *Ind. Eng. Chem. Res.* 1997;36:436-443.
15. Bernot C, Doherty MF, Malone MF. Feasibility and separation sequencing in multicomponent batch distillation. *Chem. Eng. Sci.* 1991;46:1311-1326.
16. Lotter SP and Diwekar UM. Shortcut models and feasibility considerations for emerging batch distillation columns. *Ind. Chem. Eng. Res.* 1997;36:760-770.
17. Cheong W, Barton PI. Azeotropic distillation in a middle vessel batch column. 3. Model validation. *Ind. Eng. Chem. Res.* 1999;38:1549-1564.

18. Lang P, Modla G, Benadda B, Lelkes Z. Homoazeotropic distillation of maximum azeotropes in a batch rectifier with continuous entrainer feeding I. Feasibility studies. *Comp. Chem. Eng.* 2000;24:1665-1671.

19. Venimadhavan G, Malone MF, Doherty MF. A Novel distillate policy for batch reactive distillation with application to the production of butyl acetate. *Ind. Chem. Eng. Res.* 1999;38:714-722.

20. FernholzG, Engell S, Kreul L-U, Gorak A. Optimal operation of a semi-batch reactive distillation column. *Comp. Chem. Eng.* 2000;24:1569-1575.

21. Cuille PE, Rekliaitis GV. Dynamic simulation of multicomponent batch rectification with chemical reactions. *Comp. Chem. Eng.* 1986;10:389-398.

22. Gadewar SB, Malone MF, Doherty MF. Selectivity targets for batch reactive distillation. *Ind. Eng. Chem. Res.* 2000;39:1565-1575.

23. Guo Z, Ghufran M, Lee JW. Feasible products in batch reactive distillation. *AIChE J.* 2003;49:3161-3172.

24. Lee JW. Feasibility studies on quaternary reactive distillation systems. *Ind. Eng. Chem. Res.* 2002;41:4632-4642.

25. Chin J, Kattukaran HJ, Lee JW. Generalized feasibility evaluation of equilibrated quaternary reactive distillation systems. *Ind. Eng. Chem. Res.* 2004;43:7092-7102.

26. Matsuyama H, Nishimura H. Topological and thermodynamic classification of ternary vapor-liquid equilibria. *J. Chem. Engr. Japan* 1977;10:No. 3, 181-187.

27. Aspen Plus 12.1, Aspen Engineering Suite, Aspen Tech (2005).

28. Mathematica 4.2, Wolfram Research Inc. (2002).

29. Chin J, Lee JW. Rapid generation of composition profiles for reactive and extractive cascades. *AIChE J.* 2005;51:922-930.

30. Tang YT, Chen YW, Hung SB, Huang HP, Lee MJ, Yu CC. Design of reactive distillations for acetic acid esterification. *AIChE J.* 2005;51:1683-1699.

31. Lee L, Kuo M. Phase and reaction equilibria of the acetic acid - isopropanol – isopropyl acetate – water system at 760 mmHg. *Fluid Phase Equilibria.* 1996;38:147-165.

32. Rooks RE, Julka V, Doherty MF, Malone MF. Structure of distillation regions for multicomponent azeotropic mixtures. *AIChE J.* 1998;44:1382-1391.

33. Guo Z, Lee JW. Feasible products in batch reactive extractive distillation. *AIChE J.* 2004;50:1484-1492.

34. Matlab 6.0, Using Matlab. The MathWorks, Inc.; 2000.

Chapter 5: Estimation of Still Trajectory for the Feasibility Evaluation of Batch Reactive Distillation Systems

This chapter has been submitted to AIChE Journal for review.

Abstract – This article addresses a new method for estimating the liquid still composition trajectory of batch reactive distillation systems based on material balance and reaction equilibrium data. The still trajectory information is essential to determining whether pure products are reachable from this still pot trajectory when several distillation boundaries are present, initial feed compositions can vary, and the number of components exceeds our visualization capability. For a given feed to product flow ratio with constant feed charge and product compositions, the still pot composition trajectory is mathematically confined to the intersection between the reaction equilibrium manifolds and a "material balance plane" that is the union of stoichiometric lines and material balance rays connecting still and product compositions. Starting from this estimated still pot trajectory, we can easily evaluate the feasibility of various batch reactive distillation configurations by constructing the residue curves for non-extractive cases and the feasible region formed by upper and lower bounds of reflux ratios for extractive cases.

Introduction

Reactive distillation is the combination of chemical reaction and V-L (or V-L-L) phase separation in the same unit. Conducting reaction and distillation simultaneously allows each to overcome the limitations of the other, thus allowing for potential reductions in the capital costs, operating costs, and energy usage of chemical processes[1-3]. It can greatly simplify processes that would otherwise consist of many single-operation units and sometimes avoid the use of separate extractive agents. However, the most

important question that should be answered before we integrate reaction and distillation is whether or not we can obtain pure products by combining these two tasks. Although reaction conversion and selectivity can be improved with simultaneous separation, we still have to put in additional separation units unless the products from a reactive distillation unit satisfy purity requirements.

.

Previous work[4-10] by our group has determined the feasibility criteria to produce pure products in various reactive distillation column structures in terms of residue curve maps and the upper and lower bounds of internal reflux ratios. The feasibility criteria for batch and continuous reactive columns with a single reaction of the form aK+bI ↔ cL+dH, bI ↔ cL +dH, and aK+bI ↔ dH are: 1) If residue curves connect the entire reaction equilibrium curve to a pure product, and this pure product is an unstable node in the residue curve map, then a batch reactive rectifier can produce pure product[5]. 2) If residue curves connect the entire reaction equilibrium curve to a pure product, and this pure product is a stable node in the residue curve map, then a batch reactive stripper can produce pure product[5]. 3) If residue curves connect part of the reaction equilibrium curve to two pure products where one product is a stable node and the other product is an unstable node, then a batch reactive middle-vessel column or a continuous single-feed reactive distillation column can produce pure product[5,7]. 4) If residue curves connect the reaction equilibrium curve to an unstable node azeotrope inside a liquid-liquid miscibility gap, and this azeotrope splits to an almost pure product, then a batch reactive rectifier with a decanter can produce pure product[10]. 5) If the feasibility region (defined by the upper and lower bounds of internal reflux ratios) contains the reaction equilibrium

manifold and connects it to the light product/entrainer edge of composition space, then a batch reactive extractive distillation (BRED) column or a double-feed continuous column can produce pure products[4,6,8-10].

In cases where all of composition space meets a feasibility criterion, this is easy to evaluate. For example, if there are three distillation regions, but the light product is the only unstable node, then a batch reactive rectifier can always produce pure products regardless of where the reaction equilibrium manifold is located. However, if there are multiple distillation regions and only some of those regions can possibly meet the feasibility criterion, then the feasibility depends upon where the reaction equilibrium manifold is located and what the initial feed charge is. Thus, we need to develop a method to estimate the composition trajectory of a given feed composition and to determine its feasibility by considering the relative positions of feed compositions, distillation boundaries, and reaction equilibrium manifolds.

This work will present a new method of estimating the composition trajectories of batch reactive distillation systems for given feed and product specifications and reaction/phase equilibrium information. We will mathematically derive a material balance plane that confines the liquid still pot trajectory to the union between stoichiometric lines and material balance operating lines. We will then intersect this material balance plane with reaction equilibrium manifolds to estimate the trajectory. Finally, we will demonstrate the utility of the composition trajectory estimation in promoting the selectivity of a particular reaction when two reactions occur in series.

Trajectory Estimation in Reactive Batch Columns

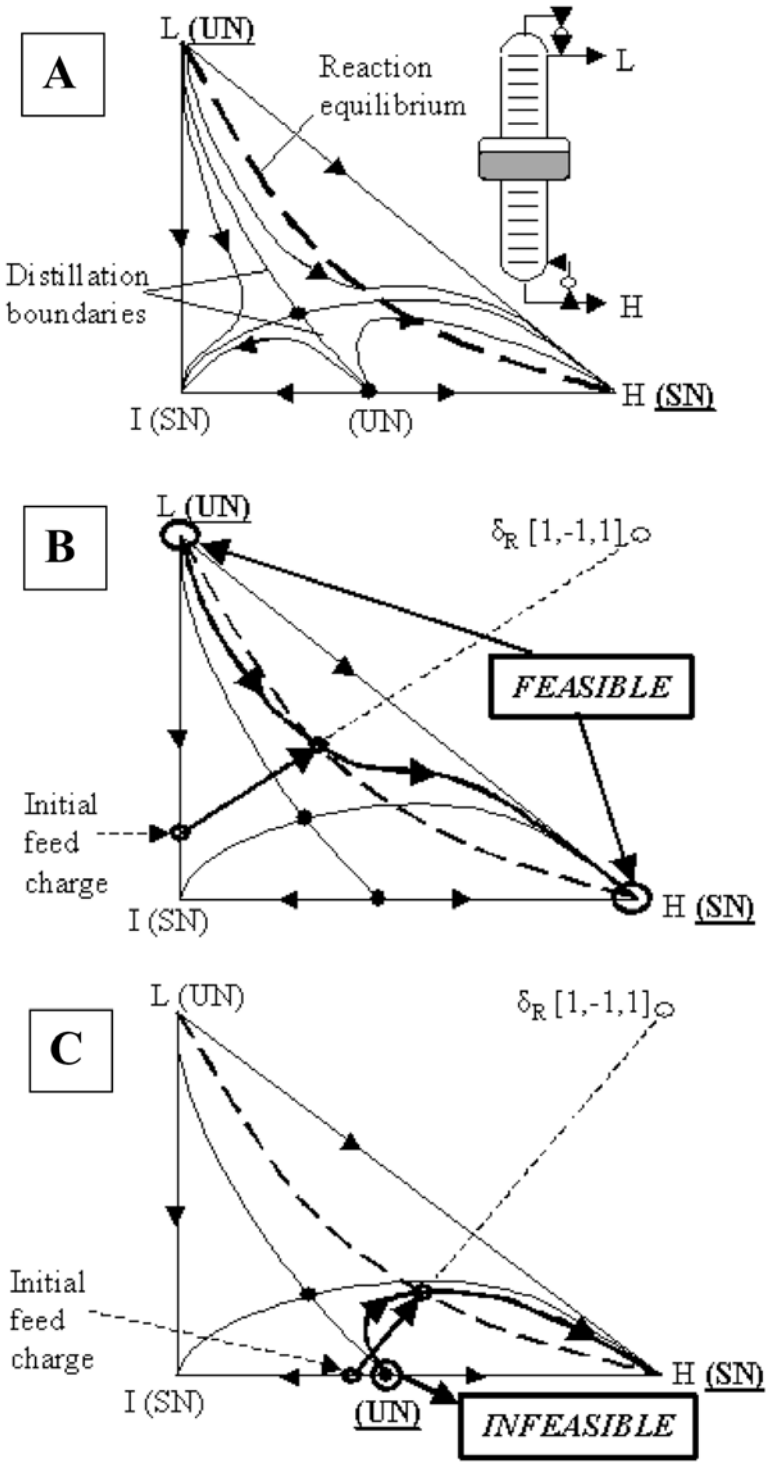

Figure 5-1. Feasibility of RCM 010-S with a reaction of I ↔ L+H.
(a) RCM with reaction equilibrium curve (dotted line), (b) Feasible feed, and (c) Infeasible feed.

Let's first examine the influence of the feed charge on column feasibility. Consider a chemical system with three components L, I, and H (the light, intermediate, and heavy-boiling components), the phase equilibrium behavior of RCM 010-S (using the RCM classification[11-12]), and the reaction I ↔ L + H. The combined phase and reaction equilibrium behavior is shown in Figure 5-1 (a). In this example, a batch reactive middle-vessel column can feasibly produce pure products because the reaction equilibrium curve lies in part of the same distillation region as pure L and pure H. But, not all feed compositions are suitable for this purpose. For the feed composition shown in Figure 5-1 (b), when the pot composition is reacted to equilibrium along the stoichiometric line connecting the feed composition and the reaction difference point ($\boldsymbol{\delta}_R$)[13], residue curves can connect the pot composition to the node products, so pure products can be produced from this feed composition. However, for the feed composition shown in Figure 5-1 (c), when the pot composition is reacted following the stoichiometric line, residue curves only connect the pot composition to pure H, but not pure L. Instead, they connect to the I-H azeotrope.

Let us now consider the influence of the reaction equilibrium manifold on column feasibility. Consider two distinct chemical systems that have different reaction equilibrium constants, but share the same phase equilibrium behavior (RCM 430), stoichiometry (I ↔ L + H), and initial feed composition (pure reactant I). Two such systems are shown in Figures 5-2 (a) and (b). In Figure 5-2(a), part of the reaction equilibrium curve lies in the infeasible distillation region where pure I is the unstable node. Thus, a batch reactive rectifier in this distillation region will not produce the

desired product. In Figure 5-2(b), however, the reaction equilibrium curve only exists in the feasible distillation region where pure L is the unstable node. Thus, a batch reactive rectifier can produce pure products.

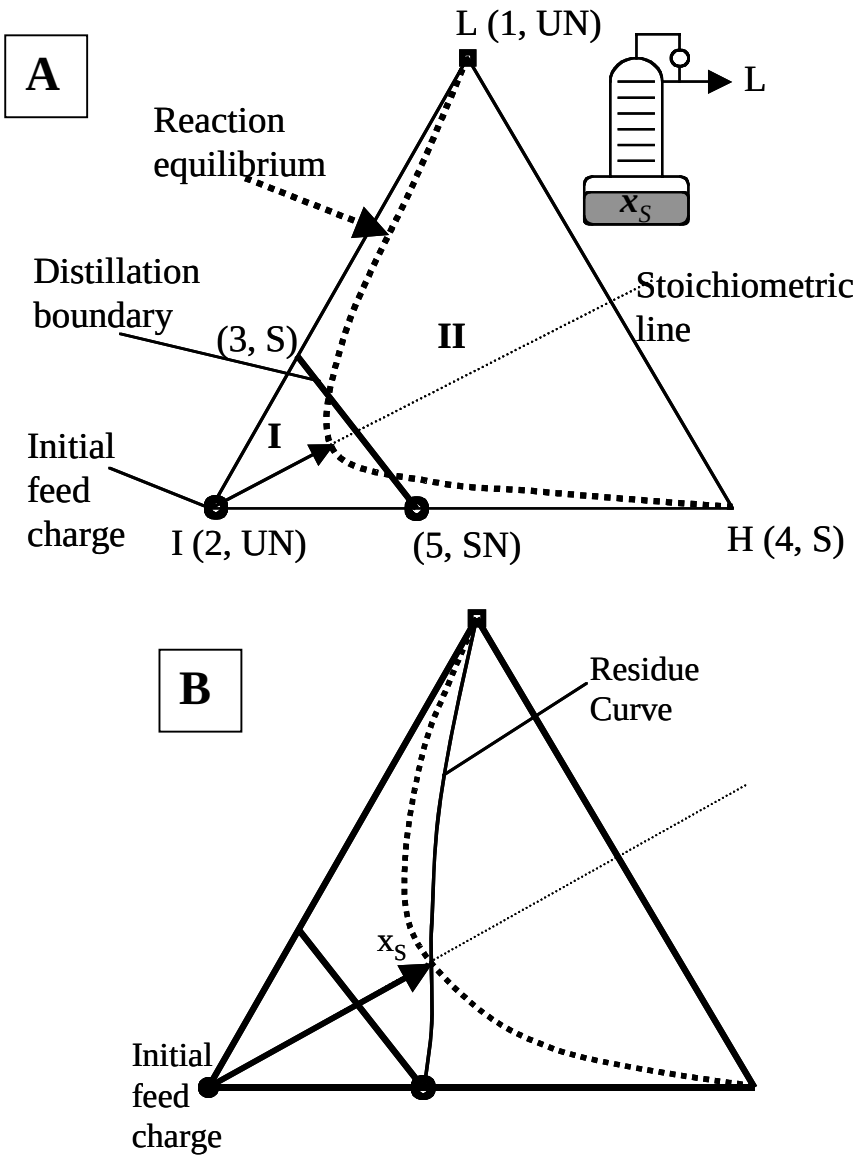

Figure 5-2. Feasibility of RCM 430 with a reaction of I ↔ L+H. (a) Infeasible reaction equilibrium and (b) Feasible reaction equilibrium. The numbers in parenthesis represent the boiling point order from lowest to highest.

From these two examples in Figures 5-1 and 5-2, it is obvious that, with respect to given feed composition and equilibrium behavior, we have to understand whether the

reactive-still composition trajectory can stay at a feasible location where pure products are reachable using non-reactive rectification, stripping, or extractive rectification. This requires us to determine which pieces of the reaction equilibrium manifold exist in which distillation regions. If an initial batch feed composition is fixed, then only a certain limited range of batch compositions will be encountered during a batch reactive distillation process. Here, we present a method for estimating the time-dependent trajectory of the still pot of a batch reactive distillation column using the reaction equilibrium manifold and the material balance constraints by assuming constant product compositions. The feasibility of the trajectory is then validated by residue curves for non-extractive columns and by the upper and lower bounds of internal reflux ratios for extractive columns.

Still Trajectory for Batch Reactive Rectifier

Consider an initial feed charge to the still pot of a batch reactive rectifier where the feed charge is reacted to chemical equilibrium prior to withdrawing a product by distillation. A residue curve is drawn through this new pot composition to both the stable and unstable nodes to determine the initial distillation region, as shown in Figure 5-2(b). We want to estimate the trajectory of the still pot composition during reactive distillation. Assume zero holdup and no reaction on the column trays, an infinite number of trays, infinite reflux, and that the reaction occurs much faster than distillation, so the still pot composition is always in reaction equilibrium. Under these assumptions (particularly the infinite reflux assumption), the column profile at any given moment in time follows the residue curves. Assume that the composition of the distillate is constant; we justify this assumption on the grounds that, for a column to be feasible, we don’t want the product

composition to change significantly. Since we want to check feasibility, we estimate the reactive still trajectory under the constant product composition assumption and then use the trajectory to check the reachability of a specified product by residue curves.

The composition of the still pot changes due to the removal of product in the distillate (or bottoms) and due to reaction. These changes are described by the following equation:

$$\frac{d\boldsymbol{x}_s}{d\xi} = (\boldsymbol{x}_s - \boldsymbol{x}_D) + \frac{H_s}{D}(\boldsymbol{\nu} - \nu_T \boldsymbol{x}_s)r \qquad (1)$$

where $\boldsymbol{x}_s$ is the composition of the still pot, $\boldsymbol{x}_D$ is the composition of the distillate product, $\boldsymbol{\nu}$ is the stoichiometric coefficient vector, ν_T is the sum of the stoichiometric coefficients, ξ is a non-dimensionalized time, H_s is the holdup in the still pot (in moles), D is the molar flow rate of distillate, and r is the reaction rate per mole of mixture in the still pot.

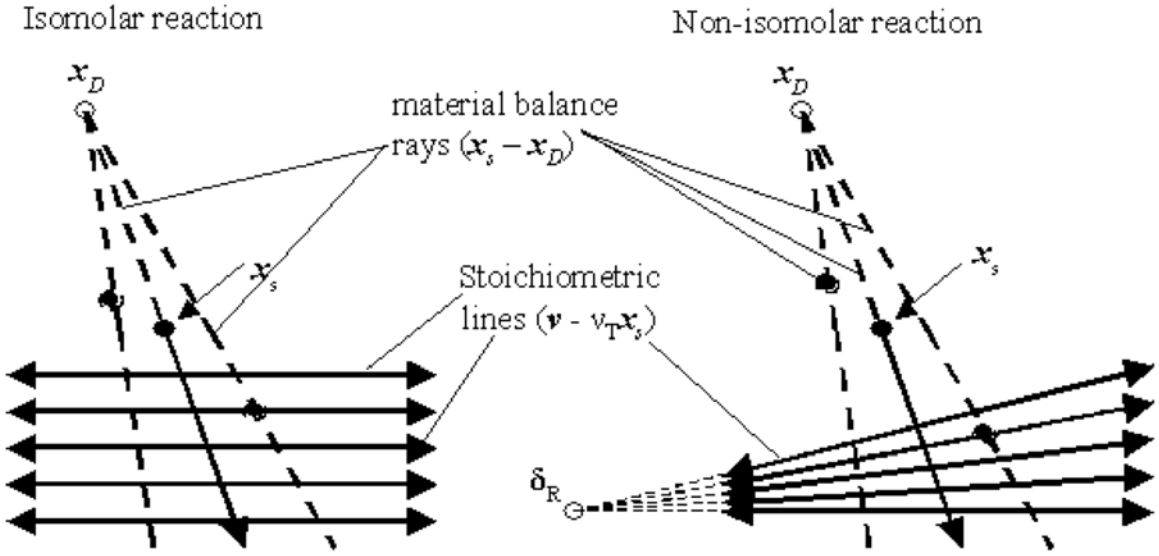

Figure 5-3. Material balance plane under the assumption of constant product composition

As the reactive distillation progresses, $\boldsymbol{x}_s$ will move through composition space in a linear combination of the vectors $(\boldsymbol{x}_s - \boldsymbol{x}_D)$ and $(\boldsymbol{\nu} - \nu_T \boldsymbol{x}_s)$. The direction of either vector will change as $\boldsymbol{x}_s$ moves along the other vector as shown in Figure 5-3. The change in either vector is always dependent on the change of the other vector. Thus, these two vectors define a plane which we shall call the "material balance plane"; the still pot composition is confined to this plane. The material balance plane does not change so long as the product composition does not change. Its mathematical proof is available in Appendix-1 and Appendix-2.

To geometrically determine the material balance plane, we start by drawing the geometric ray starting at $\boldsymbol{x}_s$ and in the direction of the vector $(\boldsymbol{x}_s - \boldsymbol{x}_D)$ (this is headed away from $\boldsymbol{x}_D$). Let us call it the "material balance ray". We then consider the set of all stoichiometric lines that pass through the material balance ray. This is the "material balance plane" discussed above. The material balance plane is shown in Figure 5-3 for a 3-component system (where the plane is coincident with all of composition space).

The next step is to find the intersection between the material balance plane and the reaction equilibrium manifold. To do this, we take an arbitrary set of points on the material balance ray and draw stoichiometric lines from each point to the reaction equilibrium manifold. This gives us a set of points that lie on both the material balance plane and the reaction equilibrium manifold simultaneously. This is our estimate of the still pot trajectory in Figure 5-4 (a). Our last step is to verify the constant-distillate assumption. The distillate composition at any given moment in time depends upon the

still pot composition, and the two are connected by a column composition profile. In the limit of infinite reflux, the column profile follows the residue curves, and a residue curve connects the still pot composition to the distillate composition. So, we then draw a residue curve from each point on our estimated still pot trajectory and follow the residue curves to the most volatile composition. If the residue curves all lead to the product composition, then the assumption of a constant product composition is correct and the column is feasible for the given feed charge. This is shown in Figure 5-4(b): all of the residue curves end at the assumed distillate composition. It should be noted that in the 3-component system, the intersection between the material balance plane and the reaction equilibrium curve is the same reaction equilibrium curve, but in the 4-component system, the intersection between the plane and the reaction equilibrium surface is a curve, a subset of the surface as shown in Figure 5-5.

For batch reactive rectifiers with a decanter, the previous analysis for columns without a decanter apply identically with the exception that the column profiles do not go to the assumed product composition, $\boldsymbol{x}_D$. Rather, the column profiles must go to an unstable node azeotrope that is inside a miscibility gap. The assumed product composition must be an endpoint of the liquid-liquid tie line that goes through this unstable node.

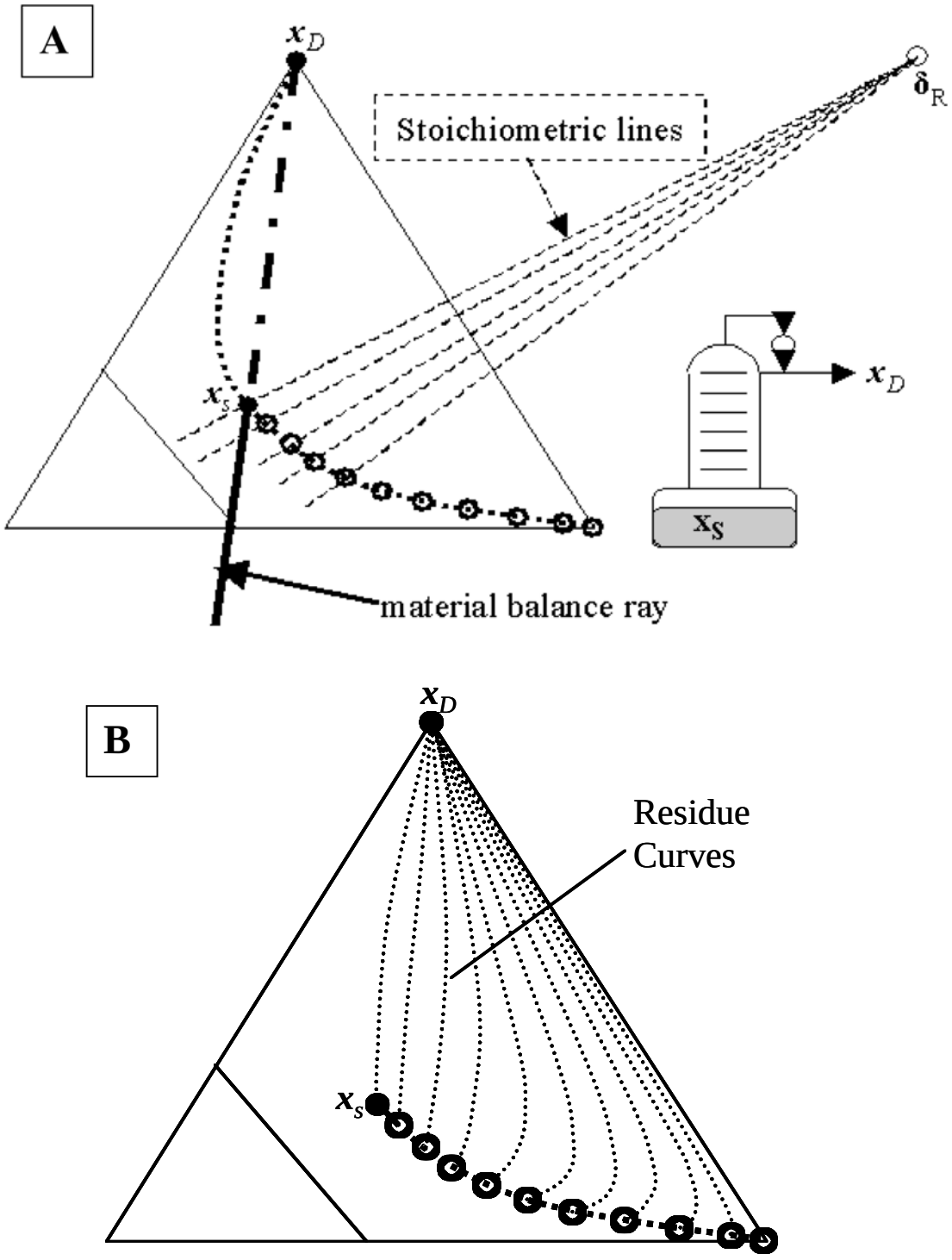

Figure 5-4. Quick estimation of the reactive-still trajectory with RCM 430. (a) Still trajectory on the reaction equilibrium curve and (b) Residue curves starting from the still trajectory.

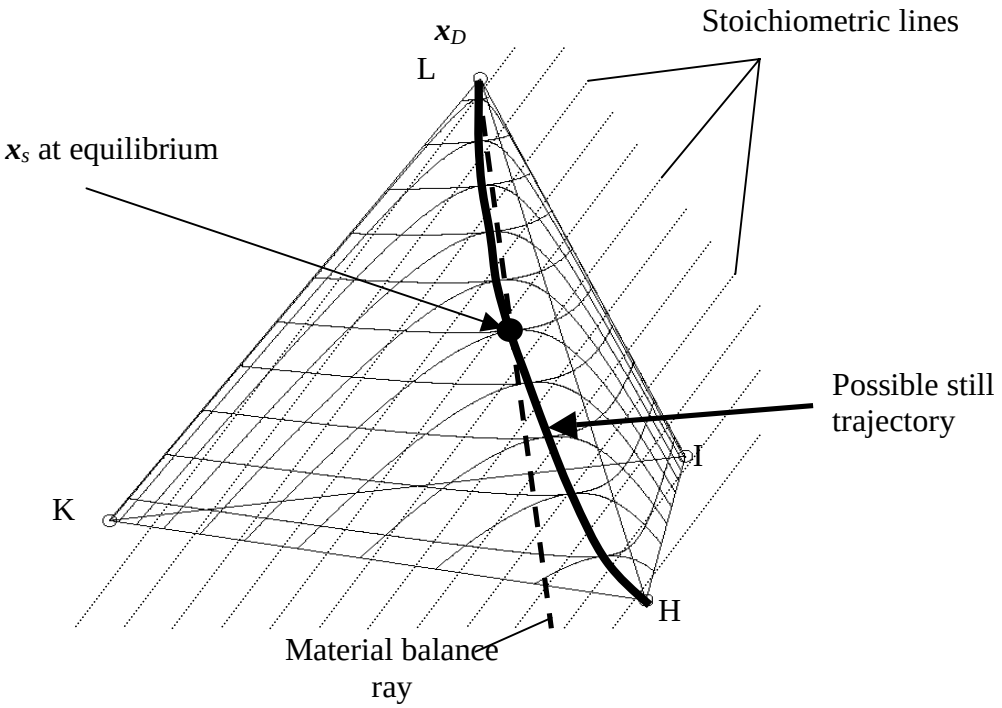

Figure 5-5. Quick estimation of the reactive-still trajectory with I+K ↔ L+H.
Solid grid curves are reaction equilibrium curve.

In the case of multiple reactions (*n* reactions), the second right-hand term is repeated for each additional reaction, and the equation becomes:

$$\frac{d\boldsymbol{x}_s}{d\xi} = \left(\boldsymbol{x}_s - \boldsymbol{x}_D\right) + \frac{H_s}{D}\sum_{i=1}^{n}\left(\boldsymbol{\nu}_i - \boldsymbol{\nu}_{Ti}\boldsymbol{x}_s\right)r_i \qquad (2)$$

The vectors still change only in proportion to each other, so the material balance plane becomes a material balance hyperplane with (*n+1*) dimensions because there are *n* reactions and is always a linear variation as proven in Appendix-3.

Batch Reactive Stripper

For batch reactive strippers, the analysis for batch reactive rectifiers applies identically. The still pot composition only changes due to two influences: the removal of bottoms product and chemical reaction. Removal of a product stream from the column will cause the still pot composition to move away from the composition of the product stream. Reaction will cause the still pot composition to move back or forth along a stoichiometric line. These two influences are material balance constraints and they only allow the still pot composition to change within a geometric plane (again, for a single-reaction case, this is a 2-dimensional linear variation regardless of how many chemical components are involved). The equation is:

$$\frac{d\boldsymbol{x}_s}{d\xi} = \left(\boldsymbol{x}_s - \boldsymbol{x}_B\right) + \frac{H_s}{B}\sum_{i=1}^{n}\left(\boldsymbol{\nu}_i - \nu_{Ti}\,\boldsymbol{x}_s\right) r_i \qquad (3)$$

where $\boldsymbol{x}_B$ is the composition of the bottoms and is assumed to be constant. To determine the material balance plane, we start by drawing the material balance ray starting at $\boldsymbol{x}_S$ and in the direction of the vector $(\boldsymbol{x}_S - \boldsymbol{x}_B)$ (this is headed away from $\boldsymbol{x}_B$). We then consider the set of all stoichiometric lines that pass through the material balance ray to find the material balance plane that the still pot composition is constrained to. The still pot trajectory must lie on the material balance plane as long as the constant-bottoms-composition assumption is true.

Consider a hypothetical three-component chemical system whose components, L, I, and H, are the light, intermediate, and heavy-boiling components respectively. The reaction is 2 I ↔ L + H where I is the reactant and L and H are the desired products. This system has the phase equilibrium behavior of RCM 120; there is a minimum-boiling node azeotrope between L and I, there is a minimum-boiling saddle azeotrope between I and H, pure L is a saddle, and both pure I and pure H are stable nodes. Two different sets of reaction equilibrium behavior are shown in Figure 5-6 to demonstrate feasibility's dependence upon the reaction equilibrium.

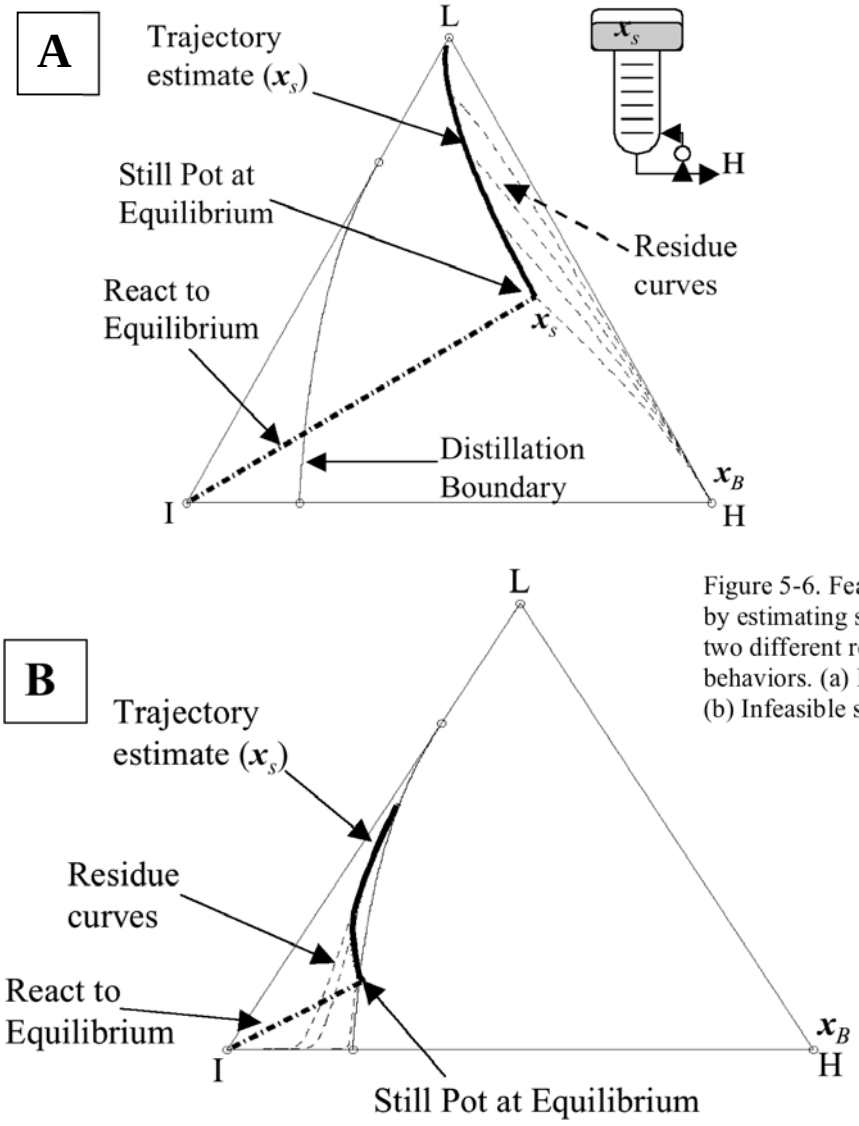

Figure 5-6. Feasibility of RCM120 by estimating still trajectories for two different reaction equilibrium behaviors. (a) Feasible system and (b) Infeasible system.

In the first case, shown in Figure 5-6 (a), the reaction equilibrium constant is 15 (based upon mole fractions) and the initial feed charge is pure I. Upon reacting this to equilibrium, we draw residue curves from the still pot to the most and least volatile compositions and we discover that the still pot composition is in the feasible distillation region where H is the stable node. We draw our material balance ray starting at the still pot composition and away from pure H (our bottoms product). We then draw the stoichiometric lines through the material balance ray to find our trajectory estimate on the reaction equilibrium curve. From points on this estimate, we then draw residue curves to the least volatile composition and find that they all lead to pure H. Thus, the assumption of a constant bottoms product is verified and a batch reactive stripper can produce pure products.

In the second case, shown in Figure 5-6(b), the reaction equilibrium constant is 0.05 (based on mole fractions). The initial feed charge is still pure I. Upon reacting this to equilibrium, we draw residue curves from the still pot to the most and least volatile compositions. As with the first case, we draw the material balance ray and the stoichiometric lines, find the trajectory estimate, and draw residue curves from the trajectory estimate. In this case, we find a large set of points in the middle of the trajectory estimate whose residue curves lead back to pure I. Thus, the assumption of a constant bottoms product is clearly incorrect and a batch reactive stripper cannot produce pure products.

Batch Reactive Middle-Vessel Column

The analysis for a batch-reactive middle vessel column is similar to the analysis for rectifiers and stripper, though $\boldsymbol{x}_s$ can now change because of three influences: removal of distillate, removal of product, and chemical reaction. If the relative flow rates of distillate and bottoms are not constrained, then $\boldsymbol{x}_s$ may vary along a material balance cube rather than a material balance plane. One can conceivably find the intersection between such a material balance cube and the reaction equilibrium manifold, but this will increase the calculation burden dramatically. We instead fix the relative flow rates and compositions of distillate and bottom product.

$$\frac{d\boldsymbol{x}_s}{d\xi} = \left(\boldsymbol{x}_s - \boldsymbol{x}_P\right) + \frac{H_s}{P}\sum_{i=1}^{n}\left(\nu_i - \nu_{Ti}\boldsymbol{x}_s\right)r_i \qquad (4)$$

where P is the total product molar flow rate ($P = D + B$) and $\boldsymbol{x}_P$ is the overall product composition ($\boldsymbol{x}_P = (D\boldsymbol{x}_D + B\boldsymbol{x}_B)/P$) which was also defined as a pseudo-feed[14].

Figure 5-7 (a) shows that if the material balance line starting at $\boldsymbol{x}_s$ is coincident with the stoichiometric line passing through $\boldsymbol{x}_s$, then the composition change due to removal of product exactly cancels the composition change due to reaction. The result is that the still pot composition is invariant with respect to time and it is only necessary to draw the residue curves from the still pot composition alone to verify feasibility. This will occur only when the initial feed composition lies on the same stoichiometric line as the overall product composition. Otherwise, the still trajectory ($\boldsymbol{x}_s$) will move along the

reaction equilibrium curve in the direction going away from the product that is being withdrawn at the faster flow rate. In Figure 5-7(b), the bottom material balance rate (B) is higher than the distillate material balance rate (D), so the still trajectory move away from the bottom product composition as distillation proceeds.

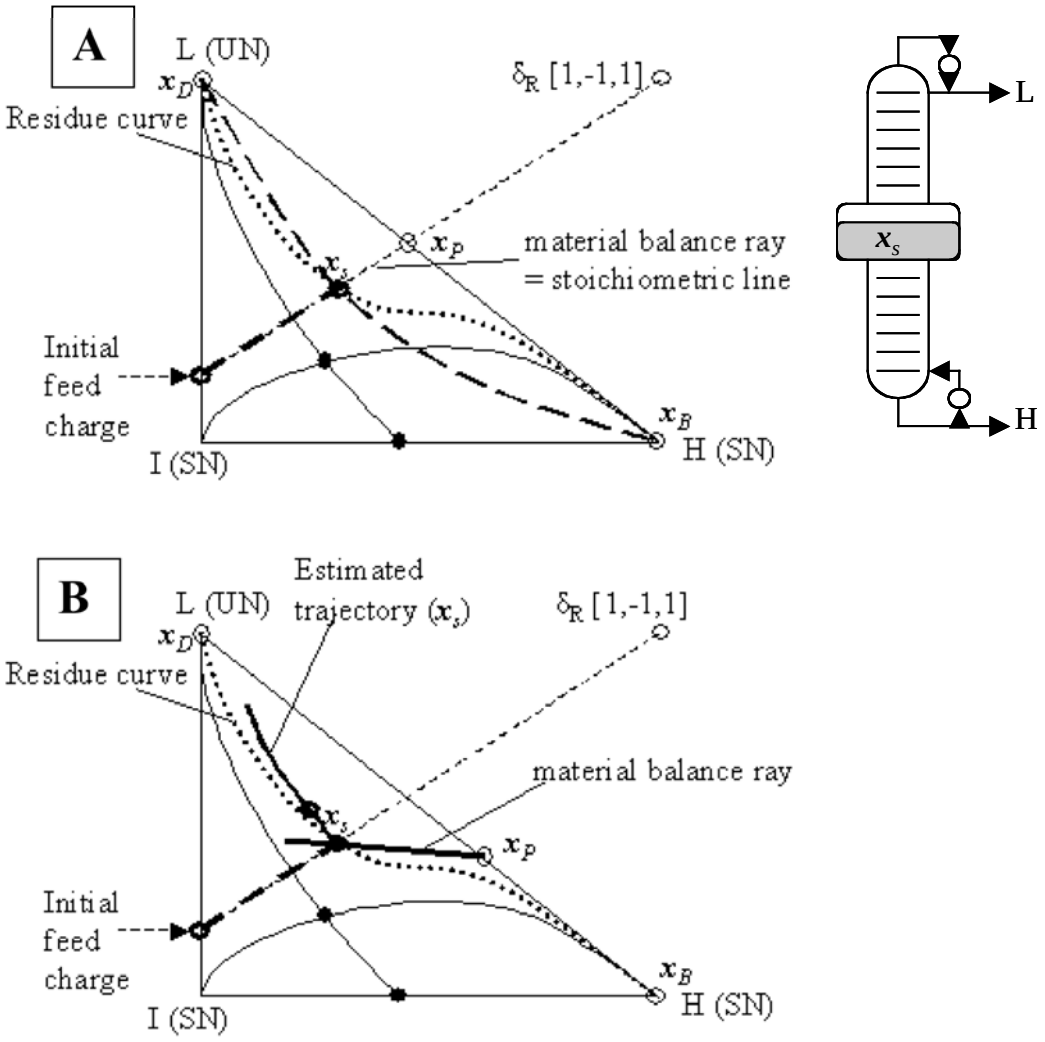

Figure 5-7. Still trajectory of MVC with RCM 010-S and a reaction of I ↔ L+H.
(a) Stationary still trajectory and (b) Moving still trajectory.

Batch Reactive Extractive Distillation Column

Consider an initial feed charge to the still pot of a batch reactive extractive distillation (BRED) column where the feed charge is reacted to chemical equilibrium prior to any other action. Assume zero holdup on the column trays, constant distillate composition, constant extractive feed composition, and that any distillation occurs slowly enough that the still pot composition is always in reaction equilibrium.

Like a batch reactive MVC, a BRED column introduces another stream, only it's an extractive feed stream instead of a bottoms stream. The derivative of $\boldsymbol{x}_S$ becomes

$$\frac{d\boldsymbol{x}_s}{d\xi} = \left(\boldsymbol{x}_s - \boldsymbol{x}_D\right) - \frac{E}{D}\left(\boldsymbol{x}_s - \boldsymbol{x}_E\right) + \frac{H_s}{D}\sum_{i=1}^{n}\left(\boldsymbol{v}_i - v_{Ti}\boldsymbol{x}_s\right)r_i \qquad (5)$$

where $\boldsymbol{x}_E$ is the composition of the extractive feed (fixed by design), and E is the extractive feed molar flow rate. We can then draw the material balance ray and the stoichiometric lines, and then estimate the still pot trajectory as before.

Verifying the feasibility of the trajectory, however, follows a different procedure because extractive sections of distillation columns do not follow residue curves. In previous work, we determined a "feasibility region" calculated from the upper and lower bounds of internal reflux ratios[4,8-10]. For a given E/D ratio, if the upper bound of the internal reflux ratio is greater than the lower bound of the internal reflux ratio at a given liquid composition, then that liquid composition is in the feasibility region and an extractive section composition profile containing that liquid composition can approach

the binary edge of composition space between the pure light product and the pure entrainer vertices.

For the BRED system, verifying the constant-product assumption then requires two conditions: 1) First, the feasible region determined by the upper and lower bounds of internal reflux ratios should include the binary edge of the light product and entrainer vertices[8-10]. 2) Second, the still trajectory estimate should remain in the feasibility region for extractive distillation.

Again consider a hypothetical L, I, H system with the reaction $2I \leftrightarrow L + H$ and a heavy inert entrainer (E). Suppose that L, I, and H, by themselves, have a phase equilibrium behavior of 313-S as used for our previous work[10]. Thus, there are 3 binary node azeotropes and a ternary saddle azeotrope. We will consider two different cases that vary only by entrainer flow rate. In the first case, shown in Figure 5-8 (a), the molar flow ratio between entrainer and distillate (or the E/D ratio) is 2.0. We take an initial pot composition of [0 0.9 0 0.1] (mole fractions of L, I, H, and E, respectively) and react it to equilibrium. Then, given the E/D ratio, we draw the material balance ray (vertical line) and the stoichiometric lines (horizontal lines) that pass through the ray. We then find where the stoichiometric lines intersect the reaction equilibrium surface; this intersection is our trajectory estimate. For the points on the trajectory, we calculate the upper and lower bounds of the internal reflux ratio, and we find that only part of the trajectory is in the feasibility region for reactive extractive distillation. Because the

trajectory leaves the feasibility region, the constant product assumption is not correct and pure L cannot be produced.

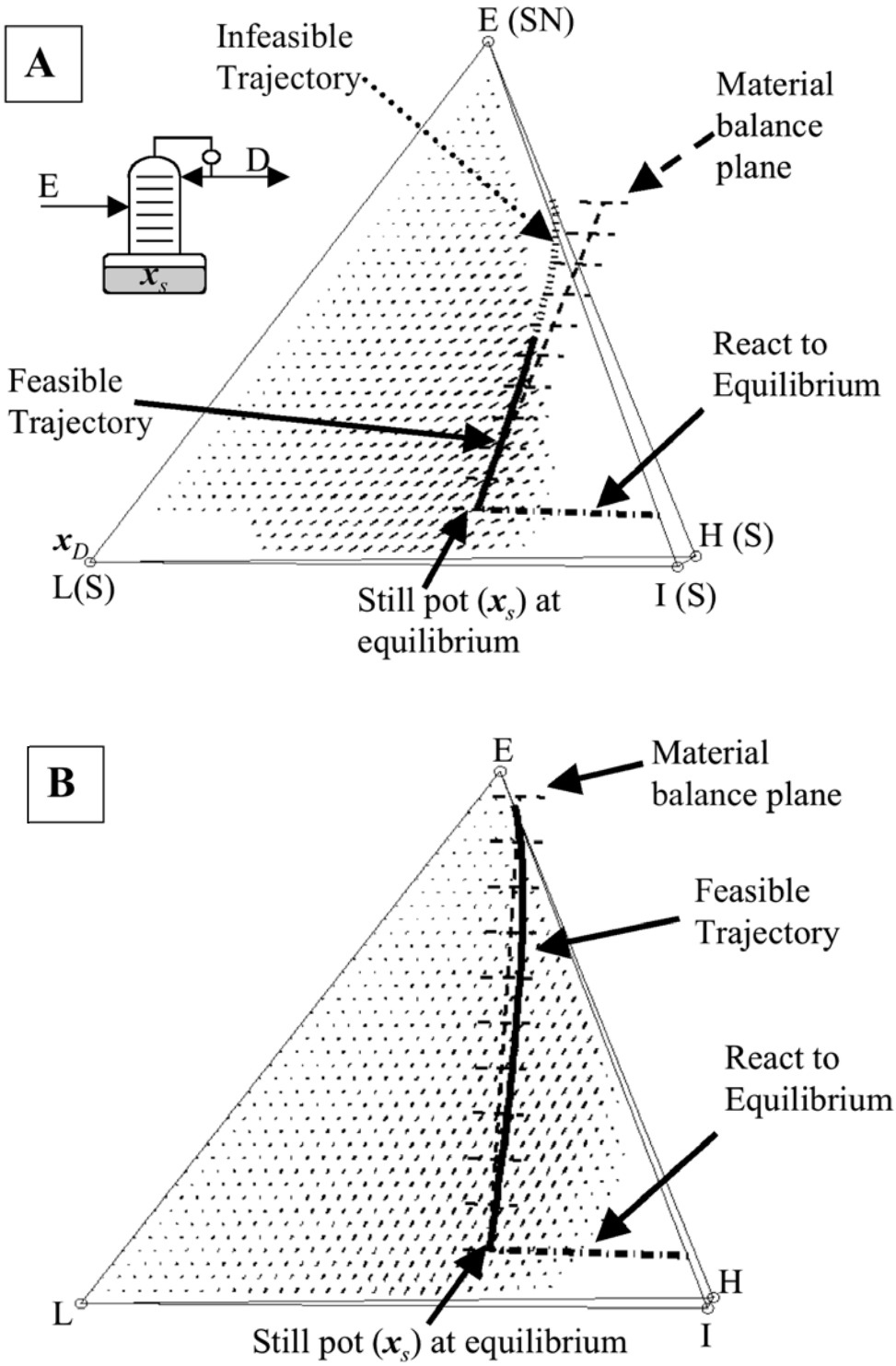

Figure 5-8. Still trajectory of Bred with RCM 313-S and a reaction of 2I ↔ L+H. (a) E/D=2.0 and (b) E/D=20.0. Dotted areas are feasible regions.

In the second case, shown in Figure 5-8(b), the E/D ratio is 20.0. We take the same pot composition and react it to equilibrium. Then, for the new E/D ratio, we draw a new material balance ray and stoichiometric lines to find a new trajectory estimate. We then calculate the upper and lower bounds and find that the trajectory is in the feasibility region for extractive distillation, so the constant product assumption is true and we can produce pure L.

Trajectory Estimation of a Multi-reaction System to Increase Reaction Selectivity

In a system with more than one reaction, if a particular undesired node component is present only because of one of the reactions, then if that reaction can be discouraged, then the undesired component can be prevented from forming in significant quantities. In the near-absence of the undesired component, the phase equilibrium behavior of the remaining components dominates and a component that was a saddle may then act as a node.

Consider the diethyl carbonate (DEC) production system[15]. The two unstable nodes are the DMC-methanol and MEC-ethanol azeotropes. DEC is the only stable node and MEC is a saddle. Thus, two unstable nodes and one stable node make two distillation regions with a common stable node in both distillation regions because there is only one pair of stable node and unstable node in a single distillation region[16]. There are two reactions in this DEC production system:

$$\begin{aligned} &H_3C\text{-}OOCOCH_3(DMC)+C_2H_5OH(EtOH) \leftrightarrow H_3C\text{-}OOCOC_2H_5(MEC)+CH_3OH\ (MeOH) \\ &H_3C\text{-}OOCOC_2H_5(MEC)+C_2H_5OH(EtOH) \leftrightarrow H_5C_2\text{-}OOCOC_2H_5(DEC)+CH_3OH\ (MeOH) \end{aligned} \quad (6)$$

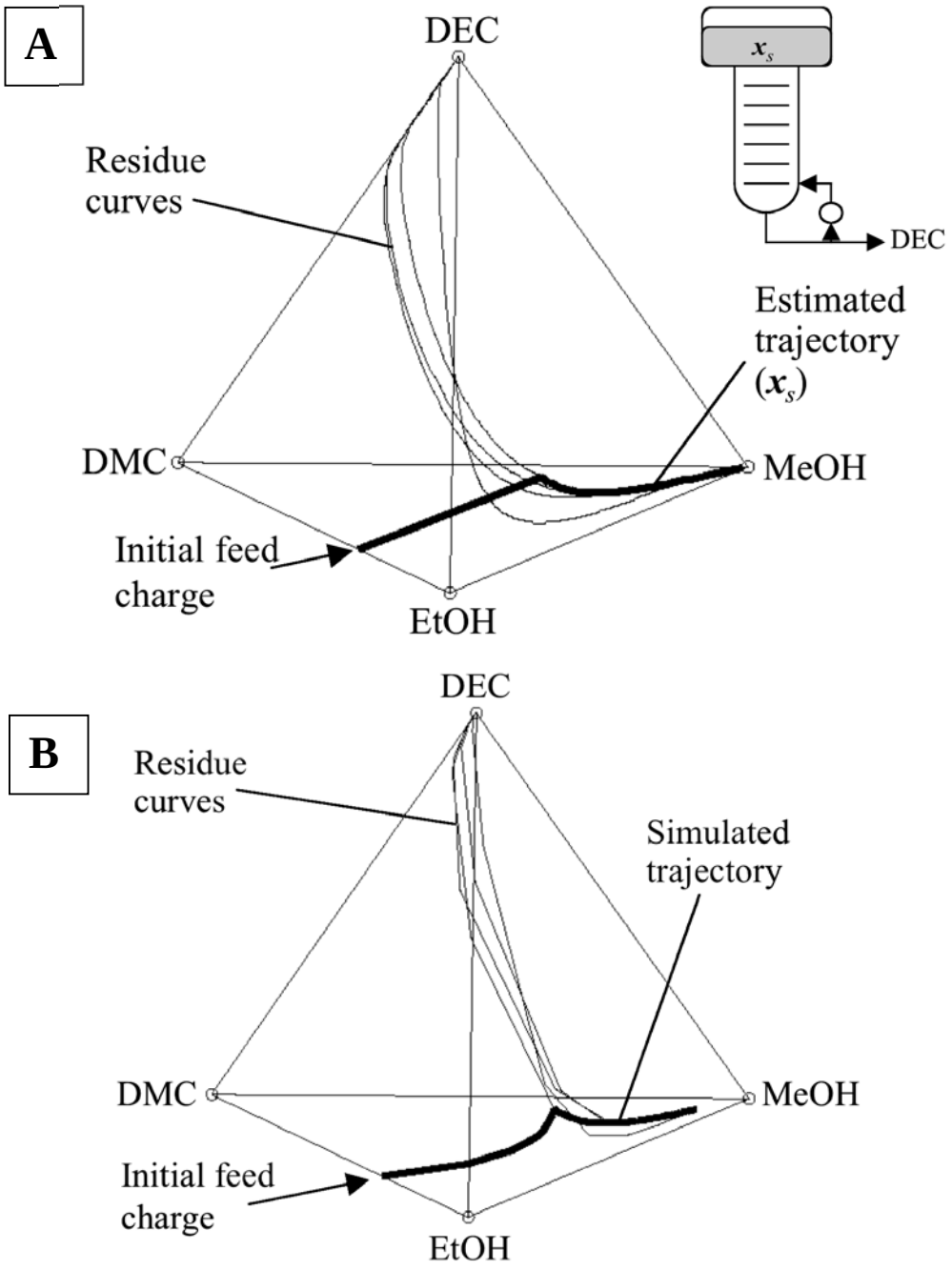

Figure 5-9. Still trajectory in MEC-projected composition space: (a) Estimation and (b) Dynamic simulation. DMC to EtOH ratio in the feed charge = 1 to 9.

If DEC is the desired final product, then both reactions should be encouraged. To accomplish this, one can use an excess of ethanol to completely consume DMC and MEC. This will promote both reactions and produce DEC preferentially over MEC. Since

DEC is the only stable node in the residue curve map and reachable from both distillation regions, the residue curves lead to the stable node DEC and a batch reactive stripper can produce pure DEC.

Figure 5-9 (a) shows an estimated still trajectory using equation (3) and Figure 5-9 (b) presents a plot of a rigorous column simulation with kinetic data available in the literature[15]. The still pot trajectory has an initial feed charge of [0.10, 0.90, 0, 0, 0] (compositions in order of DMC, ethanol, MEC, ethanol, and DEC) for both cases. The estimated still trajectory in Figure 5-9 (a) provides an excellent approximation of rigorously simulated still trajectory in Figure 5-9 (b). From any point in the still trajectory, the residue curves reach the stable node product DEC. Thus, we can produce pure DEC using a reactive batch stripper. For the dynamic simulation, we use 40 non-reactive trays with a top reactive still and use reboil ratio 2000 because the production rate (B) is so small. Our production policy is that we withdraw DEC at the bottom in proportion to the holdup of DEC in the still pot. The final yield of DEC is 98.4 % with respect to the limiting reactant of DMC.

However, if MEC is the desired product, then the first reaction should be encouraged while the second reaction is discouraged. This can be accomplished by using an excess of DMC, which only promotes the first reaction in equation (6) and consumes almost all of the ethanol. Because no large amount of DEC forms, the phase equilibrium behavior of DMC, MEC, methanol, and ethanol dominates, and among those four components, MEC is the only stable node. Starting with an initial feed charge that

contains a large excess of DMC, a stripping section can be used to isolate MEC from the reacting mixture, and a small amount of fresh ethanol can be continually fed into the still pot to continue the reaction while maintaining excess DMC in the still pot. Figure 5-10a shows an estimated trajectory by modifying the stripper equation in equation (3) as follows

$$\frac{d\boldsymbol{x}_s}{d\xi} = (\boldsymbol{x}_s - \boldsymbol{x}_B) - \frac{F}{B}(\boldsymbol{x}_s - \boldsymbol{x}_F) + \frac{H_s}{B}\sum_{i=1}^{n}(\nu_i - \nu_{Ti}\boldsymbol{x}_s)r_i \qquad (7)$$

The initial feed charge is [0.95, 0.05, 0, 0, 0] and the feed stream (F) contains pure EtOH with a fixed F/B =1, which means that EtOH is provided in the same molar amount as MEC is withdrawn at the bottom. The estimated trajectory does not contain the DEC fraction (less than 10^{-4}) and it approaches the MeOH- EtOH edge because MEC is removed from the still and DMC is consumed in the still pot as shown in Figure 5-10a. The dynamic simulation result is shown in Figure 5-10b with 20 non-reactive trays and a reboil ratio of 200. The total yield for MEC is 87.0% with respect to the limiting reactant of EtOH. The feed stream (F) is pure ethanol with a fixed ratio of F/B= 1, which means that ethanol is fed to the pot in the same amount as MEC is withdrawn at the bottom. Here the estimated trajectory in Figure 5-10a is approximately identical to the rigorously simulated trajectory in Figure 5-10b. Thus, the trajectory estimation is a very useful to determine whether a desired product in multi-reaction can be selectively produced in batch reactive distillation systems.

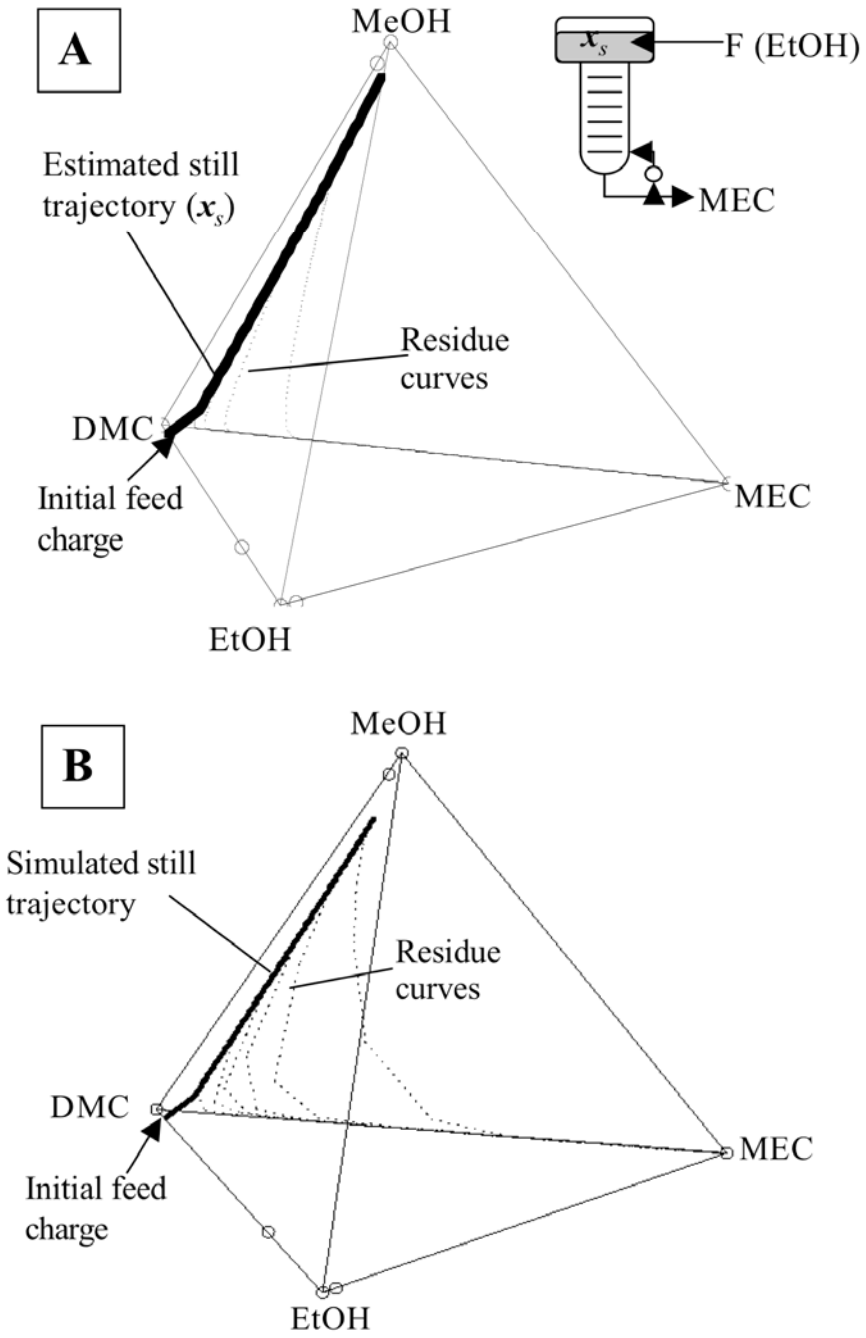

Figure 5-10. Still trajectory in DEC-projected composition space: (a) Estimation and (b) Dynamic simulation. DMC to EtOH ratio in the feed charge = 19 to 1.

Conclusions

We have presented a quick method of estimating the still pot trajectory of various batch reactive distillation columns. If we assume constant product and feed charge

compositions with constant production and feed ratios, then the still pot trajectory lies in the union of material balance rays and stoichiometric lines. The union defines a material balance plane and is a linear variation regardless of number of components. Then the still pot trajectory is estimated as the intersection between the material balance plane and a reaction equilibrium manifold. This simple estimation of still trajectory is very important especially when many distillation boundaries and multiple reactions are involved in a reacting mixture and its visualization is not possible. From the estimated trajectory, we can easily investigate the possibility of producing a desired product with high purity and selectivity in batch reactive distillation systems.

Acknowledgements

We are grateful for the support of American Chemical Society – Petroleum Research Fund (ACS-PRF). We also wish to thank Prof. Wolfgang Marquardt at RWTH Aachen for the continued use of his phase equilibrium calculation code, material properties calculation code, and quaternary system visualization program code.

Notation

B Molar flow rate of the bottom product stream (moles/time)

D Molar flow rate of the distillate product stream (moles/time)

E Molar flow rate of the entrainer feed stream (moles/time)

F Molar flow rate of reactant feed to the still pot (moles/time)

H Total molar holdup of the still pot (moles)

P (In Appendix 3) Number of non-isomolar reactions

P (Elsewhere) Sum of molar flow rates of all product streams (moles/time)

Q (In Appendix 3) Number of isomolar reactions

n Number of reactions

x_B Molar composition of the bottom product stream

x_D Molar composition of the distillate product stream

x_E Molar composition of the entrainer feed stream

x_F Molar composition of the reactant feed to the still pot

x_P Weighted average of the molar compositions of all product streams

x_S Molar composition of the still pot

r_i Molar reaction rate for reaction i (moles/time). Subscript omitted if only one reaction.

Greek Letters

ξ Dimensionless time

ν_i Stoichiometric coefficients for reaction i. Subscript omitted if only one reaction.

ν_{Ti} Sum of the stoichiometric coefficients of reaction i. Subscript omitted if only one reaction.

Appendix 5-1: Linear variation of still trajectories in the material balance plane for non-isomolar reaction.

Statement: Given only the withdrawal of a constant composition $\boldsymbol{x}_D$ and a single non-isomolar reaction along stoichiometric lines that pass through $\boldsymbol{\delta}_R$, the still trajectory, $\boldsymbol{x}_s$, is confined to the 2-dimensional linear variation that contains $\boldsymbol{x}_s$, $\boldsymbol{\delta}_R$, and $\boldsymbol{x}_D$.

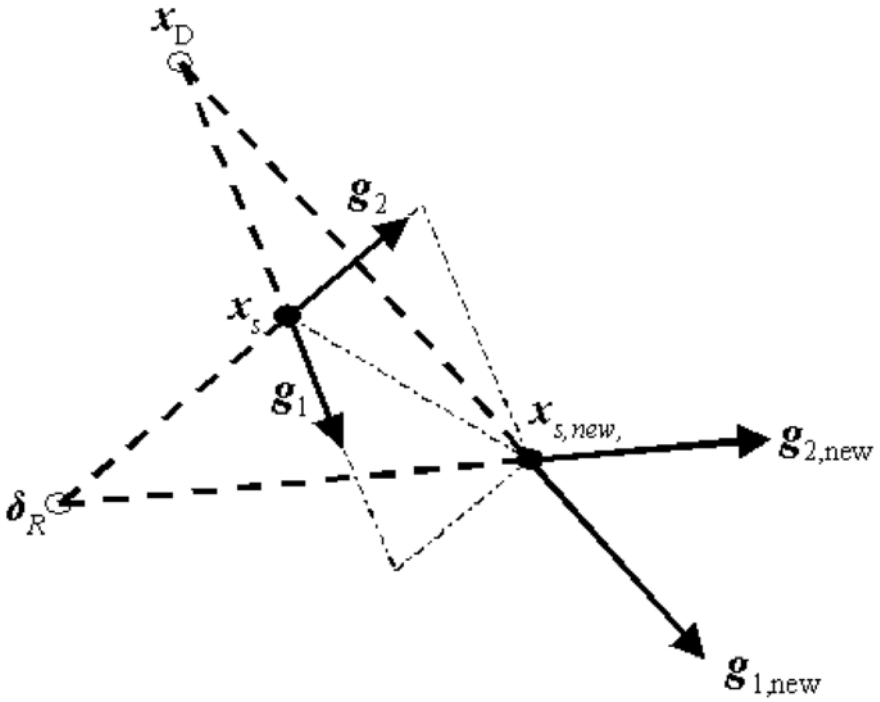

Figure 5-11. Confining the still trajectory of non-isomolar reaction in a linear 2-D material balance plane.

Proof: Because of product withdrawal, $\boldsymbol{x}_s$ is permitted to move along a vector, $\boldsymbol{g}_1 = \boldsymbol{x}_s - \boldsymbol{x}_D$. Because of chemical reaction, $\boldsymbol{x}_s$ is permitted to move along a vector, $\boldsymbol{g}_2 = \boldsymbol{x}_s - \boldsymbol{\delta}_R$. $\boldsymbol{g}_1$ and $\boldsymbol{g}_2$ constitute a basis set that defines a 2-dimensional linear variation as shown in Figure 5-11. Allow $\boldsymbol{x}_s$ to move to a new position, $\boldsymbol{x}_{s,new}$, by moving along vectors $\boldsymbol{g}_1$ and $\boldsymbol{g}_2$ with any arbitrary real magnitudes a_1 and a_2, respectively.

$$\boldsymbol{x}_{s,new} = \boldsymbol{x}_s + a_1\boldsymbol{g}_1 + a_2\boldsymbol{g}_2 \qquad \text{(A.1)}$$

Because $\boldsymbol{x}_{s,new}$ moves along a linear combination of the basis vectors, $\boldsymbol{g}_1$ and $\boldsymbol{g}_2$, it must be inside the linear variation defined by those vectors as shown in Figure 5-11. If $\boldsymbol{x}_{s,new}$ is

permitted to change further, then it changes along new vectors $\boldsymbol{g}_{1,\text{new}} = \boldsymbol{x}_{s,new} - \boldsymbol{x}_D$ and $\boldsymbol{g}_{2,\text{new}} = \boldsymbol{x}_{s,new} - \boldsymbol{\delta}_R$ whose values depend upon $\boldsymbol{x}_{s,new}$. Rewritten in terms of the original $\boldsymbol{g}_1$ and $\boldsymbol{g}_2$ in equation (A.1), $\boldsymbol{g}_{1,\text{new}}$ and $\boldsymbol{g}_{2,\text{new}}$ become:

$$\boldsymbol{g}_{1,new} = \boldsymbol{x}_s + a_1\boldsymbol{g}_1 + a_2\boldsymbol{g}_2 - \boldsymbol{x}_D \qquad \text{(A.2)}$$

$$\boldsymbol{g}_{2,new} = \boldsymbol{x}_s + a_1\boldsymbol{g}_1 + a_2\boldsymbol{g}_2 - \boldsymbol{\delta}_R \qquad \text{(A.3)}$$

(A.2) and (A.3) can be rearranged by subtracting $\boldsymbol{g}_1$ and $\boldsymbol{g}_2$:

$$\boldsymbol{g}_{1,new} - \boldsymbol{g}_1 = a_1\boldsymbol{g}_1 + a_2\boldsymbol{g}_2 \qquad \text{(A.4)}$$

$$\boldsymbol{g}_{2,new} - \boldsymbol{g}_2 = a_1\boldsymbol{g}_1 + a_2\boldsymbol{g}_2 \qquad \text{(A.5)}$$

Thus, $\boldsymbol{g}_{1,\text{new}}$ and $\boldsymbol{g}_{2,\text{new}}$ are both linearly dependent upon $\boldsymbol{g}_1$ and $\boldsymbol{g}_2$. They therefore constitute a new basis set for the same linear variation defined by $\boldsymbol{g}_1$ and $\boldsymbol{g}_2$. Therefore, $\boldsymbol{x}_s$ can only move along vectors that are linearly dependent upon $\boldsymbol{g}_1$ and $\boldsymbol{g}_2$. Therefore, $\boldsymbol{x}_s$ is confined to the linear variation (material balance) defined by the vectors $\boldsymbol{g}_1$ and $\boldsymbol{g}_2$ and the point $\boldsymbol{x}_s$.

Appendix 5-2: Linear variation of still trajectories in the material balance plane for isomolar reaction.

Statement: Given only the withdrawal of a constant composition $\boldsymbol{x}_D$ and a single isomolar reaction along stoichiometric lines in the direction of $\boldsymbol{v}$, $\boldsymbol{x}_s$ is confined to the 2-dimensional linear variation that contains $\boldsymbol{x}_D$, $\boldsymbol{x}_s$, and lines of direction $\boldsymbol{v}$ that pass through both of them.

Proof: Because of product withdrawal, $\boldsymbol{x}_s$ is permitted to move along a vector, $\boldsymbol{g}_1 = \boldsymbol{x}_s - \boldsymbol{x}_D$. Because of chemical reaction, $\boldsymbol{x}_s$ is permitted to move along a vector, $\boldsymbol{g}_2 = \boldsymbol{v}$. $\boldsymbol{g}_1$ and $\boldsymbol{g}_2$

constitute a basis set that defines a 2-dimensional linear variation. By using the same argument as in the previous appendix, we can write $\boldsymbol{g}_{1,new}$ and $\boldsymbol{g}_{2,new}$ whose values depend upon $\boldsymbol{x}_{s,new}$ as shown in Figure 5-12:

$$\boldsymbol{g}_{1,new} - \boldsymbol{g}_1 = a_1\boldsymbol{g}_1 + a_2\boldsymbol{g}_2 \qquad \text{(A.5)}$$

$$\boldsymbol{g}_{2,new} = \boldsymbol{g}_2 = \boldsymbol{v} \qquad \text{(A.6)}$$

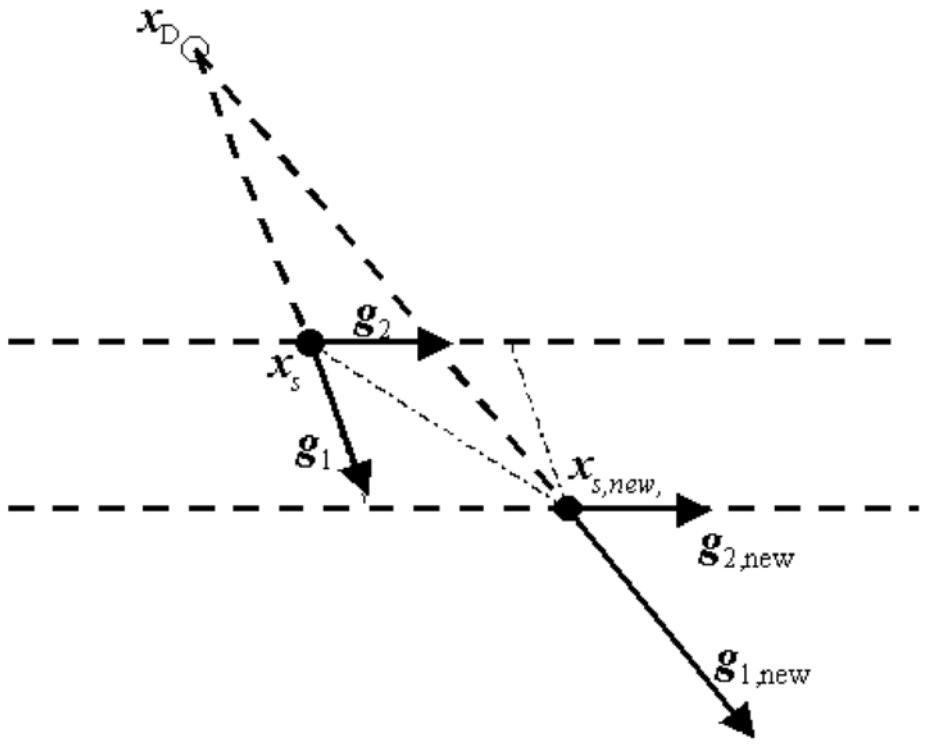

Figure 5-12. Confining the still trajectory of isomolar reaction in a linear 2-D material balance plane.

Thus, $\boldsymbol{g}_{1,new}$ and $\boldsymbol{g}_{2,new}$ are both linearly dependent upon $\boldsymbol{g}_1$ and $\boldsymbol{g}_2$. Therefore, $\boldsymbol{x}_s$ can only move along vectors that are linearly dependent upon $\boldsymbol{g}_1$ and $\boldsymbol{g}_2$ and $\boldsymbol{x}_s$ is confined to the linear variation defined by the vectors $\boldsymbol{g}_1$ and $\boldsymbol{g}_2$ and the point $\boldsymbol{x}_s$.

Appendix 5-3: Linear variation of still trajectories in the material balance plane of (n+1) dimensions for n reactions.

Statement: Given the withdrawal of a constant composition $\boldsymbol{x}_D$, P non-isomolar reactions along stoichiometric lines that each pass through a unique $\boldsymbol{\delta}_{R,i}$, and Q isomolar reactions along stoichiometric lines that each have a unique direction $\boldsymbol{v}_k$, where $n = P+Q$, $\boldsymbol{x}_s$ is confined to the (1+P+Q)-dimensional linear variation that contains $\boldsymbol{x}_s$, all of the points $\boldsymbol{\delta}_{R,i}$, and all of the lines of directions $\boldsymbol{v}_k$ that pass through them.

Proof: As in the previous sections, we define $\boldsymbol{g}_1 = \boldsymbol{x}_s - \boldsymbol{x}_D$. Because of the non-isomolar chemical reactions, $\boldsymbol{x}_s$ is permitted to move along vectors $\boldsymbol{g}_2$ through $\boldsymbol{g}_{1+P}$ that depend upon the value of $\boldsymbol{x}_s$.

$$\boldsymbol{g}_{1+i} = \boldsymbol{x}_s - \boldsymbol{\delta}_R \qquad \text{for all } 1 \le i \le P \qquad \text{(A.7)}$$

For Q isomolar reactions,

$$\boldsymbol{g}_{1+P+k} = \boldsymbol{v}_k \qquad \text{for all } 1 \le k \le Q \qquad \text{(A.8)}$$

$\boldsymbol{g}_1$ through $\boldsymbol{g}_{1+P+Q}$ constitute a basis set that defines a (1+P+Q)-dimensional linear variation. Allow $\boldsymbol{x}_s$ to move to a new position, $\boldsymbol{x}_{s,new}$, by moving along the vectors $\boldsymbol{g}_1$ through $\boldsymbol{g}_{1+P+Q}$ with any arbitrary real magnitudes a_1 through a_{1+P+Q}, respectively.

$$\boldsymbol{x}_{s,new} = \boldsymbol{x}_s + \sum_{i=1}^{1+P+Q} a_i \boldsymbol{g}_i \qquad \text{(A.9)}$$

Because $\boldsymbol{x}_{s,new}$ moves along a linear combination of the basis vectors $\boldsymbol{g}_1$ through $\boldsymbol{g}_{1+P+Q}$, it must be inside the linear variation defined by those vectors. If $\boldsymbol{x}_{s,new}$ is permitted to change further, then it changes along new vectors $\boldsymbol{g}_{1,new}$ through $\boldsymbol{g}_{1+P+Q,new}$ whose values depend upon $\boldsymbol{x}_{s,new}$.

$$\boldsymbol{g}_{1,new} = \boldsymbol{x}_s + \sum_{j=1}^{1+P+Q} a_j \boldsymbol{g}_j - \boldsymbol{x}_D = \boldsymbol{g}_1 + \sum_{j=1}^{1+P+Q} a_j \boldsymbol{g}_j \tag{A.10}$$

$$\boldsymbol{g}_{i+1,new} = \boldsymbol{x}_s + \sum_{j=1}^{1+P+Q} a_j \boldsymbol{g}_j - \boldsymbol{\delta}_{Ri} = \boldsymbol{g}_{i+1} + \sum_{j=1}^{1+P+Q} a_j \boldsymbol{g}_j \quad \text{for all } 1 \le i \le P \tag{A.11}$$

$$\boldsymbol{g}_{1+P+k,new} = \boldsymbol{g}_{1+P+k,new} = \boldsymbol{v}_k \quad \text{for all } 1 \le k \le Q \tag{A.12}$$

Thus, $\boldsymbol{g}_{1,new}$ through $\boldsymbol{g}_{1+P+Q,new}$ are all linearly dependent upon $\boldsymbol{g}_1$ through $\boldsymbol{g}_{1+P+Q}$. They therefore constitute a new basis set for the same linear variation defined by $\boldsymbol{g}_1$ through $\boldsymbol{g}_{1+P+Q}$. Therefore, $\boldsymbol{x}_s$ can only move along vectors that are linearly dependent upon $\boldsymbol{g}_1$ through $\boldsymbol{g}_{1+P+Q}$. Therefore, $\boldsymbol{x}_s$ is confined to the linear variation defined by the vectors $\boldsymbol{g}_1$ through $\boldsymbol{g}_{1+P+Q}$ and the point $\boldsymbol{x}_s$.

References

1. Doherty MF, Buzad G. Reactive Distillation by Design. *Trans. Inst. Chem. Eng.* 1992;70:448.
2. Taylor R, Krishna R. Modelling reactive distillation. *Chem Eng Sci.* 2000;55:5183-5229.
3. Malone MF, Doherty MF. Reactive distillation. *Ind Eng Chem Res.* 2000;39:3953-3957.
4. Lee JW. Feasibility studies on quaternary reactive distillation systems. *Ind Eng Chem Res*. 2002;41:4632-4642.
5. Guo Z, Ghufran M, Lee JW. Feasible products in batch reactive distillation. *AIChE J.*, 2003;49:3161-3172.
6. Guo Z, Lee JW. Feasible products in batch reactive extractive distillation. *AIChE J.* 2004;50:1484-1492.
7. Guo Z, Chin J, Lee JW. Feasibility of continuous reactive distillation with azeotropic mixtures. *Ind. Eng. Chem. Res.* 2004;43:3758-3769.
8. Chin J, Kattukaran HJ, Lee JW. Generalized feasibility evaluation of equilibrated quaternary reactive distillation systems. *Ind Eng Chem Res.* 2004;43:7092-7102.
9. Chin J, Lee JW. Rapid generation of composition profiles for reactive and extractive cascades. *AIChE J*. 2005;51:922-930.
10. Chin J, Lee JW, Choe J. Feasible Products in Complex Batch Reactive Distillation. *AIChE Journal*. 2006;52:1790.
11. Matsuyama H, Nishimura H. Topological and thermodynamic classification of ternary vapor-liquid equilibria. *J Chem Engr Japan*. 1977;10(3):181-187.
12. Doherty MF, Caldarola GA. Design and synthesis of homogeneous azeotropic distillations. 3. The sequencing of columns for azeotropic and extractive distillations. *Ind. Eng. Chem. Fundam.* 1985;24:474-485.
13. Hauan S, Westerberg AW, Lien KM. Phenomena based analysis of fixed points in reactive separation systems. *Chem. Eng. Sci.*, 2000;55:1053-1075.
14. Lee JW, Hauan S, Lien KM, Westerberg AW. Difference points in extractive and reactive cascades. II - Generating design alternatives by the lever rule for reactive systems. *Chem. Eng. Sci.* 2000;55(16):3161-3174.
15. Luo HP, Xiao WD. A Reactive Distillation Process for a Cascade and Azeotropic Reaction System: Carbonylation of Ethanol with Dimethyl Carbonate. *Chem. Eng. Sci.* 2001;56:403-410.
16. Rooks RE, Julka V, Doherty MF, Malone MF. Structure of distillation regions for multicomponent azeotropic mixtures. *AIChE J*. 1998;44:1382-1391.

Conclusions

The objective accomplished by this work was to develop a systematic method for determining the feasibility of intensifying multiple reactions with distillation in a set of basic column structures (single-feed continuous, double-feed continuous, batch rectifiers with and without entrainer, batch strippers, and batch middle-vessel columns with and without entrainer, all of which except the batch stripper may or may not have a decanter attached). The overall conclusions reached by this work are as follows:

1. A single-feed continuous reactive distillation column conducting a reaction of the form $aI \leftrightarrow bL + cH$ or $aI + bK \leftrightarrow cL + dH$ can produce pure products if the light and heavy products are stable and unstable nodes in the same distillation region as the reaction equilibrium curve *or* if the reaction equilibrium constant is large (the reaction almost goes to completion), at least one product is a node, and there is no azeotrope between the products.

2. A double-feed continuous reactive distillation column or a batch reactive extractive distillation (BRED) column conducting a reaction of the form $aI \leftrightarrow bL + cH$ or $aI + bK \leftrightarrow cL + dH$ may produce pure products under a given entrainer flow rate if the critical composition region and the feasibility region for extraction (which is determined by the upper and lower bounds of the internal reflux ratios) allow extractive section composition profiles to approach the entrainer-light product edge of composition space. For a continuous column to be feasible, the feasibility region for extraction must meet the

stripping section composition profile. For a BRED column to be feasible, the feasibility region for extraction must contain the entire still pot trajectory.

3. The pinch point trajectories for an extractive section can be found at the compositions where the upper and lower bounds of the reflux ratios are equal. Analyzing the internal reflux ratios along the pinch trajectories gives the feasible range of internal reflux ratios for the given entrainer flow rate.

4. A batch reactive rectifier with a decanter can produce pure products from a reaction of the form $aI \leftrightarrow bL + cH$ or $aI + bK \leftrightarrow cL + dH$ if an unstable node heterogenous azeotrope splits to almost-pure L or almost-pure H and this azeotrope is reachable by simple distillation from the reaction equilibrium manifold. A batch reactive middle-vessel column with a decanter can produce pure products if pure H is a stable node, an unstable node heterogenous azeotrope splits to almost-pure L, and H and the heteroazeotrope are both reachable from the same segment of the reaction equilibrium manifold by simple distillation.

5. The time-dependent still pot composition trajectory of a batch reactive distillation column, extractive or otherwise, can be estimated under the assumption of feasible product production. The still pot trajectory is confined to the intersection between the material-balance-and-stoichiometry plane and the reaction equilibrium manifold; the mathematical proof was presented in Chapter 5. For the resulting trajectory estimate, the assumption can then be verified or refuted by applying the feasibility criteria for the

particular type of column. This trajectory estimation is used for evaluating the feasibility of integrating multi-reaction and V-L-L separation and will be a very important tool for the feasibility studies on the structural variation of reactive distillation columns. An automated algorithm can be implemented to evaluate the feasibility of producing pure products from a given chemical reaction system.

Limitations of the Assumptions

We now briefly consider the various limiting-case assumptions upon which the feasibility evaluation algorithm relies and hypothesize about the possible consequences if the assumptions are violated.

For a simple batch reactive distillation column (rectifier, stripper, or middle-vessel column) to be feasible, the column composition profile must connect the still pot composition to the pure product composition(s), which must be an unstable and/or stable node(s). If the column is a rectifier with a decanter or a middle-vessel column with a decanter, then the rectifying section composition profile must connect the still pot composition to an unstable node heterogenous azeotrope whose liquid-liquid tie line falls near a pure product composition.

Assumptions concerning the column profiles

To estimate the column composition profiles with a minimum of effort, the feasibility evaluation algorithm makes the following assumptions to allow us to model the column composition profile as a simple residue curve: (1) the rectifying/stripping

sections have an infinite number of trays, (2) the reflux/reboil ratio is infinite, (3) the holdup on the trays is zero, (4) the liquid and vapor streams leaving any given tray are in phase equilibrium with each other, (5; for batch systems only) no reaction takes place on the trays, and (6; also for batch systems only) the tray compositions come to phase equilibrium faster than the still pot composition changes.

We presume that relaxing assumption (1) would result in the column composition profile not traveling all the way to the (un)stable node composition. If there are an insufficient number of trays, then the column profile may not result in a reasonably pure product composition.

Relaxing assumption (2) would result in the column profile following a path different from the residue curve; this may result in the column profile ending in a composition that is not near a pure product composition.

Assumption (3) simplifies the material balance envelopes around the trays. Relaxing this assumption would make the material balance calculations more complicated. We haven't attempted this, but we don't anticipate any implications for the validity of the feasibility calculations.

Assumption (4) allows us to ignore mass-transfer limitations; relaxing this assumption would result in the column composition profile following a path different from a residue curve.

Assumption (5) is commonly made for all distillation trays in batch systems and for the rectifying trays of a continuous reactive distillation column. The assumption cannot apply to the entirety of a continuous reactive distillation column, or else it would not be a continuous *reactive* distillation column. Chapters 1 and 2 of the present thesis discuss the modeling of column composition profiles on reactive trays. Although we have not applied these techniques to reactive trays on batch systems, we believe that adaptation to batch systems should not be especially problematic.

Assumption (6), which only applies to batch systems, allows us to treat the column composition profile as being a function only of the still pot composition, and not a function of time. If this assumption is relaxed, then it will be necessary to consider the time-dependent tray compositions in addition to the time-dependent still pot composition. Such a model would necessarily exhibit time delays between changes in the still pot composition and changes in the tray and product compositions).

Assumptions concerning chemical reaction

Whether dealing with continuous or batch systems, this work has always assumed that (7) all reactive zones are immediately in reaction equilibrium (therefore ignoring the effects of kinetics) and that (8) all reactions are reversible.

Relaxing these assumptions will allow the column composition profile on reactive trays to deviate from the reaction equilibrium manifold. The implications this has on the column profile estimation are not clear except for the fact that significant, non-trivial

changes to the column profile estimation will be needed to accommodate non-equilibrium/irreversible reactions. Such column profiles will neither be residue curves nor constrained to the reaction equilibrium manifold.

Relaxing these assumptions also means that the still pot composition of batch reactive distillation systems will not be on the reaction equilibrium manifold. Here, the implications on feasibility are a little easier to predict, provided that the assumptions concerning the column composition profile (assumptions 1 through 6, above) still hold. Namely, if the reaction equilibrium manifold lies entirely within a feasible distillation region and is nowhere near any infeasible distillation regions, then a batch reactive distillation column of the appropriate type is still feasible. However, if the reaction equilibrium manifold is close to an infeasible distillation region, then the feasibility of a batch reactive column will depend upon how closely the still pot composition approaches reaction equilibrium. In the still pot trajectory estimation technique, it would be necessary to draw residue curves, not only from the estimated trajectory (which lies on the reaction equilibrium manifold), but also from points slightly off the trajectory estimate. How far off these points need to be sampled depends upon how close or how distant the still pot approaches equilibrium.

Future Work

Significant results have been generated by this work that can be directly applied to chemical process design. As with any research, though, there are always additional

subject areas where further research may be conducted. The areas of future work in this field that we foresee are:

Complex Column Design – The scope of this work has been limited to a specific set of column structures. Namely, they include, and are limited to, batch reactive rectifiers (with and without decanters, with and without a side-fed entrainer stream), batch reactive strippers, batch reactive middle-vessel columns (with and without decanters, with and without a side-fed entrainer stream), single-feed continuous reactive distillation columns (non-extractive), and double-feed continuous reactive distillation columns. Future work can study the feasibility of reactive distillation systems using side columns, side reactors, more than two feed streams, more than two product streams, and/or more than three sections in the main column (rectifying, extractive, and stripping).

Kinetic Studies – This work developed shortcut feasibility evaluation tools under the assumption of reaction equilibrium. As yet untouched is a study of how kinetically-limited reactions affect the feasibility evaluation tools developed in this work. By implementing kinetics to our feasibility studies, we can quantitatively determine required catalyst holdup and reboiler or condenser heat duties.

Reaction Selectivity through Reactive Distillation – This work has lightly touched upon the subject of employing reactive distillation and manipulation of limiting or excess reactant to achieve different desired reaction selectivities. While it is possible to use reactive distillation and limiting reactants to produce a pure saddle product from a

multiple-reaction system, this is not yet smoothly integrated into the rest of the feasibility evaluation algorithm for non-extractive systems, all of which rely on isolating an unstable or stable node in the phase equilibrium behavior.

Thesis Appendix: Explanation of Residue Curves, Residue Curve Maps, and RCM classification

This chapter is a summary explanation of residue curves, residue curve maps, and the classification of ternary residue curve maps developed by Matsuyama and Nishimura[1].

This thesis develops feasibility criteria for reactive distillation systems using reaction equilibrium and phase equilibrium information. The phase equilibrium information is frequently expressed in the form of residue curve maps, so the preceding chapters of this thesis assume that the reader is familiar with residue curves, residue curve maps, and their systematic classification in ternary systems. The present appendix strives to provide a summary explanation of these concepts; for a detailed explanation, the reader is referred to Matsuyama and Nishimura[1].

A residue curve is defined as an integral curve of the vector equation

$$\frac{\partial x}{\partial \xi} = x - y$$

starting from any non-singular value of x, where x is a liquid-phase composition, y is a vapor-phase composition in phase equilibrium with x (and is generally a function only of x), and ξ is a dimensionless time. It is the time-dependent liquid-phase (residual) composition that would result if a liquid were boiled to continuously produce and remove an infinitesimal vapor phase. A residue curve map (RCM) is the vector field defined by the right-hand side of the above equation. At pure components and azeotropes, x and y

are equal, so pure components and azeotropes constitute singular points of the residue curve map. Pure components and azeotropes are therefore collectively referred to in this thesis as "singular points of the residue curve map" or more simply as "singular points".

All singular points are divided into three categories: stable nodes, saddles, and unstable nodes. These categories are defined by the behavior of the residue curves in the immediate vicinity of the singular point in the vector field. These categories are also independent of the singular point's nature as a pure component or azeotrope; that is to say, a pure component could be a stable node, a saddle, or an unstable node, it depends only upon how the residue curves behave near the pure component. Similarly, an azeotrope could be a stable node, a saddle, or an unstable node, it depends only upon how the residue curves behave near the azeotrope.

Stable nodes of a residue curve map are singular points where all residue curves in the immediate vicinity of the singular point tend towards that singular point. Stable nodes of a residue curve map are invariably a local temperature maximum in the phase equilibrium behavior.

Saddles of a residue curve map are singular points where some residue curves in the immediate vicinity of the singular point tend towards that singular point, while all other residue curves in the same vicinity tend away from that singular point. Saddles of a residue curve map are invariably never a temperature maximum or a temperature minimum in the phase equilibrium behavior.

Unstable nodes of a residue curve map are singular points where all residue curves in the immediate vicinity of the singular point tend away from that singular point. Unstable nodes of a residue curve map are invariably a local temperature minimum in the phase equilibrium behavior.

All residue curves start at an unstable node and end at a stable node. A "distillation region" is defined as the set of all residue curves that start at the same unstable node and end at the same stable node. A "distillation boundary" between any two (or more) distillation regions is the set of all compositions that exist in both (or all chosen) distillation regions.

Residue curves have the following properties:

1) All residue curves are continuous.

2) All residue curves start at an unstable node and end at a stable node.

3) Residue curves never intersect except at a singular point or at a distillation boundary.

4) If a residue curve has a continuous first derivative everywhere except at its unstable and stable nodes, then it never intersects other residue curves except at its unstable and stable nodes.

5) For every non-singular point in composition space that is not on a distillation boundary or boundary of composition space, there is one and only one residue curve that passes through it.

Residue curves may be drawn with or without an arrowhead on the curve. If an arrowhead is drawn, it is drawn in the direction along the curve that leads to the stable node. If an arrowhead is not drawn on a residue curve, but the singular points on the residue curve map are properly marked with temperatures or marked as stable nodes, saddles, and unstable nodes, then it is understood that the residue curve goes from the lowest-boiling temperature to the highest-boiling temperature *and also* from an unstable node to a stable node.

Matsuyama and Nishimura[1] developed a systematic classification system for all topologically-feasible three-component residue curve maps. Every ternary residue curve map has an alphanumeric label that consists of three numerals optionally followed by a hyphen and then a letter. The order of the boiling points of the three pure components must be correctly understood before giving the designation; that is, it must be known which component is the lightest-boiling (L), which is the intermediate-boiling (I), and which is the heaviest-boiling (H).

The first numeral represents the presence and nature of the binary azeotrope between L and I. The second numeral represents the presence and nature of the binary azeotrope between I and H. The third numeral represents the presence and nature of the binary azeotrope between L and H. The numerals can be:

0: No binary azeotrope

1: A binary-temperature-minimum node azeotrope (therefore an unstable node)

2: A binary-temperature-minimum saddle azeotrope

3: A binary-temperature-maximum node azeotrope (therefore a stable node)

4: A binary-temperature-maximum saddle azeotrope

The above specify *binary*-temperature-minimum or *binary*-temperature-maximum because in the case of 2 and 4, the azeotropes are local minima or local maxima in their respective binary systems but not in the ternary system. Cases 1 and 3 represent azeotropes that are minima or maxima in both their respective binary systems and in the ternary system.

If the ternary system does not have a ternary azeotrope, then the three numerals described above complete the RCM designation. If there is a ternary azeotrope, then the above three numerals are followed by a hyphen and any one of the following three letters: "S" for a ternary saddle, "m" for a ternary minimum, and "M" for a ternary maximum. This then completes the RCM designation.

Examples

Figure 1-15a, page 45: This is RCM 001. There is no azeotrope between L and I (hence, 0). There is no azeotrope between I and H (hence, 0). There is a minimum node between L and H (hence, 1). There is no ternary azeotrope (hence, no letter).

Figure 1-17a, page 47: This is RCM 031. There is no azeotrope between L and I (hence, 0). There is a maximum node between I and H (hence, 3). There is a minimum node between L and H (hence, 1). There is no ternary azeotrope (hence, no letter).

Figure 4-2, page 128: This is RCM 202-m. There is a minimum saddle between L and I (hence, 2). There is no azeotrope between I and H (hence, 0). There is a minium saddle between L and H (hence, 2). There is a ternary minimum azeotrope (hence, m).

Figure 4-5, page 134: This is RCM 222-m. There is a minimum saddle between L and I (hence, 2). There is a minimum saddle between I and H (hence, 2). There is a minium saddle between L and H (hence, 2). There is a ternary minimum azeotrope (hence, m). It is worth noting that the presence of a liquid-liquid miscibility gap has no bearing on the RCM designation, though the "x" used in the residue curve equation is taken as being the mole-average composition of the two liquid phases wherever two liquid phases exist.

Figure 5-2, page 177: This is RCM 430. There is a maximum saddle between L and I (hence, 4). There is a maximum node between I and H (hence, 3). There is no azeotrope between L and H (hence, 0). There is no ternary azeotrope (hence, no letter).

References

1. Matsuyama H, Nishimura H. Topological and thermodynamic classification of ternary vapor-liquid equilibria. *J Chem Engr Japan*. 1977;10(3):181-187.

Bibliography

Agreda VH, Partin LR. Reactive distillation process for the production of methyl acetate. U.S. Patent 4,435,595: 1984.

Agreda VH, Partin LR, Heise WH. High purity methyl acetate via reactive distillation. *Chem Eng Prog*. 1990;86(2):40-46.

Al-Arfaj MA, Luyben WL. Design and Control of an Olefin Metathesis Reactive Distillation Column. *Chem. Eng. Sci.* 2002;57:715.

Allen DT, Shonnard D. Green Engineering: Environmentally Conscious Design of Chemical Processes, Prentice Hall PTR, Upper Saddle River, NJ, (2002).

Andersen HW, Laroche L, Morari M. Effect of design on the operation of homogeneous azeotropic distillation. *Comp. Chem. Eng*. 1995;19:105-122.

Aspen Plus 12.1, Aspen Engineering Suite, Aspen Tech; 2005.

Backhaus AA. Continuous process for the manufacture of ester. US Patent 1,400,849: 1921.

Balashov MI, Serafimov LA. Analysis of statics of continuous combined reaction-fractionation process. *Theor. Found. Chem. Engr.* 1980;14:495-500.

Balashov MI, Patlasov VP, Serafimov LA. Rules of Primary Reaction Zone Spread in Continuous Combined Reaction-Fractionation Processes, *Theor. Found. Chem. Engr.* 1981;15:406-413

Barbosa D, Doherty MF. Theory of phase diagrams and azeotropic conditions for two-phase reactive system. *Proc. R. Soc. London* 1987;A413:443-458.

Barbosa D, Doherty MF. A new set of composition variables for the representation of reactive phase diagram. *Proc. R. Soc. London* 1987;A413:459-464.

Barbosa D, Doherty MF. The Influence of Equilibrium Chemical Reactions on Vapor-Liquid Phase Diagrams, *Chem. Engr. Sci.*, 1988;43:529-540.

Barbosa D, Doherty MF. The Simple Distillation of Homogenous Reactive Mixtures. *Chem. Engr. Sci.*, 1988;43:541.

Barbosa D, Doherty MF. Design and Minimum-Reflux Calculations for Single-Feed Multicomponent Reactive Distillation Columns. *Chem. Engr. Sci.*, 1988;43:1523.

Barbosa D, Doherty MF. Design and Minimum-Reflux Calculations for Double-Feed Multicomponent Reactive Distillation Columns. *Chem. Engr. Sci.*, 1988;43:2377.

Baur R, Taylor R, Krishna R. Dynamic Behaviour of Reactive Distillation Columns Described by a Nonequilibrium Stage Model. *Chem. Eng. Sci.* 2001;56:2085.

Bausa J, Watzdorf Rv, Marquardt W. Shortcut methods for nonideal multicomponent distillation: 1. Simple columns. *AIChE J*. 1998;44:2181-2198.

Bernot C, Doherty MF, Malone MF. Feasibility and separation sequencing in multicomponent batch distillation. *Chem Eng Sci*. 1991;46:1311-1326.

Bonny L. Multicomponent batch distillation: study of operating parameters. *Ind Eng Chem Res.* 1999;38:4759-4768.

Brüggemann S, Marquardt W. Shourtcut methods for nonideal multicomponent distillation: 3. Extractive distillation columns. *AIChE J*. 2004;50;1129-1149.

Buzad G, Doherty MF. Design of three-component kinetically controlled reactive distillation columns using fixed-point methods. *Chem. Eng. Sci.* 1994;49:1947-1963.

Buzad G, Doherty MF. New Tools for the Design of Kinetically Controlled Reactive Distillation Columns for Ternary Mixtures. *Comp. Chem. Engr.* 1995;19:395.

Chadda N, Malone MF, Doherty MF. Feasible products for kinetically controlled reactive distillation of ternary mixtures. *AIChE J.* 2000;46:923-936.

Chadda N, Malone MF, Doherty MF. Effect of Chemical Kinetics on Feasible Splits for Reactive Distillation. *AIChE Journal*. 2001;47:590

Cheong W, Barton PI. Azeotropic distillation in a middle vessel batch column. 3. Model validation. *Ind Eng Chem Res*. 1999;38:1549-1564.

Chin J, Kattukaran HJ, Lee JW. Generalized feasibility evaluation of equilibrated quaternary reactive distillation systems. *Ind Eng Chem Res.* 2004;43:7092-7102.

Chin J, Lee JW. Rapid generation of composition profiles for reactive and extractive cascades. *AIChE J*. 2005;51:922-930.

Chin J, Lee JW, Choe J. Feasible Products in Complex Batch Reactive Distillation. *AIChE Journal*. 2006;52:1790.

Ciric AR, Gu D. Synthesis of nonequilibrium reactive distillation processes by MINLP optimization. *AIChE J.* 1994;40:1479-1487.

Cuille PE, Rekliaitis GV. Dynamic simulation of multicomponent batch rectification with chemical reactions. *Comp Chem Eng.* 1986;10:389-398.

Degarmo JL, Parulekar VN, Pinjala V. Consider Reactive Distillation. *Chem. Eng. Prog.* 1992;88(3):43.

Doherty MF, Buzad G. Reactive distillation by design. *Chemical Engineering Research and Design, Transactions of the Institution of Chemical Engineers, Part A*. 1992;70:448.

Doherty MF, Caldarola GA. Design and synthesis of homogeneous azeotropic distillations. 3. The sequencing of columns for azeotropic and extractive distillations. *Ind. Eng. Chem. Fundam.* 1985;24:474-485.

Doherty MF, Perkins JD. On the dynamics of distillation process. III. The topological structure of ternary residue curve maps. *Chem. Eng. Sci*. 1979;34:1401-1414.

Dyk BV, Nieuwoudt I. Design of Solvents for Extractive Distillation. *Ind. Eng. Chem. Res*., 2000;39:1423.

Espinosa J, Aguirre P, Perez G. Product Composition Regions of Single-Feed Reactive Distillation Columns: Mixtures Containing Inerts. *Ind. Eng. Chem. Res.* 1995;34:853.

Espinosa J, Aguirre P, Perez G. Some Aspects in the Design of Multicomponent Reactive Distillation Columns Including Nonreactive Species. *Chem. Eng. Sci.* 1996;50:469.

Fernholz G, Engell S, Kreul L-U, Gorak A. Optimal operation of a semi-batch reactive distillation column. *Comp Chem Eng*. 2000;24:1569-1575.

Foucher ER, Doherty MF, Malone MF. Automatic Screening of Entrainers for Homogeneous Azeotropic Distillation. *Ind. Eng. Chem. Res*., 1991;30:760.

Gadewar SB, Malone MF, Doherty MF. Selectivity targets for batch reactive distillation. *Ind Eng Chem Res*. 2000;39:1565-1575.

Giessler S, Danilov RY, Pisarenko YA, Serafimov LA, Hasabe S, Hashimoto I. Feasibility Study of Reactive Distillation Using the Analysis of the Statics. *Ind. Eng. Chem. Res.* 1998;37:4375-4382.

Guo Z, Chin J, Lee JW. Feasibility of continuous reactive distillation with azeotropic mixtures. *Ind. Eng. Chem. Res.* 2004;43:3758-3769.

Guo Z, Ghufran M, Lee JW. Feasible products in batch reactive distillation. *AIChE J.*, 2003;49:3161-3172.

Guo Z, Lee JW. Feasible products in batch reactive extractive distillation. *AIChE J.* 2004;50:1484-1492.

Hasebe S, Noda M, Hashimoto I. Optimal operation policy for multieffect batch distillation system. *Comp Chem Eng.* 1997;21:S1221–S1226.

Hauan S, Ciric AR, Westerberg AW, Lien KM. Difference points in extractive and reactive cascades. I - Basic properties and analysis. *Chem. Eng. Sci.* 2000;55(16):3145-3159.

Hauan S, Omtveit T, Lien KM. Analysis of Reactive Separation Systems. Presented at the AIChE Annual Meeting, Chicago, IL, Nov 10-15, 1996; Paper 5f.

Hauan S, Westerberg AW, Lien KM. Phenomena based analysis of fixed points in reactive separation systems. *Chem. Eng. Sci.*, 2000;55:1053-1075.

Hoffman EJ. Azoetropic and extractive distillation; Wiley (Interscience); New York, 1964.

Hoffmaster W, Hauan S. Analysis of complex separation schemes in the presence of chemical reactions. *Sep. Sci. Technol.* 2003;38:2763.

Ismail SR, Papalexandri KP, Pistikopoulos EN. Synthesis of Reactive and Combined Reactor/Separation Systems Utilizing a Mass/Heat Transfer Exchange Module. *Chem. Engr. Sci.* 1999;54:2721.

Jackson JR, Grossmann IE. A disjunctive programming approach for the optimal design of reactive distillation columns. *Comp. Chem. Eng.* 2001;25:1661-1673.

Julka V, Doherty MF. Geometric behavior and minimum flows for nonideal multicomponent distillation. *Chem. Eng. Sci*. 1990;45:1801-1822.

Kim K, Diwekar UM. Comparing batch column configurations: parametric study involving multiple objectives. *AIChE J.* 2000;46:2475-2488.

Knapp JP, Doherty MF. Thermal integration of homogeneous azeotropic distillation sequence. *AIChE J.* 1990;36:969-984.

Knapp JP, Doherty MF. Minimum entrainer flows for extractive distillation: a bifurcation theoretic approach. *AIChE J*. 1994;40:243-268.

Kreul LU, Górak A, Barton PI. Modeling of Homogeneous Reactive Separation Processes in Packed Columns. *Chem. Eng. Sci.* 1999;54:19.

Lang P, Modla G, Benadda B, Lelkes Z. Homoazeotropic distillation of maximum azeotropes in a batch rectifier with continuous entrainer feeding I. Feasibility studies. *Comp Chem Eng*. 2000;24:1665-1671.

Lee JW. Feasibility studies on quaternary reactive distillation systems. *Ind Eng Chem Res*. 2002;41:4632-4642.

Lee JW, Brüggemann S, Marquardt W. Shortcut method for kinetically controlled reactive distillation systems. *AIChE J*. 2003;49:1471-1487.

Lee JW, Hauan S, Lien KM, Westerberg AW. Difference points in extractive and reactive cascades. II - Generating design alternatives by the lever rule for reactive systems. *Chem. Eng. Sci.* 2000;55(16):3161-3174.

Lee JW, Hauan S, Lien KM, Westerberg AW. A Graphical Method for Designing Reactive Distillation Columns I: The Ponchon—Savarit Diagram. *Proc. R. Soc. London, Ser. A* 2000;456:1953-1964.

Lee JW, Hauan S, Lien KM, Westerberg AW. A Graphical Method for Designing Reactive Distillation Columns II: The McCabe—Thiele Diagram. *Proc. R. Soc. London, Ser. A* 2000;456:1965-1978.

Lee JW, Hauan S, Westerberg AW. Circumventing an azeotrope in reactive distillation. *Ind. Eng. Chem. Res.* 2000;39:1061.

Lee JW, Hauan S, Westerberg AW. Feasibility of a reactive distillation column with ternary mixtures. *Ind. Eng. Chem. Res.* 2001;40:2714-2728.

Lee JW, Westerberg AW. Visualization of Stage Calculations in Ternary Reacting Mixtures. *Comput. Chem. Eng.* 2000;24:639.

Lee JW, Westerberg AW. Graphical design applied to MTBE and methyl acetate reactive distillation processes. *AIChE J*., 2001;47:1333.

Lee L, Kuo M. Phase and reaction equilibria of the acetic acid - isopropanol - isopropyl acetate - water system at 760 mmHg. *Fluid Phase Equilibria.* 1996;38:147-165.

Lelkes Z, Lang P, Benadda B, Moszlowicz P. Feasibility of extractive distillation in a batch rectifier. *AIChE J.* 1998;44:810-822.

Lelkes Z, Lang P, Moszlowicz P, Benadda B, Otterbein M. Batch extractive distillation: the process and the operational policies. *Chem Eng Sci*. 1998;53:1331-1348.

Lotter SP, Diwekar UM. Shortcut models and feasibility considerations for emerging batch distillation columns. *Ind Chem Eng Res.* 1997;36:760-770.

Luo HP, Xiao WD. A Reactive Distillation Process for a Cascade and Azeotropic Reaction System: Carbonylation of Ethanol with Dimethyl Carbonate. *Chem. Eng. Sci.* 2001;56:403-410.

Malone MF, Doherty MF. Reactive distillation. *Ind Eng Chem Res*. 2000;39:3953-3957.

Masamoto J, Matsuzaki K. Development of Methylal Synthesis by Reactive Distillation. *J. Chem. Engr. Japan.* 1994;27(1):1-5.

Matlab 6.0, Using Matlab. The MathWorks, Inc.; 2000.

Mathematica 4.2, Wolfram Research, Inc.; 2002.

Matsuyama H, Nishimura H. Topological and thermodynamic classification of ternary vapor-liquid equilibria. *J Chem Engr Japan*. 1977;10(3):181-187.

Nisoli A, Malone MF, Doherty MF. Attainable regions for reaction with separation. *AIChE J.* 1997;43:374.

Okasinski MJ, Doherty MF. Design Method for Kinetically Controlled, Staged Reactive Distillation Columns. *Ind. Eng. Che. Res.* 1998;37:2821.

Papalexandri KP, Pistikopoulos EN. Generalized modular representation framework for process synthesis. *AIChE J.* 1996;42:1010-1032.

Patlasov VP, Balashov MI, Serafimov LA. Computer Analysis of the Statics of Continuous Integrated Reaction-Rectification Processes. *Theor. Found. Chem. Technol.* 1980;14(1):67-72

Peng J, Lextrait S, Edgar TF, Eldridge RB. A Comparison of Steady-State Equilibrium and Rate-Based Models for Packed Reactive Distillation Columns. *Ind. Eng. Che. Res*. 2002;41:2735.

Pérez-Cisneros ES, Gani R, Michelsen ML. Reactive separation systems. Part I: Computation of physical and chemical equilibrium. *Chem Eng. Sci.* 1997;52:527-543.

Phimister JR, Seider WD. Semicontinuous, middle-vessel extractive distillation. *Comp Chem Eng*. 2000;24:879-885.

Phimister JR, Seider WD. Semicontinuous, middle-vessel distillation of ternary mixtures. *AIChE J.* 2000;46:1508-1520.

Pisarenko YA, Balashov MI. Statics of Reaction Systems with Selective Exchange. *Teor. Osn. Khim. Teknol.* 1986;20:539.

Pisarenko YA, Danilov RY, Serafimov LA. Infinite-Efficiency Operating Conditions in Analysis of the Statics of Reactive Rectification. *Theor. Found. Chem. Engr.* 1995;29:556.

Pisarenko YA, Serafimov LA. Assessing Influence of Selective Transfer on Chemical Conversion in Open Systems. *Theor. Found. Chem. Engr.* 1992;26:611.

Reder C, Remme U, Bausa J, Marquardt W. Design of reactive distillation processes using a new shortcut method for minimum-reflux calculation. AIChE Annual Meeting, Miami, November (1998).

Rihko LK, Krause AO. Kinetics of Heterogeneously Catalyzed *tert*-Amyl Methyl Ether Reactions in the Liquid Phase. *Ind. Eng. Chem. Res.* 1995;34:1172.
Robinson CS, Gilliland ER. Elements of fractional distillation; Interscience Publisher; New York, 1961.

Rooks RE, Julka V, Doherty MF, Malone MF. Structure of distillation regions for multicomponent azeotropic mixtures. *AIChE J.* 1998;44:1382-1391.

Safrit BT, Westerberg AW. Improved operation policies for batch extractive distillation columns. *Ind Eng Chem Res.* 1997;36:436-443.

Safrit BT, Westerberg AW, Diwekar U, Wahnschafft OM. Extending continuous conventional and extractive distillation feasibility insights to batch distillation. *Ind Eng Chem Res.* 1995;34:3257-3264.

Seider WD, Brengel DD, Widagdo S. Nonlinear analysis in process design. AIChE J. 1991;37:1-38.

Seydel R, Hlavacek V. Role of continuation in engineering analysis. *Chem. Eng. Sci.* 1987;42:1281-1295.

Shoemaker JD, Jones EM. Cumene by Catalytic Distillation. *Hydrocarbon Processing*. 1987;66(6):57-58.

Siirola JJ. An industrial perspective on process synthesis. *AIChE Symp Ser*. 1995;304:222-233.

Smith LA. Catalytic Distillation Process. U.S. Patent 4,307,254: 1981.

Song W, Venimadhavan G, Manning JM, Malone MF, Doherty MF. Measurement of residue curve maps and heterogeneous kinetics in methyl acetate synthesis. *Ind. Eng. Chem. Res.* 1998;37:1917-1928.

Stankiewicz A, Moulijn JA. Process Intensification. *Ind. Engr. Chem Res.* 2002;41(8):1920-1924.

Stichlmair JG, Fair JR. *Distillation: Principle and Practice*; Wiley-VCH: New York, 1998.

Sundmacher K, Uhde G, Hoffmann U. Multiple reactions in catalytic distillation processes for the production of the fuel oxygenates MTBE and TAME: Analysis by rigorous model and experimental validation. *Chem. Eng. Sci.* 1999;54:2839.

Tang YT, Chen YW, Hung SB, Huang HP, Lee MJ, Yu CC. Design of reactive distillations for acetic acid esterification. *AIChE J*. 2005;51:1683-1699.

Taylor R, Krishna R. Modelling reactive distillation. *Chem Eng Sci.* 2000;55:5183-5229.

Ung S, Doherty MF. Vapor-liquid phase equilibrium in systems with multiple chemical reactions. Chem. Eng. Sci. 1995;50:23.

Velo E, Puigjaner L, Recasens F. Inhibition by product in the liquid-phase hydration of isobutene to tert-butyl alcohol: Kinetics and equilibrium studies. Ind. Eng. Chem. Res. 1988;27:2224.

Venimadhavan G, Buzad G, Doherty MF. Effects of Kinetics on Residue Curve Maps for Reactive Distillation. *AIChE J.* 1994;39:169.

Venimadhavan G, Malone MF, Doherty MF. A novel distillate policy for batch reactive distillation with application to the production of butyl acetate. *Ind Chem Eng Res*. 1999;38:714-722.

Wahnschafft OM, Westerberg AW. The product composition regions of azeotropic distillation columns. 2. Separability in two-feed columns and entrainer selection. *Ind. Eng. Chem. Res.* 1993;32:1108-1120.

Watzdorf Rv, Bausa J, Marquardt W. Shortcut method for non-ideal multicomponent distillation: 2. Complex columns. *AIChE J*. 1999;45:1615-1628.

Westerberg AW, Wahnschafft OM. Synthesis of Distillation-Based Separation Systems. *Adv. Chem. Eng*. 1996;23:63.

Wibowo C, Ng KM. Visualization of High-Dimensional Systems via Geometric Modeling with Homogenous Coordinates. *Ind. Eng. Chem. Res.* 2002;41:2213.